Preliminary Cruise Report

R/V Hakuho-maru KH93-3 Research Cruise
July 8 - September 17, 1993

Rodriguez Triple Junction Expedition in the Indian Ocean

(InterRidge and ODP)

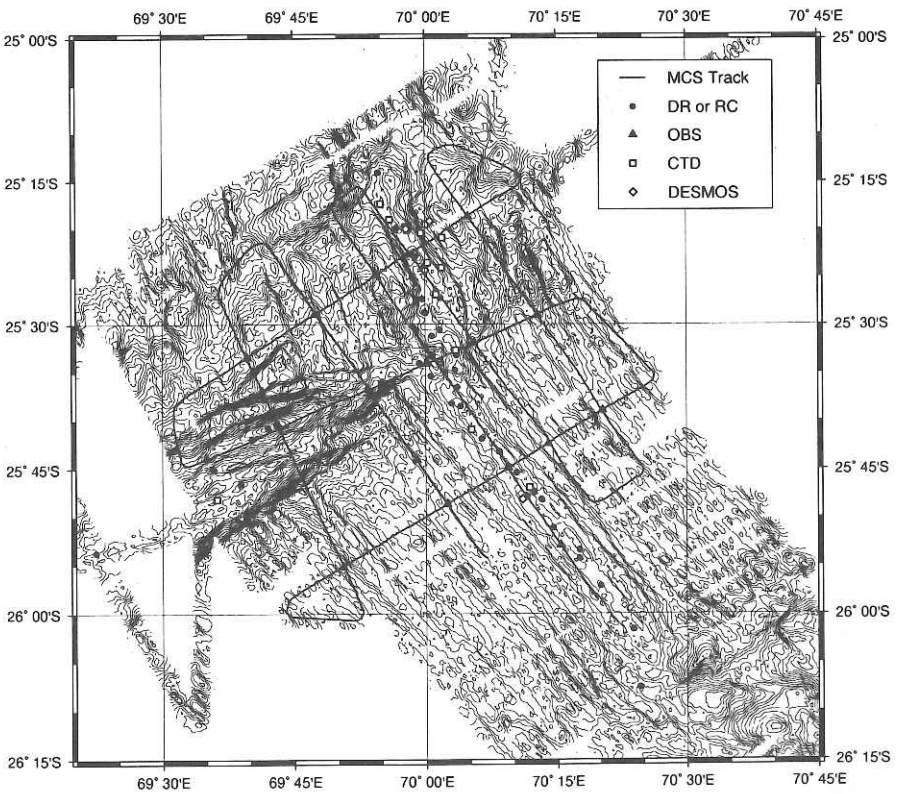

Ocean Research Institute
University of Tokyo
March 1995

Preliminary Cruise Report

R/V Hakuho-maru KH93-3 Research Cruise
July 8 - September 17, 1993

Rodriguez Triple Junction Expedition in the Indian Ocean

(InterRidge and ODP)

Edited by
Kensaku Tamaki and Hiromi Fujimoto

Ocean Research Institute
University of Tokyo
March 1995

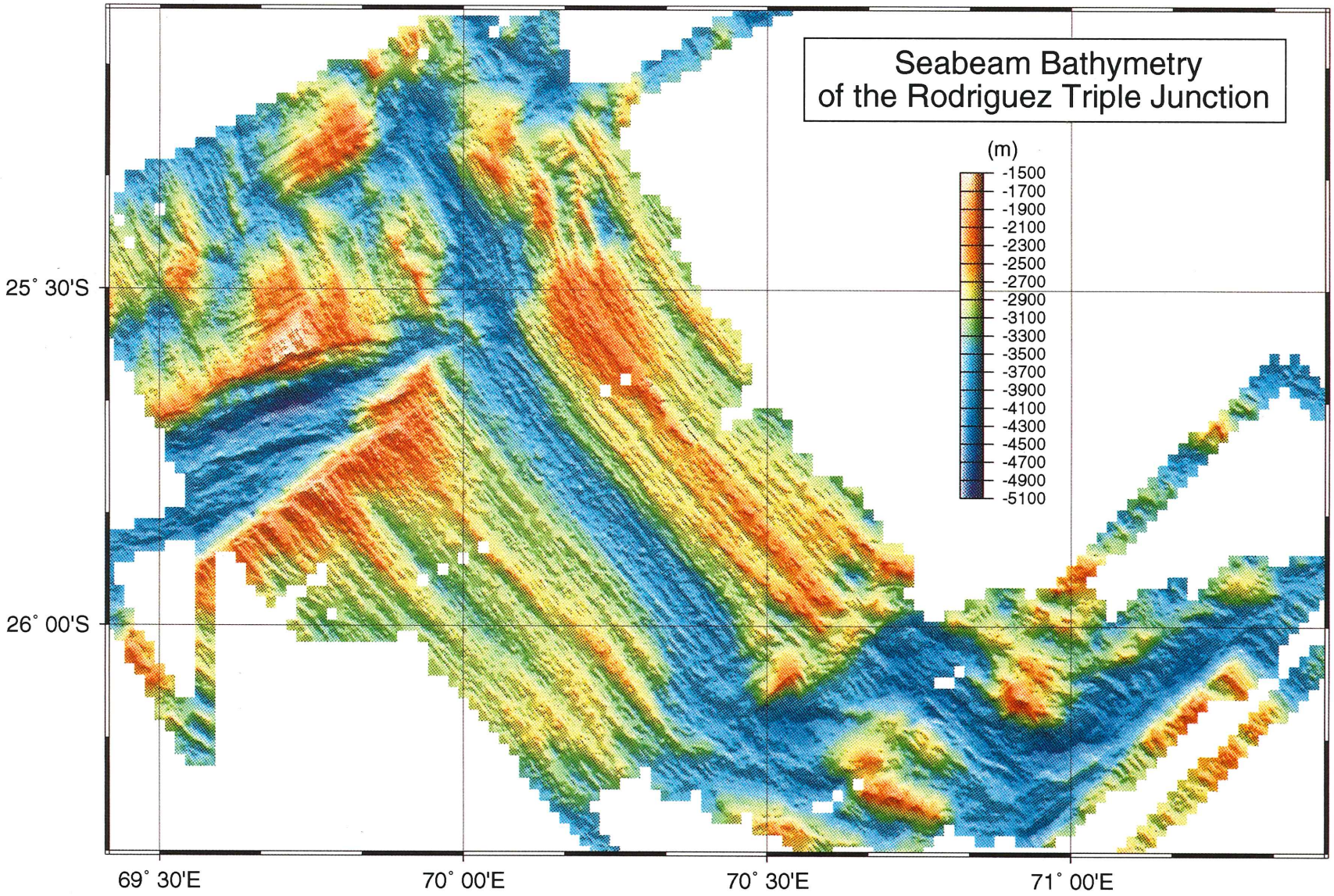
Seabeam Bathymetry
of the Rodriguez Triple Junction
(m)
-1500
-1700
-1900
-2100
-2300
-2500
-2700
-2900
-3100
-3300
-3500
-3700
-3900
-4100
-4300
-4500
-4700
-4900
-5100
25° 30'S
26° 00'S
69° 30'E
70° 00'E
70° 30'E
71° 00'E

PREFACE

The mid-oceanic ridge plays a principal role in solid earth dynamics as well as in ocean dynamics by thermal, chemical, and biological interaction. In spite of the importance of the mid-oceanic ridge system on earth science, Japanese scientists have long been isolated from the exciting progress of mid-oceanic ridge research mainly because all mid-oceanic ridges are far from Japan. The KH93-3 Research Cruise was planned as the first intensive seagoing research at a mid-oceanic ridge for Japanese university scientists and graduate students and intended to start robust research activity of mid-oceanic ridges in Japan.

The KH93-3 cruise formed an integral part of InterRidge Japan Project as well as a preliminary site survey for the Ocean Drilling Program. The Rodriguez Triple Junction in the center of the Indian Ocean was selected as a target survey area because of its intriguing tectonic setting. Three different types of mid-oceanic ridges meet at the Rodriguez Triple Junction and provide various opportunities to investigate mid-oceanic ridge processes in a small area and within a limited time. A multidisciplinary survey was conducted with underway geophysical survey, multichannel seismic reflection survey, deployment of ocean bottom seismometers for seismic refraction measurements and earthquake observation, bottom rock sampling, deep sea hydrocasts, and deep sea TV observation. As the R/V Hakuho-maru has the size of 3,980 tons, she is fully suitable for such multidisciplinary research work.

The KH93-3 cruise was a highly successful expedition as fully described in the subsequent reports in this volume and in the online cruise report published on the Internet (http://www.ori.u-tokyo.ac.jp). We owe the success of the cruise to the support of the following people. Captain H. Shimamune and all of the officers and crew provided their skillful support for twenty-four hours a day at sea to carry out intensive research works. The administration office of the Ocean Research Institute (ORI), University of Tokyo safely prepared and planned the 72 days of the cruise. Drs. M. Munschy and R. Schlich (IPG Strasbourg) allowed us to use all the geophysical data obtained near the Rodriguez Triple Junction by the R/V Jean Charcot in 1984. Dr. P. Patriat (IPG Paris) kindly sent us a new swath bathymetric map of the Southwestern Indian Ridge. Drs. W. Plüger and P. Herzig (Aachen, Germany) sent us results of their geochemical survey in the Central Indian Ridge. Drs. A. Briais (GRGS, France), L. Parson (IOS, UK), J. Delaney (InterRidge Office), and T. Stroh (InterRidge Office) helped us in the planning of the cruise. A. Hatanaka of ORI converted the manuscripts to Tex format. T. Mizutani, A. Hatanaka, C. Tamura, and W. Hatanaka of ORI prepared the printing formats of all the figures. C. Honsho designed the cover page. We sincerely thank all of the above people for their support.

Kensaku Tamaki and Hiromi Fujimoto
Ocean Research Institute, University of Tokyo

March 1st, 1995

CONTENTS

Scientists aboard the R/V Hakuho-maru Cruise KH93-3

Co-chief scientists

Kensaku Tamaki (Legs 1, 2, 3)
Ocean Research Institute, University of Tokyo, 1-15-1 Minamidai, Nakano-ku, Tokyo 164, Japan
tamaki@ori.u-tokyo.ac.jp
Hiromi Fujimoto (Legs 2, 3, 4)
Ocean Research Institute, University of Tokyo, 1-15-1 Minamidai, Nakano-ku, Tokyo 164, Japan
fujimoto@ori.u-tokyo.ac.jp

Underway Geophysics (SeaBeam, Gravity, Magnetics)

Chie Honsho (Lega 1, 2, 3, 4)
Ocean Research Institute, University of Tokyo, 1-15-1 Minamidai, Nakano-ku, Tokyo 164, Japan
honsho@minerva.ori.u-tokyo.ac.jp
Keiichi Furuya (Legs 1, 2)
Department of Earth Science, Faculty of Science, Chiba University, 1-33 Yayoi, Inage-ku, Chiba 263, Japan
efuruya@nature.s.chiba-u.ac.jp
Kin-ichiro Koizumi (Legs 1, 2)
Ocean Research Institute, University of Tokyo, 1-15-1 Minamidai, Nakano-ku, Tokyo 164, Japan
Brian P. West (Leg 3)
School of Oceanography, Univ. of Washington (Marine Geophysics), UW, WB-10, Seattle, WA 98195, USA
bpw@ocean.washington.edu
Laurent Roux (Leg 3)
GRUS-Observatoire Midi-Pyrenees, Avenue Edouard Belin, Toulouse, France
roux@pontos.cnej.fr

Seismology

Junzo Kasahara (Legs 1, 2)
Earthquake Research Institute, University of Tokyo, 1-1-1 Yayoi, Bunkyo-ku, Tokyo 113, Japan
kasa2@obs1.eri.u-tokyo.ac.jp
Naoshi Hirata (Leg 2)
Earthquake Research Institute, University of Tokyo, 1-1-1 Yayoi, Bunkyo-ku, Tokyo 113, Japan
hirata@eri.u-tokyo.ac.jp
Toshinori Sato (Legs 3, 4)
Earthquake Research Institute, University of Tokyo, 1-1-1 Yayoi, Bunkyo-ku, Tokyo 113, Japan
satot@obs1.eri.u-tokyo.ac.jp
Ryota Hino (Leg 2)
Observation Center for Prediction of Earthquakes and Volcanic Eruptions, Faculty of Science, Tohoku Univ., Aza-Aoba, Aoba, Sendai-city, Miyagi 980, Japan
hino@aob.geophys.tohoku.ac.jp
Chiaki Igarashi (Legs 1, 2)
Ocean Research Institute, University of Tokyo, 1-15-1 Minamidai, Nakano-ku, Tokyo 164, Japan
igarashi@ori.u-tokyo.ac.jp
Sadayuki Koresawa (Legs 1, 2)
Earthquake Research Institute, University of Tokyo, 1-1-1 Yayoi, Bunkyo-ku, Tokyo 113, Japan

Narumi Takahashi (Legs 2, 3)
Department of Earth Science, Faculty of Science, Chiba University, 1-33 Yayoi, Inage-ku, Chiba 263, Japan
narumi@cuphd.nd.chiba-u.ac.jp
Kei Katsumata (Legs 3, 4)
Earthquake Research Institute, University of Tokyo, 1-1-1 Yayoi, Bunkyo-ku, Tokyo 113, Japan
(Present address : Reserch Center for Earthquake Prediction, Faculty of Science, Hokkaido Univ., Sapporo 060, Japan. e-mail : katsu@eos.hokudai.ac.jp)
Mayumi Sekine (Legs 1, 2)
Department of Earth Science, Faculty of Science, Chiba University, 1-33 Yayoi, Inage-ku, Chiba 263, Japan
(Present address : Earthquake Research Institute, University of Tokyo, 1-1-1 Yayoi, Bunkyo-ku, Tokyo 113, Japan. e-mail : mayumi@eri.u-tokyo.ac.jp)

Petrology

Toshitsugu Fujii (Leg 2)
Earthquake Research Institute, University of Tokyo, 1-1-1 Yayoi, Bunkyo-ku, Tokyo 113, Japan
fujii@magma.eri.u-tokyo.ac.jp
Setsuya Nakada (Leg 3)
Department of Earth and Planetary Sciences, Faculty of Science, Kyushu Univ., 6-10-1 Hakozaki, Higashi-ku, Fukuoka 812, Japan
(Present address : Earthquake Research Institute, University of Tokyo, 1-1-1 Yayoi, Bunkyo-ku, Tokyo 113, Japan. e-mail : nakada@eri.u-tokyo.ac.jp)
Teruaki Ishii (Legs 2, 3)
Ocean Research Institute, University of Tokyo, 1-15-1 Minamidai, Nakano-ku, Tokyo 164, Japan
ishii@ori.u-tokyo.ac.jp
Charles H. Langmuir (Leg 2)
Lamount-Doherty Earth Observatory of Columbia University (Geochemistry), Palisades, NY 10964-8000, USA
langmuir@ldeo.columbia.edu
Shigeru Yamashita (Legs 2, 3)
Earthquake Research Institute, University of Tokyo, 1-1-1 Yayoi, Bunnkyo-ku, Tokyo 113, Japan
(Present address : Institute for Study of the Earth's Interior Okayama University, Misasa, Tottori 682-01, Japan. e-mail : shigeru@msewsl.okayama-u.ac.jp)
Yoshiaki Tainosho (Legs 1, 2)
Faculty of Human Development, Div. of Earth Environment, Kobe Univ., 3-11 Tsurukabuto, Nada, Kobe-city, Hyogo 657, Japan
Satoshi Matsumoto (Leg 3)
Department of Geology, Osaka City Univ., 3-3-138 Sugimoto, Sumiyoshi-ku, Osaka 558, Japan
Yasushi Harada (Leg 3)
Department of Earth and Planetaly Phisics, Univ. of Tokyo, 2-11-16 Yayoi, Bunnkyo-ku, Tokyo 113, Japan
harada@gpsun01.geoph.s.u-tokyo.ac.jp

Water Chemistry

Toshitaka Gamo (Legs 2, 3, 4)
Ocean Research Institute, University of Tokyo, 1-15-1 Minamidai, Nakano-ku, Tokyo 164, Japan
gamo@ori.u-tokyo.ac.jp
Hiroshi Hasumoto (Legs 2, 3)
Ocean Research Institute, University of Tokyo, 1-15-1 Minamidai, Nakano-ku, Tokyo 164, Japan
kansok@ori.u-tokyo.ac.jp

Eiichiro Nakayama (Leg 2)
Faculty of Science, Kyoto University, Kitashirakawa Oiwake, Sakyo-ku, Kyoto 606-01, Japan
Kenji Isshiki (Legs 3, 4)
Department of Applied Science, Kochi Women's University, 5-15 Eikokuji, Kochi-city, Kochi 780, Japan
gec00011@niftyserve.or.jp
Tamotsu Oomori (Legs 2, 3)
Department of Chemistry, Univ. of the Ryukyus, 1 Senbaru, Nisihara, Okinawa 903-01, Japan
Kiminori Shitashima (Legs 2, 3)
Central Research Institute of Electric Power Industry, 1646 Abiko, Abiko-city, Chiba 270-11, Japan
shita@abiko.denken.or.jp
Hajime Obata (Legs 2, 3)
Faculty of Science, Kyoto University, Kitashirakawa Oiwake, Sakyo-ku, Kyoto 606-01, Japan
Shinji Kanayama (Legs 1, 2, 3, 4)
Dep. of Earth Sciences, Faculty of Science, Yamagata Univ., 1-4-12 Koshirakawa, Yamagata-city, Yamagata 990, Japan
Takayuki Koizumi (Legs 2, 3)
Department of Chemistry, Univ. of the Ryukyus, 1 Senbaru, Nisihara, Okinawa 903-01, Japan
Kei Okamura (Legs 3, 4)
Faculty of Science, Kyoto University, Kitashirakawa Oiwake, Sakyo-ku, Kyoto 606-01, Japan

Biology

Suguru Ohta (Legs 3, 4)
Ocean Research Institute, University of Tokyo, 1-15-1 Minamidai, Nakano-ku, Tokyo 164, Japan
sohta@ori.u-tokyo.ac.jp
Kenji Shimizu (Legs 3, 4)
Ocean Research Institute, University of Tokyo, 1-15-1 Minamidai, Nakano-ku, Tokyo 164, Japan
shimizu@ori.u-tokyo.ac.jp
Masaharu Watanabe (Legs 1, 2, 3, 4)
Ocean Research Institute, University of Tokyo, 1-15-1 Minamidai, Nakano-ku, Tokyo 164, Japan
Harumi Kobayashi (Legs 1, 2, 3, 4)
Ocean Research Institute, University of Tokyo, 1-15-1 Minamidai, Nakano-ku, Tokyo 164, Japan
mxe01511@niftyserve.or.jp
Maki Ito (Legs 3, 4)
Dept. Ocean Sci. and Technology, Tokai Univ., 3-20-1 Orido, Shimizu-city, Shizuoka 424, Japan
(Present address : Technical Development, Metal Mining Agency of Japan.)

Atmospheric Chemistry

Tatsuo Tanji (Legs 1, 2)
Muroran Institute of Technology, 27-1 Mizumoto, Muroran-city, Hokkaido 050, Japan
Michio Okino (Legs 3, 4)
Muroran Institute of Technology, 27-1 Mizumoto, Muroran-city, Hokkaido 050, Japan
Kei Saito (Legs 3, 4)
Faculty of Science, Science University of Tokyo, 1-3 Kagurazaka, Shinjyuku-ku, Tokyo 162, Japan

Meteorology

Shigenori Haginoya (Legs 3, 4)
Physical Meteorology Research Department, Meteorological Research Institute, 1-1 Nagamine, Tsukuba-city, Ibaraki 305, Japan
Nobuyuki Kinoshita (Legs 3, 4)
Physical Meteorology Research Department, Meteorological Research Institute, 1-1 Nagamine, Tsukuba-city, Ibaraki 305, Japan
nkinoshi@mri-1.mri-jma.gp.jp

Cosmic Ray

Masahide Furukawa (Legs 1, 2)
Division of Environmental Health, National Institute of Radiological Sciences, 4-9-1 Anagawa, Inage-ku, Chiba 263, Japan

Introduction : Outline of the R/V Hakuho-maru KH93-3 Reserch Cruise

Kensaku TAMAKI[1] and Hiromi FUJIMOTO[1]

[1] *Ocean Research Institute, University of Tokyo*

1. Outline

KH93-3 Research Cruise by the R/V Hakuho-maru of Ocean Research Institute, University of Tokyo, is the first intensive seagoing research at mid-oceanic ridge conducted by the Japanese scientist group. The shiptime for this cruise was endorsed on behalf of InterRidge Project by the Ocean Research Institute, University of Tokyo, who is the owner of the vessel. The target survey area was set at the Rodriguez Triple Junction (RTJ) in the Indian Ocean. Port calls of the cruise are as follows; leaving Tokyo on July 8, 1993, Singapore from July 17 to 21, Mauritius from August 10 to 14, Penang from September 2 to 6, and arriving at Tokyo on September 17. Co-chief scientists are K. Tamaki and H. Fujimoto of Ocean Research Institute. Forty five scientists on board are composed of five research groups; mapping geophysics, seismology, petrology, water chemistry, and benthic biology. Mapping geophysics group is directed by K. Tamaki and H. Fujimoto, seismology group by Kasahara and N. Hirata (both at Earthquake Research Institute, University of Tokyo), petrology group by N. Fujii (ERI), T. Ishii (ORI), C. Langmuir (LDEO), and S. Nakada (Kyushu Univ.), water chemistry group by T. Gamo (ORI), and biology group by S. Ohta (ORI). As the R/V Hakuho-maru has the size of 3,980 ton, she is fully suitable for above multidisciplinary research groups all through the cruise.

2. Objectives of the expedition at the Rodriguez Triple Junction

The Rodriguez Triple Junction is the world most remarkable R-R-R triple junction, which has been controlling the evolution of the major portion of the Indian Ocean. Three ridges with different spreading rates, the Central Indian Ridge (CIR), the Southwest Indian Ridge (SWIR), and the Southeast Indian Ridge (SEIR) meet at the junction. The topographic features of the three rift valleys are quite different, suggesting either the difference in the thermal structure of the underlying mantle or the difference in the crustal structure. It is also expected that the thermal condition of the mantle just beneath the triple junction could be different from those of normal ridges. Principal objectives of the expedition at the RTJ are summarized as follows.
(1) A comprehensive crustal studies at the RTJ by multichannel reflection seismics, ocean bottom seismometer (OBS) refraction crustal studies, and tomograhic analyses of OBS data.
(2) Observation of natural earthquakes at the RTJ.
(3) Geophysical mapping by swath bathymetry, gravity and magnetics for the SEIR to study segmentation of ridges and crustal accretion process by the inversion of magnetic and gravity data.
(4) Detailed bottom rock sampling along spreading center to study melt genesis and mantle dynamics beneath the spreading center.
(5) Study of water chemistry along spreading center to detect chemical flux and to discover active hydrothermal vent area.

(6) Study of benthic community at the spreading center.

3. Methods of the expedition at the Rodriguez Triple Junction

The triple junction was previously surveyed by GLORIA system of UK group (Mitchell, 1991; Michell and Parson, 1993) and SeaBeam system of the R/V Jean Charcot (Munschy and Schlich, 1989, 1990). We planned to conduct all the principal survey in the area previously mapped by the R/V Jean Charcot. This approach saved the time for mapping bathymetry by the R/V Hakuho-maru and allowed us to allocate more time for multichannel seismics, OBS related works, rock sampling, water sampling, and deep-sea TV observation of the seabottom.

Research methods accomplished during the KH93-3 cruise at the RTJ are as follows.

(1) Geophysical mapping of swath bathymetry, gravity, magnetics (total intensity and three component) for the SEIR outside the box surveyed by R/V Jean Charcot.

(2) Seismic refraction studies at the RTJ by OBS and large air gun sound sources. Eighteen OBSs are deployed in a grid configuration as shown in Figure 1, and seventeen OBSs are recovered.

(3) Crustal structure studies at the RTJ by multichannel seismics (MCS). Eight MCS tracks in a grid pattern were achieved as shown in Figure 2.

(4) Seismic tomographic studies at the RTJ by OBSs and large air gun sound sources.

(5) Observation of natural earthquake activity at RTJ by OBSs. Duration of observations is more than 15 days.

(6) Detailed bottom rock sampling at 41 sites (27 dredges and 14 rock cores) along three axes of spreading centers at the RTJ.

(7) Water sampling by CTD-rossette hydrocasts (13 sites, one site is northeast of the RTJ box area) and tow-yo surveys (5 sites).

(8) Observation of the sea bottom and benthic biological community by Deep Sea Monitoring System (DESMOS) at 5 sites (one site is at north of the RTJ box area).

To accomplish the above survey, we have spent 19 days and 8 hours (10 days and 4 hours for Leg 2 and 9 days and 4 hours for Leg 3) in total in the area. 24 hours operation of any of research items were done all through these days. The sea state and weather condition at the RTJ area are fairly good all through the survey time. None of research items were abandoned because of weather condition. The research program was done almost as scheduled.

4. Initial results of the expedition at the Rodriguez Triple Junction

Preliminary results at the RTJ are summarized as follows.

(1) A topographic map around the triple junction was compiled from the observed Sea Beam data combined with the data obtained by the French R/V Jean Charcot.

(2) Bouguer gravity anomalies show "bull's eye negative anomalies on the SEIR and CIR, indicating focused accretion in these segments. The source of the negative gravity anomalies will be clarified by the results of the seismic experiments.

(3) Preliminary analysis of the OBS data show high seismic activities in the area, earthquake swarms being near the RTJ.

(4) Teleseismics events such as a big earthquake occurred near Guam Island were observed by the OBSs.

(5) High-density rock sampling covered a whole range of a single segment on each of the

three different ridges. Fresh glassy basalts were recovered from 23 sites on the SEIR and CIR. Relatively old basaltic rocks with relatively thick Mn-coat were recovered from the southern part of the SWIR. Highly altered (weakly metamorphosed) basalts, dolerites, and gabbros were found along steep fault scarps in the SWIR and RTJ.
(6) Basalt glasses analyzed preliminarily range in MgO from 7.2 to 8.8 wt. differentiated composition in comparison with those in the CIR and SEIR. A little older basalt glasses from the SWIR have the composition similar to fresh glasses in the CIR and SEIR.
(7) A distinct hydrothermal plume was detected close in the CIR. The center of the plume was in a shallow depth around 2200m, about 1800m higher than the bottom of the rift valley. Judging from the areal distribution of the plume, its source is suggested to be somewhere at the eastern off-axis area.
(8) Visual observations of the seafloor suggest that the volcanism at the Indian Ridges contains two stages: sheet lava flow stage and the following volcanic cone stage.

Unfortunately we could not observe any vent area nor biological colony in the RTJ box area by deep-sea TV system although we could detect substantial chemical anomaly in the water column at the CIR. We finally moved to the Sonne Hydrothermal Plume area at 24 00.3'S, 69 39.6'E (Pluger et al., 1988) 60 nautical miles north of the RTJ box area and confirmed the existence of high signature of hydrothermal plume by the anomaly of transmissometer during CTD tow-yo survey (CTD-17). We executed 16 hours of DESMOS deep sea TV observation at the supposed anomaly area. But we could not observe any signature of hydrothermal activity on the sea bottom.

5. Surveys during transit

During the transit from Tokyo to Singapore, Singapore to RTJ, RTJ to Mauritius, Mauritius to RTJ, RTJ to Penang, and Penang to Tokyo, following observations were executed.
(1) Underway geophysics by SeaBeam, gravity, magnetics, and 3.5 kHz echo sounder. Systematic grid surveys were done at two areas of the Ryukyu Trench.
(2) Sampling of plankton by ORI net at 18 sites. Six sites among 18 sites were done at the RTJ box area while waiting for popping up of the OBSs.
(3) Meteorological observation by OMEGA-sonde system at 80 sites during the transit from Mauritius through Penang to Tokyo.
(4) Oceanographic observation by XBT system at 53 sites during the transit from Mauritius through Penang to Tokyo.
(5) Measurements of radon and its daughters, aerosols and electrical conductivity in the atmosphere near the sea surface. The measurements were executed all through the cruise from Tokyo to Tokyo.
(6) Measurements of cosmic-ray intensity by spectro survey meter. The measurements were executed from Tokyo to Singapore, and Singapore to Mauritius.

6. Summary

A multidisciplinary approach for the study of the crustal accretion process of the Rodriguez Triple Junction was successfully executed by detailed geophysical mapping, seismic reflection and refraction crustal studies, tomographic crustal studies, dense bottom rock sampling along

spreading axes, tow-yo and hydrocast water sampling at spreading centers, and geological and biological sea-bottom observation by deep-sea monitoring system. A further synthetic analyses of geophysical mapping, seismic crustal studies, and dense bottom rock sampling will provide a real three-dimensional picture of sea floor spreading process through upper mantle to the surface volcanism at three different spreading systems of CIR, SWIR, and SEIR ridges. Although we could not find hydrothermal vent area, the accumulated chemical data of water sample will provide valuable datasets to understand the chemical flux at the Indian Ocean spreading centers.

7. Acknowledgments

We thank Captain H. Shimamune and all of the officers and crew for their skillful support for twenty-four hours of research works on board. Drs. M. Munschy and R. Schlich, IPG, France, allowed us to use all the geophysical data obtained near the Rodriguez Triple Junction by the R/V Jean Charcot in 1984. Dr. P. Patriat kindly sent us a swath bathymetric map of the SWIR. Dr. W. Plüger and P. Herzig, Aachen, Germany, sent us results of their geochemical survey in the CIR. Drs. A. Briais, L. Parson, J. Delaney, and T. Stroh helped us in the planning of the cruise.

REFERENCES

Jean-Baptiste, P., F. Mantisi, H. Pauwells, D. Grimaud, and P. Patiriat, Hydrothermal 3He and manganese plumes at 19° 29′S on the central Indian Ridge, *Geophys. Res. lett., 17*, 1787-1790, 1992.

Herzig, P. M., and W. L. Plűger, Exploration for hydorthermal activity near Rodriguez Triple Junction, Indian Ocean, *Canadian Mineralogist, 26*, 721-736, 1988.

Mahoney, J. J., J. H. Natland, W. M. White, R. Poreda, S. H. Bloomer, R. L. Fisher, and A. N. Baxter, Isotopic and geochemical provinces of the Western Indian Ocean spreading centers, *J. Geophys. Res., 94*, 4033-4052, 1989.

Mitchell, N. C., Distributed extension at the Indian Ocean Triple Juntion, *J. Geophys. Res., 96*, 8019-8043, 1991.

Mitchell, N. C., An evolving ridge system around the Indian Ocean Triple Junction, *Marine Geophys. Res., 13*, 173-201, 1991.

Mitchell, N. C., and L. M. Parson, The tectonic evolution of the Indian Ocean Triple Junction, anomaly 6 to precent, *J. Geophys. Res., 98*, 1793-1812, 1993.

Munschy, M., and R. Schlich, The Rodriguez Triple Junction (Indian Ocean): structure and evolution for the past one million years, *Mar. Geophys. Res., 11*, 1-14, 1989.

Munschy, M., and R. Schlich, The Rodriguez Triple Junction (Indian Ocean): structure and evolution for the past one million years, *Geologica Acta, S10*, 129-142, 1990.

Norton, I. O., and J. G. Sclater, A model for the evolution of the Indian Ocean and the breakp of Gondwanaland, *J. Geophys. Res., 84*, 6803-6830, 1979.

Patriat, P., and J. Segoufin, Reconstruction of the central Indian Ocean, *Tectonophys.,155*, 211-234, 1988.

Patriat, P., and L. Parson, A survey of the Indian Ocean Triple Junctin trace within the Antractic Plate. Implications for the junction evolution since 15 Ma, *Mar. Geophys. Res., 11*, 89-100, 1989.

Patriot, P., and V. Courtillot, On the stsbility, of triple junction and its relation to episodicity in speading, *Tectonics, 3*, 317-332, 1984.

Plűger, W. L., P. M. Herzig, K. P. Becker, G. Dessmann, D. Schops, J. Lange, A. Jenisch, S. Ladage, H. H. Richnow, T. Schulze, and W. Michaelis, Discovery of hydrothermal fields at the Central Indian Ocean, *Marine Mining, 9*, 73-86, 1990.

Royer, J-Y., and R. Schlich, Southeast Indian Ridge between the Rodriquez Treple Junction and the Amsterdam and Saint-Paul Islands: Detailed kinematics of the past 20 m.y., *J. Geophys. Res., 93*, 13524-13550, 1988.

Sauter, D., H. Whitechurch, M. Munschy, and E. humler, Periodicity in the accretion precess on the Southwest Indian ridge at 27° 40′ S, *Tectonophys., 195*, 47-64, 1991.

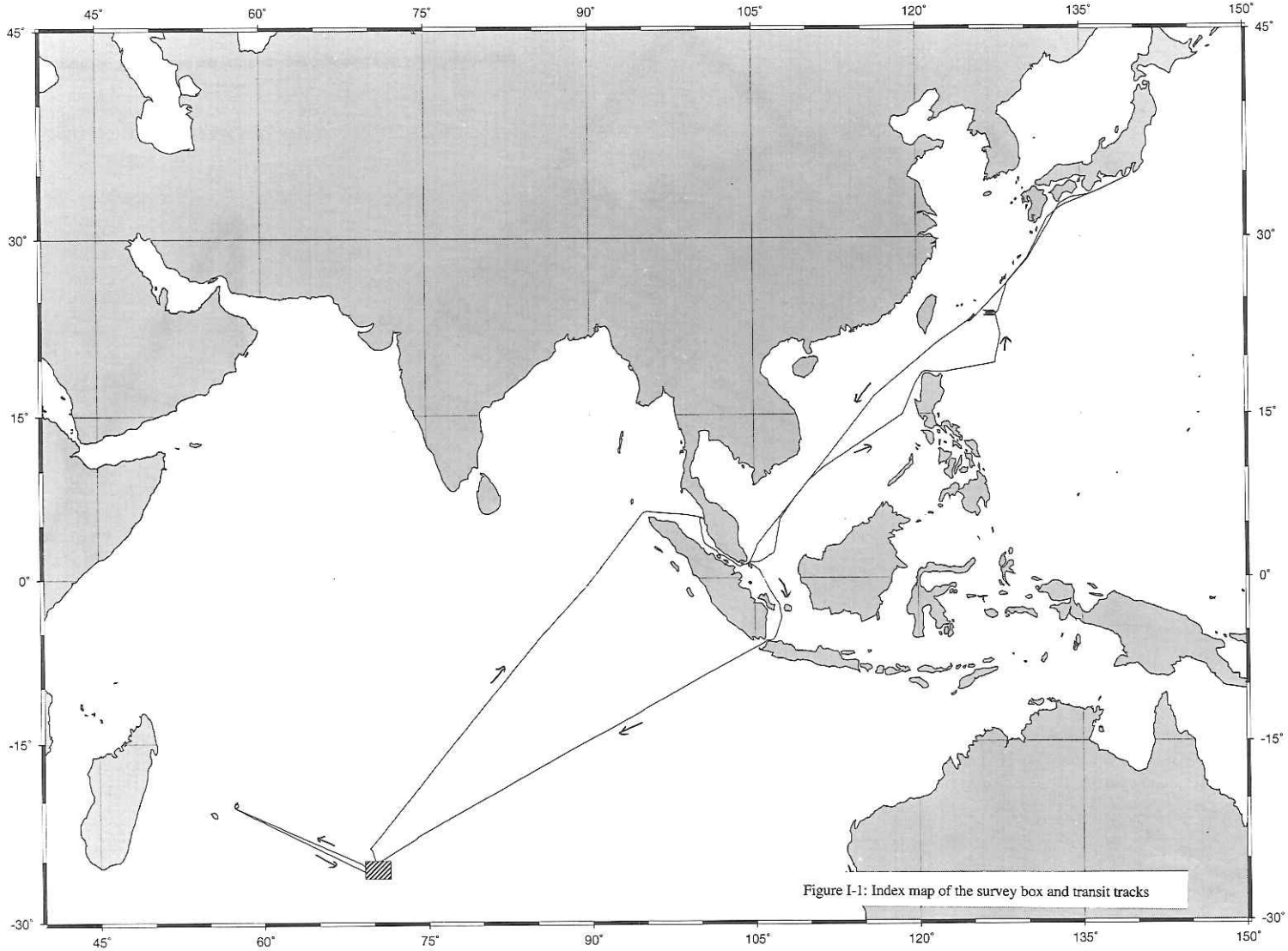

Figure I-1: Index map of the survey box and transit tracks

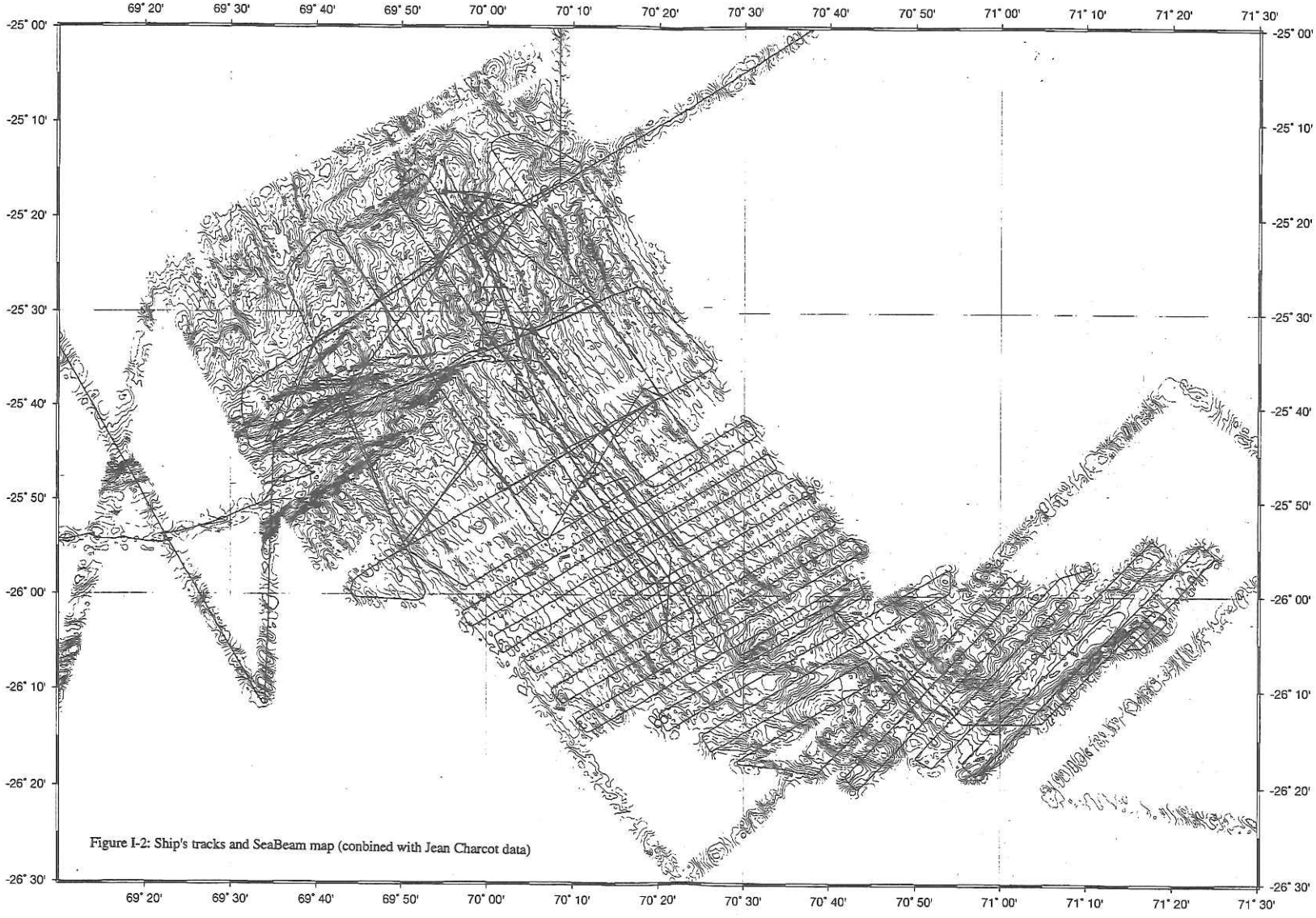

Figure I-2: Ship's tracks and SeaBeam map (conbined with Jean Charcot data)

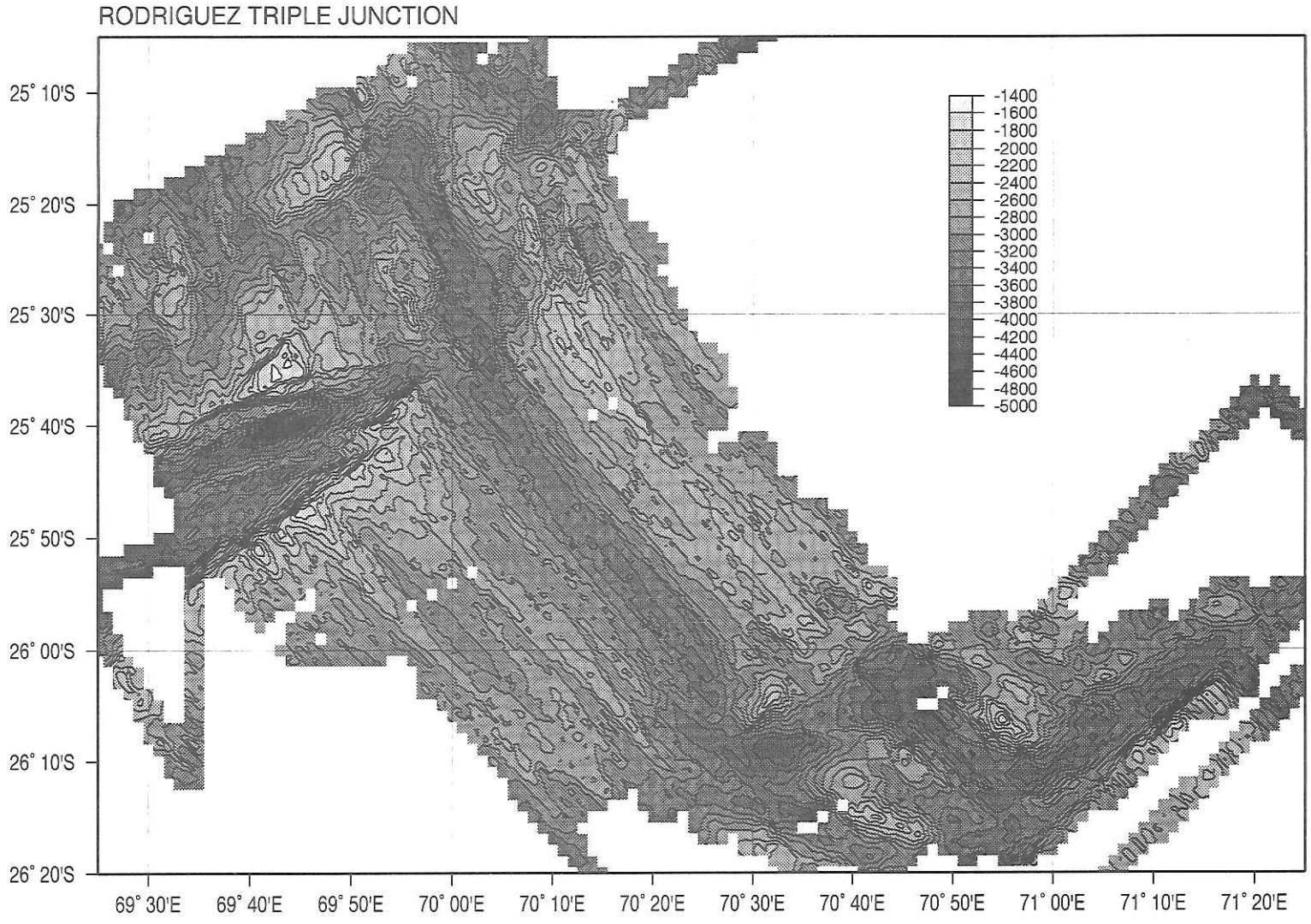

Fig. I-3. SeaBeam map (combined with Jean Charcot Data).

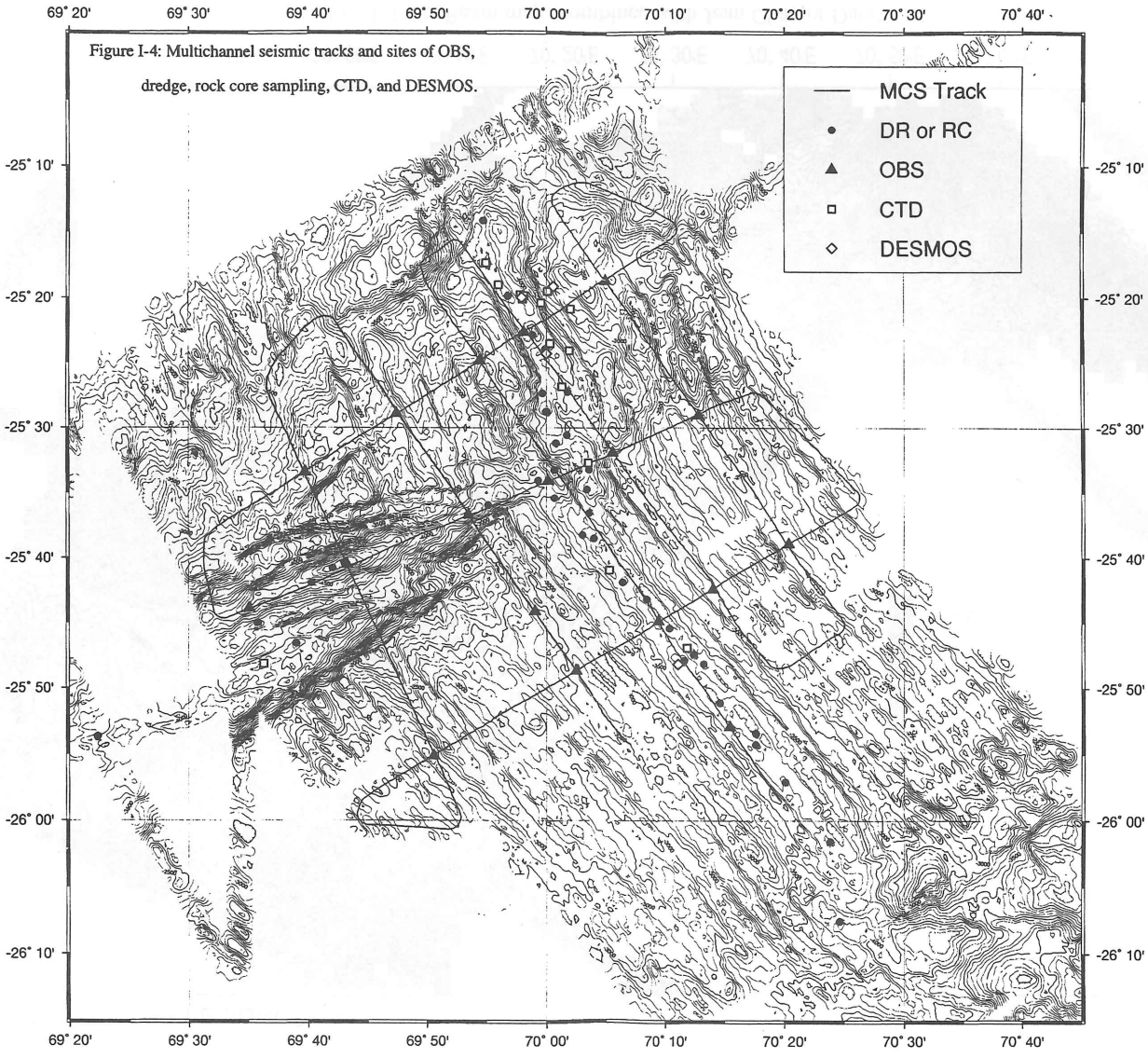

Figure I-4: Multichannel seismic tracks and sites of OBS, dredge, rock core sampling, CTD, and DESMOS.

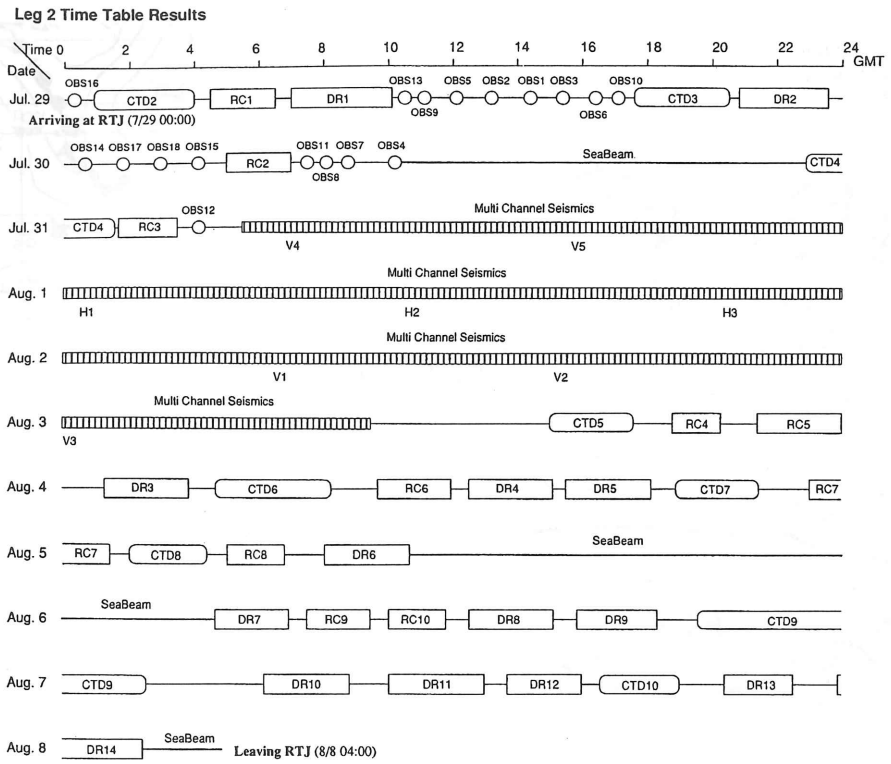

Fig. I-5. Leg 2 time table

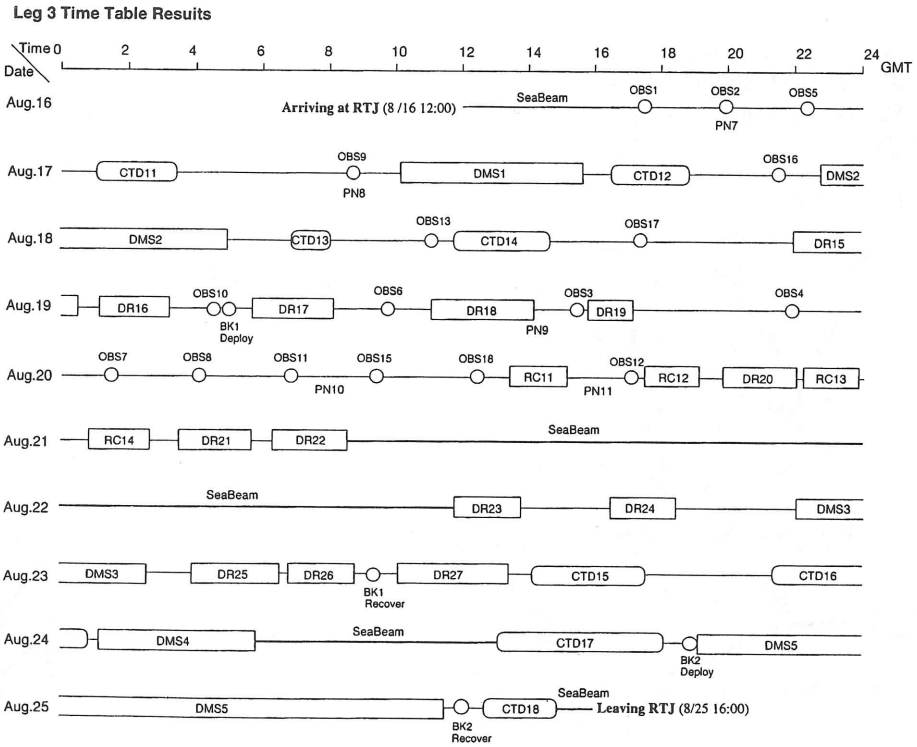

Fig. I-6. Leg 3 time table

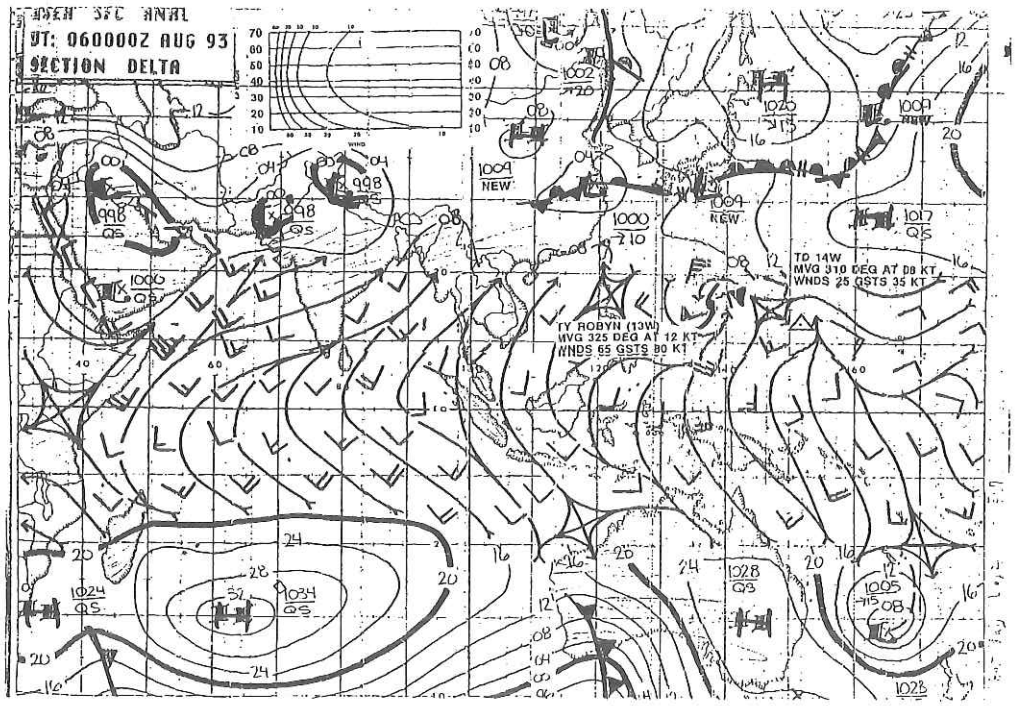

Fig. I-7. Contours of atmospheric pressure of one of the best days in Leg2 (August 6).

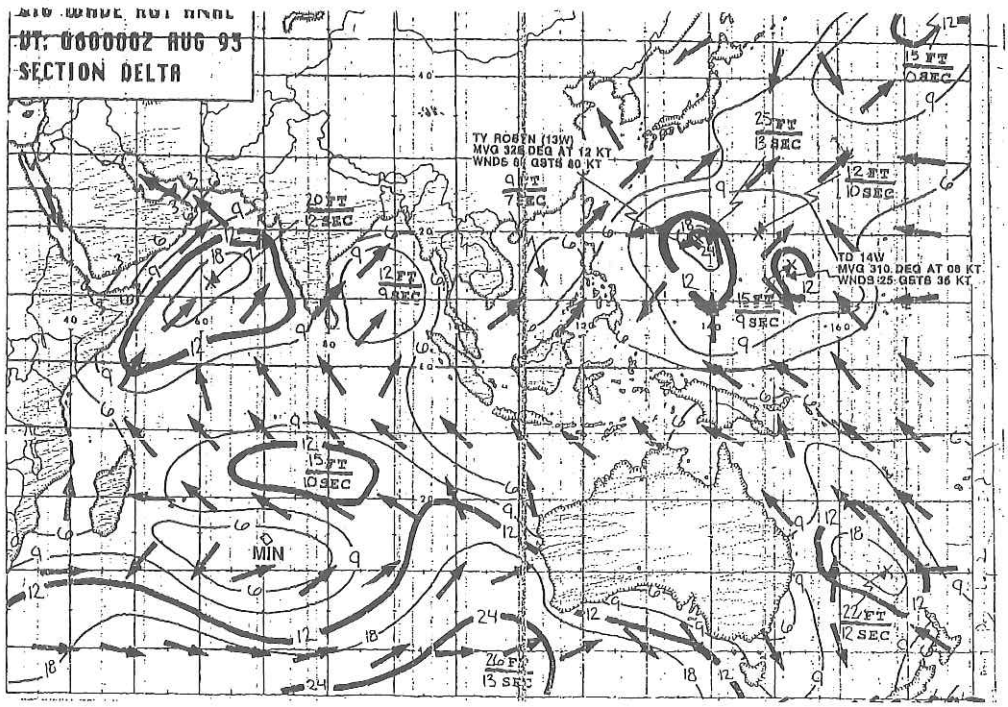

Fig. I-8. Contours of wave hights in feet of one of the best days in Leg2 (August 6).

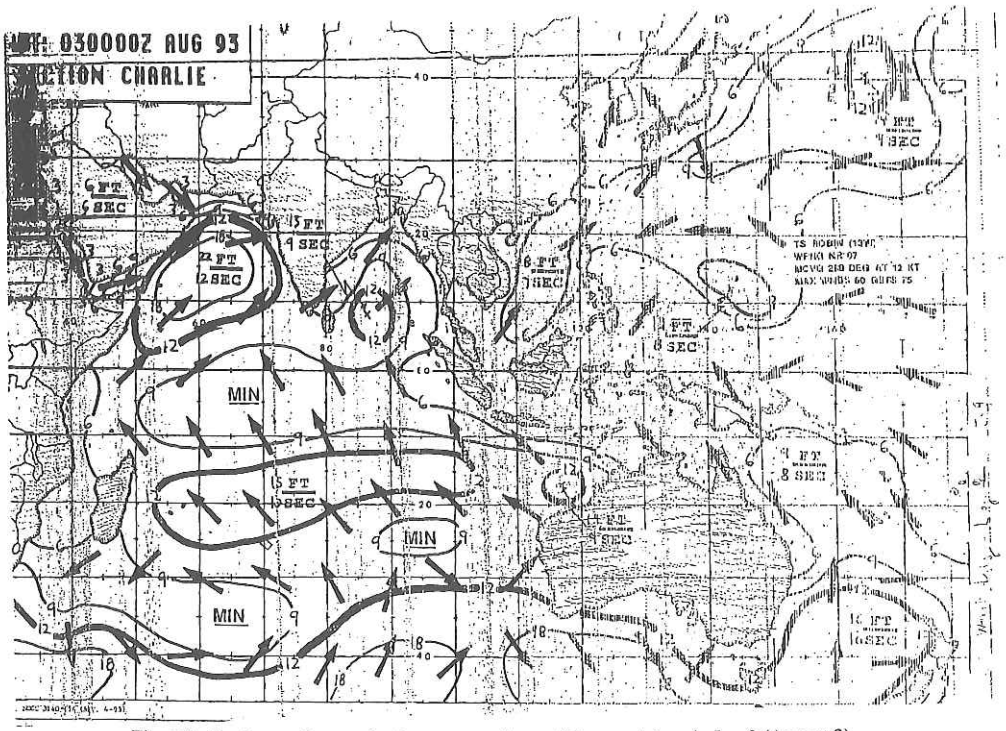

Fig. I-9. Contours of atmospheric pressure of one of the worst days in Leg2 (August 3).

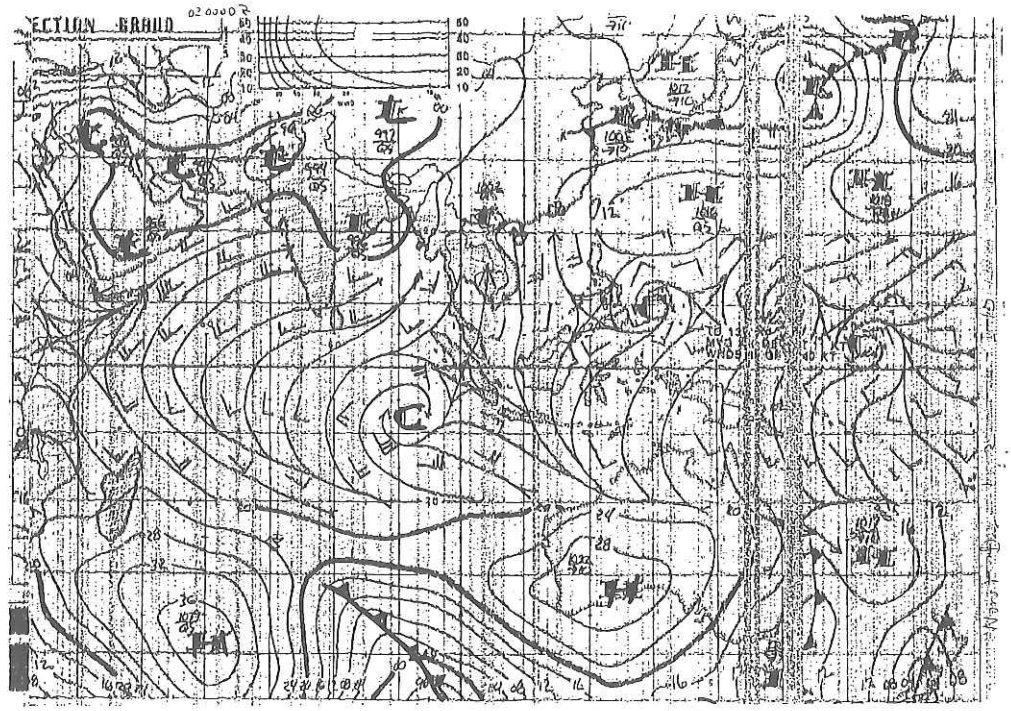

Fig. I-10. Contours of wave of hights in feet of one of the worst days in Leg2 (August 3).

Table I-1. Station and working leg of KH93-3

Y.M.D. GMT+T	LAT.	LONG.	DEPTH	ST.NO	CURRENT	COMENT
930708 0834+09	34-55.395N	139-39.877E	6	S6	288 0.6	s/co to 207fl
930712 1424+09	20-06.550N	120-24.250E	3883	PN-1	000 0.0	ORI NET START
930712 1443+09	20-06.340N	120-23.980E	3883	PN-1	000 0.0	ORI NET START
930712 1447+09	20-06.270N	120-23.900E	3897	PN-1	000 0.0	ORI NET DEEPEST
930712 1503+09	20-06.000N	120-23.510E	4041	PN-1	000 0.0	ORI SIDE NET FINISH
930712 1511+09	20-05.860N	120-23.260E	4051	PN-1	000 0.0	ORI NET FINISH
930713 1418+09	16-26.010N	115-53.200E	4107	PN-2	000 0.0	ORI NET START
930713 1423+09	16-25.910N	115-53.250E	4111	PN-2	000 0.0	ORI SIDE NET START
930713 1439+09	16-25.510N	115-53.280E	4120	PN-2	000 0.0	ORI NET DEEPEST
930713 1442+09	16-25.420N	115-53.300E	4119	PN-2	000 0.0	ORI SIDE NET FINISH
930713 1457+09	16-25.040N	115-53.380E	4124	PN-2	000 0.0	ORI NET FINISH
930714 1408+09	11-46.980N	112-11.150E	4162	PN-3	050 1.5	ORI NET START
930714 1411+09	11-46.860N	112-11.080E	4158	PN-3	056 0.9	ORI SIDE NET START
930714 1424+09	11-46.360N	112-10.740E	4096	PN-3	000 0.0	ORI NET DEEPEST
930714 1430+09	11-46.150N	112-10.540E	4011	PN-3	000 0.0	ORI SIDE NET FINISH
930714 1441+09	11-45.730N	112-10.340E	3881	PN-3	000 0.0	ORI NET FINISH
930724 1612+07	12-06.540S	094-43.760E	5015	PN-4	098 1.4	ORI NET START
930724 1616+07	12-06.760S	094-43.900E	5000	PN-4	000 0.0	ORI SIDE NET START
930724 1625+07	12-07.130S	094-44.180E	4997	XBT 1	000 0.0	XBT
930724 1627+07	12-07.240S	094-44.240E	4996	PN-4	000 0.0	ORI NET DEEPEST
930724 1638+07	12-07.620S	094-44.500E	4838	PN-4	000 0.0	ORI SIDE NET FINISH
930724 1652+07	12-08.100S	094-44.890E	4815	PN-4	000 0.0	ORI NET FINISH
930724 1657+07	12-08.310S	094-44.920E	4835	XBT 1	000 0.0	XBT
930728 0540+05	22-59.970S	074-00.040E	4128	CTD 1	000 0.0	CTD-RMS DEEPEST
930728 0652+05	23-00.000S	074-00.190E	4130	CTD 1	000 0.0	CTD-RMS FINISH
930729 0105+05	25-23.930S	069-59.790E	4092	CTD 2	000 0.0	CTD-RMS START
930729 0236+05	25-23.520S	070-00.270E	4202	CTD 2	000 0.0	CTD-RMS DEEPEST
930729 0402+05	25-22.850S	070-00.390E	3922	CTD 2	000 0.0	CTD-RMS FINISH
930729 0422+05	25-23.930S	069-59.880E	4113	RC 01	000 0.0	ROCK CORING STARTED
930729 0525+05	25-23.910S	069-59.920E	4106	RC 01	000 0.0	ROCK CORER LANDED
930729 0624+05	25-23.940S	069-59.930E	4116	RC 01	000 0.0	ROCK CORING ENDED
930729 0651+05	25-22.790S	069-58.860E	3857	DR 01	000 0.0	DREDGE START DOWN
930729 0803+05	25-22.870S	069-58.840E	3886	DR 01	000 0.0	DREDGE ON BOTTOM
930729 0857+05	25-22.030S	069-59.480E	4413	DR 01	000 0.0	DREDGE OFF BOTTOM
930729 1000+05	25-21.860S	069-59.850E	3923	DR 01	000 0.0	DREDGE ON DECK
930729 1008+05	25-21.790S	069-59.740E	4033	DR 01	000 0.0	SLOW AHEAD ENG
930729 1028+05	25-22.690S	069-58.100E	4195	OBS13	000 0.0	LAUNCH OF SEISMOMETER
930729 1106+05	25-24.830S	069-54.250E	2841	OBS 9	000 0.0	LAUNCH OF SEISMOMETER
930729 1212+05	25-28.990S	069-47.280E	2543	OBS 5	000 0.0	LAUNCH OF SEISMOMETER
930729 1314+05	25-33.400S	069-39.660E	2767	OBS 2	000 0.0	RUNG UP ENGINES
930729 1425+05	25-43.920S	069-35.070E	4538	OBS 1	000 0.0	LAUNCH OF SEISMOMETER
930729 1520+05	25-40.380S	069-43.150E	5061	OBS 3	000 0.0	LAUNCH OF SEISMOMETER
930729 1622+05	25-36.870S	069-53.490E	3975	OBS 6	000 0.0	LAUNCH OF SEISMOMETER
930729 1704+05	25-34.030S	069-59.990E	3404	OBS10	274 1.0	LAUNCH OF SEISMOMETER
930729 1737+05	25-33.040S	070-03.490E	4200	CTD 3	000 0.0	CTD-RMS START
930729 1857+05	25-32.690S	070-03.490E	4132	CTD 3	000 0.0	CTD-RMS DEEPEST
930729 2025+05	25-32.180S	070-03.500E	4166	CTD 3	000 0.0	CTD-RMS FINISH
930729 2046+05	25-33.130S	070-03.390E	4222	DR 02	000 0.0	DREDGE START DOWN
930729 2155+05	25-33.190S	070-03.510E	4194	DR 02	000 0.0	DREDGE ON BOTTOM
930729 2244+05	25-33.580S	070-03.350E	4172	DR 02	000 0.0	DREDGE OFF BOTTOM
930729 2340+05	25-33.350S	070-03.500E	4164	DR 02	000 0.0	DREDGE ON DECK
930730 0049+05	25-32.040S	070-05.510E	3043	OBS14	000 0.0	LAUNCH OF SEISMOMETER
930730 0147+05	25-29.210S	070-12.820E	2289	OBS17	000 0.0	LAUNCH OF SEISMOMETER
930730 0301+05	25-38.940S	070-20.380E	2906	OBS18	307 1.2	LAUNCH OF SEISMOMETER
930730 0414+05	25-42.340S	070-14.050E	2876	OBS15	000 0.0	LAUNCH OF SEISMOMETER
930730 0458+05	25-45.400S	070-10.280E	3609	RC 2	000 0.0	ROCK CORING STARTED
930730 0552+05	25-45.420S	070-10.330E	3602	RC 2	000 0.0	ROCK CORER LANDED
930730 0600+05	25-45.440S	070-10.360E	3590	RC 2	000 0.0	ROCK CORER LANDED
930730 0657+05	25-45.440S	070-10.370E	3596	RC 2	000 0.0	ROCK CORING ENDED
930730 0720+05	25-44.890S	070-09.420E	3658	OBS11	000 0.0	LAUNCH OF SEISMOMETER
930730 0810+05	25-48.650S	070-02.540E	3115	OBS 8	035 1.8	LAUNCH OF SEISMOMETER
930730 0847+05	25-44.140S	069-59.080E	2926	OBS 7	150 1.3	LAUNCH OF SEISMOMETER
930730 2234+05	25-47.040S	070-11.850E	3612	CTD 4	000 0.0	CTD-RMS START
930730 2358+05	25-46.910S	070-11.810E	3618	CTD 4	000 0.0	CTD-RMS DEEPEST
930731 0124+05	25-47.140S	070-12.030E	3606	CTD 4	000 0.0	CTD-RMS FINISH
930731 0138+05	25-47.400S	070-12.360E	3513	RC 3	000 0.0	ROCK CORING STARTED
930731 0240+05	25-47.370S	070-12.380E	3530	RC 3	000 0.0	ROCK CORER LANDED

Y.M.D. GMT+T	LAT.	LONG.	DEPTH	ST.NO	CURRENT	COMENT
930731 0332+05	25-47.590S	070-12.780E	3591	RC 3	000 0.0	ROCK CORING ENDED
930731 0406+05	25-50.550S	070-13.810E	3844	OBS12	286 0.9	LAUNCH OF SEISMOMETER
930731 0516+05	25-53.780S	070-11.720E	2995	MCS	000 0.0	LAUNCH OF STREAMER CABLE
930731 0535+05	25-54.710S	070-11.060E	3093	MCS	000 0.0	AIR-GUN STARTED
930731 0601+05	25-55.200S	070-09.260E	2974	MCS	000 0.0	PROTON SURVEY START
930731 0652+05	25-53.160S	070-05.850E	3056	MCS	000 0.0	START OF SEISMIC SURVEY
930731 0653+05	25-53.040S	070-05.740E	3044	MCS	000 0.0	STARTED V4 LINE SURVEY
930731 0713+05	25-51.720S	070-04.630E	3016	MCS	286 0.7	PICKED UP ONE AIRGUN FOR REPAIR
930731 1309+05	25-26.740S	069-46.020E	2724	MCS	000 0.0	SUNSET & PUT ON REGULATION LIGHTS
930731 1410+05	25-22.670S	069-42.870E	3392	MCS	000 0.0	CLEARED OUT OF LINE V4
930731 1427+05	25-21.510S	069-41.930E	3187	MCS	258 0.7	COM'CED ALTERING COURSE
930731 1543+05	25-27.600S	069-36.780E	3702	MCS	237 0.1	s/co on 156fl
930731 2233+05	25-59.540S	069-52.780E	3174	MCS	000 0.0	END OF MCC LINE V5
930731 2235+05	25-59.670S	069-52.840E	3200	MCS	000 0.0	COM'CED ALTER COURSE
930731 2359+05	26-00.310S	069-44.940E	3224	MCS	068 0.6	COM'CED ALTERING COURSE
930801 0027+05	25-58.290S	069-44.750E	3175	MCS	000 0.0	a/co to 059fl
930801 0031+05	25-58.090S	069-45.090E	3080	MCS	000 0.0	ENTERED IN LINE H1
930801 0826+05	25-36.020S	070-25.830E	2895	MCS	335 0.2	END OF MCS LINE H1
930801 1037+05	25-27.440S	070-16.860E	3070	MCS	153 0.5	ENTERED ON LINE H2 s/co on 246fl
930801 1912+05	25-44.600S	069-33.310E	4240	MCS	005 0.9	END OF MCS LINE H2
930801 2028+05	25-38.010S	069-31.900E	2766	MCS	005 0.4	ENTERED OF MCS LINE H3
930802 0202+05	25-22.740S	069-57.880E	4220	MCS	000 0.0	SUNRISE & PUT OFF REGULAION LIGHTS
930802 0447+05	25-15.610S	070-10.300E	3306	MCS	000 0.0	FINISHED SURVEY ON LINE H3
930802 0504+05	25-14.080S	070-10.420E	3745	MCS	280 1.7	s/co to 300fl
930802 0600+05	25-11.290S	070-03.670E	3652	MCS	311 0.8	USED COURSE VARIOUSLY
930802 0636+05	25-12.960S	070-00.540E	3008	MCS	000 0.0	s/co to 145fl &STARTED SURVEY ON LINE V
930802 1318+05	25-40.710S	070-21.550E	2934	MCS	132 0.4	PICKED UP ONE OF AIR-GUN
930802 1409+05	25-44.020S	070-24.310E	2894	MCS	000 0.0	CLEARED OUT LINE V1
930802 1420+05	25-44.850S	070-24.950E	2755	MCS	272 0.0	COM'CED ALTERING COURSE
930802 1528+05	25-47.960S	070-18.580E	2793	MCS	360 1.0	s/co on 324fl & STARTED SURVEY ON LINE
930802 2301+05	25-15.870S	069-52.890E	3776	MCS	239 0.3	END OF MCS LINE V2
930802 2348+05	25-17.990S	069-49.610E	2775	MCS	000 0.0	s/co on 146fl
930803 0001+05	25-18.950S	069-49.970E	3278	MCS	000 0.0	ENTERED IN LINE V3
930803 0201+05	25-27.470S	069-56.340E	3024	MCS	110 0.2	SUNRISE & PUT OFF REGULAION LIGHTS
930803 0930+05	25-58.440S	070-19.560E	3430	MCS	355 0.2	END OF SEISMIC SURVEY
930803 1454+05	25-20.070S	069-57.690E	5787	CTD 5	000 0.0	CTD-RMS START
930803 1614+05	25-19.750S	069-57.830E	4268	CTD 5	000 0.0	CTD-RMS DEEPEST
930803 1738+05	25-19.320S	069-57.760E	4229	CTD 5	000 0.0	CTD-RMS FINISH
930803 1800+05	25-19.830S	069-56.810E	3950	RC 4	000 0.0	ROCK CORING STARTED
930803 1857+05	25-19.880S	069-56.790E	4036	RC 4	000 0.0	ROCK CORER LANDED
930803 1905+05	25-19.880S	069-56.810E	3962	RC 4	000 0.0	ROCK CORER RELANDED
930803 2020+05	25-19.740S	069-56.480E	4037	RC 4	000 0.0	ROCK CORING ENDED
930803 2122+05	25-17.400S	069-55.030E	3906	RC-5	000 0.0	ROCK CORING STARTED
930803 2311+05	25-17.410S	069-55.050E	3877	RC-5	000 0.0	ROCK CORER LANDED
930804 0017+05	25-17.440S	069-55.030E	3901	RC-5	000 0.0	ROCK CORING ENDED
930804 0057+05	25-13.750S	069-55.060E	5787	DR 3	000 0.0	DREDGE START DOWN
930804 0156+05	25-13.940S	069-54.950E	4070	DR 3	000 0.0	DREDGE ON BOTTOM
930804 0256+05	25-14.110S	069-54.500E	5357	DR 3	000 0.0	DREDGE OFF BOTTOM
930804 0352+05	25-14.180S	069-54.780E	4022	DR 3	000 0.0	DREDGE ON DECK
930804 0446+05	25-19.960S	069-57.970E	4252	CTD 6	321 1.8	CTD-RMS START
930804 0614+05	25-19.850S	069-58.100E	4218	CTD 6	000 0.0	CTD-RMS DEEPEST
930804 0820+05	25-19.910S	069-57.690E	3838	CTD 6	000 0.0	CTD-RMS FINISH
930804 0933+05	25-27.200S	070-01.570E	3903	RC-6	000 0.0	ROCK CORING STARTED
930804 1051+05	25-27.240S	070-01.710E	3891	RC-6	000 0.0	ROCK CORER LANDED
930804 1057+05	25-27.290S	070-01.750E	4083	RC-6	000 0.0	ROCK CORER LANDED
930804 1158+05	25-27.410S	070-02.340E	3981	RC-6	000 0.0	ROCK CORING ENDED
930804 1230+05	25-27.490S	069-59.500E	4175	DR 4	000 0.0	DREDGE START DOWN
930804 1328+05	25-27.340S	069-59.650E	4174	DR 4	000 0.0	DREDGE ON BOTTOM
930804 1417+05	25-27.820S	069-59.880E	4168	DR 4	000 0.0	DREDGE OFF BOTTOM
930804 1515+05	25-27.700S	070-00.010E	4171	DR 4	000 0.0	DREDGE ON DECK
930804 1534+05	25-28.720S	069-59.930E	4311	DR 5	000 0.0	DREDGE START DOWN
930804 1632+05	25-28.770S	070-00.000E	4222	DR 5	000 0.0	DREDGE ON BOTTOM
930804 1718+05	25-29.330S	070-00.170E	4195	DR 5	000 0.0	DREDGE OFF BOTTOM
930804 1819+05	25-28.890S	070-00.450E	4112	DR 5	000 0.0	DREDGE ON DECK
930804 1847+05	25-26.920S	070-00.830E	4059	CTD 7	000 0.0	CTD-RMS START
930804 2006+05	25-26.860S	070-01.220E	4115	CTD 7	000 0.0	CTD-RMS DEEPEST
930804 2011+05	25-26.860S	070-01.230E	4111	CTD 7	000 0.0	CTD-RMS DEEPEST

Y.M.D. GMT+T	LAT.	LONG.	DEPTH	ST.NO	CURRENT	COMENT
930804 2131+05	25-26.600S	070-01.380E	3951	CTD 7	000 0.0	CTD-RMS FINISH
930804 2307+05	25-41.250S	070-06.300E	3714	RC 7	000 0.0	ROCK CORING STARTED
930805 0029+05	25-41.860S	070-06.380E	4315	RC 7	000 0.0	ROCK CORER LANDED
930805 0039+05	25-41.900S	070-06.360E	3874	RC 7	000 0.0	ROCK CORER LANDED
930805 0129+05	25-41.800S	070-06.400E	3645	RC 7	000 0.0	ROCK CORING ENDED
930805 0154+05	25-40.870S	070-05.040E	3788	CTD 8	000 0.0	CTD-RMS START
930805 0310+05	25-40.930S	070-05.260E	3773	CTD 8	000 0.0	CTD-RMS DEEPEST
930805 0423+05	25-40.850S	070-05.110E	3728	CTD 8	000 0.0	CTD-RMS EINISH
930805 0504+05	25-43.180S	070-08.390E	3592	RC 8	000 0.0	ROCK CORING STARTED
930805 0556+05	25-43.180S	070-08.410E	3888	RC 8	000 0.0	ROCK CORER LANDED
930805 0646+05	25-42.890S	070-08.260E	3675	RC 8	000 0.0	ROCK CORING ENDED
930805 1040+05	25-48.620S	070-13.700E	3595	DR 6	000 0.0	DREDGE ON DECK
930806 0446+05	25-38.510S	070-04.000E	3785	DR 7	000 0.0	DREDGE START DOWN
930806 0528+05	25-38.500S	070-03.970E	3753	DR 7	000 0.0	DREDGE ON BOTTOM
930806 0559+05	25-38.870S	070-04.210E	3787	DR 7	000 0.0	DREDGE OFF BOTTOM
930806 0654+05	25-39.230S	070-04.560E	3833	DR 7	000 0.0	DREDGE ON DECK
930806 0730+05	25-38.160S	070-02.990E	3724	RC 9	000 0.0	ROCK CORING STARTED
930806 0829+05	25-38.230S	070-02.970E	3729	RC 9	000 0.0	ROCK CORER LANDED
930806 0834+05	25-38.240S	070-03.000E	3726	RC 9	000 0.0	ROCK CORER LANDED
930806 0927+05	25-38.500S	070-03.200E	3772	RC 9	000 0.0	ROCK CORING ENDED
930806 0959+05	25-36.590S	070-03.500E	3801	RC 10	000 0.0	ROCK CORING STARTED
930806 1056+05	25-36.550S	070-03.540E	3810	RC 10	000 0.0	ROCK CORER LANDED
930806 1148+05	25-36.800S	070-04.100E	3929	RC 10	000 0.0	ROCK CORING ENDED
930806 1232+05	25-33.350S	070-00.620E	3218	DR 8	150 0.9	DREDGE START DOWN
930806 1329+05	25-33.240S	070-00.620E	3222	DR 8	000 0.0	DREDGE ON BOTTOM
930806 1422+05	25-33.440S	069-59.970E	3174	DR 8	000 0.0	DREDGE OFF BOTTOM
930806 1505+05	25-33.690S	070-00.100E	3227	DR 8	000 0.0	DREDGE ON DECK
930806 1543+05	25-30.580S	070-01.600E	4068	DR 9	000 0.0	DREDGE START DOWN
930806 1645+05	25-30.560S	070-01.650E	4057	DR 9	000 0.0	DREDGE ON BOTTOM
930806 1719+05	25-29.920S	070-01.570E	4016	DR 9	000 0.0	DREDGE OFF BOTTOM
930806 1814+05	25-29.720S	070-02.220E	3895	DR 9	000 0.0	DREDGE ON DECK
930806 1934+05	25-20.120S	069-57.970E	4272	CTD 8	000 0.0	CTD-RMS START
930806 2101+05	25-19.970S	069-57.990E	4254	CTD 8	000 0.0	CTD-RMS DEEPEST B-1
930806 2148+05	25-19.520S	069-58.450E	3912	CTD 8	000 0.0	POINT S-1
930806 2211+05	25-19.340S	069-58.650E	3765	CTD 8	000 0.0	B-2
930806 2235+05	25-19.110S	069-58.910E	3548	CTD 8	000 0.0	S-2
930806 2257+05	25-18.830S	069-59.120E	3311	CTD 8	000 0.0	B-3
930806 2323+05	25-18.590S	069-59.320E	2963	CTD 8	000 0.0	S-3
930806 2346+05	25-18.420S	069-59.490E	3050	CTD 8	000 0.0	B-4
930807 0004+05	25-18.260S	069-59.650E	3037	CTD 8	000 0.0	S-4
930807 0023+05	25-18.100S	069-59.840E	3014	CTD 8	000 0.0	B-5
930807 0044+05	25-17.910S	070-00.010E	3067	CTD 8	000 0.0	S-5
930807 0110+05	25-17.730S	070-00.150E	3099	CTD 8	000 0.0	B-6
930807 0157+05	25-17.600S	070-00.410E	3012	CTD 8	000 0.0	SUNRISE & PUT OFF REGULAION LIGHTS
930807 0207+05	25-17.530S	070-00.410E	3006	CTD 8	000 0.0	CTD-RMS FINISH
930807 0413+05	25-40.740S	069-41.810E	5045	DR 10	352 1.2	DREDGE START DOWN
930807 0520+05	25-40.770S	069-42.040E	5054	DR 10	000 0.0	DREDGE OFF BOTTOM
930807 0712+05	25-39.260S	069-41.340E	3472	DR 10	000 0.0	DREDGE OFF BOTTOM
930807 0818+05	25-39.470S	069-41.240E	3676	DR 10	000 0.0	DREDGE ON DECK
930807 0924+05	25-44.990S	069-35.700E	3540	DR 11	000 0.0	DREDGE START DOWN
930807 1036+05	25-44.990S	069-35.790E	3397	DR 11	000 0.0	DREDGE ON BOTTOM
930807 1142+05	25-44.870S	069-35.600E	3809	DR 11	000 0.0	DREDGE OFF BOTTOM
930807 1235+05	25-44.830S	069-35.910E	3689	DR 11	000 0.0	DREDGE ON DECK
930807 1313+05	25-46.530S	069-38.910E	3737	DR 12	000 0.0	DREDGE START DOWN
930807 1409+05	25-46.540S	069-38.960E	3679	DR 12	000 0.0	DREDGE ON BOTTOM
930807 1437+05	25-46.980S	069-39.220E	3962	DR 12	000 0.0	DREDGE OFF BOTTOM
930807 1527+05	25-47.140S	069-39.840E	3983	DR 12	000 0.0	DREDGE ON DECK
930807 1602+05	25-48.250S	069-36.230E	3933	CTD10	029 1.2	CTD-RMS START
930807 1718+05	25-48.150S	069-36.310E	3924	CTD10	000 0.0	CTD-RMS DEEPEST
930807 1833+05	25-47.660S	069-36.220E	3970	CTD10	000 0.0	CTD-RMS FINISH
930807 2004+05	25-53.640S	069-22.160E	4011	DR 13	000 0.0	DREDGE START DOWN
930807 2109+05	25-53.670S	069-22.370E	3927	DR 13	000 0.0	DREDGE ON BOTTOM
930807 2135+05	25-54.040S	069-22.320E	3997	DR 13	000 0.0	DREDGE OFF BOTTOM
930807 2232+05	25-54.370S	069-22.350E	3982	DR 13	000 0.0	DREDGE ON DECK
930807 2351+05	25-54.160S	069-14.480E	3975	DR 14	000 0.0	DREDGE START DOWN
930808 0053+05	25-54.120S	069-14.810E	4029	DR 14	000 0.0	DREDGE ON BOTTOM
930808 0139+05	25-53.970S	069-13.990E	4011	DR 14	000 0.0	DREDGE OFF BOTTOM

Y.M.D. GMT+T	LAT.	LONG.	DEPTH	ST.NO	CURRENT	COMENT
930808 0234+05	25-53.630S	069-14.120E	3992	DR 14	000 0.0	DREDGE ON DECK
930808 1803+05	24-05.680S	065-04.780E	4428	PN-5	110 2.1	ORI NET START
930808 1807+05	24-05.670S	065-04.650E	4390	PN-5	106 1.5	ORI SIDE NET START
930808 1819+05	24-05.640S	065-04.280E	4350	PN-5	000 0.0	ORI NET DEEPEST
930808 1827+05	24-05.630S	065-04.070E	4440	PN-5	000 0.0	ORI SIDE NET FINISH
930808 1838+05	24-05.630S	065-03.740E	4332	PN-5	000 0.0	ORI NET FINISH
930809 1633+04	21-24.710S	059-10.720E	3654	PN 6	132 2.1	ORI NET START
930809 1636+04	21-24.800S	059-10.620E	3646	PN 6	135 1.6	ORI SIDE NET START
930809 1649+04	21-25.100S	059-10.220E	3412	PN 6	000 0.0	ORI NET DEEPEST
930809 1656+04	21-25.280S	059-09.960E	3349	PN 6	000 0.0	ORI SIDE NET FINISH
930809 1709+04	21-25.610S	059-09.530E	3447	PN 6	000 0.0	ORI NET FINISH
930814 1548+04	20-48.660S	058-00.640E	4033	058	078 0.5	XBT
930814 1932+04	21-13.280S	058-59.960E	3722	059	346 0.4	XBT
930814 2320+04	21-38.510S	060-00.000E	4431	X 060	194 0.2	XBT
930815 0315+04	22-03.360S	061-00.130E	3964	X 061	003 0.9	XBT
930815 0708+04	22-28.140S	062-00.010E	4016	X 062	290 0.6	XBT
930815 1059+04	22-52.780S	063-00.000E	3780	X-063	150 0.3	XBT
930815 1446+04	23-17.490S	064-00.050E	4137	X 064	346 0.7	XBT
930815 1827+05	23-41.980S	065-00.020E	4098	X 065	158 0.3	XBT
930815 2216+05	24-06.420S	066-00.000E	3925	X-066	254 0.3	XBT
930816 0217+05	24-32.600S	067-04.460E	3806	X 067	038 0.6	XBT
930816 0541+05	24-55.170S	068-00.030E	3343	X 068	112 0.4	XBT
930816 0922+05	25-19.400S	069-00.040E	3826	X-069	023 0.8	XBT
930816 1520+05	25-43.960S	069-34.830E	4516	OBS 1	000 0.0	RELEASE FOR OBS
930816 1550+05	25-43.800S	069-34.690E	4459	NOR 1	000 0.0	NORPAC-NET START
930816 1641+05	25-43.410S	069-34.690E	4354	OBS 1	000 0.0	POPPING UP OF OBS
930816 1642+05	25-43.410S	069-34.700E	4346	NOR 1	000 0.0	NORPAC-NET FINISH
930816 1728+05	25-43.920S	069-34.120E	4334	OBS 1	000 0.0	FINISH TO RETREIVE OF OBS
930816 1835+05	25-33.170S	069-39.860E	2690	OBS 2	171 0.6	RELEASE FOR OBS
930816 1838+05	25-33.110S	069-39.910E	2677	PN 7	000 0.0	ORI NET START
930816 1840+05	25-33.010S	069-39.950E	2628	PN 7	000 0.0	ORI SIDE NET START
930816 1849+05	25-32.650S	069-40.200E	2587	O 01	000 0.0	OMEGA-ZONDE RELEASED
930816 1854+05	25-32.410S	069-40.290E	2545	PN 7	000 0.0	ORI NET DEEPEST
930816 1900+05	25-32.180S	069-40.420E	2554	PN 7	000 0.0	ORI SIDE NET FINISH
930816 1909+05	25-31.840S	069-40.570E	2641	PN 7	000 0.0	ORI NET FINISH
930816 1950+05	25-33.100S	069-39.800E	2704	OBS 2	000 0.0	FINISH TO RETREIVE OF OBS
930816 2104+05	25-28.680S	069-47.470E	2708	OBS 5	000 0.0	RELEASE FOR OBS
930816 2208+05	25-28.820S	069-47.250E	2552	OBS 5	000 0.0	POPPING UP OF OBS
930816 2220+05	25-28.790S	069-47.110E	2614	OBS 5	000 0.0	FINISH TO RETREIVE OF OBS
930817 0035+05	25-20.540S	069-59.680E	3488	O-02	000 0.0	OMEGA-ZONDE RELEASED
930817 0103+05	25-20.530S	069-59.560E	3652	CTD11	000 0.0	CTD-RMS POSITION CHECK B-1
930817 0135+05	25-20.230S	069-59.180E	3820	CTD11	000 0.0	CTD-RMS POSITION CHECK S-1
930817 0155+05	25-20.090S	069-58.920E	3903	CTD11	000 0.0	CTD-RMS POSITION CHECK B-2
930817 0213+05	25-19.870S	069-58.820E	3913	CTD11	000 0.0	CTD-RMS POSITION CHECK S-2
930817 0230+05	25-19.650S	069-58.650E	3902	CTD11	000 0.0	CTD-RMS POSITION CHECK B-3
930817 0251+05	25-19.370S	069-58.450E	3846	CTD11	000 0.0	CTD-RMS POSITION CHECK S-3
930817 0310+05	25-19.140S	069-58.220E	3878	CTD11	000 0.0	CTD-RMS POSITION CHECK B-4
930817 0324+05	25-19.070S	069-58.040E	3921	CTD11	000 0.0	CTD-RMS POSITION CHECK S-4
930817 0328+05	25-19.010S	069-58.060E	3920	0 03	000 0.0	OMEGA-ZONDE RELEASED
930817 0329+05	25-19.000S	069-58.060E	3932	O 03	000 0.0	OMEGA-ZONDE RELEASED
930817 0504+05	25-18.200S	069-57.250E	3992	CTD11	000 0.0	CTD-RMS POSITION CHECK B-6
930817 0601+05	25-17.870S	069-57.490E	3922	CTD11	000 0.0	CTD-RMS FINISH
930817 0610+05	25-17.990S	069-57.670E	3892	O 04	000 0.0	OMEGA-ZONDE RELEASED
930817 0716+05	25-24.770S	069-54.250E	2830	OBS 9	000 0.0	RELEASE FOR OBS
930817 0722+05	25-24.840S	069-54.140E	2813	PN 8	000 0.0	ORI NET START
930817 0727+05	25-24.980S	069-54.130E	2775	PN 8	000 0.0	ORI SIDE NET START
930817 0736+05	25-25.180S	069-54.010E	2782	PN 8	000 0.0	ORI NET DEEPEST
930817 0743+05	25-25.350S	069-53.960E	2750	PN 8	000 0.0	ORI SIDE NET FINISH
930817 0749+05	25-25.540S	069-53.910E	2720	PN 8	000 0.0	ORI NET FINISH
930817 0832+05	25-24.840S	069-54.290E	2840	OBS 9	000 0.0	POPPING UP OF OBS
930817 0842+05	25-24.730S	069-54.140E	2902	OBS 9	000 0.0	FINISH TO RETREIVE OF OBS
930817 0855+05	25-23.950S	069-54.640E	2955	O-06	000 0.0	OMEGA-ZONDE RELEASED
930817 1006+05	25-20.140S	069-57.950E	4260	DMS 1	000 0.0	DESMOS START DOWN
930817 1142+05	25-19.990S	069-58.000E	4256	DMS 1	000 0.0	DESMOS NEAR BOTTOM
930817 1203+05	25-19.850S	069-58.180E	4164	O-07	000 0.0	OMEGA-ZONDE RELEASED
930817 1445+05	25-18.020S	069-59.900E	3016	DMS 1	000 0.0	DESMOS LEAVE BOTTOM
930817 1541+05	25-17.560S	069-59.970E	3209	DMS 1	000 0.0	DESMOS ON DECK

Y.M.D. GMT+T	LAT.	LONG.	DEPTH	ST.NO	CURRENT	COMENT
930817 1628+05	25-17.380S	069-55.050E	3910	CTD12	000 0.0	CTD-RMS START
930817 1746+05	25-17.340S	069-54.950E	3925	CTD12	000 0.0	CTD-RMS DEEPEST
930817 1859+05	25-17.400S	069-54.730E	4015	CTD12	000 0.0	CTD-RMS FINISH
930817 2003+05	25-18.690S	070-05.070E	2942	NOR 2	000 0.0	NORPAC-NET START
930817 2005+05	25-18.670S	070-05.110E	2962	OBS16	000 0.0	RELEASE FOR OBS
930817 2053+05	25-17.740S	070-05.160E	2939	NOR 2	000 0.0	NORPAC-NET FINISH
930817 2117+05	25-18.870S	070-04.990E	2924	OBS16	000 0.0	POPPING UP OF OBS
930817 2137+05	25-18.480S	070-04.810E	3004	OBS16	000 0.0	RELEASE FOR OBS
930817 2241+05	25-24.350S	070-00.050E	4140	DSM 2	000 0.0	DESMOS START DOWN
930818 0008+05	25-24.300S	070-00.070E	4151	DSM02	000 0.0	DESMOS NEAR BOTTOM
930818 0345+05	25-22.160S	069-58.760E	3967	DSM02	000 0.0	DESMOS LEAVE BOTTOM
930818 0400+05	25-22.050S	069-58.760E	4012	O 08	000 0.0	OMEGA-ZONDE RELEASED
930818 0455+05	25-21.660S	069-58.810E	4172	DSM02	000 0.0	DESMOS ON DECK
930818 0532+05	25-23.950S	070-01.870E	3776	CTD13	315 1.1	CTD-RMS START
930818 0648+05	25-24.080S	070-01.880E	3725	CTD13	000 0.0	CTD DEEPEST
930818 0759+05	25-23.980S	070-01.910E	3763	CTD13	000 0.0	CTD-RMS FINISH
930818 0901+05	25-22.550S	069-58.040E	4177	OBS13	000 0.0	RELEASE FOR OBS
930818 1029+05	25-22.650S	069-58.070E	4213	OBS13	000 0.0	POPPING UP OF OBS
930818 1104+05	25-22.270S	069-57.910E	4102	OBS13	000 0.0	FINISH TO RETREIVE OF OBS
930818 1146+05	25-18.970S	069-55.860E	4097	CTD14	000 0.0	CTD-RMS START
930818 1313+05	25-19.010S	069-56.030E	4074	CTD14	000 0.0	CTD-RMS DEEPEST
930818 1400+05	25-18.970S	069-55.960E	4076	O-10	000 0.0	OMEGA-ZONDE RELEASED
930818 1437+05	25-18.680S	069-55.870E	4083	CTD14	000 0.0	CTD-RMS FINISH
930818 1610+05	25-29.240S	070-12.760E	2297	NOR 3	295 2.1	NORPAC-NET START
930818 1612+05	25-29.220S	070-12.740E	2294	OBS17	000 0.0	RELEASE FOR OBS
930818 1650+05	25-28.980S	070-12.360E	2409	NOR 3	000 0.0	NORPAC-NET FINISH
930818 1722+05	25-29.250S	070-12.560E	2390	OBS17	000 0.0	FINISH TO RETREIVE OF OBS
930818 2118+05	25-31.700S	070-03.650E	4100	OBS14	300 0.5	NO RESPONSE FROM OBS & IT DID NOT PO
930818 2153+05	25-31.160S	070-00.800E	4044	DR 15	000 0.0	DREDGE START DOWN
930818 2259+05	25-31.180S	070-00.740E	4040	DR 15	000 0.0	DREDGE ON BOTTOM
930818 2331+05	25-31.150S	070-00.390E	4099	DR 15	000 0.0	DREDGE OFF BOTTOM
930819 0029+05	25-31.280S	069-59.560E	3918	DR 15	000 0.0	DREDGE ON DECK
930819 0110+05	25-33.870S	069-59.430E	3448	DR 16	000 0.0	DREDGE START DOWN
930819 0200+05	25-34.000S	069-59.360E	3410	DR 16	000 0.0	DREDGE ON BOTTOM
930819 0226+05	25-34.270S	069-59.060E	3490	DR 16	000 0.0	DREDGE OFF BOTTOM
930819 0243+05	25-34.230S	069-58.850E	3485	OBS10	000 0.0	RELEASE FOR OBS
930819 0300+05	25-34.090S	069-59.170E	3449	O-11	000 0.0	OMEGA-ZONDE RELEASED
930819 0314+05	25-33.850S	069-59.140E	3457	DR 16	000 0.0	DREDGE ON DECK
930819 0337+05	25-33.850S	069-59.910E	3361	X 070	000 0.0	XBT
930819 0402+05	25-33.980S	069-59.960E	3395	OBS10	000 0.0	POPPING UP OF OBS
930819 0430+05	25-33.910S	069-59.340E	3405	OBS10	000 0.0	FINISH TO RETREIVE OF OBS
930819 0452+05	25-34.990S	070-00.400E	3429	BK 1	000 0.0	LAUNCH OF BAITE TRAP
930819 0455+05	25-35.030S	070-00.320E	3385	BK 1	000 0.0	FINISH TO LAUNCH OF BAITE TRAP
930819 0541+05	25-36.020S	069-55.260E	3780	DR 17	106 0.3	DREDGE START DOWN
930819 0649+05	25-35.930S	069-55.140E	3775	DR 17	000 0.0	DREDGE ON BOTTOM
930819 0717+05	25-36.250S	069-54.720E	3869	DR 17	000 0.0	DREDGE OFF BOTTOM
930819 0742+05	25-36.170S	069-54.530E	3912	OBS 6	000 0.0	RELEASE FOR OBS
930819 0809+05	25-36.230S	069-54.250E	3953	DR 17	000 0.0	DREDGE ON DECK
930819 0900+05	25-36.980S	069-53.180E	3962	O-12	000 0.0	OMEGA-ZONDE RELEASED
930819 0933+05	25-36.810S	069-53.420E	3954	OBS 6	000 0.0	POPPING UP OF OBS
930819 0947+05	25-36.740S	069-53.310E	3855	OBS 6	000 0.0	FINISH TO RETREIVE OF OBS
930819 1101+05	25-41.920S	069-40.160E	4488	DR 18	000 0.0	DREDGE START DOWN
930819 1208+05	25-41.930S	069-40.260E	4454	DR 18	000 0.0	DREDGE ON BOTTOM
930819 1258+05	25-42.450S	069-40.590E	4443	DR 18	000 0.0	DREDGE OFF BOTTOM
930819 1305+05	25-42.460S	069-40.680E	4443	O 13	000 0.0	OMEGA-ZONDE RELEASED
930819 1353+05	25-41.680S	069-41.260E	4720	OBS 3	000 0.0	RELEASE FOR OBS
930819 1414+05	25-41.460S	069-41.110E	4835	DR 18	000 0.0	DREDGE ON DECK
930819 1415+05	25-41.440S	069-41.110E	4844	PN 9	000 0.0	ORI NET START
930819 1418+05	25-41.400S	069-41.140E	4871	PN 9	000 0.0	ORI SIDE NET START
930819 1431+05	25-41.310S	069-41.340E	4975	PN 9	000 0.0	ORI NET DEEPEST
930819 1434+05	25-41.300S	069-41.340E	5019	PN 9	000 0.0	ORI SIDE NET FINISH
930819 1453+05	25-41.140S	069-41.620E	5030	PN 9	000 0.0	ORI NET FINISH
930819 1511+05	25-40.500S	069-42.890E	5058	OBS 3	000 0.0	POPPING UP OF OBS
930819 1527+05	25-40.530S	069-42.860E	5060	OBS 3	000 0.0	FINISH TO RETREIVE OF OBS
930819 1543+05	25-40.480S	069-42.930E	5056	DR 19	000 0.0	DREDGE START DOWN
930819 1653+05	25-40.430S	069-43.020E	5058	DR 19	000 0.0	DREDGE ON BOTTOM
930819 1749+05	25-40.130S	069-43.670E	5058	O 14	000 0.0	OMEGA-ZONDE RELEASED

Y.M.D. GMT+T	LAT.	LONG.	DEPTH	ST.NO	CURRENT	COMENT
930819 1803+05	25-40.060S	069-43.750E	5028	DR 19	000 0.0	DREDGE OFF BOTTOM
930819 1912+05	25-39.430S	069-43.270E	4457	DR 19	000 0.0	DREDGE ON DECK
930819 2043+05	25-55.180S	069-50.290E	3087	OBS 4	318 2.0	RELEASE FOR OBS
930819 2142+05	25-55.030S	069-50.070E	3122	OBS 4	000 0.0	POPPING UP OF OBS
930819 2153+05	25-55.130S	069-50.200E	3064	OBS 4	000 0.0	FINISH TO RETREIVE OF OBS
930819 2335+05	25-44.130S	069-59.440E	3003	OBS 7	000 0.0	RELEASE FOR OBS
930820 0115+05	25-44.180S	069-58.980E	2913	OBS 7	000 0.0	POPPING UP OF OBS
930820 0132+05	25-44.270S	069-58.540E	2814	OBS 7	000 0.0	FINISH TO RETREIVE OF OBS
930820 0225+05	25-48.840S	070-02.260E	3010	OBS 8	000 0.0	RELEASE FOR OBS
930820 0323+05	25-48.860S	070-01.340E	2964	O 15	000 0.0	OMEGA-ZONDE RELEASED
930820 0350+05	25-48.700S	070-02.480E	3083	O 15	000 0.0	OMEGA-ZONDE OBSERVATION ENDEI
930820 0350+05	25-48.690S	070-02.470E	3075	OBS 8	000 0.0	POPPING UP OF OBS
930820 0404+05	25-48.990S	070-02.120E	3062	OBS 8	000 0.0	FINISH TO RETREIVE OF OBS
930820 0510+05	25-44.680S	070-09.090E	3684	OBS11	000 0.0	RELEASE FOR OBS
930820 0641+05	25-44.910S	070-09.350E	3676	OBS11	000 0.0	POPPING UP OF OBS
930820 0653+05	25-44.820S	070-09.070E	3704	OBS11	000 0.0	FINISH TO RETREIVE OF OBS
930820 0749+05	25-42.120S	070-13.900E	2891	OBS15	000 0.0	RELEASE FOR OBS
930820 0754+05	25-42.140S	070-13.820E	2879	PN 10	000 0.0	ORI NET START
930820 0755+05	25-42.170S	070-13.810E	2874	PN 10	000 0.0	ORI SIDE NET START
930820 0808+05	25-42.510S	070-13.620E	2794	PN 10	000 0.0	ORI NET DEEPEST
930820 0816+05	25-42.730S	070-13.530E	2879	PN 10	000 0.0	ORI SIDE NET FINISH
930820 0827+05	25-43.020S	070-13.390E	3000	PN 10	000 0.0	ORI NET FINISH
930820 0907+05	25-42.150S	070-13.790E	2874	O-16	000 0.0	OMEGA-ZONDE RELEASED
930820 0910+05	25-42.110S	070-13.720E	2867	OBS15	000 0.0	POPPING UP OF OBS
930820 0925+05	25-42.200S	070-13.650E	2847	OBS15	000 0.0	FINISH TO RETREIVE OF OBS
930820 1020+05	25-38.880S	070-20.140E	2877	OBS18	000 0.0	RELEASE FOR OBS
930820 1130+05	25-38.820S	070-20.500E	2900	OBS18	000 0.0	POPPING UP OF OBS
930820 1223+05	25-38.130S	070-18.550E	2731	OBS18	000 0.0	FINISH TO RETREIVE OF OBS
930820 1328+05	25-48.030S	070-11.620E	3608	RC 11	000 0.0	ROCK CORING STARTED
930820 1330+05	25-48.050S	070-11.560E	3558	O 17	000 0.0	OMEGA-ZONDE RELEASED
930820 1424+05	25-47.860S	070-11.550E	3502	RC 11	000 0.0	ROCK CORER LANDED
930820 1513+05	25-47.180S	070-10.980E	3765	RC 11	000 0.0	ROCK CORING ENDED
930820 1555+05	25-50.650S	070-13.580E	3804	OBS12	000 0.0	RELEASE FOR OBS
930820 1601+05	25-50.670S	070-13.540E	3790	PN 11	000 0.0	ORI NET START
930820 1603+05	25-50.690S	070-13.570E	3788	PN 11	000 0.0	ORI SIDE NET START
930820 1616+05	25-50.740S	070-13.890E	3820	PN 11	000 0.0	ORI NET DEEPEST
930820 1622+05	25-50.700S	070-14.030E	3832	PN 11	000 0.0	ORI SIDE NET FINISH
930820 1635+05	25-50.750S	070-14.270E	3839	PN 11	000 0.0	ORI NET FINISH
930820 1659+05	25-50.500S	070-13.760E	3818	OBS12	000 0.0	POPPING UP OF OBS
930820 1707+05	25-50.480S	070-13.510E	3794	OBS12	000 0.0	FINISH TO RETREIVE OF OBS
930820 1735+05	25-51.130S	070-14.390E	3726	RC 12	000 0.0	ROCK CORING STARTED
930820 1825+05	25-51.080S	070-14.570E	3662	RC 12	000 0.0	ROCK CORER LANDED
930820 1915+05	25-51.480S	070-14.950E	3782	RC 12	000 0.0	ROCK CORING ENDED
930820 1954+05	25-53.350S	070-17.520E	3710	DR 20	000 0.0	DREDGE START DOWN
930820 2048+05	25-53.400S	070-17.600E	3671	DR 20	000 0.0	DREDGE ON BOTTOM
930820 2108+05	25-53.600S	070-17.830E	3750	DR 20	000 0.0	DREDGE OFF BOTTOM
930820 2202+05	25-54.040S	070-17.480E	3712	DR 20	000 0.0	DREDGE ON DECK
930820 2217+05	25-54.240S	070-17.550E	3669	RC 13	000 0.0	ROCK CORING STARTED
930820 2309+05	25-54.260S	070-17.600E	3680	RC 13	000 0.0	ROCK CORER LANDED
930820 2359+05	25-54.590S	070-16.170E	3674	RC 13	000 0.0	ROCK CORING ENDED
930821 0048+05	25-56.810S	070-19.860E	3718	RC 14	000 0.0	ROCK CORING STARTED
930821 0148+05	25-57.100S	070-20.050E	3634	RC 14	000 0.0	ROCK CORER LANDED
930821 0238+05	25-56.270S	070-19.710E	3855	RC 14	000 0.0	ROCK CORING ENDED
930821 0305+05	25-59.020S	070-21.830E	3850	O 18	252 0.6	OMEGA-ZONDE RELEASED
930821 0328+05	26-01.580S	070-23.630E	3738	DR 21	000 0.0	DREDGE START DOWN
930821 0420+05	26-01.560S	070-23.800E	3712	DR 21	000 0.0	DREDGE ON BOTTOM
930821 0452+05	26-01.820S	070-24.010E	3778	DR 21	000 0.0	DREDGE OFF BOTTOM
930821 0541+05	26-02.900S	070-23.900E	3811	DR 21	000 0.0	DREDGE ON DECK
930821 0620+05	26-07.410S	070-24.450E	3864	DR 22	320 1.3	DREDGE START DOWN
930821 0713+05	26-07.520S	070-24.580E	3833	DR 22	000 0.0	DREDGE ON BOTTOM
930821 0742+05	26-07.820S	070-24.780E	3870	DR 22	000 0.0	DREDGE OFF BOTTOM
930821 0835+05	26-08.020S	070-24.570E	3909	DR 22	000 0.0	DREDGE ON DECK
930821 0856+05	26-07.600S	070-25.100E	3894	O-19	000 0.0	OMEGA-ZONDE RELEASED
930821 1327+05	26-06.780S	070-35.580E	3520	O 20	265 0.4	OMEGA-ZONDE RELEASED
930822 0304+05	26-12.360S	070-54.850E	3972	O 21	175 0.3	OMEGA-ZONDE RELEASED
930822 0722+05	26-13.310S	071-00.040E	3301	X-071	138 0.3	XBT
930822 0857+05	26-06.380S	071-10.520E	3515	O-22	036 0.3	OMEGA-ZONDE RELEASED

Y.M.D. GMT+T	LAT.	LONG.	DEPTH	ST.NO	CURRENT	COMENT
930822 1145+05	26-02.150S	071-18.630E	3785	DR 23	000 0.0	DREDGE START DOWN
930822 1241+05	26-02.000S	071-18.650E	3727	DR 23	000 0.0	DREDGE ON BOTTOM
930822 1252+05	26-02.140S	071-18.760E	3869	DR 23	000 0.0	DREDGE OFF BOTTOM
930822 1315+05	26-02.280S	071-19.200E	3787	O 23	000 0.0	OMEGA-ZONDE RELEASED
930822 1344+05	26-01.990S	071-19.310E	3849	DR 23	000 0.0	DREDGE ON DECK
930822 1623+05	26-07.110S	070-48.150E	4218	DR 24	000 0.0	DREDGE START DOWN
930822 1721+05	26-07.300S	070-48.420E	4132	DR 24	000 0.0	DREDGE ON BOTTOM
930822 1733+05	26-07.050S	070-48.370E	4200	DR 24	000 0.0	DREDGE OFF BOTTOM
930822 1827+05	26-06.840S	070-47.430E	4239	DR 24	000 0.0	CHANGED PROPULSION TO DIESEL ENGIN
930822 1827+05	26-06.840S	070-47.410E	4232	DR 24	000 0.0	DREDGE ON DECK
930822 2202+05	25-48.490S	070-11.360E	3740	DSM 3	000 0.0	DESMOS START DOWN
930822 2314+05	25-48.060S	070-11.140E	3724	DSM 3	000 0.0	DESMOS NEAR BOTTOM
930823 0135+05	25-47.310S	070-12.880E	3591	DSM 3	000 0.0	DESMOS LEAVE BOTTOM
930823 0237+05	25-47.090S	070-12.140E	3602	DSM 3	000 0.0	DESMOS ON DECK
930823 0301+05	25-44.520S	070-12.560E	3300	O 24	296 2.0	OMEGA-ZONDE RELEASED
930823 0358+05	25-34.590S	070-03.120E	4209	DR 25	115 0.9	DREDGE START DOWN
930823 0455+05	25-34.730S	070-03.380E	4262	DR 25	000 0.0	DREDGE ON BOTTOM
930823 0531+05	25-35.090S	070-03.660E	4280	DR 25	000 0.0	DREDGE OFF BOTTOM
930823 0629+05	25-35.160S	070-02.940E	4015	DR 25	000 0.0	DREDGE ON DECK
930823 0648+05	25-35.330S	070-00.690E	3402	DR 26	076 0.4	DREDGE START DOWN
930823 0726+05	25-35.360S	070-00.670E	3408	KAGO	000 0.0	RELEASE FOR KAGO NET
930823 0739+05	25-35.390S	070-00.620E	3399	DR 26	000 0.0	DREDGE ON BOTTOM
930823 0757+05	25-35.160S	070-00.920E	3494	DR 26	000 0.0	DREDGE OFF BOTTOM
930823 0822+05	25-34.810S	070-00.770E	3330	KAGO	000 0.0	POPPING UP OF KAGO NET
930823 0843+05	25-34.680S	070-00.370E	3407	DR 26	000 0.0	DREDGE ON DECK
930823 0900+05	25-34.760S	069-59.650E	3499	O-25	000 0.0	OMEGA-ZONDE RELEASED
930823 0912+05	25-34.750S	069-59.290E	3508	KAGO	000 0.0	FINISHED TO RETREIVE OF KAGO NET
930823 1006+05	25-28.790S	069-59.980E	4308	DR 27	000 0.0	DREDGE START DOWN
930823 1104+05	25-28.750S	069-59.950E	4306	DR 27	000 0.0	DREDGE ON BOTTOM
930823 1220+05	25-27.370S	069-59.700E	4173	DR 27	000 0.0	DREDGE OFF BOTTOM
930823 1323+05	25-25.580S	069-59.870E	4120	DR 27	000 0.0	DREDGE ON DECK
930823 1326+05	25-25.510S	069-59.840E	4097	O 26	000 0.0	OMEGA-ZONDE RELEASED
930823 1411+05	25-20.890S	070-01.960E	2926	CTD15	000 0.0	CTD-RMS START
930823 1508+05	25-20.870S	070-01.940E	2922	CTD15	000 0.0	CTD-RMS POSITION CHECK B1
930823 1523+05	25-20.690S	070-01.880E	2875	CTD15	000 0.0	CTD-RMS POSITION CHECK S1
930823 1538+05	25-20.450S	070-01.670E	2820	CTD15	000 0.0	CTD-RMS POSITION CHECK B2
930823 1550+05	25-20.360S	070-01.590E	2859	CTD15	000 0.0	CTD-RMS POSITION CHECK S2
930823 1603+05	25-20.230S	070-01.500E	2859	CTD15	000 0.0	CTD-RMS POSITION CHECK B3
930823 1615+05	25-20.040S	070-01.440E	2856	CTD15	000 0.0	CTD-RMS POSITION CHECK S3
930823 1631+05	25-19.810S	070-01.260E	2857	CTD15	000 0.0	CTD-RMS POSITION CHECK B4
930823 1643+05	25-19.660S	070-01.130E	2811	CTD15	000 0.0	CTD-RMS POSITION CHECK S4
930823 1657+05	25-19.410S	070-01.100E	2794	CTD15	000 0.0	CTD-RMS POSITION CHECK B5
930823 1709+05	25-19.220S	070-01.100E	2785	CTD15	000 0.0	CTD-RMS POSITION CHECK S5
930823 1723+05	25-19.000S	070-00.920E	2784	CTD15	000 0.0	CTD-RMS POSITION CHECK B6
930823 1734+05	25-18.890S	070-00.730E	2769	CTD15	000 0.0	CTD-RMS POSITION CHECK S6
930823 1753+05	25-18.520S	070-00.570E	2863	CTD15	000 0.0	CTD-RMS POSITION CHECK B7
930823 1807+05	25-18.280S	070-00.440E	2893	CTD15	000 0.0	CTD-RMS POSITION CHECK S7
930823 1822+05	25-18.040S	070-00.310E	3013	CTD15	000 0.0	CTD-RMS POSITION CHECK B8
930823 1835+05	25-17.890S	070-00.180E	3105	CTD15	000 0.0	CTD-RMS POSITION CHECK S8
930823 1847+05	25-17.670S	070-00.080E	3191	CTD15	000 0.0	CTD-RMS POSITION CHECK B9
930823 1932+05	25-17.520S	069-59.620E	3101	CTD15	000 0.0	CTD-RMS FINISH
930823 2119+05	25-19.530S	070-00.080E	3097	CTD16	000 0.0	CTD-RMS POSITION CHECK (D-1)
930823 2136+05	25-19.340S	070-00.330E	3049	CTD16	000 0.0	CTD-RMS POSITION CHECK (S-1)
930823 2148+05	25-19.250S	070-00.450E	2967	CTD16	000 0.0	CTD-RMS POSITION CHECK (D-2)
930823 2158+05	25-19.150S	070-00.540E	2930	CTD16	000 0.0	CTD-RMS POSITION CHECK S-2)
930823 2210+05	25-19.040S	070-00.700E	2782	CTD16	000 0.0	CTD-RMS POSITION CHECK (D-3)
930823 2221+05	25-18.960S	070-00.870E	2782	CTD16	000 0.0	CTD-RMS POSITION CHECK (S-3)
930823 2232+05	25-19.010S	070-01.010E	2753	CTD16	000 0.0	CTD-RMS POSITION CHECK (D-4)
930823 2242+05	25-19.030S	070-01.140E	2684	CTD16	000 0.0	CTD-RMS POSITION CHECK (S-4)
930823 2257+05	25-19.010S	070-01.390E	2639	CTD16	000 0.0	CTD-RMS POSITION CHECK (D-5)
930823 2307+05	25-19.020S	070-01.540E	2710	CTD16	000 0.0	CTD-RMS POSITION CHECK (S-5)
930823 2330+05	25-18.970S	070-01.460E	2670	CTD16	000 0.0	CTD-RMS POSITION CHECK B-6
930823 2347+05	25-18.750S	070-01.520E	2651	CTD16	000 0.0	CTD-RMS POSITION CHECK S-6
930823 2358+05	25-18.650S	070-01.650E	2536	CTD16	000 0.0	CTD-RMS POSITION CHECK B-7
930824 0043+05	25-18.640S	070-01.560E	2590	CTD16	000 0.0	CTD-RMS FINISH
930824 0108+05	25-19.230S	070-00.510E	2961	DSM 3	000 0.0	DESMOS START DOWN
930824 0202+05	25-19.140S	070-00.610E	2895	DSM 4	000 0.0	DESMOS NEAR BOTTOM

Y.M.D. GMT+T	LAT.	LONG.	DEPTH	ST.NO	CURRENT	COMENT
930824 0300+05	25-18.680S	070-01.110E	2644	O 27	000 0.0	OMEGA-ZONDE RELEASED
930824 0501+05	25-19.790S	070-00.660E	3096	DSM 4	000 0.0	DESMOS LEAVE BOTTOM
930824 0553+05	25-20.300S	070-00.040E	3242	DSM 4	000 0.0	DESMOS ON DECK
930824 0852+05	24-44.120S	070-00.010E	2367	O-28	072 0.3	OMEGA-ZONDE RELEASED
930824 1306+05	24-00.250S	069-39.630E	3341	CTD17	000 0.0	CTD-RMS START
930824 1314+05	24-00.260S	069-39.540E	3220	O 29	000 0.0	OMEGA-ZONDE RELEASED
930824 1410+05	24-00.190S	069-39.640E	3353	CTD17	000 0.0	CTD-RMS POSITION CHECK B-1
930824 1430+05	24-00.210S	069-39.310E	3144	CTD17	000 0.0	CTD-RMS POSITION CHECK S-1
930824 1454+05	24-00.230S	069-38.910E	2891	CTD17	000 0.0	CTD-RMS POSITION CHECK B-2
930824 1512+05	24-00.240S	069-38.580E	3061	CTD17	000 0.0	CTD-RMS POSITION CHECK S-2
930824 1531+05	24-00.220S	069-38.270E	3054	CTD17	000 0.0	CTD-RMS POSITION CHECK B3
930824 1545+05	24-00.220S	069-38.030E	3446	CTD17	000 0.0	CTD-RMS POSITION CHECK S3
930824 1607+05	24-00.220S	069-37.640E	3682	CTD17	000 0.0	CTD-RMS POSITION CHECK B4
930824 1623+05	24-00.180S	069-37.420E	3788	CTD17	000 0.0	CTD-RMS POSITION CHECK S4
930824 1649+05	24-00.160S	069-36.940E	4058	CTD17	000 0.0	CTD-RMS POSITION CHECK B5
930824 1805+05	24-00.130S	069-36.190E	3913	CTD17	000 0.0	CTD-RMS FINISH
930824 1859+05	24-00.370S	069-40.000E	3384	DMS 5	000 0.0	DESMOS START DOWN
930824 2013+05	24-00.450S	069-40.030E	3385	DMS 5	000 0.0	DESMOS NEAR BOTTOM
930825 0307+05	23-58.370S	069-39.000E	2925	O 30	000 0.0	OMEGA-ZONDE RELEASED
930825 0852+05	24-00.210S	069-38.860E	2871	O-31	000 0.0	OMEGA-ZONDE RELEASED
930825 1001+05	23-59.240S	069-38.730E	3082	DSM 5	000 0.0	DESMOS LEAVE BOTTOM
930825 1103+05	23-59.700S	069-39.270E	3169	KAGO	000 0.0	RELEASE FOR KAGO NET
930825 1133+05	23-59.650S	069-39.410E	3196	DSM 5	000 0.0	DESMOS ON DECK
930825 1242+05	24-00.280S	069-39.650E	3342	CTD18	000 0.0	CTD-RMS START
930825 1321+05	24-00.130S	069-39.770E	3422	O 32	000 0.0	OMEGA-ZONDE RELEASED
930825 1347+05	24-00.290S	069-39.900E	3397	CTD18	000 0.0	CTD-RMS DEEPEST
930825 1455+05	23-59.870S	069-40.210E	3139	CTD18	000 0.0	CTD-RMS FINISH
930826 0003+05	22-13.420S	071-12.210E	3920	O 33	321 0.3	OMEGA-ZONDE RELEASED
930826 0034+05	22-07.130S	071-17.750E	3880	O 33	303 0.7	OMEGA-ZONDE OBSERVATION ENDEI
930826 0442+05	21-19.150S	072-00.030E	3708	X 072	248 0.4	XBT
930826 0550+05	21-05.900S	072-11.630E	3826	O 34	249 0.3	OMEGA-ZONDE RELEASED
930826 1029+05	20-10.340S	073-00.070E	4566	X-073	316 0.7	XBT
930826 1148+05	19-54.050S	073-14.260E	4394	O 35	006 1.0	OMEGA-ZONDE RELEASED
930826 1606+05	19-01.400S	074-00.010E	4901	X 074	356 0.7	XBT
930826 1800+05	18-38.410S	074-19.890E	4841	O 36	300 0.6	OMEGA-ZONDE RELEASED
930826 2152+05	17-51.690S	075-00.010E	5439	X-075	323 0.9	XBT
930826 2358+05	17-26.790S	075-21.370E	4554	O 37	304 0.6	OMEGA-ZONDE RELEASED
930827 0339+05	16-42.190S	075-59.490E	5002	X 076	005 0.5	XBT
930827 0551+05	16-15.230S	076-22.670E	5015	O 38	355 0.7	OMEGA-ZONDE RELEASED
930827 0924+05	15-31.660S	077-00.030E	5031	X-077	288 0.7	XBT
930827 1202+05	14-59.500S	077-27.170E	5110	O-39	136 0.9	OMEGA-ZONDE RELEASED
930827 1514+05	14-20.010S	078-00.100E	5127	X 078	317 0.6	XBT
930827 1702+05	13-59.100S	078-17.860E	5087	PN 12	240 2.3	ORI NET START
930827 1706+05	13-59.170S	078-17.910E	5071	PN 12	244 1.9	ORI SIDE NET START
930827 1717+05	13-59.390S	078-18.110E	5043	PN 12	000 0.0	ORI NET DEEPEST
930827 1727+05	13-59.650S	078-18.250E	5033	PN 12	000 0.0	ORI SIDE NET FINISH
930827 1732+05	13-59.710S	078-18.340E	5035	PN 12	000 0.0	ORI NET FINISH
930827 1757+05	13-56.570S	078-21.400E	5128	O 40	344 0.7	OMEGA-ZONDE RELEASED
930827 2148+06	13-08.980S	079-00.010E	5301	X-079	340 0.4	XBT
930828 0001+06	12-41.780S	079-22.880E	5035	O 41	349 0.6	OMEGA-ZONDE RELEASED
930828 0339+06	11-57.340S	080-00.000E	5175	X 080	312 0.9	XBT
930828 0552+06	11-30.110S	080-22.720E	4985	O 42	304 0.9	OMEGA-ZONDE RELEASED
930828 1006+06	10-44.960S	081-00.210E	5058	X 081	306 1.3	XBT
930828 1154+06	10-22.720S	081-18.640E	5166	O 43	321 1.0	OMEGA-ZONDE RELEASED
930828 1559+06	09-34.180S	081-59.590E	5368	X 082	209 2.3	XBT
930828 1603+06	09-34.310S	081-59.630E	5364	PN 13	228 2.3	ORI NET START
930828 1606+06	09-34.340S	081-59.710E	5360	PN 13	000 0.0	ORI SIDE NET START
930828 1617+06	09-34.620S	081-59.840E	5357	PN 13	000 0.0	ORI NET DEEPEST
930828 1626+06	09-34.830S	082-00.030E	5353	PN 13	000 0.0	ORI SIDE NET FINISH
930828 1631+06	09-34.970S	082-00.140E	5352	PN 13	000 0.0	ORI NET FINISH
930828 1750+06	09-20.230S	082-12.040E	5080	O 44	319 0.8	OMEGA-ZONDE RELEASED
930828 2237+06	08-20.100S	083-00.020E	5028	X 083	336 0.6	XBT
930828 2359+06	08-02.850S	083-14.300E	5045	O 45	001 0.4	OMEGA-ZONDE RELEASED
930829 0422+06	07-07.590S	084-00.000E	4942	X 084	000 0.4	XBT
930829 0556+06	06-47.800S	084-16.310E	4880	O 46	343 0.4	OMEGA-ZONDE RELEASED
930829 1010+06	05-54.620S	085-00.000E	5046	X 085	314 0.3	XBT
930829 1149+06	05-33.920S	085-17.000E	5005	O 47	307 0.2	OMEGA-ZONDE RELEASED

Y.M.D.	GMT+T	LAT.	LONG.	DEPTH	ST.NO	CURRENT	COMENT
930829	1545+06	04-45.240S	086-00.030E	4959	X 086	048 0.5	XBT
930829	1602+06	04-43.430S	086-02.200E	4963	PN 14	220 1.9	ORI NET START
930829	1605+06	04-43.540S	086-02.180E	4963	PN 14	000 0.0	ORI SIDE NET START
930829	1617+06	04-43.920S	086-02.120E	4962	PN 14	000 0.0	ORI NET DEEPEST
930829	1626+06	04-44.180S	086-02.120E	4964	PN 14	000 0.0	ORI SIDE NET FINISH
930829	1631+06	04-44.370S	086-02.130E	4966	PN 14	000 0.0	ORI NET FINISH
930829	1742+06	04-31.360S	086-13.770E	4937	O 48	040 0.3	OMEGA-ZONDE RELEASED
930829	2151+06	03-38.480S	087-00.020E	4873	X-087	008 1.0	XBT
930829	2355+07	03-12.200S	087-23.680E	4847	O 49	000 1.2	OMEGA-ZONDE RELEASED
930830	0307+07	02-31.840S	088-00.040E	4819	X 088	351 1.2	XBT
930830	0547+07	01-58.980S	088-29.710E	4740	O 50	003 1.0	OMEGA-ZONDE RELEASED
930830	0847+07	01-25.420S	089-00.010E	2918	X-089	007 1.1	XBT
930830	1149+07	00-51.560S	089-30.330E	2470	O 51	006 1.2	OMEGA-ZONDE RELEASED
930830	1506+07	00-12.630S	090-00.000E	3127	X 090	339 1.0	XBT
930830	1802+07	00-22.380N	090-26.730E	4259	O-52	359 0.8	OMEGA-ZONDE RELEASED
930830	2143+07	01-06.050N	091-00.000E	4438	X 091	057 0.2	XBT
930830	2359+07	01-33.030N	091-20.660E	4345	O 53	083 0.4	OMEGA-ZONDE RELEASED
930831	0457+07	02-24.550N	092-00.000E	4233	X 092	053 0.8	XBT
930831	0558+07	02-34.450N	092-07.630E	4200	O-54	072 0.7	OMEGA-ZONDE RELEASED
930831	1158+07	03-31.710N	092-51.380E	4384	O 55	138 0.6	OMEGA-ZONDE RELEASED
930831	1313+07	03-41.220N	092-58.770E	4500	PN 15	000 0.0	ORI NET START
930831	1316+07	03-41.280N	092-58.810E	4500	PN 15	000 0.0	ORI SIDE NET START
930831	1326+07	03-41.580N	092-59.010E	4501	PN 15	000 0.0	ORI NET DEEPEST
930831	1336+07	03-41.820N	092-59.170E	4500	PN 15	000 0.0	ORI SIDE NET FINISH
930831	1340+07	03-41.890N	092-59.230E	4502	PN 15	000 0.0	ORI NET FINISH
930831	1352+07	03-42.930N	093-00.000E	4509	X 093	182 0.9	XBT
930831	1756+08	04-35.660N	093-40.310E	1050	O-56	141 0.8	OMEGA-ZONDE RELEASED
930831	1950+08	05-01.310N	094-00.010E	1515	X-094	347 0.7	XBT
930901	0120+08	06-09.810N	094-59.730E	6205	X 095	061 1.2	XBT
930901	0121+08	06-09.880N	095-00.070E	5987	X 095	065 0.9	XBT
930901	0506+08	06-05.090N	096-00.000E	1286	X-096	290 0.9	XBT
930901	1008+08	05-59.970N	097-00.425E	1242	X 097	205 1.4	XBT
930907	2351+08	04-42.980N	106-33.370E	93	O 57	192 0.5	OMEGA-ZONDE RELEASED
930908	0253+08	05-20.480N	107-04.050E	63	O 58	172 0.5	OMEGA-ZONDE RELEASED
930908	0600+08	06-02.170N	107-36.860E	72	O- 59	105 0.5	OMEGA-ZONDE RELEASED
930908	0856+08	06-41.100N	108-08.100E	86	O 60	119 0.5	OMEGA-ZONDE RELEASED
930908	1158+08	07-20.450N	108-39.770E	121	O 61	131 0.4	OMEGA-ZONDE RELEASED
930908	1456+08	07-57.770N	109-10.480E	128	O 62	167 0.5	OMEGA-ZONDE RELEASED
930908	1749+08	08-34.790N	109-39.680E	78	O-63	151 0.5	OMEGA-ZONDE RELEASED
930908	1948+08	09-00.000N	110-00.000E	1806	X-110	195 0.4	XBT & a/co to 048ñ
930908	1952+08	09-00.700N	110-00.770E	1784	X1102	160 0.6	XBT
930908	2049+08	09-11.360N	110-12.640E	2068	O 64	157 0.1	OMEGA-ZONDE RELEASED
930908	2353+08	09-46.320N	110-51.640E	3188	O 65	084 1.1	OMEGA-ZONDE RELEASED
930909	0032+08	09-53.920N	111-00.000E	3315	X 111	090 0.8	XBT
930909	0303+08	10-21.160N	111-35.050E	3855	O 66	134 1.2	OMEGA-ZONDE RELEASED
930909	0510+08	10-38.140N	112-00.000E	4024	X-112	072 0.9	XBT
930909	0557+08	10-45.820N	112-11.630E	4073	O-67	078 1.0	OMEGA-ZONDE RELEASED
930909	0856+08	11-14.940N	112-55.810E	4264	O 68	059 0.8	OMEGA-ZONDE RELEASED
930909	0914+08	11-17.700N	113-00.020E	4275	X 113	086 0.6	XBT
930909	1159+08	11-44.390N	113-40.510E	4334	O 69	100 1.0	OMEGA-ZONDE RELEASED
930909	1318+08	11-57.190N	114-00.000E	4355	X 114	099 1.4	XBT
930909	1455+08	12-13.280N	114-24.570E	4371	O 70	102 2.6	OMEGA-ZONDE RELEASED
930909	1716+09	12-36.570N	115-00.000E	4342	X-115	048 0.7	XBT
930909	1747+09	12-41.380N	115-07.310E	4380	O-71	329 0.4	OMEGA-ZONDE RELEASED
930909	2047+09	13-09.830N	115-50.890E	4307	O 72	131 0.5	OMEGA-ZONDE RELEASED
930909	2126+09	13-15.800N	116-00.010E	4333	X 116	153 0.9	XBT
930909	2350+09	13-38.220N	116-34.270E	4304	O 73	115 0.3	OMEGA-ZONDE RELEASED
930910	0136+09	13-54.990N	117-00.000E	4221	X 117	056 0.3	XBT
930910	0316+09	14-10.650N	117-24.030E	4247	O-74	140 0.6	OMEGA-ZONDE RELEASED
930910	0548+09	14-34.040N	118-00.010E	3626	X-118	206 0.6	XBT
930910	0606+09	14-36.780N	118-04.200E	4234	O-78	175 0.4	OMEGA-ZONDE RELEASED
930910	0855+09	15-04.340N	118-41.910E	4003	O 76	266 0.2	OMEGA-ZONDE RELEASED
930910	1143+09	15-47.000N	119-00.000E	2972	X 119	182 0.7	XBT
930910	1155+09	15-50.170N	119-01.350E	2952	O 77	181 0.4	OMEGA-ZONDE RELEASED
930910	1453+09	16-35.810N	119-20.870E	2570	O 78	311 0.4	OMEGA-ZONDE RELEASED
930910	1746+09	17-20.470N	119-39.990E	2895	O-79	358 0.5	OMEGA-ZONDE RELEASED
930910	2011+09	17-57.420N	120-00.000E	2948	X 120	007 0.4	XBT

Y.M.D.	GMT+T	LAT.	LONG.	DEPTH	ST.NO	CURRENT	COMENT
930910	2047+09	18-05.960N	120-05.630E	1945	O 80	004 0.8	OMEGA-ZONDE RELEASED
930912	1250+09	23-01.550N	127-22.950E	5623	PN 16	000 0.0	ORI NET START
930912	1255+09	23-01.490N	127-23.180E	5612	PN 16	000 0.0	ORI SIDE NET START
930912	1305+09	23-01.390N	127-23.640E	5659	PN 16	000 0.0	ORI NET DEEPEST
930912	1315+09	23-01.350N	127-24.050E	5639	PN 16	000 0.0	ORI SIDE NET FINISH
930912	1323+09	23-01.310N	127-24.350E	5620	PN 16	000 0.0	ORI NET FINISH
930914	1233+09	29-09.020N	130-38.110E	3205	PN 17	176 1.5	ORI NET START
930914	1236+09	29-09.110N	130-38.160E	3202	PN 17	178 1.1	ORI SIDE NET START
930914	1248+09	29-09.540N	130-38.510E	3171	PN 17	000 0.0	ORI NET DEEPEST
930914	1256+09	29-09.870N	130-38.820E	3122	PN 17	000 0.0	ORI SIDE NET FINISH
930914	1306+09	29-10.180N	130-39.050E	3112	PN 17	000 0.0	ORI NET FINISH
930915	1233+09	33-33.570N	136-37.000E	2093	PN 18	259 2.1	ORI NET START
930915	1236+09	33-33.620N	136-37.090E	2093	PN 18	256 1.5	ORI SIDE NET START
930915	1249+09	33-33.830N	136-37.580E	2094	PN 18	000 0.0	ORI NET DEEPEST
930915	1257+09	33-33.910N	136-37.840E	2093	PN 18	000 0.0	ORI SIDE NET FINISH
930915	1310+09	33-34.010N	136-38.240E	2095	PN 18	000 0.0	ORI NET FINISH

1. Bathymetric Mapping by SeaBeam

Chie HONSHO[1], Kensaku TAMAKI[1], Hiromi FUJIMOTO[1],
Brian P. WEST[2], Lourent ROUX[3], Keiichi FURUYA[4],
Mayumi SEKINE[4], and Masahide FURUKAWA[5]

[1]*Ocean Research Institute, University of Tokyo*
[2]*School of Oceanography, University of Washington*
[3]*GRUS-Observatorie Midi-Pyrenees*
[4]*Department of Earth Science, Faculity of Science, Chiba University*
[5]*Division of Environmental Health, National Institute of Radiological Sciences*

1. Outline of Survey and Objectives

The Rodriguez Triple Junction connects three ridges in the Indian Ocean: the Central Indian Ridge (CIR), the Southeast Indian Ridge (SEIR) and the Southwest Indian Ridge (SWIR). There are several precedent surveys by SeaBeam near the Triple Junction. The center of the Triple Junction was surveyed by a French R/V Jean Charcot in 1984 (Munschy and Schlich,1989), and the CIR by a German R/V Sonne from 1987 to 1988, the SWIR was surveyed by a French R/V Le Atlante only a few months before our survey. The tracks of the Jean Charcot and the Hakuho-maru during this cruise are shown in Figure 1-1.

SeaBeam survey during the cruise was forcused on the topographic mapping of the SEIR succeeding the J.C.'s survey. The main objective of our survey was to clarify the features of the first segment and the transform fault of the ridge. The segment was shorter than we had expected, then we could extend the survey to the beginning of the third segment.

The another task of SeaBeam in the region is to confirm the real locations of sites for dredge, rock core, or CTD that were decided on maps made from J.C.'s SeaBeam data. Using the realtime mapping system connected to SeaBeam, we compared these maps with real topography. About 0.1 nautical mile shifts were often seen between these maps and real topography, but these shifts were not systematic.

2. System Configuration

Block diagram of the SeaBeam swath mapping system equipped with the Hakuho maru is shown in Figure 1-2. There are two data logging systems (to magnetic tape and hard disc) and three realtime mapping systems. The ZETA plotter is a roll plotter along the ship's track, and the another plotter is a XY_plotter. The mapping using colour dots on the display was carried out every ping, so it was helpful when we need to monitour the present topography.

The SeaBeam survey of the SEIR was divided into three parts over Leg 2 and Leg 3 for the efficiency of our schedule, and it took about 54 hours in total. The operation of the SeaBeam was completely automatic and the ship's speed was almost constant, around 16 knots. Each survey track in the first segment was about 70 km in length, with spacing of two nautical miles (3,700 m). The direction of the tracks was N60°E northwest of one of the lines of J.C. and N44°E beyond it (see Figure 1-1). As the SeaBeam has its swath width of 43°, about 78 % of the depth can be covered by one track. The coverage was around 70 % in most of the survey

area, but the rift valley in the first segment was almost fully covered by means of tracks along the axis.

3. Topography of SEIR

The topography of SEIR is shown in Figure 1-3. In the first segment, the rift valley is shallowest (3,700 m) a little north of the midst of the segment and becomes deeper toward both northwestern and southeastern ends. The depth at the southeastern end is more than 4,300 m, and the length of the segment is about 85 km. The inside corner high at 70° 32′E, 26° 05′S and features like overlapping spreading at 70° 25′E,26° 05′S can be seen. Though rather good correspondence between the eastern and western flanks can be recognized, it is remarkable that the eastern flank is shallower than the western as a whole.

The second segment shifts by 21 km toward northeast, and begins at 70° 45′E, 26° 05′S. We can see deep rift valley of more than 4,200 m and high abyssal hills on both sides of the ridge. Compared with the first segment, the second segment is short (about 33 km) and appears to be rotated counterclockwisely. The segment ends at another transform fault and the corner is more than 4,500 m deep. It is the deepe point in the SEIR we surveyed. The third segment begins at 70° 17′E, 26° 02′S, about 42 km apart from the end of the second segment. Topographic lineaments of the third segment running NW-SE can be seen clearly.

The second and third segments are almost parallel in the direction of about N46°W and the transform fault connecting them is orthogonal to them, while the first segment has a slightly different direction of about N38°W and the transform fault between the first and the second segments show less clear feature than that between the second and the third segments.

REFERENCES

Munschy,M. and Schlich,R.,1989, The Rodriguez Triple Junction (Indian Ocean): Structure and Evolution for the Past One Million Years, *Marine Geophys.Res. 11*, 1-14

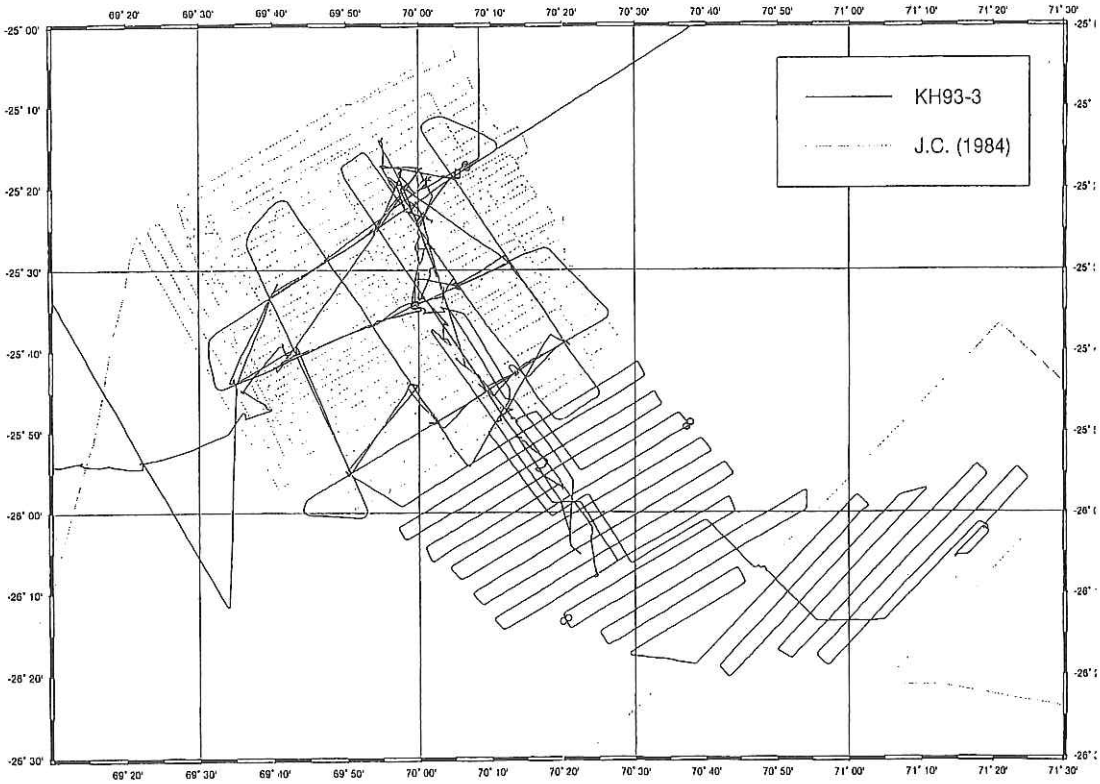

Fig. 1-1. SeaBeam tracks of the Jean Charcot (1984) and the cruise KH93-3.

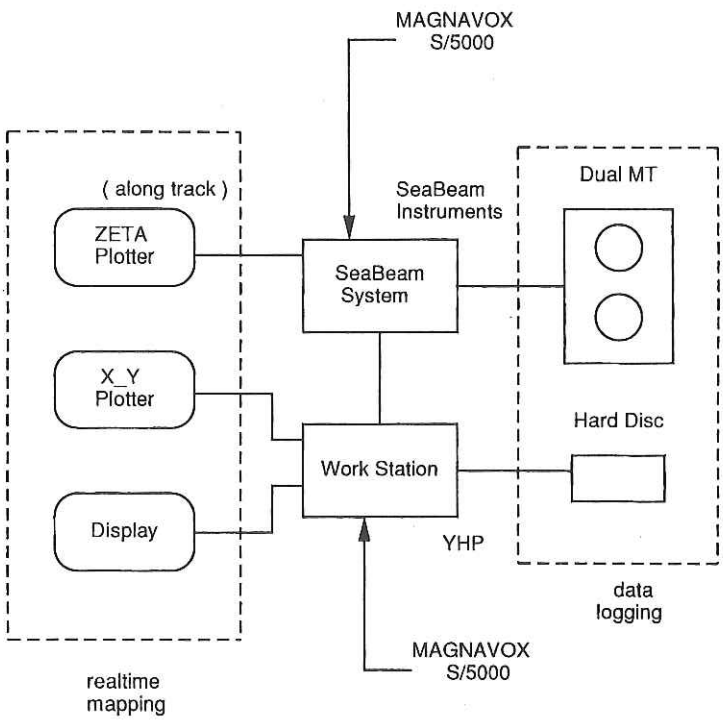

Fig. 1-2. Block diagram of the SeaBeam swath mapping system.

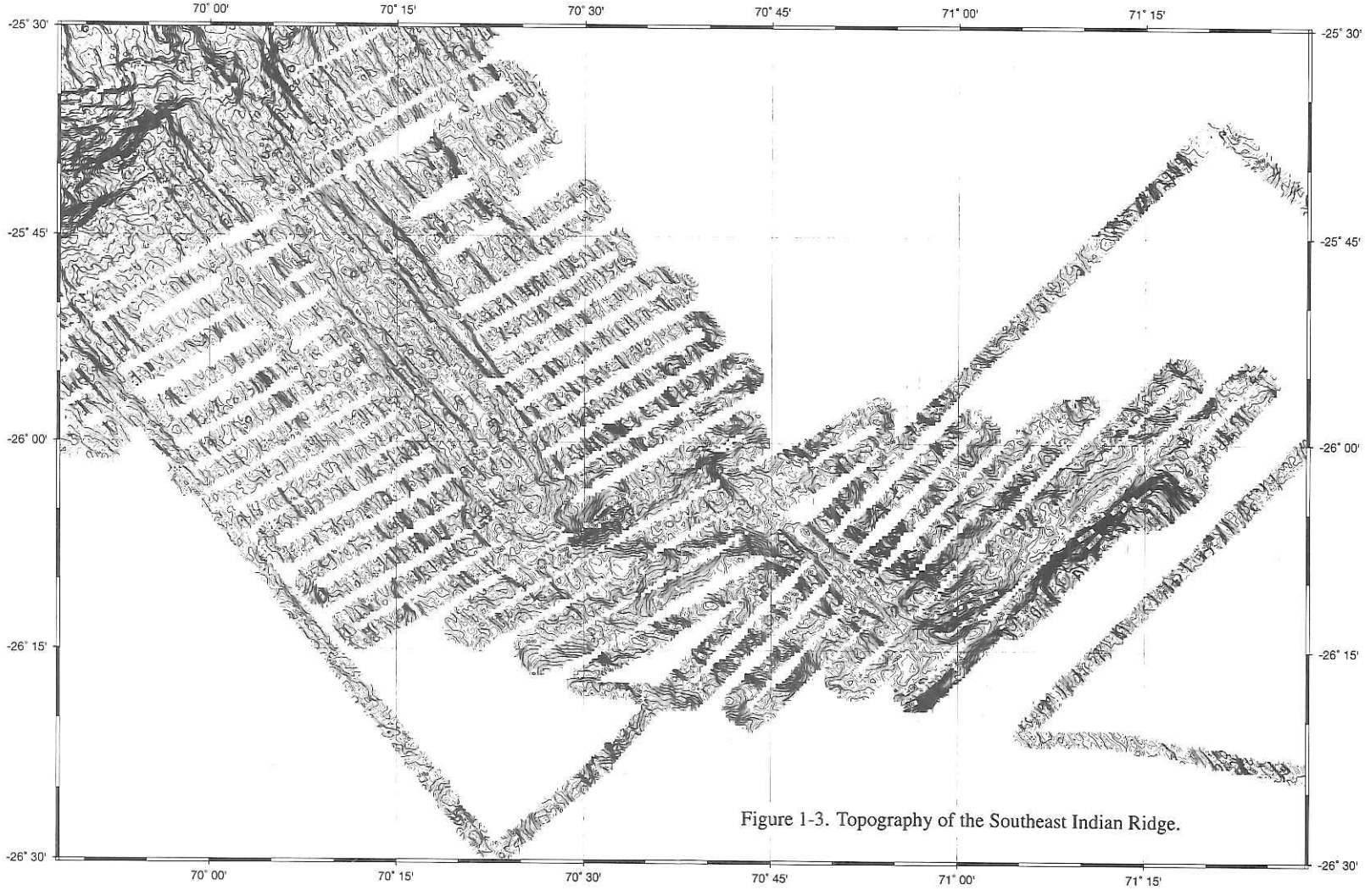

Figure 1-3. Topography of the Southeast Indian Ridge.

2-1. Geomagnetic Total Intensity Measurement by Proton Magnetometer

Chie HONSHO[1], Kensaku TAMAKI[1], Masaharu WATANABE[1],
Keiich FURUYA[2], Mayumi SEKINE[2], and Masahiko FURUKAWA[3]

[1]*Ocean Research Institute, University of Tokyo*
[2]*Department of Earth Science, Faculty of Science, Chiba University*
[3]*Division of Environmental Health, National Institute of Radiological Sciences*

1. Systems and Outline of Survey

Geomagnetic total force was measured by one of a proton precession magnetometers as one of the foundamental geophysical data. The measurement was done all through the cruise including transits, except while the ship was at a stop for dredging or other observations. Figure 2.1-1 shows tracks near the Rodriguez Triple Junction along which the measurement of geomagnetic total force was done.

We used two types of system for measurement: the ORI's original system which sensor was assembled in the ship for the cruise and EG & G Geometrics Model G-811G Proton Gradiometer equipped with the ship. Figure 2.1-2(a) is a block diagram of the ORI system. The towing length of the cable is about 250m. The data were processed and recorded by a micro-computer(PC9801VM) together with navigation data sent from the navigation system MAGNAVOX every one minute. In the latter half of the cruise, the data were sent through LAN and recorded in the MAGNAVOX system.

A block diagram of the G-811G system is shown in Figure 2.1-2(b). We used the system only during the multi-channel seismic reflection survey(MCS) because the towing system must be towed at a speed slower than 6.5 knots. The idea of gradiometer is to reduce the short-period time variations of the geomagnetic field by using difference between values of a slave sensor(forward) and a master sensor(trailing). But the signal of the master sensor was so week, that we could not get enough data for the time variation analysis. We do not know the reason yet, but it seems to be some trouble with the master sensor itself. So, we only got total force measured by the slave sensor along the MCS track.

2. Onboard Results

Geomagnetic anomalies near the Rodroiguez Triple Junction are shown in Figure 2.1-3. IGRF90 was used for the reference field. It was compiled using the data obtained by the Hakuho-maru and a French R/V Jean Charcot (1984). The data along MCS tracks by G811-G is not included because they have not been processed yet.

In Figure 2.1-3 we can see the following :

i) There are remarkable magnetic lineations along the CIR and the first two segments of the SEIR.
ii) The magnetic lineations along the SEIR are continuous to those near the triple junction observed by the Jean Charcot.

iii) Other than the magnetic lineations, the topographic effects can be seen, especilly along the CIR.

iv) In the first segment of the SEIR, the amplitude of anomalies is smaller in the north part than the central part. The area with smaller amplitude agrees with the area where the "bull's eye" negative gravity anomaly is seen, then it may be caused by focused accretion.

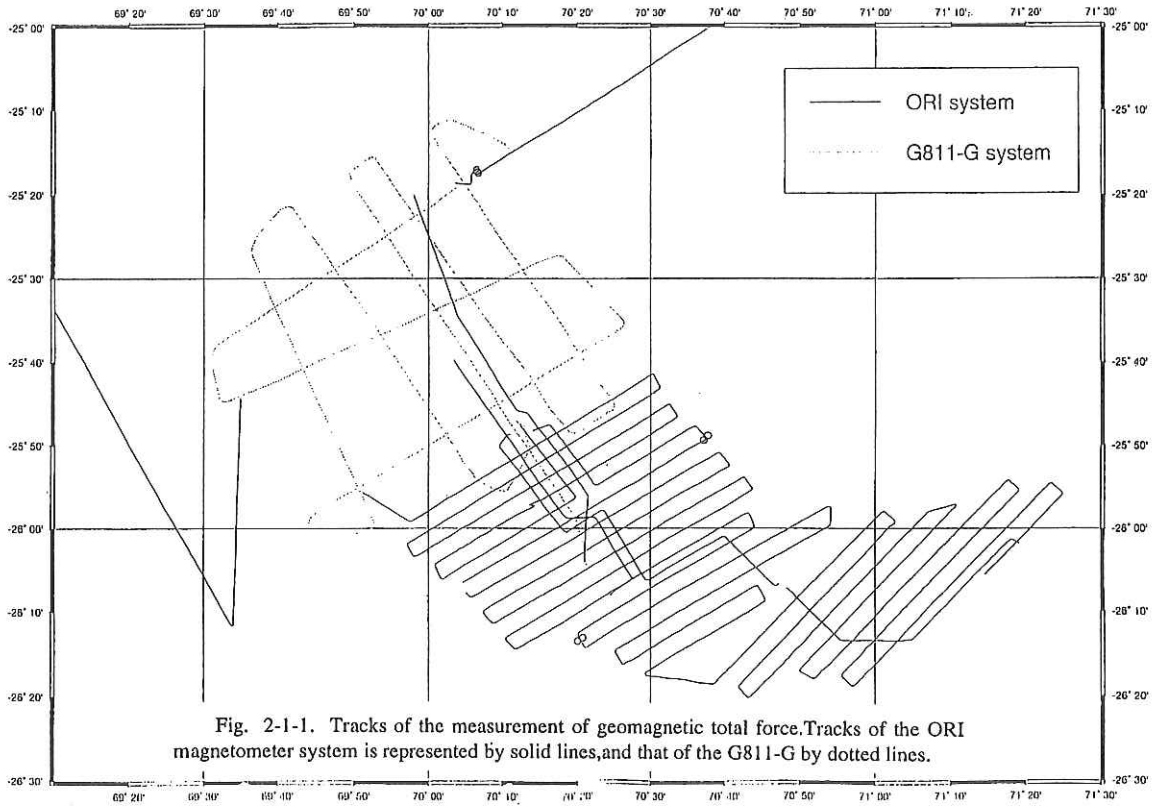

Fig. 2-1-1. Tracks of the measurement of geomagnetic total force.Tracks of the ORI magnetometer system is represented by solid lines,and that of the G811-G by dotted lines.

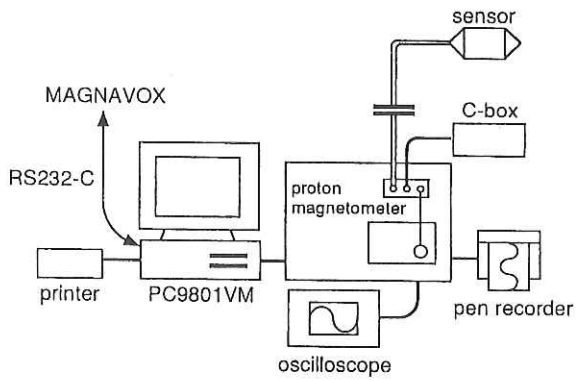

Fig. 2-1-2(a). The ORI magnetometer system.

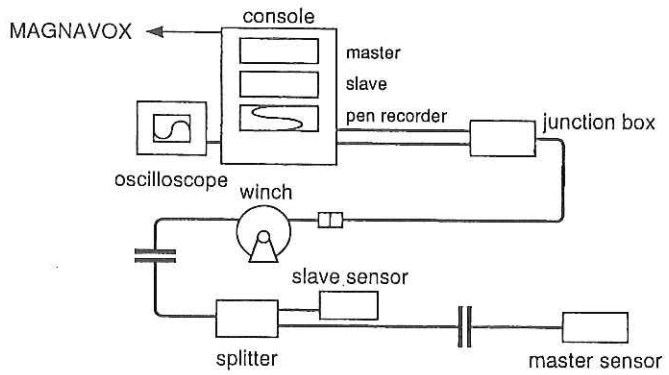

Fig. 2-1-2(b). The Model G811-G Proton Gradiometer System.

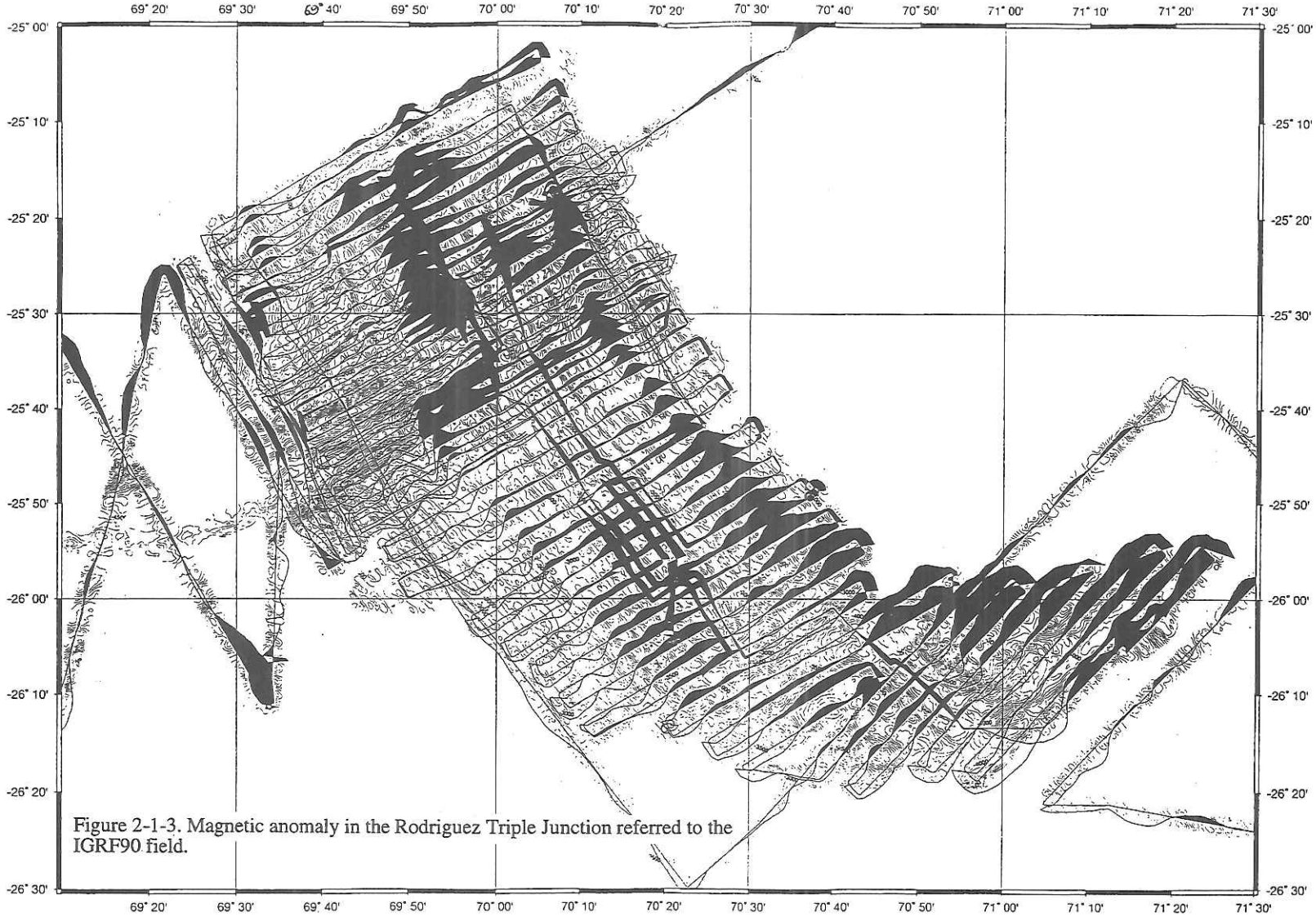

Figure 2-1-3. Magnetic anomaly in the Rodriguez Triple Junction referred to the IGRF90 field.

2-2. Measurement of Geomagnetic Three-Component Anomalies over the Rodriguez Triple Junction

Keiichi FURUYA[1], Chie HONSHO[2], Mayumi SEKINE[1],
Narumi TAKAHASHI[1], and Masahiko FURUKAWA[3]

[1]*Department of Earth Science, Faculty of Science, Chiba University*
[2]*Ocean Research Institute, University of Tokyo*
[3]*Division of Environmental Health, National Institute of Radiological Sciences*

1. Introduction

We used the ORI's STCM (Shipboard Three Component Magnetmeter;Isezaki et al .,1986) to measure the three components of the geomagnetic field. The main charactaristics of three component anomalies are as follows. 1) One can be determined even a single measurement line if the geomagnetic source body is two or three dimensional . 2) The dip and strike of two dimensional source body can be determined directly without any assumption. 3) The three component anomaly is not affected both by ambient geomagnetic field and by the trend of geomagnetic anomaly lineation, therefore it can be observed even at the geomagnetic equator, while the total intensity anomaly becomes very small if the lineation trend NS. 4) The bottom depth of the two dimensional source body can be estimated directly (e.g.Isezaki ,1986; Seama et al., 1992; Kitahara et al.,1994).

2. The STCM Systems

The STCM system of the R/V Hakuho-maru is shown in Figure 2.2- 1. This system was controlled by a personal computer (NEC PC- 9801) which collected all data. The geomagnetic vector field were measured by three fluxgate-type sensors set up on the upper deck. The ships heading, rolling and piching angles were measured by the precise gyrocompass (SGC-l) in Lab.9 and were sent to Lab.l through the LAN (Local AreaNetwerk) system of the R/V Hakuho-maru. These six data (Northward-X, Eastward-Y, Downward-Z components of geomagnetic field, heading, rolling and pitching angles) are stored in a hard disk every one second. Position, depth, speed, gravity and temperature data were also obtained from the general information in the Hakuho-maru LAN system every one minute. The STCM had collected these data during the entire period of the cruise.

3. Figure "8" steering data

The field around the sensor is affected by the additional magnetic field producted by the metallic vessel body because the sensor were set up on the upper deck during the entire period of the cruise.12 constants can remove these effects to obtain the true X, Y, Z components of the geomagnetic field (Isezaki,1986) and these 12 constants are determined using the observed data obtained while the ship steers figure "8" at nine places (Table.2.2-1).

4. The three component geomagnetic anomalies over the Rodriguez Triple junction

We calculated the three component geomagnetic anomalies. At first, the effects of the induced and permanent magnetic field by the ship were removed from the observed data using the 12 constants and IGRF90 sabtracted. Then short wave length anomalies which appear to be noise were removed using low-pass filter. The along-track geomagnetic anomaly profiles of the north,east and downward components are shown in Fig.2.2-2. Then we examined whether the magnetic source body is two-dimensional structure using the geomagnetic anomaly profiles. According to Isezaki (1986), when the magnetic source body is two-dimensional structure, the phase difference between the horizontal and the downward component anomaly profile is $\pi/2$. Fig.2.2-3 shows downward anomaly profiles with $\pi/2$ phase shifted and horizontal anomaly profiles. The phase shifted component from line1 to line12 (correspond to the first segment) and line18, 19 (correspond to the second segment) are similar to the horizontal component although the others are not. Thus, we comfirmed that the first and second segments in the SEIR are two-dimensional structure magnetically.

Table.2-2-1 Figure "8" steering location and the 12 constants.

Station No.	Date	Latitude	Longitude
KH93-3.R1	93.7.11	23°49.35'N	125°43.02'E
KH93-3.R2	93.7.14	13°38.06'N	113°39.48'E
KH93-3.R3	93.7.26	16°52.32'S	85°52.20'E
KH93-3.R4	93.7.29	25°17.57'S	70° 6.72'E
KH93-3.R5	93.8.5	25°49.08'S	70°37.58'E
KH93-3.R6	93.8.21	26°13.30'S	70°20.35'E
KH93-3.R7	93.8.28	11° 4.00'S	80°43.90'E
KH93-3.R8	93.9.9	10°21.40'N	111°34.69'E
KH93-3.R9	93.9.12	23° 1.04'N	127°22.40'E

B(1,1)	-0.1657	B(1,1)	-1.15578	B(1,1)	0.05366
B(1,2)	1.0295	B(1,2)	0.00737	B(1,2)	0.08596
B(1,3)	0.04167	B(1,3)	-0.05997	B(1,3)	0.94706
Hph	-104.8	Hps	0.94706	Hpv	-8450.5

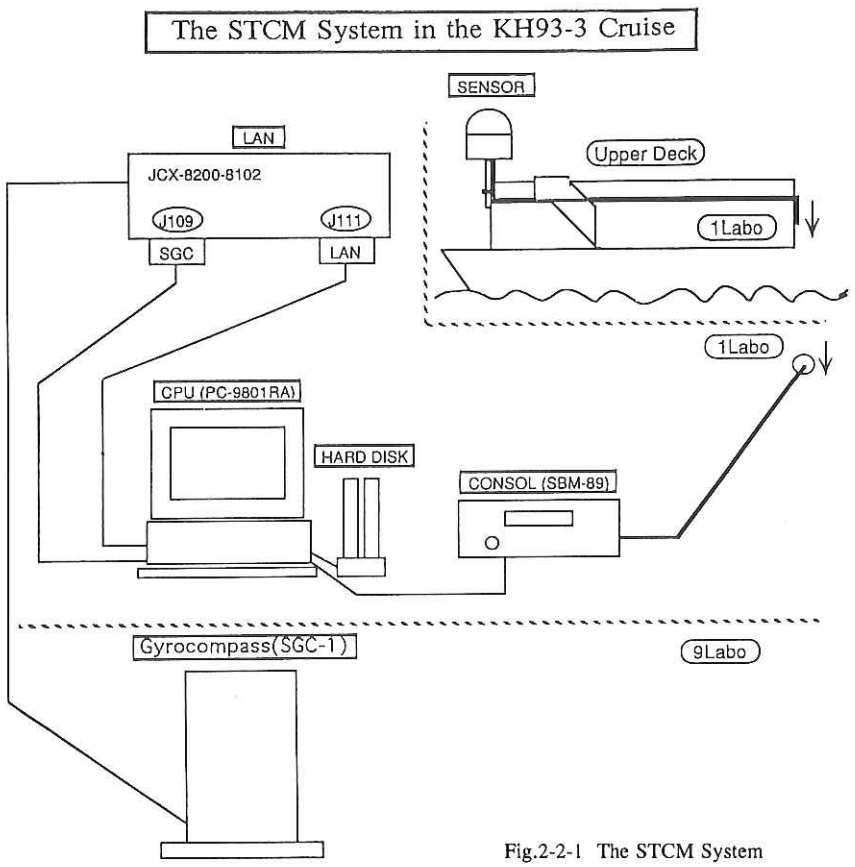

Fig.2-2-1 The STCM System

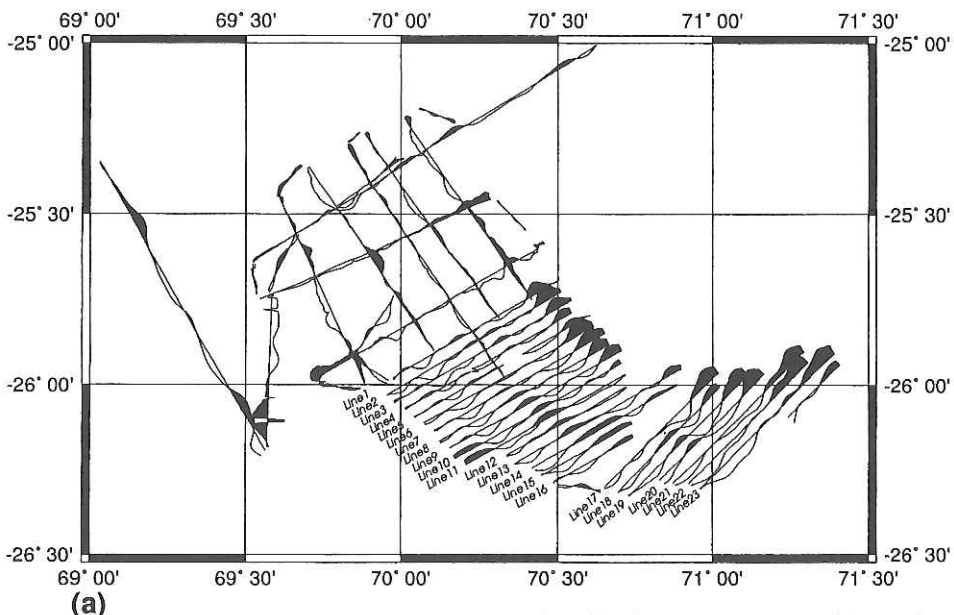

Fig.2-2-2 The along track geomagnetic anomaly profiles. (a), (b) and (c) are north, east and downward component respectively. Positive anomalies are shaded.

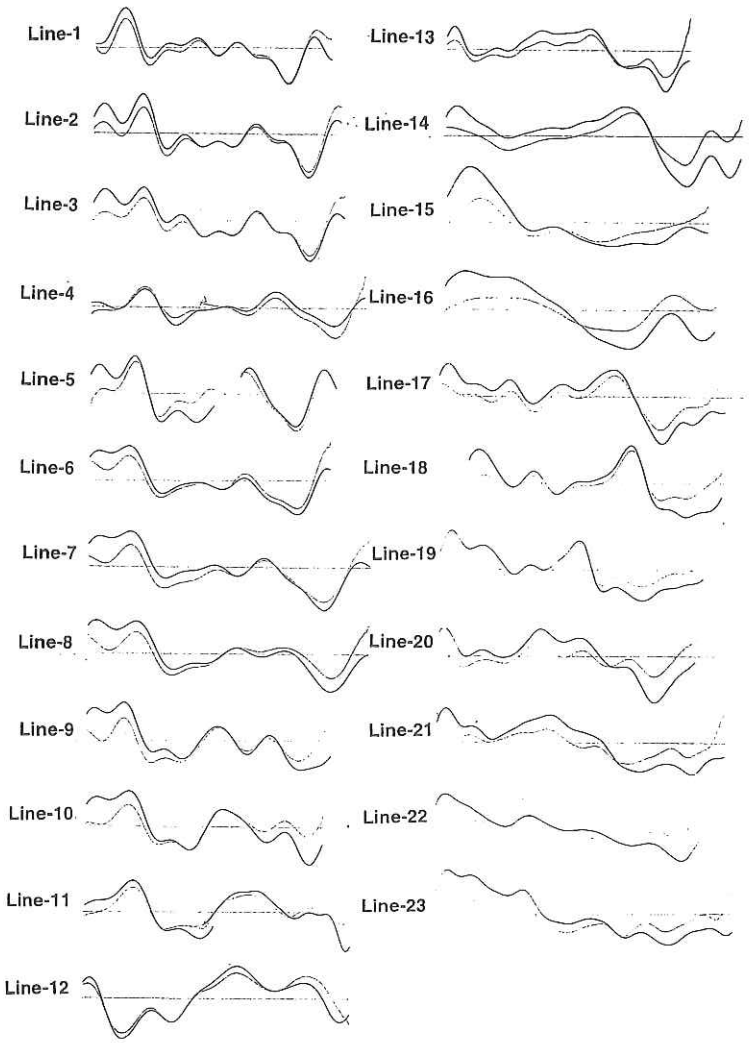

Fig.2-2-3 The downward anomaly profiles with $\pi/2$ phase shifted (sorid lines) and the horizontal anomaly profiles(dotted lines).

3. Mapping of Gravity Anomalies around the Rodriguez Triple Junction

Hiromi FUJIMOTO[1], Kin-ichiro KOIZUMI[1], Chie HONSHO[1], Kensaku TAMAKI[1], Brian P. WEST[2], Laurent ROUX[3], Maki ITO[4], Keiichi FURUYA[5], Mayumi SEKINE[5], and Yasushi HARADA[6]

[1]*Ocean Research Institute, University of Tokyo*
[2]*School of Oceanography, University of Washington, U.S.A*
[3]*GRUS-Observatorie Midi-Pyrenees, France*
[4]*Department of Ocean Science and Technology, Tokai University*
[5]*Department of Earth Science, Faculty of Science, Chiba University*
[6]*Department of Earth and Planetary Physics, University of Tokyo*

1. Objective

The Rodriguez Triple Junction (RTJ) is a R-R-R triple junction among the Indian, African, and Antarctic Plates. Three mid-ocean ridges meet at the junction: the Cental Indian Ridge (CIR), Southwest Indian Ridge (SWIR), and Southeast Indian Ridge (SEIR). Mapping of seafloor topography and gravity anomalies around the RTJ was carried out in 1984 during a transit of the French R/V Jean Charcot. Intensive geophysical expeditions have been performed during the KH93-3 cruise in 1993 following the French cruise. The objective of the expeditions was to clarify the geodynamics which controls ridge activities of the three segments nearest to the triple junction.

There are two approaches to geodynamics from the mapping of gravity anomalies. One is interpretations of free-air anomalies combined with seafloor topography. Because free-air anomalies show deviation of the subterranean structure from hydrostatic equilibrium, free-air anomalies are supported by some forces. Generally speaking, free-air anomalies at sea with wavelength shorter than several tens of kilometers are supported by the strength of the lithosphere. Longer wavelength components are supported by dynamic forces or flexure rigidity of the lithosphere. We can estimate the geodynamic forces acting around the RTJ or variation in thickness of the lithosphere by analysing the free-air anomalies combined with seafloor topography.

The SWIR is associated with large amplitude of topographic reliefs. The geophysical mechanism driving the rifting and supporting the topographic highs is one of interesting targets of this study. Gravity anomalies will be valuable to understand the tectonics around the two transform faults on the SEIR near the RTJ.

Another approach to geodynamics is gravity modeling of subterranean structures. A few kinds of Bouguer anomalies are used for the analysis as is discussed in the next section. One of the most interesting subjects is whether the three segments nearest to the RTJ are associated with "bull's eye" negative gravity anomalies like the Mid Atlantic Ridge (Kuo and Forsyth, 1988; Lin et al., 1990) or not. Two models have been proposed for the "bull's eye" gravity anomalies. One model postulates that the anomalies are an evidence for central upwelling plumes in the underlying mantle. The other model attributes the anomalies to along-axis crustal thickness variations. Either explanation indicates focused magma supply in a ridge segment.

The underway geophysics group proposes most probable subterranean structures based on gravity anomalies and seafloor topography. Although the area covered by seismic experiments is limited, the seismic group can examine and revise the structures near the RTJ. And finally we get mantle Bouguer anomalies near the RTJ which show density anomalies in the underlying mantle. Gravity modeling of the density anomalies in the upper mantle is an important approach to the geodynamics of the triple junction.

The geophysical data of the Jean Charcot cruise covers a whole segment on the CIR and half segments on the SWIR and SEIR. Most of the data are on the NE-SW track lines. A French R/V Atalante, newly built in place of the Jean Charcot, has recently extended the geophysical survey near the RTJ on the SWIR. Considering these conditions, we carried out geophysical surveys around the RTJ focused on the following targets: (1) 3-D analyses of subterranean structures around the RTJ by carrying out available geophysical measurements simultaneously on 8 seismic lines: Sea Beam, gravity, total force and 3-component magnetics, multi-channel seismic profiling, and OBS observation (see the chapter on seismics). (2) Investigation of focused accretion in the segment on the SEIR by extending geophysical surveys on the SEIR. (3) Investigation of tectonics around the two transform faults on the SEIR. (4) Investigation of the subterranean structure of the SWIR by adding geophysical profiles across the SWIR.

2. Instrumentation and data compilation

2.1 Instrumentation

Gravity measurements during this cruise were carried out by using a NIPR-ORI gravimeter which was developed jointly by National Institute for Polar Research (NIPR) and Ocean Research Institute (ORI), University of Tokyo, and manufactured by Tokimec Ltd. (Segawa, 1990). The gravity sensor of the gravimeter is a servo accelerometer. Most serious problem of the gravimeter is an extraordinarily large drift rate of the servo accelerometer. The drift rate is more than 2 mgal/day; a drift rate of a sea gravimeter is usually less than 1 mgal/month. The second problem is on the scale value of the gravimeter, that is, a ratio of a gravity value to the output voltage. As a constant scale value fixed by the manufacturer brought about irregular drift values depending on gravity values, we recalculated the scale value. Although the effects of these problems are mixed on measured gravity values and make the post processing complicated, the effcets will be removed as is discussed below. The third problem is on the system to keep the gravimeter vertical. The system adopts a Schuler gyroscope with a period of 84 minutes in order to be free from the effcets of course changes of the ship. However, off-leveling errors amounted to some 10 mgals for about 30 minutes after the ship changed the course by 180 ¡ with turning to the left. In this case we neglected the measured values. Some parameters of the leveling system may not be well adjusted. Off leveling errors are negligibly small 1 hour after a change of the course or the speed. Gravity acceleration is computed every one minute by the data processing system of the gravimeter. Eotvoes correction is also computed by using navigation data distributed to every laboratory through an optical local area network (LAN) utilizing RS-232C mọdems for real-time data processing. These gravity values are also distributed in the ship through the RS-232C LAN, and logged in two ways: both on a hard disk of a work station and on magnetic tapes of Magnavox Series 5000 navigation and data logging system. Several UNIX work stations are networked on board the vessel through an optical Ethernet LAN. Two work stations are connected to both the RS-232C LAN and the Ethernet LAN. One is used for real time mapping of the Sea Beam swath bathymetry data. The other is used for real time logging of navigational, geophysical, and meteorological

data. Gravity data are logged every one minute with MGD77 Format by the work station. Compilation of gravity data was carried out by using the data files in MGD77 Format.

2.2 Data compilation

Gravity data are distributed on the RS-232C LAN with delay time of 500 seconds. The delay is not adjusted in the file of the data logging work station. Therefore the first step of the gravity data compilation is adjustment of the delay time. And then Eotvoes correction was recomputed based on the position data within 4 minutes from the time of gravity measurements.

Most serious step of processings of the measured gravity data is a correction for the large drift of gravity sensor combined with the effect of the scale value. The drift value was checked at each port call by using a LaCoste & Romberg land gravimeter (model G), which has a drift rate about 0.1 mgal/year. We have also estimated the drift rate during the cruise by computing internal cross-over errors (ICOE) at intersections of straight ship's tracks. ICOE is free from the effect of the scale value. There are 100 ICOEs during Leg 2 with conditions that ship's velocity is faster than 4 knots and that variation of Eotvoes correction is less than 3 mgal/min. We got a minimum ICOE with a drift rate of -2.2 mgal/day for 10 days during the Leg 2. The root mean square of the ICOEs was 2.1 mgals. Considering that the value of the JC8404 gravity data around the RTJ was 3.8 mgals, the drift of our gravimeter during Leg 2 was fairly constant and well corrected. Drift rate during the Leg 3 was determined in the same way to be -1.0 mgal/day.

Drift rates obtained in this way are:

Singapore	(17 July - 21 July)	-2.0 mgal/day
Leg 2	(21 July - 10 Aug.)	-2.2 mgal/day
Port Louis	(10 Aug. - 14 Aug.)	-1.75 mgal/day
Leg 3	(14 Aug. - 02 Sep.)	-1.0 mgal/day
Penang	(02 Sep. - 06 Sep.)	-0.5 mgal/day

The scale value was then determined so as to give the most smooth drift curve. Gravity values in the surveyed area were firstly so adjusted after drift correction that the root mean square of the cross-over errors with the JC8404 cruise data became minimum. Final result is to be computed after the ship return to Tokyo, because the observed gravity value at Tokyo is critical to detemine the drift curve.

Overall root mean square of the cross-over errors of the combined gravity data near the Triple Junction obtained during the KH93-3 cruise and JC8404 cruise is some 3 mgals.

3. Data reductions and results

3.1 Free-air anomalies

Figure 3.1 shows a map of free-air anomalies based on the compiled gravity data mentioned above. Absolute values of free-air anomalies were determined based on the Jean Charcot gravity data. Average value of the free-air anomalies is about +10 mgals. If this is the case, some forces are necessary to support the positive free-air anomalies. Small fluctuations of the contours are due to navigation errors, imperfect correction of the drift effect, and the off-leveling errors mentioned above.

Variation of free-air anomalies well correlates with seafloor topography. Each of the three ridges is associated with negative free-air anomalies over the axial rift valley and positive anomalies on both sides. As is the case with topography, amplitudes of the gravity anomalies

are largest on the SWIR. Transform faults on the SEIR are associated with large negative free-air anomalies.

3.2 Bouguer anomalies

A few kinds of Bouguer anomalies are used for gravity modeling of subterranean structures. Standard Bouguer anomalies are obtained from free-air anomalies by correcting for the gravimetric effect of the seafloor topography. The correction is called Bouguer correction, and is obtained by computing the gravimetric effect of replacing the sea water of the density 1030 kg/m^3 with crustal rocks. Bouguer anomalies show density anomalies below the seafloor, and are usually interpreted by crustal structures, especially by variation of the Moho depth.

Bouguer correction was computed in two different ways. One is direct computation of the gravimetric effect of the seafloor topography. Although this method is time consuming, the result is accurate. The other uses Fourier transform on the assumption that the relief of the seafloor topography is small. As is shown in the following results, the two methods give much the same results on the SEIR and CIR, where topographic relief is relatively small. Different results are obtained on the SWIR. Maps of Bouguer anomalies obtained by Fourier transform show residual anomalies with the average value subtracted in order to estimate variation of crustal thickness.

An average crustal structure commonly used for gravity modeling of the mid-ocean ridges consists of the upper crust of the thickness 2 km and density 2730 kg/m^3 and the lower crust 4 km and 2930 kg/m^3. The average crustal density is 2860 kg/m^3. Bouguer anomalies with the crustal density of 2860 kg/m^3 are shown in Figure 3.2.

"Bull's eye" negative anomalies are observed in the northern part of the first segment on the SEIR. The same kind of negative anomalies with slightly small amplitude are on the CIR. Although observed data are limited, negative anomalies are recognized on the third segment of the SEIR. These negative anomalies indicate focused accretion in each of the segments. Negative anomalies are not prominent on the second segment of the SEIR, where negative free-air anomalies are large.

Although Bouguer anomalies in Figure 3.2.(a) are flat on the SWIR, Figure 3.2.(b) show anomalies related with topography. The difference results from the approximate computation for Figure 3.2(a) as mentioned above.

Another kind of Bouguer anomalies are also presented. If the crustal thickness is assumed to be constant, so-called mantle Bouguer anomalies (Figure 3.3) are obtained from free-air anomalies by correcting for the gravimetric effect of the sea water and crustal layers. The anomalies should be called mantle "pseudo" Bouguer anomalies, because the assumption of the constant crustal thickness is not always valid. If the assumption is the case, the anomalies present density anomalies in the underlying mantle. From this point of view, the "bull's eye" negative anomalies observed on the SEIR and CIR are an evidence of central upwelling plumes supposed in the mid-ocean ridge segments. It is another way of interpretation to discuss on variations of crustal thickness from the anomalies, because mantle pseudo Bouguer anomalies show deviation from the assumption of constant crustal thickness. The result is shown below.

Another kind of Bouguer anomalies are necessary for the modeling of crustal structures. Because thickness of the upper crust is considered to be fairly constant on the mid-ocean ridges, we define here "lower crust pseudo Bouguer anomalies" (Figure 3.4), which are obtained on the assumption of constant thickness of the upper crust. The gravity anomalies show density anomalies in the lower crust or mantle, and most probably show variation in the thickness of the layer 3. From this point of view, the "bull's eye" negative gravity anomalies show

thickening of the lower crust in the central part of the segments on the SEIR and CIR.

3.3 Variation of crustal thickness

Mantle pseudo Bouguer anomalies can be interpreted to show deviation from the assumption of constant crustal thickness as is discussed above. Variation of crustal thickness obtained from the result of Figure 3.3 is shown in Figure 3.5. As is indicated from Bouguer anomalies discussed above, the figure shows crustal thickening on the SEIR and CIR. Variation of the thickness of the layer 3 is most clearly estimated from the lower crust pseudo Bouguer anomalies.

he assumption of constant crustal thickness as is discussed above. Variation of crustal thickness obtained from the result of Figure 3.3 is shown in Figure 3.5. As is indicated from Bouguer anomalies discussed above, the figure shows crustal thickening on the SEIR and CIR. Variation of the thickness of the layer 3 is most clearly estimated from the lower crust pseudo Bouguer anomalies.

4. Summary

Although the sea gravimeter on board the Hakuho-maru had some problems, all the errors have successfully been removed in the off-line processings. Mapping of gravity anomalies were carried out based on the observed gravity data combined with those obtained during a Jean Charcot cruise. Judging from cross-over errors at intersections of the ship's tracks, relative variation of gravity anomalies has been measured with accuracies of about 3 mgals.

"Bull's eye" negative Bouguer gravity anomalies were observed on the Southwest Indian Ridge and Central Indian Ridge, which indicate focused accretion in the central part of each segment. The negative anomalies were not observed on the Southwest Indian Ridge.

REFERENCES

Kuo, B. Y. and D. W. Forsyth: Gravity anomalies of the ridge-transform system in the south Atlantic between 31 and 34.5 S: upwelling centers and variations in crustal thickness. Mar. Geophys. Res., 10, 205-232, 1988.

Lin, J., G. M. Purdy, H. Shouten, J.-C. Sempere, and C. Zervas: Evidence from gravity data for focuesd magmatic accretion along the Mid-Atlantic Ridge. Nature, 344, 627-632, 1990.

Segawa, J.: Gravity measurements and test of inertial navigator. Prel. Rep. of the Hakuho Maru Cruise KH-89-1. 25-29, 1990.

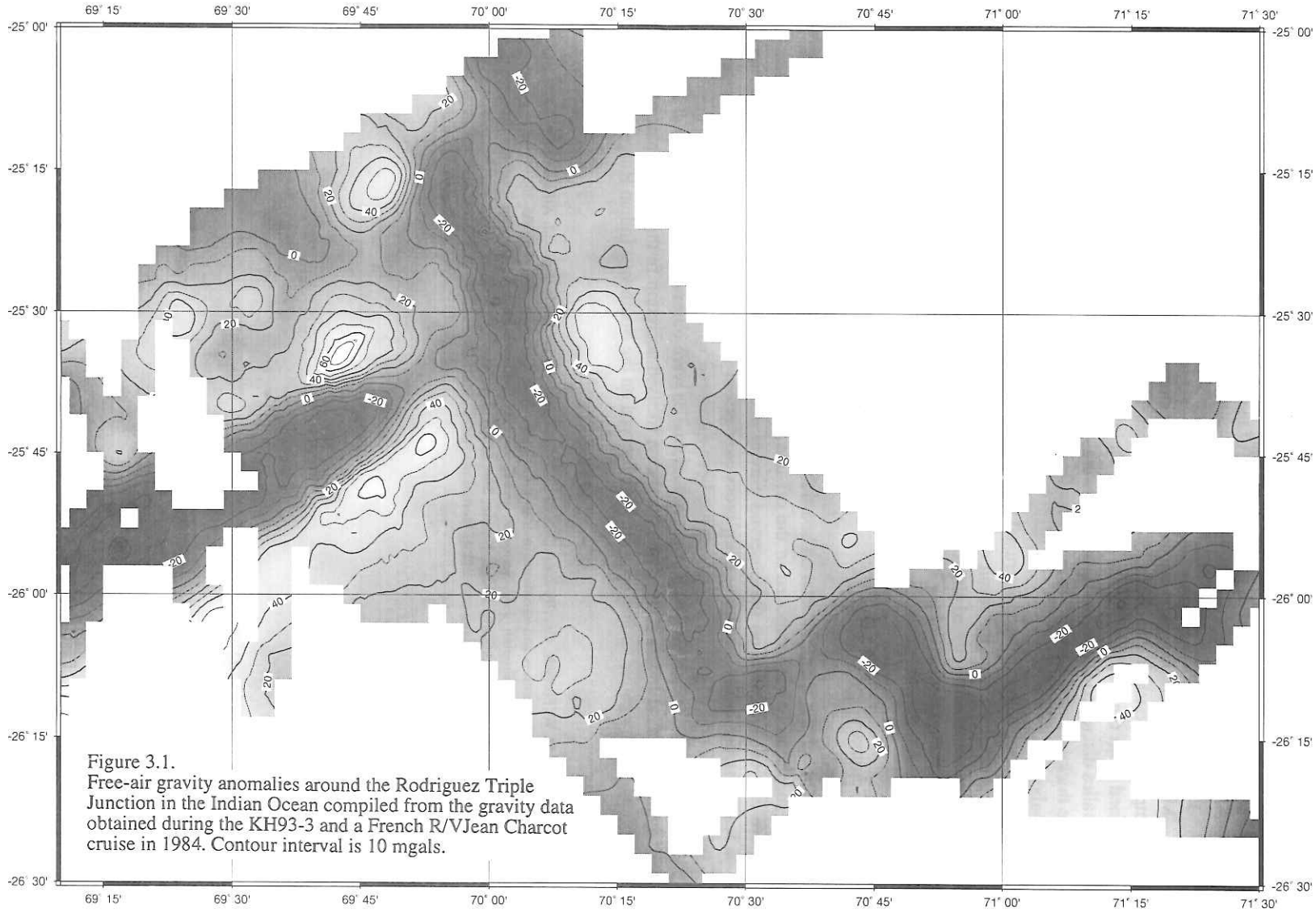

Figure 3.1.
Free-air gravity anomalies around the Rodriguez Triple Junction in the Indian Ocean compiled from the gravity data obtained during the KH93-3 and a French R/VJean Charcot cruise in 1984. Contour interval is 10 mgals.

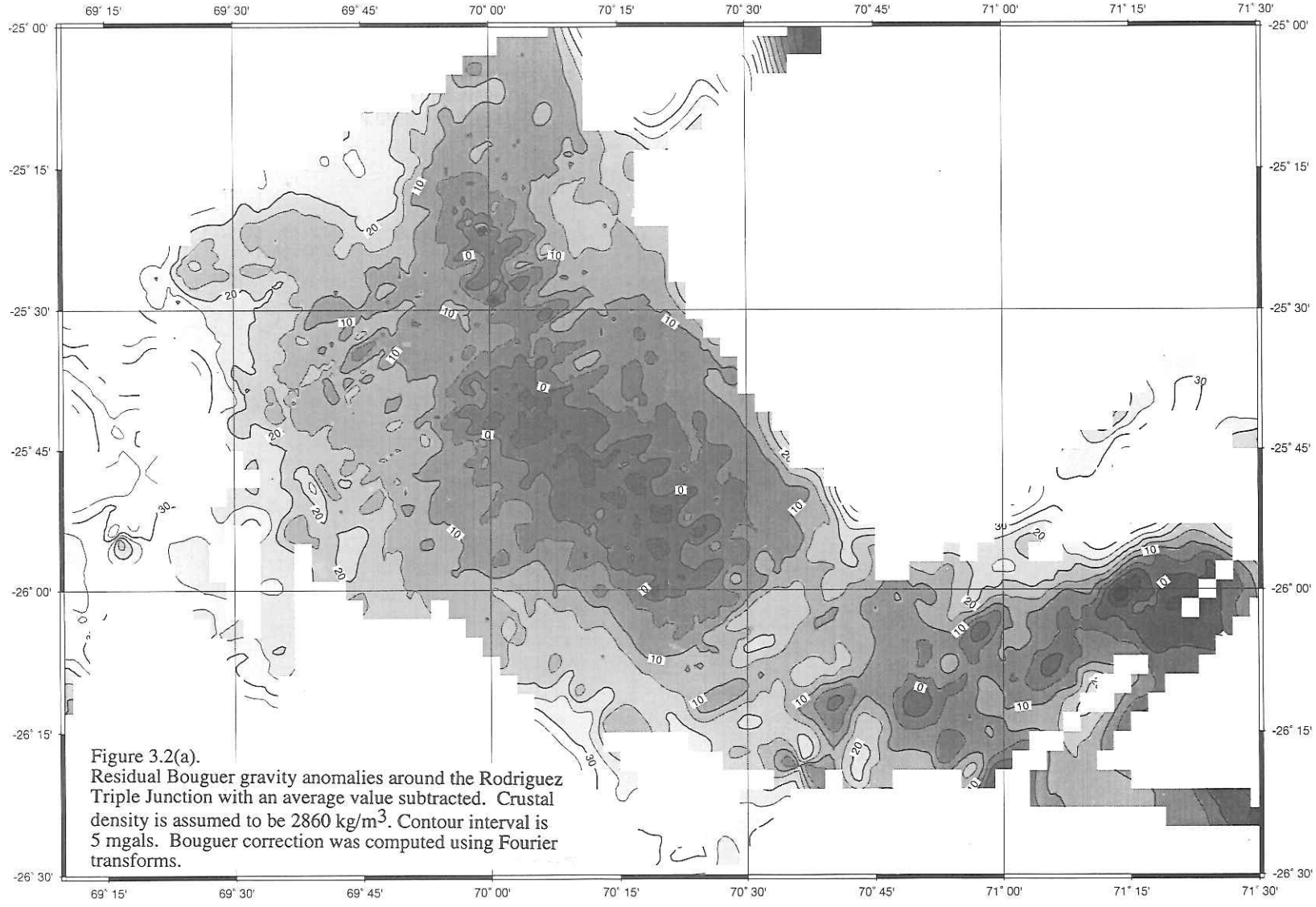

Figure 3.2(a).
Residual Bouguer gravity anomalies around the Rodriguez Triple Junction with an average value subtracted. Crustal density is assumed to be 2860 kg/m^3. Contour interval is 5 mgals. Bouguer correction was computed using Fourier transforms.

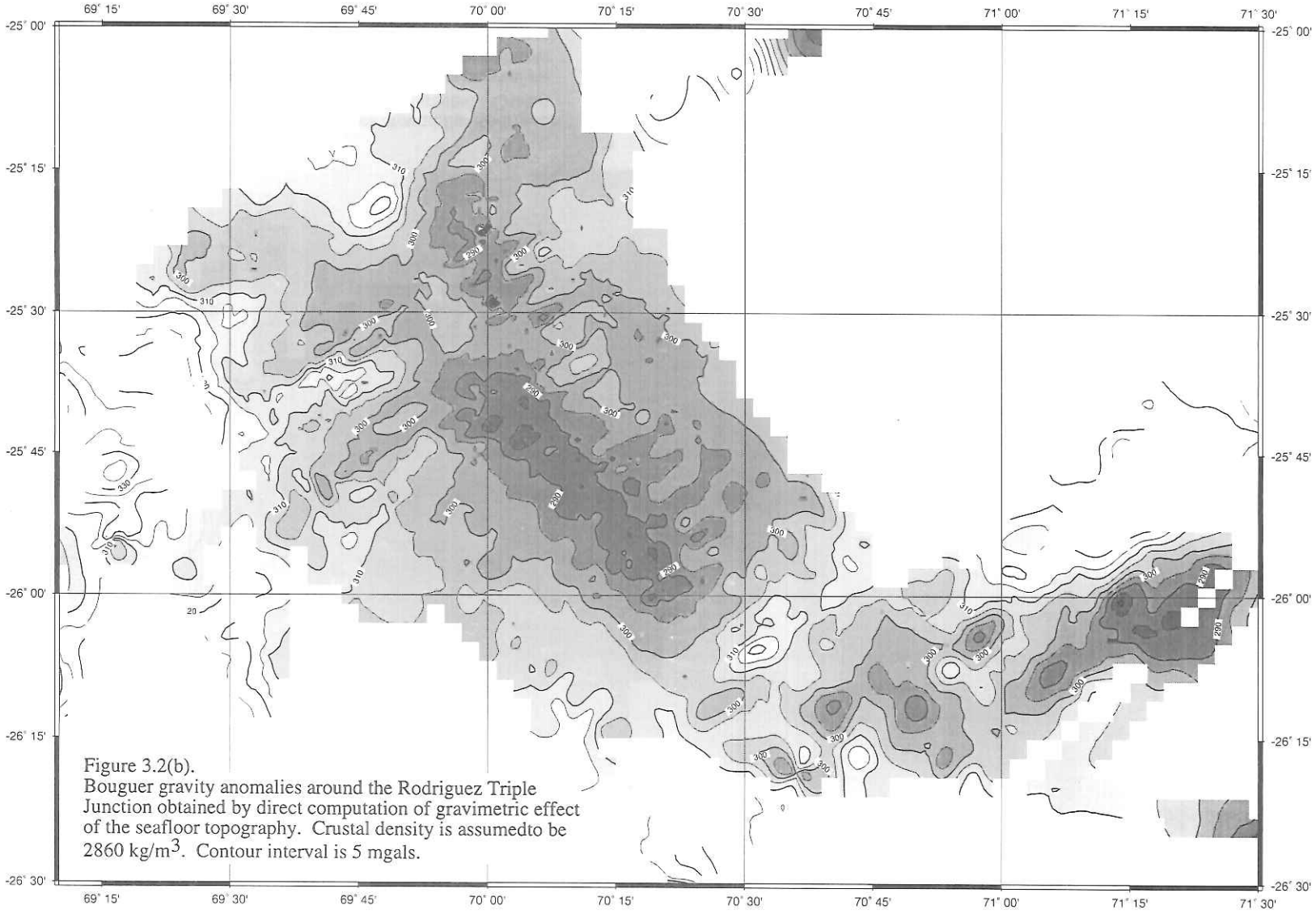

Figure 3.2(b).
Bouguer gravity anomalies around the Rodriguez Triple Junction obtained by direct computation of gravimetric effect of the seafloor topography. Crustal density is assumedto be 2860 kg/m^3. Contour interval is 5 mgals.

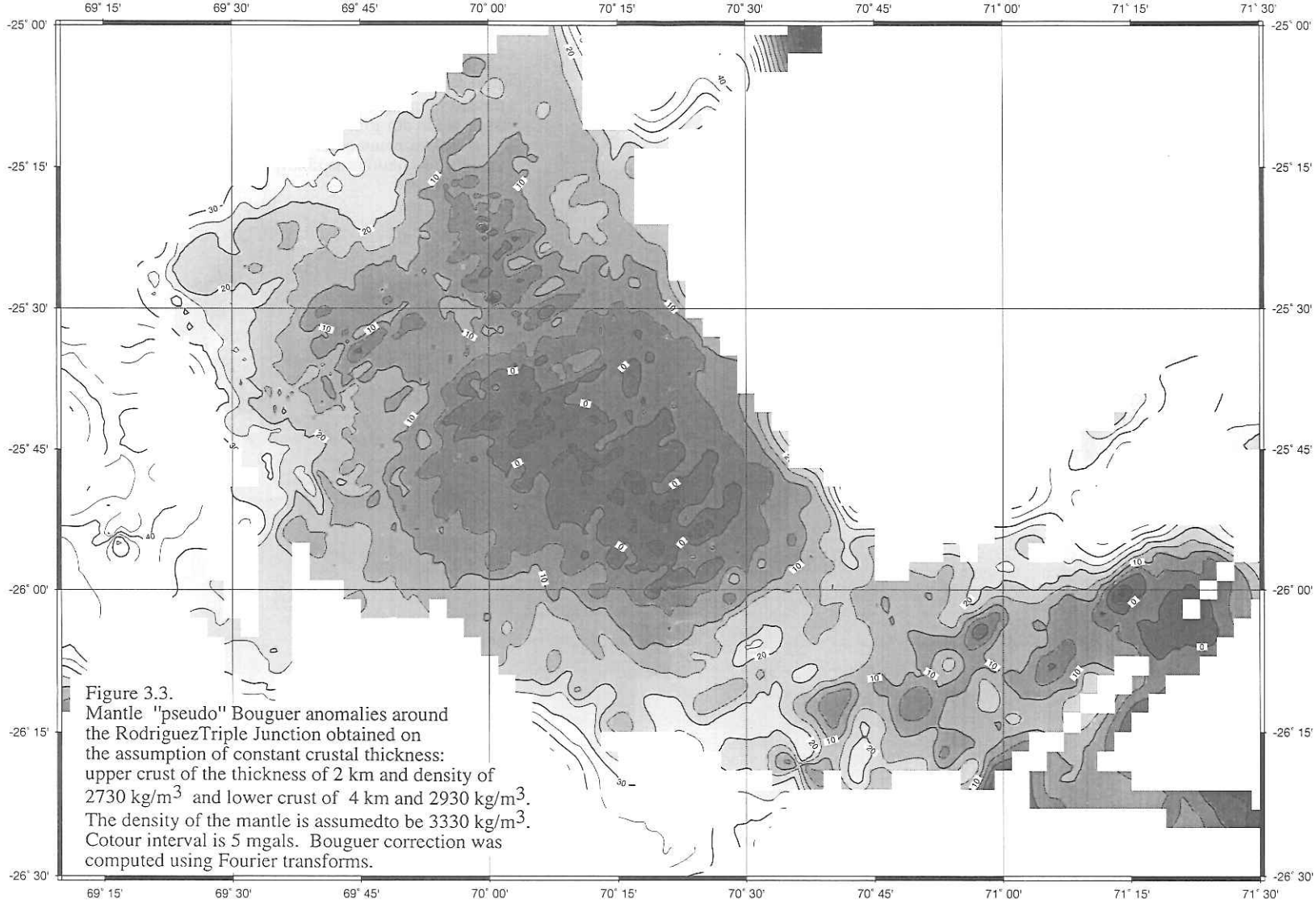

Figure 3.3.
Mantle "pseudo" Bouguer anomalies around the RodriguezTriple Junction obtained on the assumption of constant crustal thickness: upper crust of the thickness of 2 km and density of 2730 kg/m^3 and lower crust of 4 km and 2930 kg/m^3. The density of the mantle is assumedto be 3330 kg/m^3. Cotour interval is 5 mgals. Bouguer correction was computed using Fourier transforms.

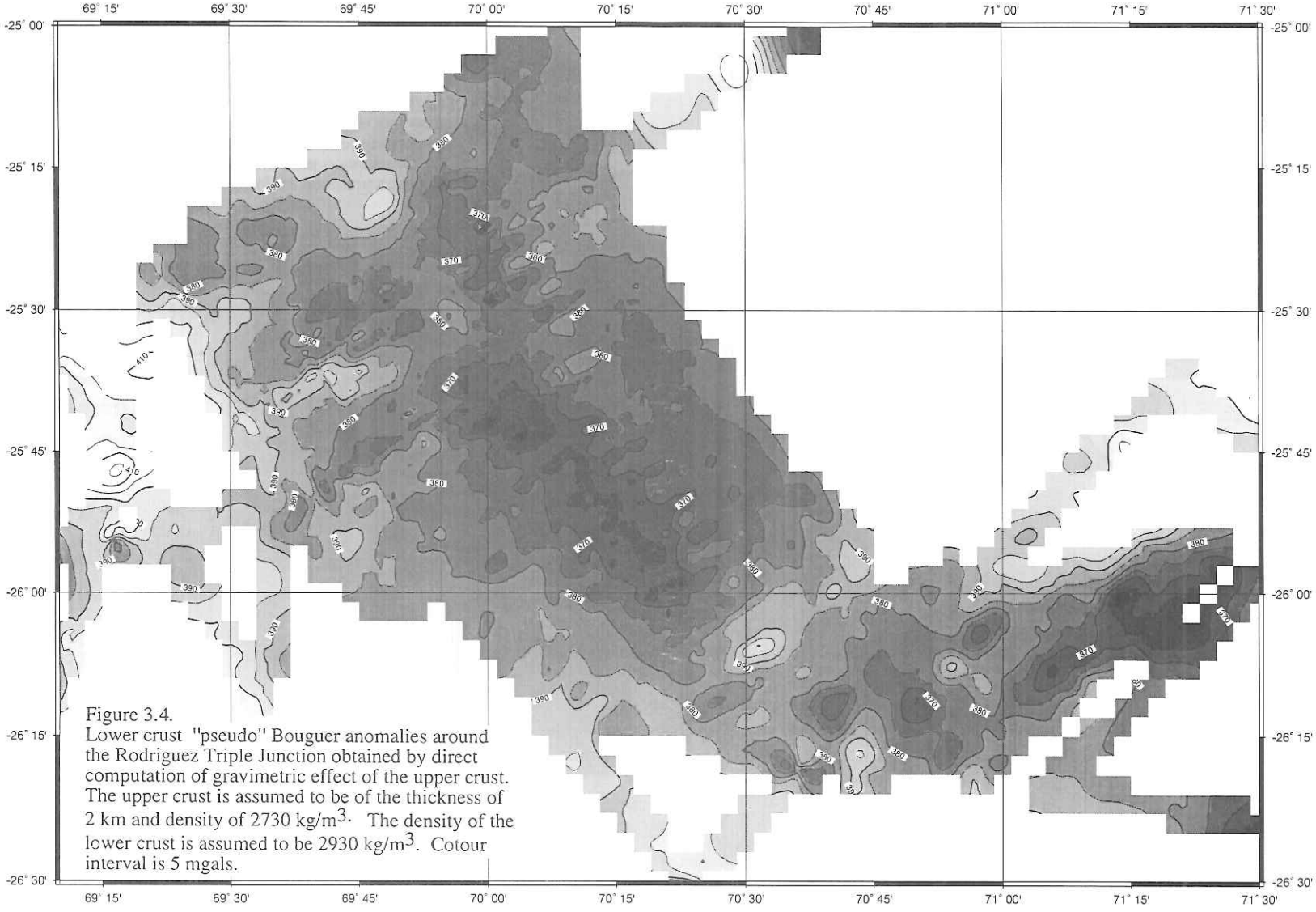

Figure 3.4.
Lower crust "pseudo" Bouguer anomalies around the Rodriguez Triple Junction obtained by direct computation of gravimetric effect of the upper crust. The upper crust is assumed to be of the thickness of 2 km and density of 2730 kg/m^3. The density of the lower crust is assumed to be 2930 kg/m^3. Cotour interval is 5 mgals.

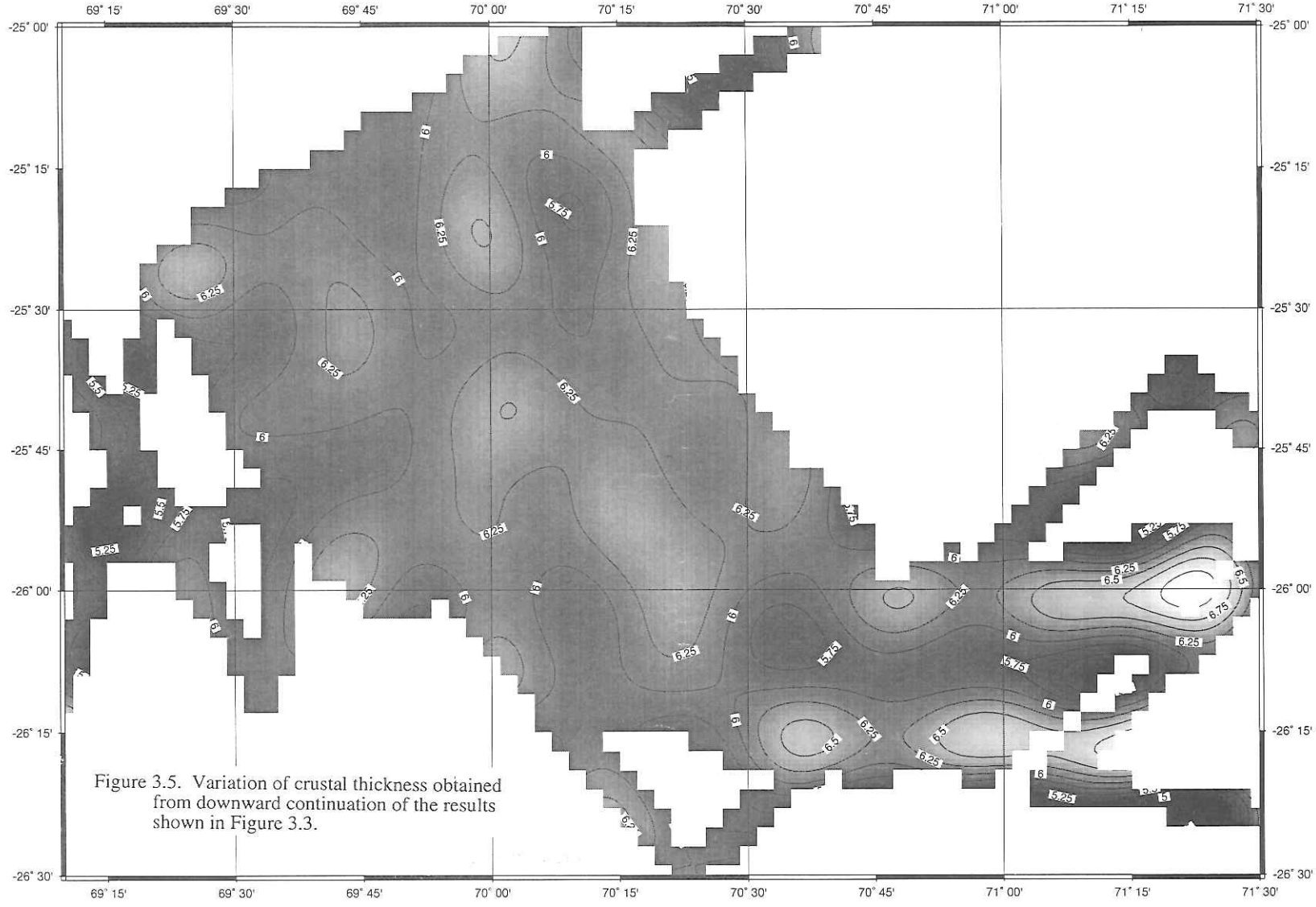

Figure 3.5. Variation of crustal thickness obtained from downward continuation of the results shown in Figure 3.3.

4. Seismic experiment in the Rodriguez Triple Junction area

Naoshi HIRATA[1], Junzo KASAHARA[1], Toshinori SATO[1], Sadayuki KORESAWA[1],
Kei KATSUMATA[1], Ryota HINO[2], Narumi TAKAHASHI[3],
Mayumi SEKINE[3], and Chiaki IGARASHI[4]

[1]*Earthquake Research Institute, University of Tokyo*
[2]*Observation Center for Earthquake and Volcanic Eruptions, Faculty of Science, Tohoku University*
[3]*Departent of Earth Science, Faculty of Science, Chiba University*
[4]*Ocean Research Institute, University of Tokyo*

We conducted a seismic reflection/refraction experiment and a natural earthquake observation during the KH93-3 cruise of the R/V Hakuho-maru. We deployed 18 ocean bottom seismometers (OBS) from three institutions, including Earthquake Research Institute, the University of Tokyo, Tohoku University, and Chiba University, in the Indian Ocean ridge-ridge-ridge triple junction area. Along eight lines we shot an airgun array, signals from which were recorded simultaneously by the OBSs and a multichannel seismic profiler (MCS). Deployment of the OBS and the airgun shooting operation were completed during Leg 2 of the cruise. The OBSs were retrieved during Leg 3. Some data were processed during Leg 3 and Leg 4.

1. Objectives

The Rodriguez Triple Junction (RTJ) is a junction of three Indian Ocean spreading ridges located near 25° 30′S and 70°E, 900 km southwest of the Rodriguez Island. The Southeast Indian Ridge (SEIR) has an intermediate spreading rate of 2.99 cm a^{-1} (half), trending N140°, and the Central Indian Ridge (CIR) slightly changes its trend to N152° with a half spreading rate of 2.73 cm a^{-1}. In the contrast , the Southwestern Indian Ridge (SWIR) has a deep rift valley which corresponds to a very slow spreading rate of 0.65 cm a^{-1} (Munschy and Schlich, 1989).

To understand the dynamics of the oceanic crustal generation at the triple junction area, the seismic crustal structure in the vicinity of the junction is essential. We need a clear seismic image of the crust and the upper mantle there. The basic questions to be clarified are (1) variation of crustal thickness across and/or along the Central and Southeastern Indian Ridges with age and relative position in a ridge segment, including the question if an axial magma chamber exists or not at the intermediate spreading center, (2) deep structure of the rift valley in SWIR, where a very young oceanic crust generated along IR and SEIR is stretched and a deep rift valley is well developed. We can expect seismic activity associated with development of the rift structure with extensional faulting.

2. Operation

2.1 OBS deployment

During the Leg 2 of the KH93-3 cruise, we deployed 18 ocean bottom seismometer (OBSs), including ERI type (Kasahara et al., 1985), and TK type. The latter type of OBS consisted of those developed in the Faculty of Science, the University of Tokyo (Yamada et al.,

1981) and those developed in the Department of Earth Sciences, Chiba University (Matsuda et al., 1986). The OBSs were equipped with one vertical component geophone and one or two horizontal geophones with a natural frequency of 2.0 or 4.5 Hz. Some of OBSs had also a hydrophone.

We could take full advantage of a detailed topographic data previously acquired by SeaBeam (Munschy and Schlich, 1989) for design of the airgun shooting line and selection of the exact place for OBS deployment. Because we planed the experiment for both a controlled seismic experiment and observation of natural earthquakes, we distributed the OBSs approximately equal spacing about 10 n.m. (20 km) as shown in Fig.1. Exceptions are in the vicinity of the triple junction where the OBSs are located about every 10 km.

Before deployment of each OBS we made a detailed topographic map at a scale of about 1/50,000 and chose a position with relatively smooth topography for the OBS site. As was shown by the 3.5-kHz profiling data, the see floor is extremely rough and seemed no sediment. All OBS positions were examined using a detailed topographic map, which were made by the SeaBeam data acquired during the present cruise by the R/V Hakuho- maru. We found a small discrepancy between the previous and the present SeaBeam topographic data depending on location in the surveyed area. In general, the difference is from 0.1 to 0.2 n.m. We shifted the scheduled position of the OBS after acquisition of swath mapping data on board. The detailed topography near the individual OBSs are shown in Fig.2 in which the scheduled position and actually deployed position are displayed with SeaBeam topography acquired during the present cruise.

Positions and times of deployment for individual OBSs are listed in Table 1. It took less than half an hour to complete deployment of the OBS after arriving at the scheduled position. We deployed the OBSs from the northeast OBS, RTJ16, towards southwest. The order and time of the operation of each OBS are summarized in Table 2. It took about 20 hrs to complete all the OBSs including transit between sites.

The procedure of deployment is as follows. First, we surveyed the topography by the current SeaBeam data with the previous data, and then, slightly changed the location if needed. After determination of the location, the R/V Hakuho-maru slowly approached there and slowed down the ship's speed to less than 2 kt. We lifted the OBS by a crane from a rear deck, then lowered it to the sea surface. When the ship arrived at the location, we released the rope to lower the OBS in the sea.

2.2 Airgun shooting

We shot an array of Bolt type airguns on eight lines. Originally, we plancd to use three guns, but it turned out very difficult to tow three guns behind the ship with a hydrophone streamer cable and a proton magnetic cable under the rough sea condition. So, the array in the present experiment consisted of two Bolt 1500C airguns with a 20- liter (1,200 in^3) chamber, 40 liter in total. We shot guns every 20 s at a pressure of 130 bar (1800 psi). We fired 12,228 shot for 64 hrs on 322 n.m. (596 km) in total. Positions and times for the airgun operation are summarized in Table 3. We had to stop the operation of one or two airguns several times due to leakage of air from either an air hose or an airgun assembly.

2.3 Multichannel reflection survey (MCS)

We conducted a multichannel seismic reflection survey (MCS) during airgun shooting on OBSs. The airgun signals were recorded simultaneously by the OBSs and MCS system. The MCS consisted of a 24-channel hydrophone cable, signals of which were acquired on magnetic

tapes after analogue-to-digital conversion by the DFS-V. We stored the data on 38 tapes (2400 ft, 6250 bpi) during the present operation. Originally we supposed to use two tape drive units for continuous recording, but one tape unit broke down and we could use only one of the tape units. Eventually, we lost some shot during exchange of tapes. Usually we missed ten to fifteen shots between tapes.

Before the airgun-MCS operation, we made profiles of topography and gravity anomaly using previously acquired data. We display the profiles in Figs. 3 through 10 with free air anomaly and Bouguer anomaly.

2.4 OBS retrieval

During the Leg 3, we tried to retrieve 18 OBSs. We succeeded in retrieving 17 OBSs, and could not get an OBS, RTJ14. Although we called this OBS by an acoustic transmitter from several directions, the OBS did not reply at all. Positions and times of retrieval for individual OBSs are listed in Table 1. A summary of the operation are shown in Table 4. The OBSs were called just above them, except two OBSs, RTJ3 and 6, which were called at a distance (2-4 n. m.) during dredges for time saving. At some stations, the operation of plankton net was conducted while the OBS was coming to the sea surface.

3. Initial Results

3.1 MCS

We obtained onboard monitor records using signals from the nearest channel of the hydrophone cable. In general, the data had poor signal-to-noise ratio due to rough sea condition. But Lines H3 and V1 show some reflection events, travel times of which is consistent to the reflection from Moho although the amplitude is not large enough to be definitely identified. We need to process the MCS data carefully.

3.2 Seismicity

We processed the data on RTJ2, 4, 10, 12, 16, 17, and 18 during the Leg 3 and Leg 4. From analogue recording tapes we made visible monitors on paper. We counted events which were over some threshold level. Figure 11 shows daily number of events at each station. During about 20 days observation, RTJ2 recorded 561 events (37 events per day), RTJ4 1554 (90/day), RTJ10 3089 (182/day), RTJ12 5284 (288/day), RTJ16 5005 (301/day), RTJ17 974 (59/day), and RTJ18 734 (40/day).

These results suggest that the Rodriguez Triple Junction has very high seismicity. Many events seem to occur at ridge axes, segment boundaries, and fracture zones in the Central Indian Ridge and the Southeast Indian Ridge, because the OBSs which were deployed near the Ridges recorded many events (RTJ10, 12, 16). RTJ10 and 16 had many swarms. RTJ10 and 12 had many small events. At RTJ2 and 4, which were deployed near the Southwest Indian Ridge, the number of events is relatively small, but the size of recorded events are relatively large.

3.3 Hypocenter distribution

We tried to determine hypocenter location of some events during the Leg 4. We chose five stations (RTJ2, 4, 10, 16, 18), and selected events which were recorded at all the stations. The selected events were recorded on paper using jet-pen recorder. Then we picked up P- and S-wave arrival times. The earth structure used for estimation of hypocenter locations was a

water layer of 4km thick, the layer 2 of 1km thick (Vp 5.0km/s), the layer 3 of 3km thick (Vp 6.7km/s), and upper mantle (Vp 8.0km/s). The algorithm of hypocenter determination was HYPOMH (Hirata and Matsu'ura, 1987).

We determined hypocenter locations of 55 events (7/30 1700 - 8/5 530). The preliminary results of epicenter distributions are shown in Fig. 12. The hypocenter locations is listed in Table 5. The value of depth has much uncertainty. From the epicenter distributions, most of events occurred at segment boundaries and fracture zones in the Central and Southeast Indian Ridges. Especially, many events including a swarm occurred at the segment boundary between RTJ10 and 16. In the Southwest Indian Ridge, events seem to occur its side walls.

4. Summary

We conducted a seismic reflection/refraction experiment and a natural earthquake observation. We deployed 18 OBSs and retrieved 17 OBSs. Because of rough sea conditions, we used only two airguns, and so the MCS data had poor S/N ratio. The OBSs recorded many events. From these data, we can make the structure and seismicity of this region clear. These studies will give a great help for understanding the dynamics of R-R-R triple junctions.

REFERENCES

Hirata, N., and M. Matsu'ura, Maximum-liklihood estimation of hypocenter with origin time eliminated using nonlinear inversion technique, Phys. Earth Planet. Inter., 47, 50- 61, 1987

Kasahara, J., M. Takahashi, T. Matsubara, and M. Komiya, Mass storage digital ocean bottom seismometer and hydrophone (DOBSH) controlled by micro-processors using ADPCM voice synthesizing, Bull. Earthq. Res. Inst., Univ. Tokyo, 60, 23- 37, 1985.

Munschy, M. and R. Schlich, The Rodriguez Triple Junction (Indian Ocean): Structure and evolution for the past one million years, Mar. Geophys. Res., 11, 1-14, 1989.

Yamada, T., A. Asada, and H. Shimamura, A pop-up ocean bottom seismograph (in Japanese), Prog. Abs. seismo. Soc. Jpn., 2, 126, 1981.

Fig. 4-1. A map showing the positions of OBSs (solid triangles) and MCS lines (thick solid lines).

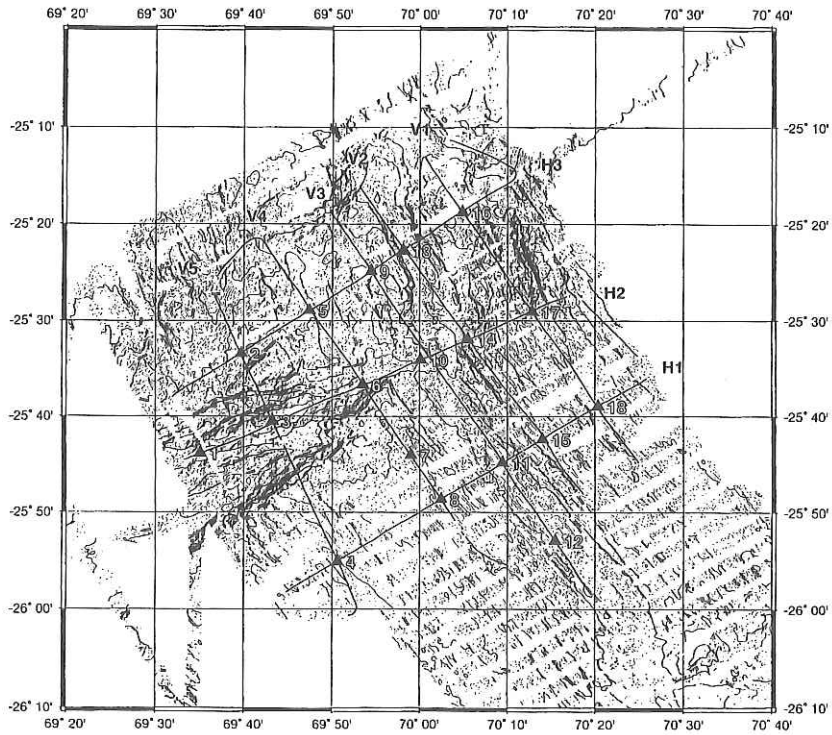

Position	OBS	Institute	Deployment	Deployment position			Retrieval	Retrieval position		
Name	Sation Name		time (GMT)	Latitude (S)	Longitude (E)	Depth(m)	time (GMT)	Latitude (S)	Longitude (E)	Depth(m)
OBS 1	RTJ 1	CHU	7/29 14:25	25° 43.92'	69° 35.07'	4538	8/16 17:38	25° 43.91'	69° 34.12'	4252
OBS 2	RTJ 2	ERI	7/29 13:14	25° 33.40'	69° 39.66'	2768	8/16 19:53	25° 33.11'	69° 39.80'	2704
OBS 3	RTJ 3	ERI	7/29 15:20	25° 40.38'	69° 43.15'	5065	8/19 15:28	25° 40.54'	69° 42.83'	3401
OBS 4	RTJ 4	ERI	7/30 10:14	25° 55.16'	69° 50.51'	3056	8/19 21:54	25° 55.12'	69° 50.21'	3083
OBS 5	RTJ 5	CHU	7/29 12:12	25° 28.99'	69° 47.28'	2543	8/16 22:21	25° 28.80'	69° 47.11'	2613
OBS 6	RTJ 6	THK	7/29 16:22	25° 36.87'	69° 53.49'	3975	8/19 09:47	25° 36.74'	69° 53.31'	3855
OBS 7	RTJ 7	THK	7/30 08:46	25° 44.14'	69° 59.08'	2927	8/19 01:31	25° 44.25'	69° 58.57'	3419
OBS 8	RTJ 8	THK	7/30 08:09	25° 48.64'	70° 02.53'	3115	8/20 04:01	25° 48.94'	70° 02.19'	3075
OBS 9	RTJ 9	CHU	7/29 11:06	25° 24.83'	69° 54.25'	2841	8/17 08:42	25° 24.72'	69° 54.14'	2827
OBS 10	RTJ 10	ERI	7/29 17:04	25° 34.03'	69° 59.58'	3404	8/19 04:31	25° 33.90'	69° 59.32'	3400
OBS11	RTJ 11	THK	7/30 07:20	25° 44.89'	70° 09.42'	3658	8/20 06:52	25° 44.83'	70° 09.08'	3702
OBS 12	RTJ 12	ERI	7/31 04:06	25° 50.54'	70° 13.80'	3824	8/20 17:07	25° 50.48'	70° 13.52'	3797
OBS 13	RTJ 13	CHU	7/29 10:28	25° 22.69'	69° 58.09	4202	8/18 11:07	25° 22.23'	69° 57.95'	4090
OBS 14	RTJ 14	ERI	7/30 00:49	25° 32.05'	70° 05.52'	3052	not retrieve			
OBS 15	RTJ 15	THK	7/30 04:13	25° 42.34'	70° 14.04'	2876	8/20 09:25	25° 42.19'	70° 13.66'	2846
OBS 16	RTJ 16	ERI	7/29 00:14	25° 18.93'	70° 04.99'	2930	8/17 21:37	25° 18.48'	70° 04.82'	3011
OBS 17	RTJ 17	ERI	7/30 01:45	25° 29.22'	70° 12.85'	2294	8/18 17:20	25° 29.23'	70° 12.56'	2354
OBS 18	RTJ 18	ERI	7/30 03:01	25° 38.94'	70° 20.38'	2900	8/20 12:23	25° 38.12'	70°18.55'	2766

CHU:Chiba University , ERI:Earthquake Research Institute University of Tokyo , THK:Tohoku University

Table 4-1. Position and time of deployment and retrieval of OBSs.

Table 4-2. Summary of operation of OBS deployment

Event	GMT	OBS station name
Arrival at OBS16	7/28/93 23:50	
Deployment of OBS16	7/29/93 00:14	RTJ16
Leave for CTD16		
S/B of OBS13	7/29/93 10:10	
Deployment of OBS13	7/29/93 10:18	RTJ13
Deployment of OBS9	7/29/93 11:06	RTJ9
Deployment of OBS5	7/29/93 12:12	RTJ5
Deployment of OBS2	7/29/93 13:14	RTJ2
Deployment of OBS1	7/29/93 14:25	RTJ1
Deployment of OBS3	7/29/93 15:20	RTJ3
Deployment of OBS6	7/29/93 16:23	RTJ6
Deployment of OBS10	7/29/93 17:04	RTJ10
Leave for CTD3		
Approaching of OBS14	7/29/93 23:50	
Deployment of OBS14	7/30/93 00:49	RTJ14
Deployment of OBS17	7/30/93 01:45	RTJ17
Deployment of OBS18	7/30/93 03:01	RTJ18
Deployment of OBS15	7/30/93 04:13	RTJ15
Leave for RC2		
Deployment of OBS11	7/30/93 07:20	RTJ11
Deployment of OBS8	7/30/93 08:09	RTJ8
Deployment of OBS7	7/30/93 08:46	RTJ7
Deployment of OBS4	7/30/93 10:14	RTJ4
Start SeaBeam		
Deployment of OBS12	7/31/93 04:06	RTJ12

Table 4-3. Summary of airgun operation.

Line		GMT	Local	Latitude °S '	Longitude °E '	Length n.m.
V4	start 20 L x2	7/31/93 6:52	7/31 11:52	25 52.50	70 5.25	37.13
	20 L	7/31/93 7:04	7/31 12:04			
	stop	7/31/93 7:09	7/31 12:09			
	20 L x 2	7/31/93 7:24	7/31 12:24			
	end	7/31/93 14:23	7/31 19:23	25 21.72	69 42.18	
		7.50 hrs				
V5	start 20 + 12 L	7/31/93 15:43	7/31 20:43	25 27.65	69 36.80	34.70
	stop	7/31/93 18:50	7/31 23:50			
	20 L start	7/31/93 19:14	8/1 0:14			
	20 L x 2	7/31/93 19:46	8/1 0:46			
	end	7/31/93 22:33	8/1 3:33	25 59.25	69 52.67	
		6.83 hrs				
H1	start 20 L x 2	8/1/93 0:28	8/1 5:28	25 58.24	69 44.87	40.80
	20 L	8/1/93 5:26	8/1 10:26			
	stop	8/1/93 5:31	8/1 10:31			
	20 L start	8/1/93 5:33	8/1 10:33			
	stop	8/1/93 5:35	8/1 10:35			
	20 L x 2 start	8/1/93 5:39	8/1 10:39			
	end	8/1/93 8:25	8/1 13:25	25 37.19	70 23.74	
		7.93 hrs				
H2	start 20 L x 2	8/1/93 10:39	8/1 15:39	25 27.48	70 16.71	41.66
	end	8/1/93 19:12	8/2 0:12	25 44.17	69 34.43	
		8.55 hrs				
H3	start 20 L x 2	8/1/93 20:28	8/2 1:28	25 37.97	69 31.95	41.30
	end	8/2/93 4:47	8/2 9:47	25 15.55	70 10.42	
		8.32 hrs				
V1	start 20 L x 2	8/2/93 6:37	8/2 11:37	25 12.98	70 0.55	38.80
	20 L x1	8/2/93 13:00	8/2 18:00			
	end	8/2/93 14:19	8/2 19:19	25 44.88	70 24.97	
		7.70 hrs				
V2	start 20 L x 2	8/2/93 15:27	8/2 20:27	25 48.09	70 18.69	39.41
	end	8/2/93 22:57	8/3 3:57	25 16.11	69 53.10	
		7.50 hrs				
V3	start 20 L x 2	8/2/93 23:55	8/3 4:55	25 18.55	69 49.75	48.18
	end	8/3/93 9:31	8/3 14:31	25 58.47	70 19.59	
		9.59 hrs				
	Total	74.63 hrs	(63.93 hrs)	12228 shots		
		321.98 n.m.		(596.30 km)		

Table 4-4. Summary of operation of OBS retrieval

Event	GMT	OBS etc. station	Position Latitude (S)	Position Longitude (E)	Remarks
Arrival at OBS 1, call RTJ 1	8/16/93 15:05	RTJ 1	25° 43.98'	69° 34.99'	NOR-1
Leave OBS 1 for OBS 2	8/16/93 17:38	RTJ 1	25° 43.91'	69° 34.12'	Retrieve RTJ 1
Arrival at OBS 2, call RTJ 2	8/16/93 18:30	RTJ 2	25° 33.23'	69° 39.79'	PN-7
Leave OBS 2 for OBS 5	8/16/93 19:53	RTJ 2	25° 33.11'	69° 39.80'	Retrieve RTJ 2
Arrival at OBS 5, call RTJ 5	8/16/93 20:47	RTJ 5	25° 28.90'	69° 47.33'	
Leave OBS 5 for CTD 11	8/16/93 22:21	RTJ 5	25° 28.80'	69° 47.11'	Retrieve RTJ 5
Arrival at OBS 9, call RTJ 9	8/17/93 06:56	RTJ 9	25° 24.83'	69° 54.26'	PN-8
Leave OBS 9 for DESMOS 1	8/17/93 08:42	RTJ 9	25° 24.72'	69° 54.14'	Retrieve RTJ 9
Arrival at OBS 16, call RTJ 16	8/17/93 19:59	RTJ 16	25° 18.78'	70° 05.09'	NOR-2
Leave OBS 16 for DESMOS 2	8/17/93 21:37	RTJ 16	25° 18.48'	70° 04.82'	Retrieve RTJ 16
Arrival at OBS 13, call RTJ 13	8/18/93 08:42	RTJ 13	25° 22.71'	69° 58.04'	
Leave OBS 13 for OBS 17	8/18/93 11:07	RTJ 13	25° 22.23'	69° 57.95'	Retrieve RTJ 13
Arrival at OBS 17, call RTJ 17	8/18/93 16:07	RTJ 17	25° 18.78'	70° 12.80'	NOR-3
Leave OBS 17 for OBS 14	8/18/93 17:23	RTJ 17	25° 29.25'	70° 12.56'	Retrieve RTJ 17
Arrival at OBS 14, call RTJ 14	8/18/93 18:29	RTJ 14	25° 31.96'	70° 05.27'	
Leave OBS14 for DR 15	8/18/93 21:03	RTJ 14	25° 31.94'	70° 05.36'	Not retrieve RTJ 14
Arrival at OBS 10, call RTJ 10	8/19/93 02:32	RTJ 10	25° 34.32'	69° 58.96'	
Leave OBS 10 for DR 17	8/19/93 04:31	RTJ 10	25° 33.90'	69° 59.32'	Retrieve RTJ 10
Call RTJ 6 during DR 17	8/19/93 07:21	PET 40	25° 36.22'	69° 54.67'	
Leave DR 17 for OBS 6	8/19/93 08:10	PET 40			
Leave OBS 6 for DR 18	8/19/93 09:47	RTJ 6	25° 36.74'	69° 53.31'	Retrieve RTJ 6
Call RTJ 3 during DR 18	8/19/93 13:10	PET 42	25° 42.43'	69° 40.64'	
Leave DR 18 for OBS 3	8/19/93 14:01	PET 42			PN-9
Leave OBS 3 for DR 19	8/19/93 15:28	RTJ 3	25° 40.54'	69° 42.83'	Retrieve RTJ 3
Arrival at OBS 4, call RTJ 4	8/19/93 20:38	RTJ 4	25° 55.21'	69° 50.42'	
Leave OBS 4 for OBS 7	8/19/93 21:54	RTJ 4	25° 55.12'	69° 50.21'	Retrieve RTJ 4
Arrival at OBS 7, call RTJ 4	8/19/93 23:08	RTJ 7	25° 44.23'	69° 59.82'	
Leave OBS 7 for OBS 8	8/19/93 01:31	RTJ 7	25° 44.25'	69° 58.57'	Retrieve RTJ 7
Arrival at OBS 8, call RTJ 8	8/20/93 02:11	RTJ 8	25° 48.82'	70° 02.53'	
Leave OBS 8 for OBS 11	8/20/93 04:01	RTJ 8	25° 48.94'	70° 02.19'	Retrieve RTJ 8
Arrival at OBS 11, call RTJ 11	8/20/93 04:50	RTJ 11	25° 44.87'	70° 09.35'	
Leave OBS 11 for OBS 15	8/20/93 06:52	RTJ 11	25° 44.83'	70° 09.08'	Retrieve RTJ 11
Arrival at OBS 15, call RTJ 15	8/20/93 07:35	RTJ 15	25° 42.27'	70° 14.17'	PN-10
Leave OBS 15 for OBS 18	8/20/93 09:25	RTJ 15	25° 42.19'	70° 13.66'	Retrieve RTJ 15
Arrival at OBS 18, call RTJ 18	8/20/93 10:16	RTJ 18	25° 38.92'	70° 20.23'	
Leave OBS 18 for RC 11	8/20/93 12:23	RTJ 18	25° 38.12'	70° 18.55'	Retrieve RTJ 18
Arrival at OBS 12, call RTJ 12	8/20/93 15:48	RTJ 12	25° 50.62'	70° 13.76'	PN-11
Leave OBS 12 for RC 12	8/20/93 17:07	RTJ 12	25° 50.48'	70° 13.52'	Retrieve RTJ 12

DR and RC mean a dredge and a rock core, respectively. PET is the station name for sampling of rocks.
NOR and PN are the station names for collection of plankton using NORPAC Net and ORI Net, respectively.

Table 4-5. A list of hypocenter locations.

origin time (GMT)		latitude (°S)	longitude (°E)	depth (km)
7/30	17:04:56.519	24.922	70.040	9.167
7/30	17:25:27.972	25.446	70.010	4.135
7/30	18:33:07.811	25.263	69.933	8.674
7/30	20:33:17.517	26.138	70.445	10.254
7/30	21:13:06.107	25.241	69.950	27.844
7/30	22:06:09.666	24.816	69.916	9.114
7/31	0:44:47.652	25.872	69.772	5.061
7/31	1:49:50.680	24.960	70.013	8.245
7/31	3:29:58.367	25.568	70.012	9.220
7/31	4:22:42.804	25.518	70.066	4.485
8/3	10:19:00.907	25.150	69.943	8.144
8/3	11:12:07.556	25.547	70.059	10.431
8/3	13:57:10.516	26.165	70.432	9.259
8/3	19:43:29.026	25.664	70.092	16.825
8/4	3:46:23.962	25.059	69.830	9.424
8/4	5:38:18.721	26.003	70.409	8.211
8/4	16:01:46.903	25.151	69.987	8.220
8/4	16:13:35.790	25.507	70.054	8.690
8/4	17:44:39.289	25.494	70.034	10.434
8/4	17:43:02.820	25.491	70.032	9.059
8/4	17:41:54.076	25.485	70.021	8.192
8/4	17:42:06.867	25.501	70.035	8.015
8/4	19:23:46.951	25.566	70.072	4.926
8/4	20:25:59.440	25.501	70.029	4.868
8/4	20:42:15.887	25.490	70.030	5.041
8/4	20:43:13.225	25.491	70.036	4.655
8/4	20:43:33.668	25.480	70.034	6.354
8/4	20:44:23.334	25.574	70.118	8.177
8/4	20:44:41.397	25.491	70.026	9.871
8/4	20:46:14.031	25.483	70.027	6.437
8/4	20:47:31.882	25.490	70.018	8.693
8/4	20:48:55.458	25.501	70.027	4.657
8/4	20:49:34.055	25.491	70.027	5.601
8/4	20:50:40.471	25.479	70.031	5.246
8/4	20:52:54.940	25.490	70.030	4.353
8/4	20:55:14.788	25.514	69.981	8.034
8/4	20:59:17.007	25.498	70.045	9.299
8/4	21:04:02.154	25.486	70.037	4.768
8/4	21:05:41.940	25.516	70.040	12.858
8/4	21:32:14.185	25.575	69.893	6.048
8/4	22:49:18.052	25.491	70.024	4.990
8/4	23:13:34.537	25.486	70.024	8.396
8/4	23:22:39.304	25.481	70.026	5.367
8/4	23:33:45.573	25.515	69.991	14.203
8/4	23:36:12.362	25.489	70.032	6.462
8/4	23:53:28.982	25.483	70.029	5.817
8/5	0:19:08.889	25.481	70.026	6.370
8/5	0:26:49.126	25.483	70.033	6.919
8/5	0:27:51.178	25.491	70.038	3.412
8/5	1:08:27.511	25.478	70.052	5.136
8/5	4:30:42.976	25.487	70.036	5.907
8/5	4:38:15.776	25.501	70.031	6.588
8/5	5:18:11.969	25.647	70.089	6.786
8/5	5:28:14.053	25.577	69.866	8.867

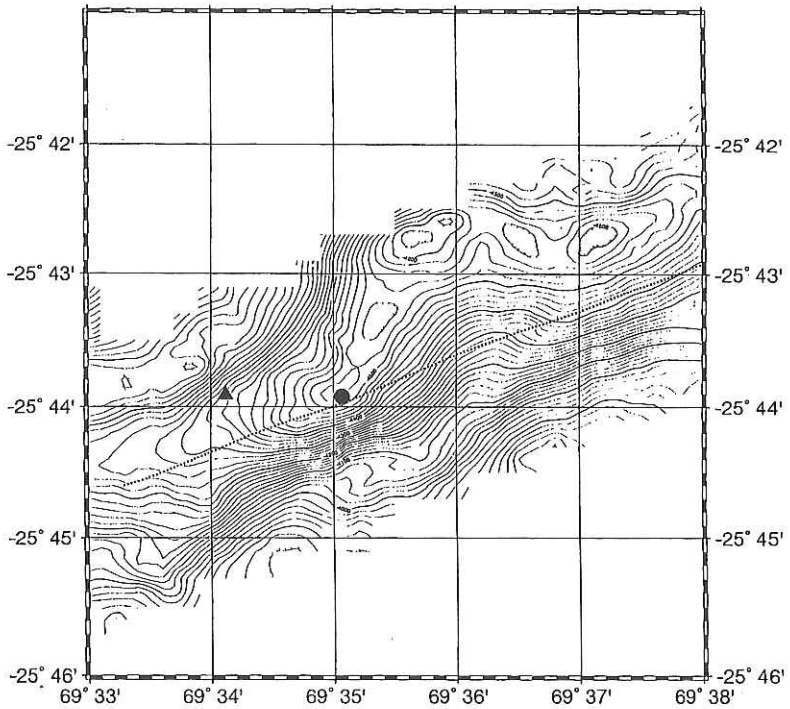

Fig. 4-2(a). Detailed maps of OBS position with topography. A circle and a triangle show the deployed and retrieved locations, respectively. Airgun shootings are shown by dots.

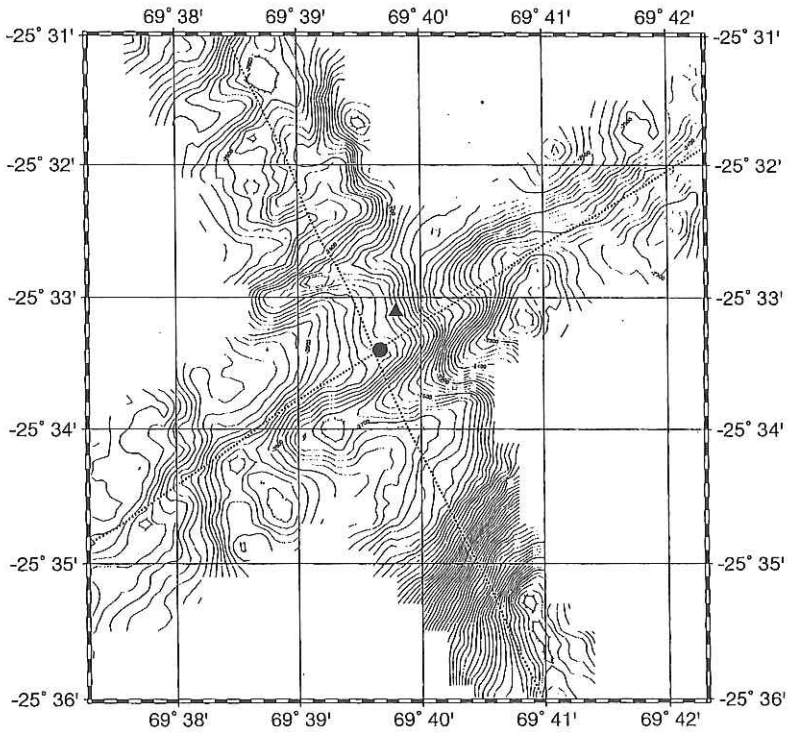

Fig. 4-2(b). Detailed maps of OBS position with topography. A circle and a triangle show the deployed and retrieved locations, respectively. Airgun shootings are shown by dots.

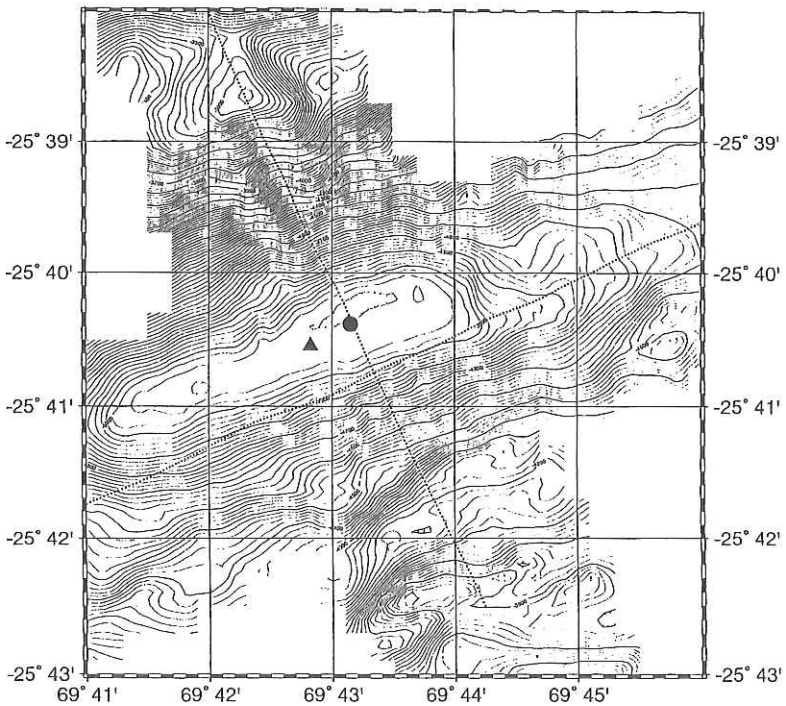

Fig. 4-2(c). Detailed maps of OBS position with topography. A circle and a triangle show the deployed and retrieved locations, respectively. Airgun shootings are shown by dots.

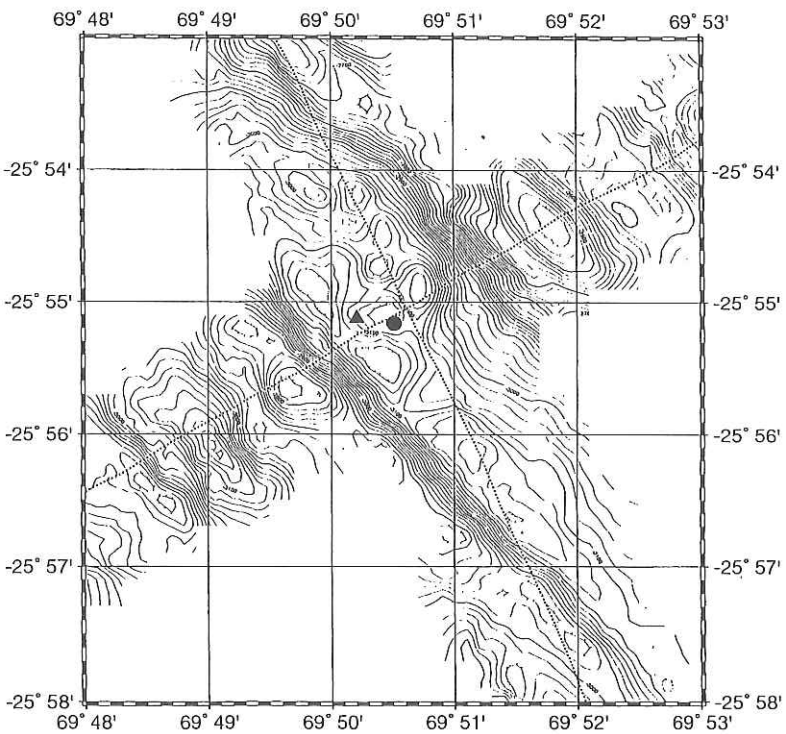

Fig. 4-2(d). Detailed maps of OBS position with topography. A circle and a triangle show the deployed and retrieved locations, respectively. Airgun shootings are shown by dots.

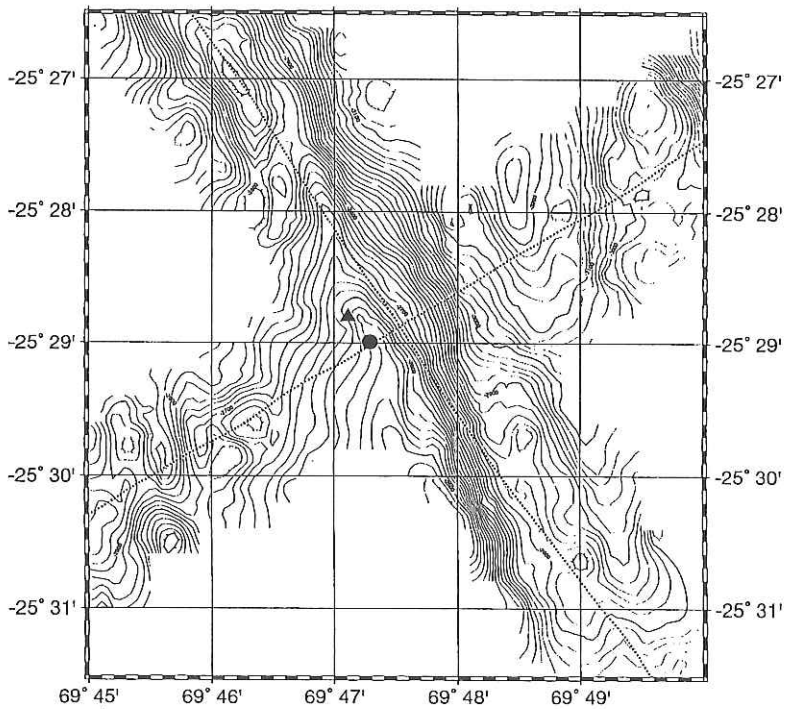

Fig. 4-2(e). Detailed maps of OBS position with topography. A circle and a triangle show the deployed and retrieved locations, respectively. Airgun shootings are shown by dots.

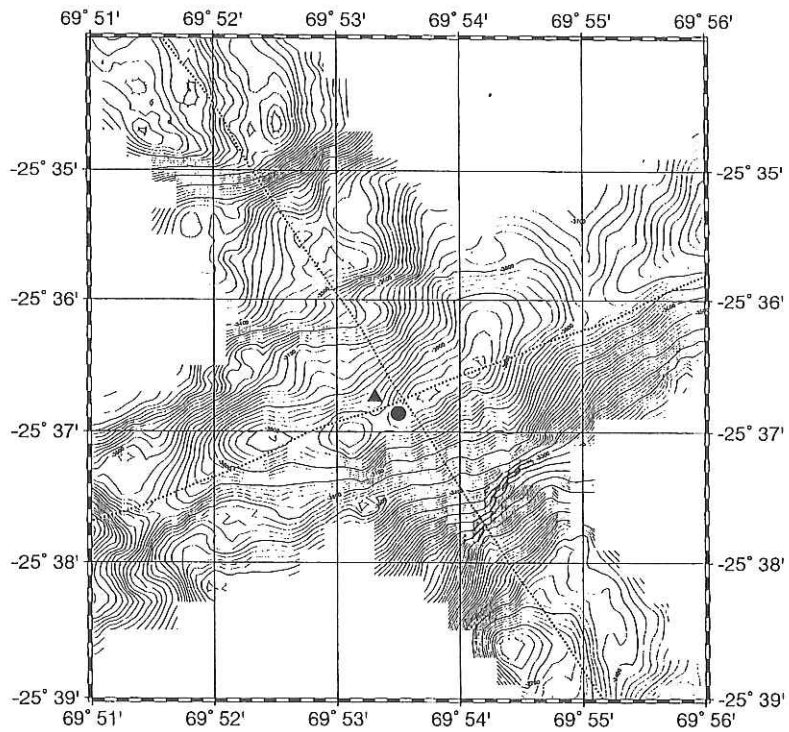

Fig. 4-2(f). Detailed maps of OBS position with topography. A circle and a triangle show the deployed and retrieved locations, respectively. Airgun shootings are shown by dots.

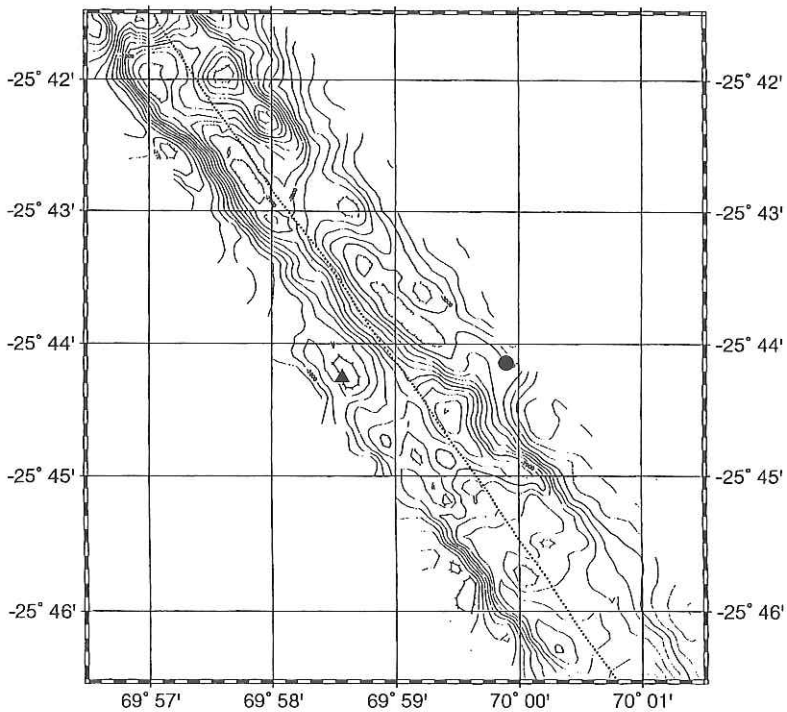

Fig. 4-2(g). Detailed maps of OBS position with topography. A circle and a triangle show the deployed and retrieved locations, respectively. Airgun shootings are shown by dots.

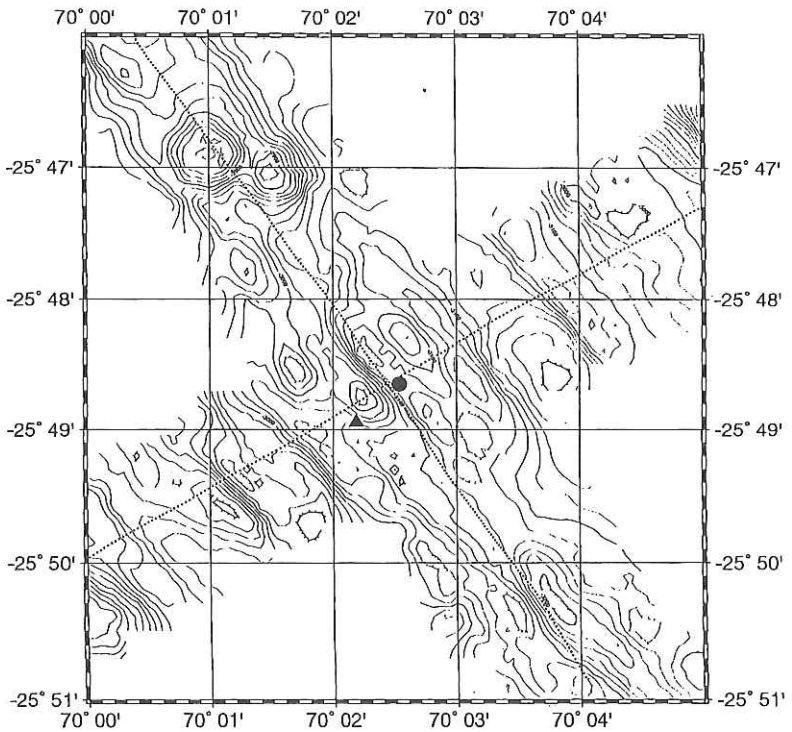

Fig. 4-2(h). Detailed maps of OBS position with topography. A circle and a triangle show the deployed and retrieved locations, respectively. Airgun shootings are shown by dots.

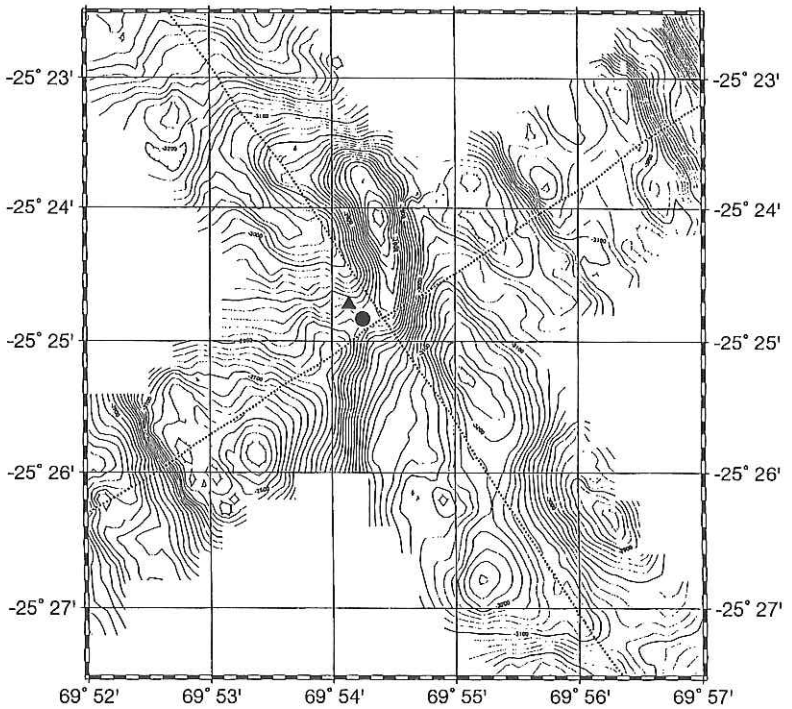

Fig. 4-2(i). Detailed maps of OBS position with topography. A circle and a triangle show the deployed and retrieved locations, respectively. Airgun shootings are shown by dots.

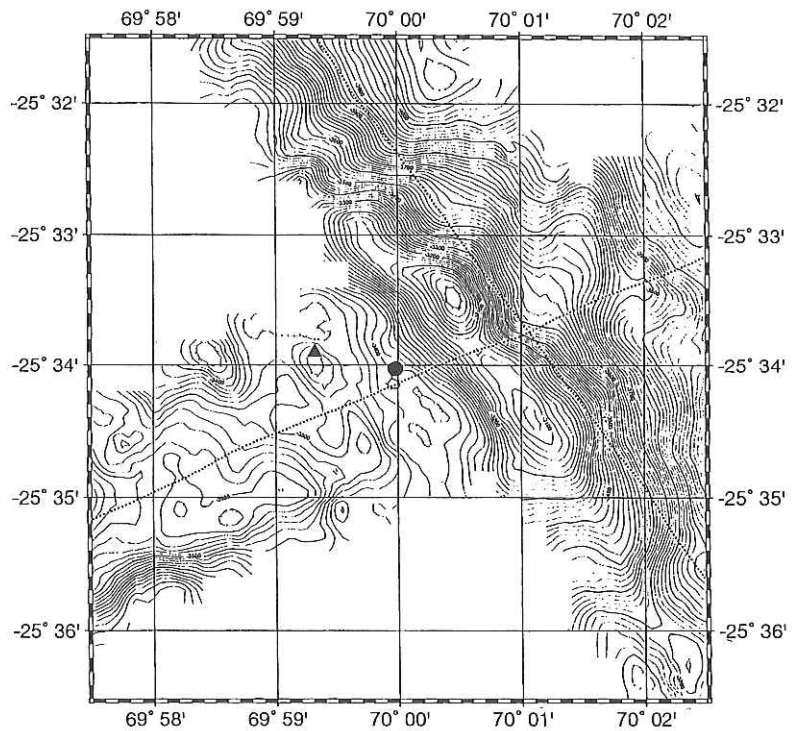

Fig. 4-2(j). Detailed maps of OBS position with topography. A circle and a triangle show the deployed and retrieved locations, respectively. Airgun shootings are shown by dots.

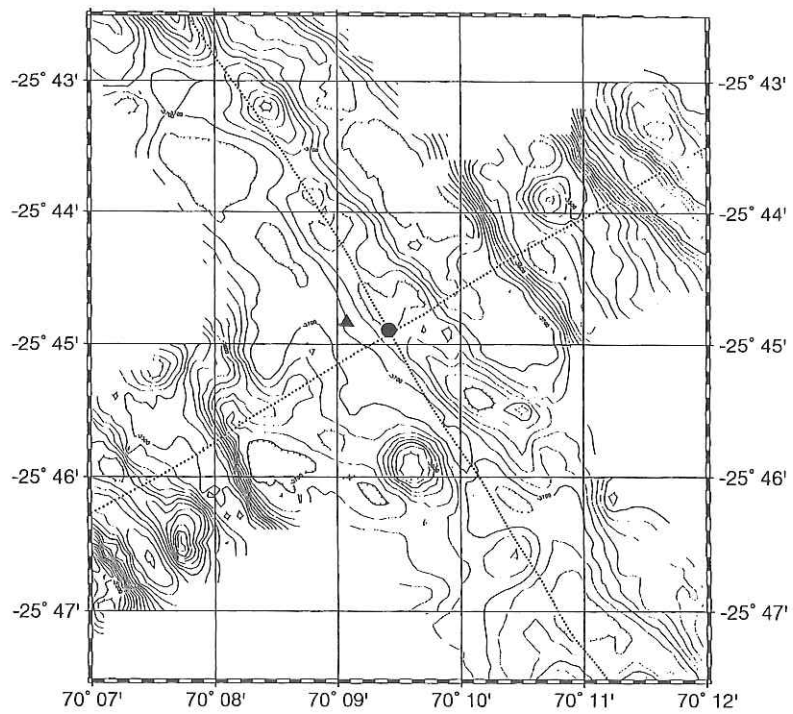

Fig. 4-2(k). Detailed maps of OBS position with topography. A circle and a triangle show the deployed and retrieved locations, respectively. Airgun shootings are shown by dots.

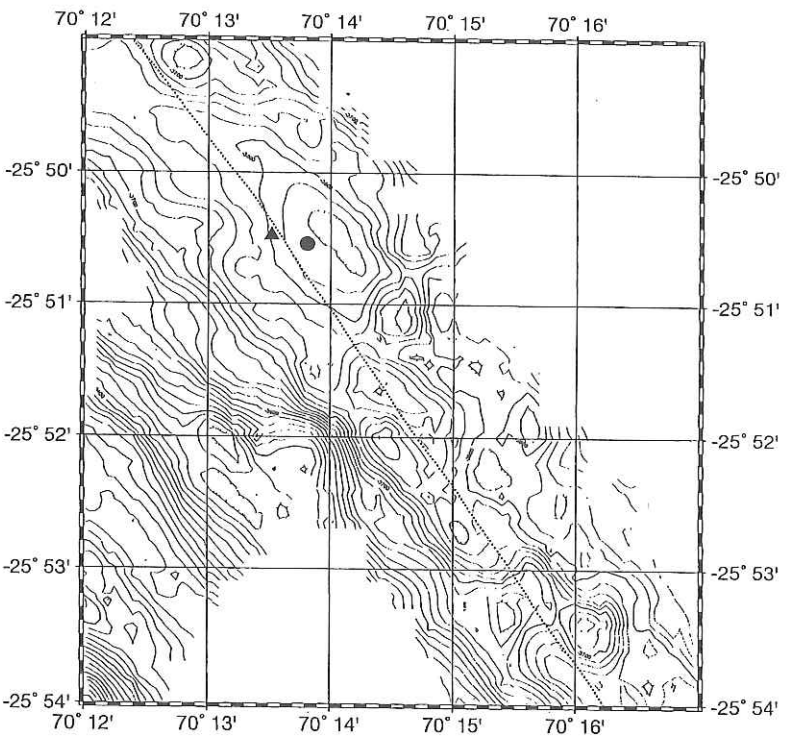

Fig..4-2(l). Detailed maps of OBS position with topography. A circle and a triangle show the deployed and retrieved locations, respectively. Airgun shootings are shown by dots.

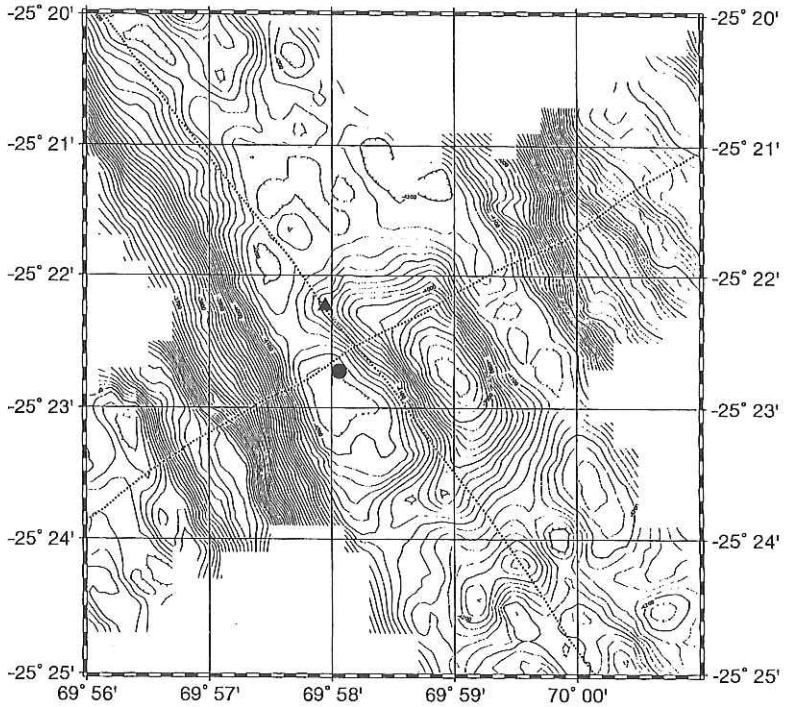

Fig. 4-2(m). Detailed maps of OBS position with topography. A circle and a triangle show the deployed and retrieved locations, respectively. Airgun shootings are shown by dots.

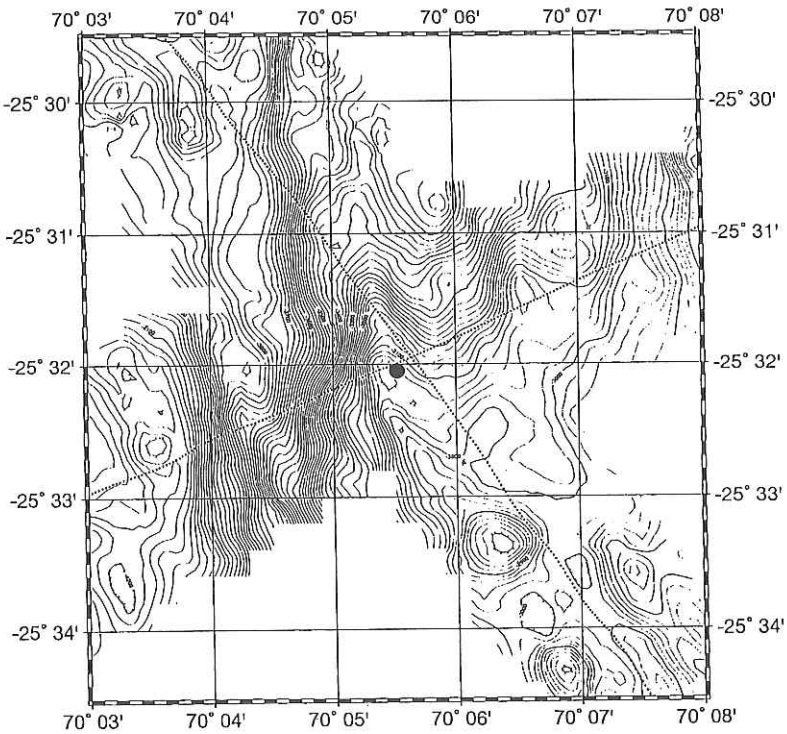

Fig. 4-2(n). Detailed maps of OBS position with topography. A circle and a triangle show the deployed and retrieved locations, respectively. Airgun shootings are shown by dots.

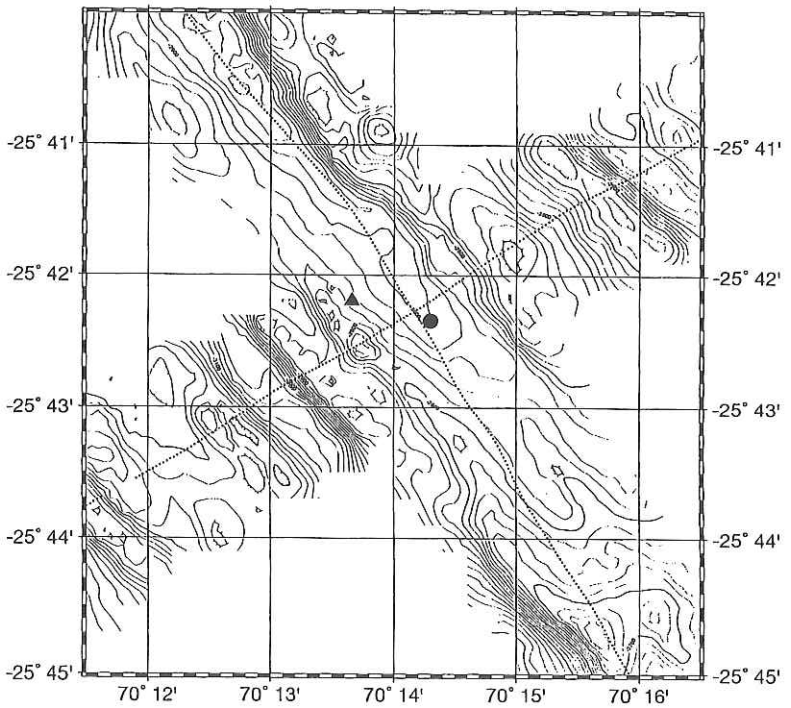

Fig. 4-2(o). Detailed maps of OBS position with topography. A circle and a triangle show the deployed and retrieved locations, respectively. Airgun shootings are shown by dots.

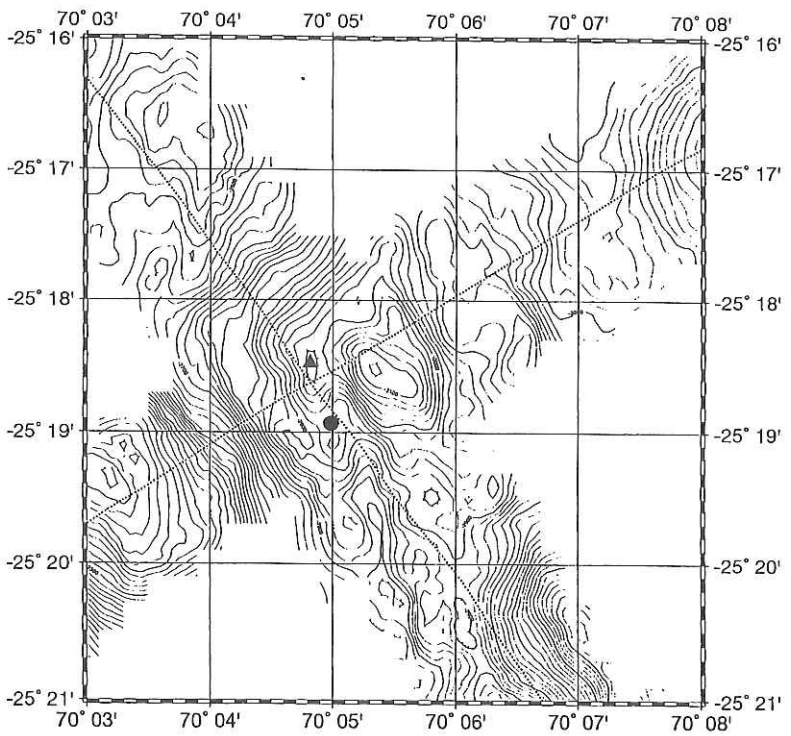

Fig. 4-2(p). Detailed maps of OBS position with topography. A circle and a triangle show the deployed and retrieved locations, respectively. Airgun shootings are shown by dots.

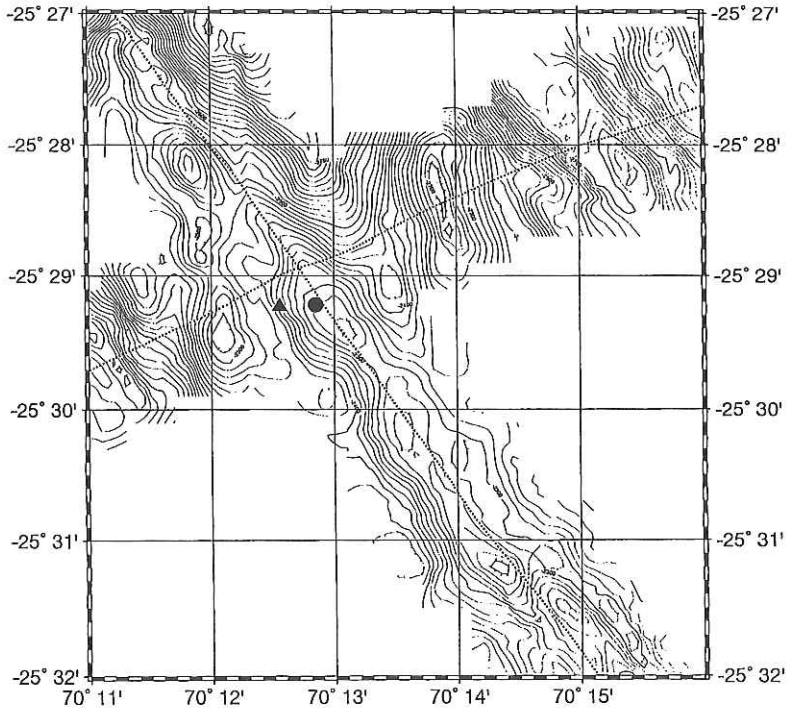

Fig. 4-2(q). Detailed maps of OBS position with topography. A circle and a triangle show the deployed and retrieved locations, respectively. Airgun shootings are shown by dots.

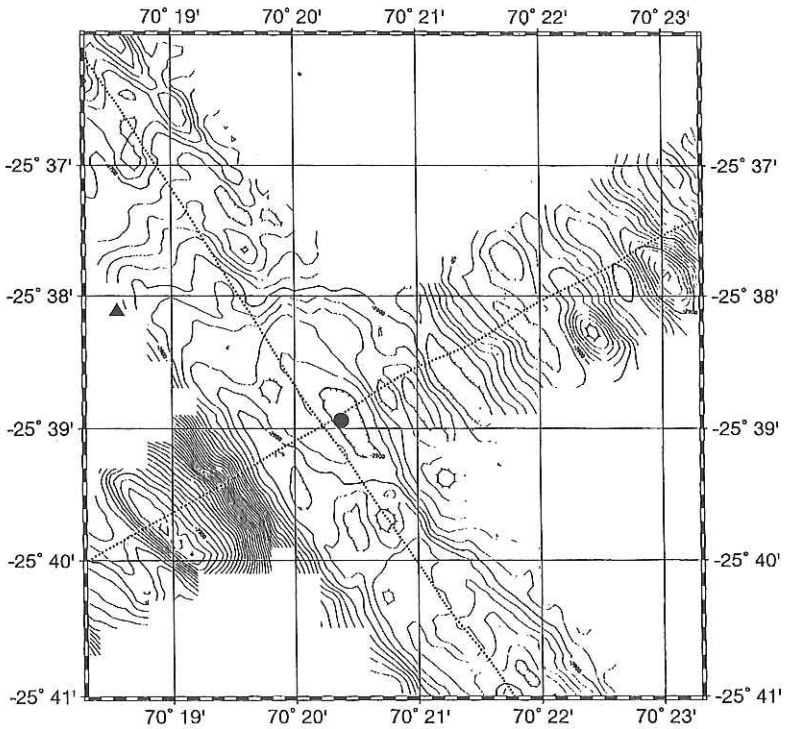

Fig. 4-2(r). Detailed maps of OBS position with topography. A circle and a triangle show the deployed and retrieved locations, respectively. Airgun shootings are shown by dots.

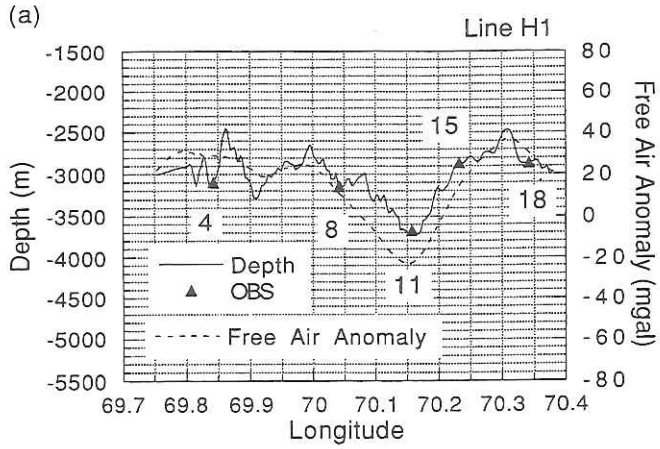

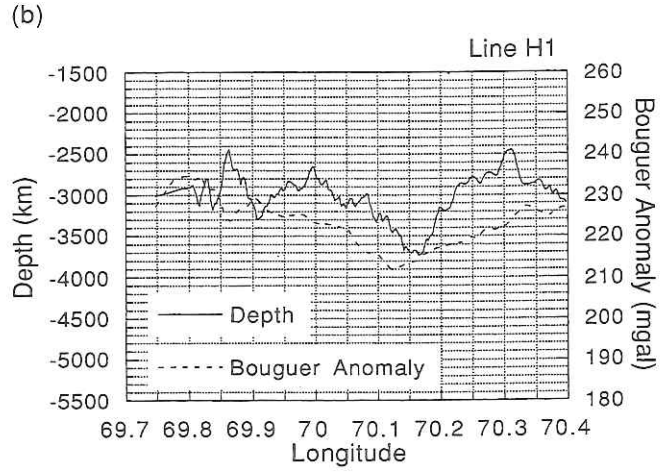

Fig. 4-3. Profiles of topography and gravity anomaly for Line H1.
(a) Depth and free air gravity anomaly.
(b) Depth and Bouguer anomaly where a density of 2.67 g cm^{-3} is assumed.

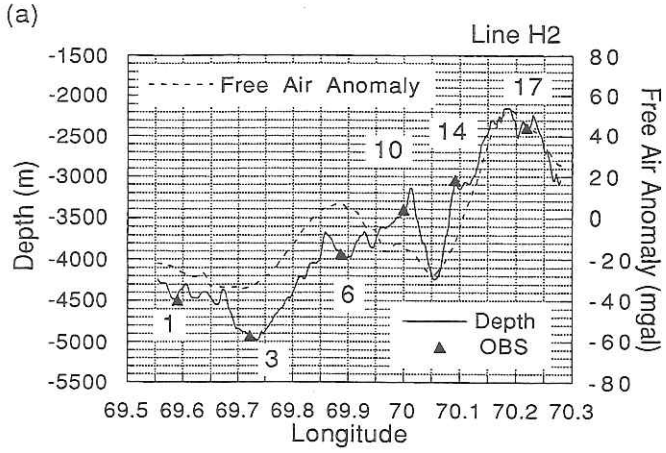

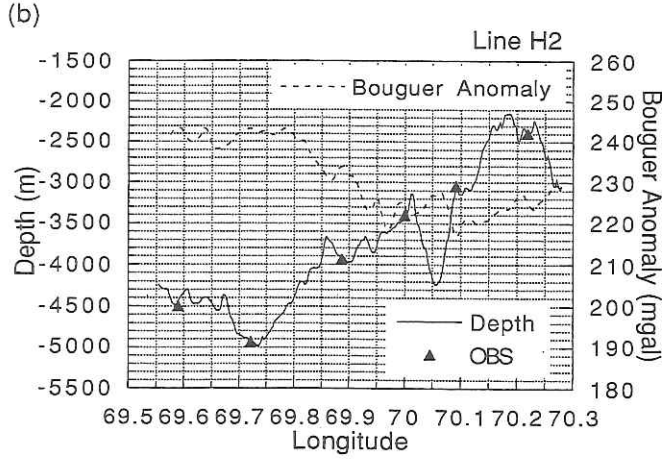

Fig. 4-4. Profiles of topography and gravity anomaly for Line H2.
(a) Depth and free air gravity anomaly.
(b) Depth and Bouguer anomaly where a density of 2.67 g cm^{-3} is assumed.

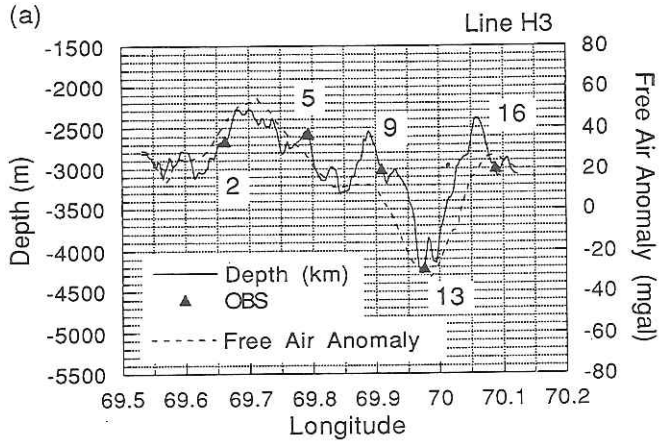

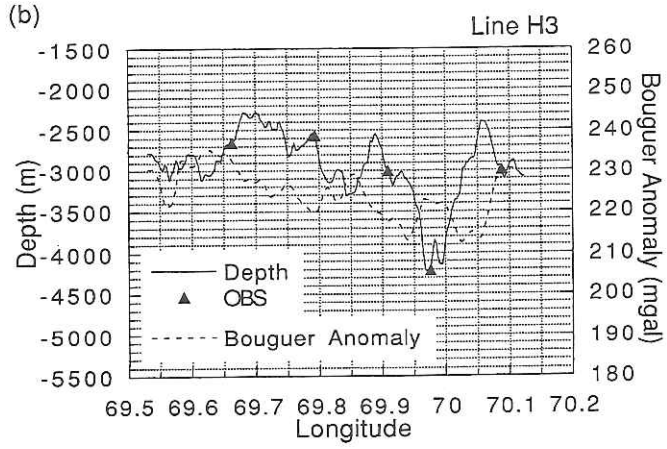

Fig. 4-5. Profiles of topography and gravity anomaly for Line H3.
(a) Depth and free air gravity anomaly.
(b) Depth and Bouguer anomaly where a density of 2.67 g cm^{-3} is assumed.

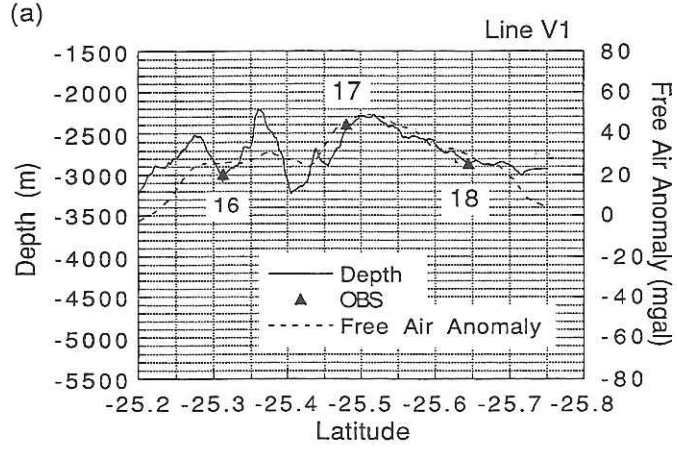

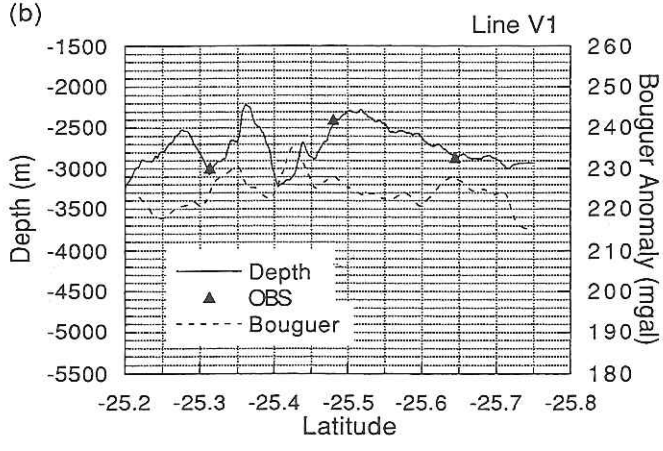

Fig. 4-6. Profiles of topography and gravity anomaly for Line V1.
(a) Depth and free air gravity anomaly.
(b) Depth and Bouguer anomaly where a density of 2.67 g cm^{-3} is assumed.

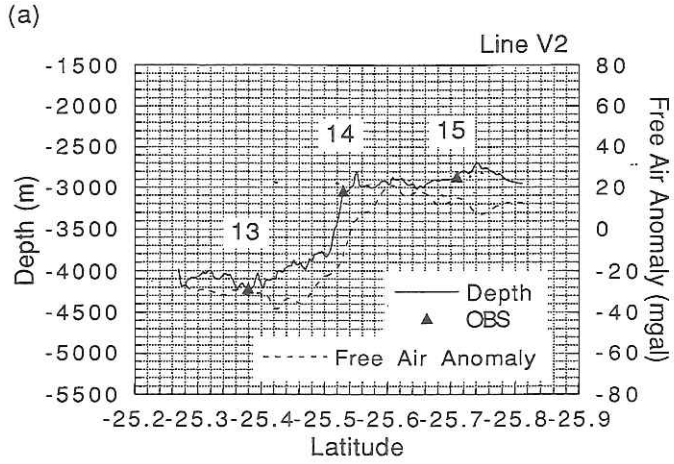

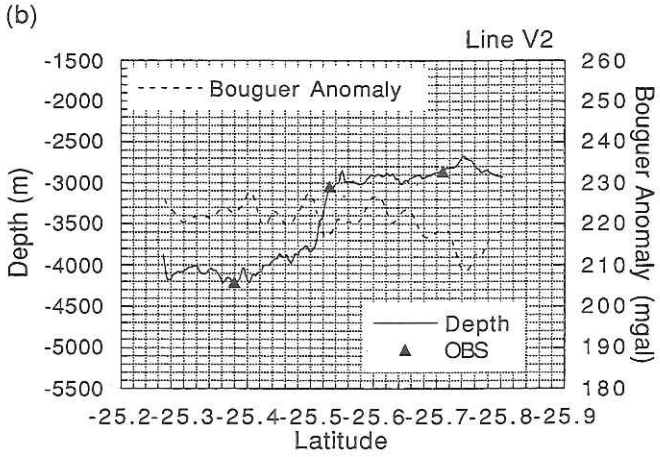

Fig. 4-7. Profiles of topography and gravity anomaly for Line V2.
(a) Depth and free air gravity anomaly.
(b) Depth and Bouguer anomaly where a density of 2.67 g cm^{-3} is assumed.

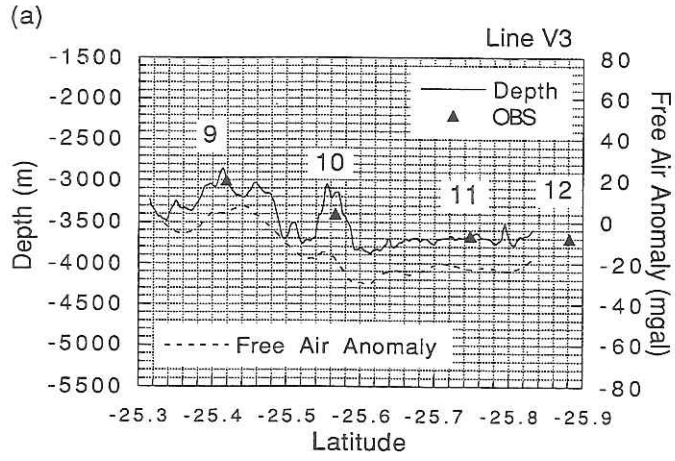

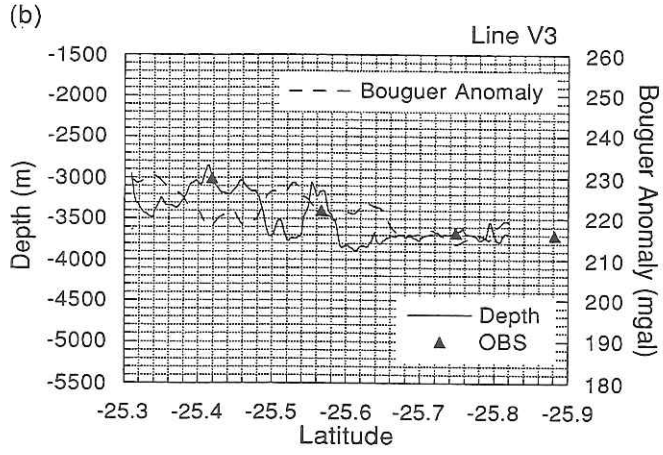

Fig. 4-8. Profiles of topography and gravity anomaly for Line V3.
(a) Depth and free air gravity anomaly.
(b) Depth and Bouguer anomaly where a density of 2.67 g cm^{-3} is assume.

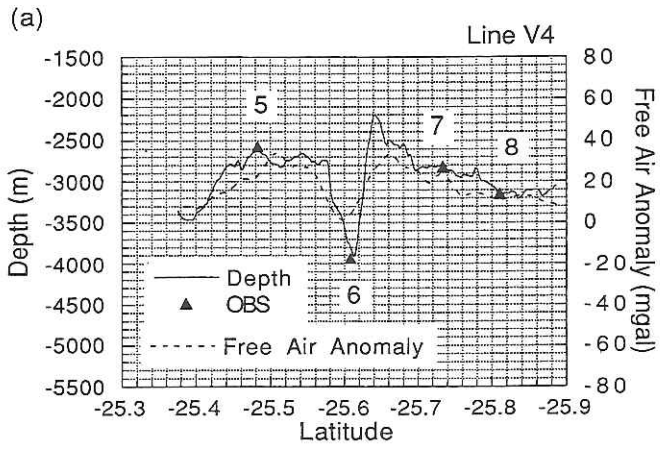

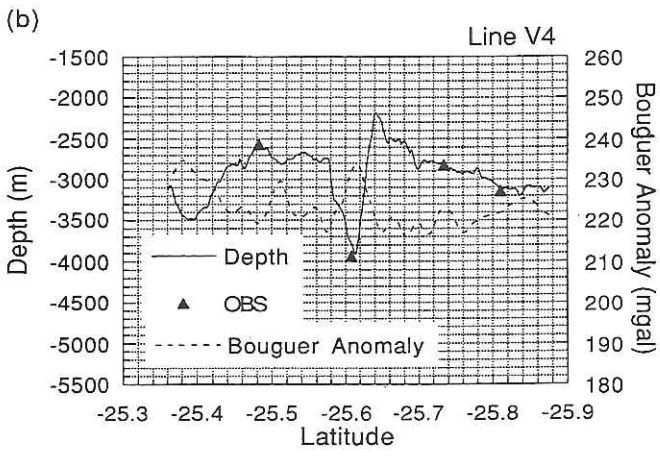

Fig. 4-9. Profiles of topography and gravity anomaly for Line V4.
(a) Depth and free air gravity anomaly.
(b) Depth and Bouguer anomaly where a density of 2.67 g cm^{-3} is assumed.

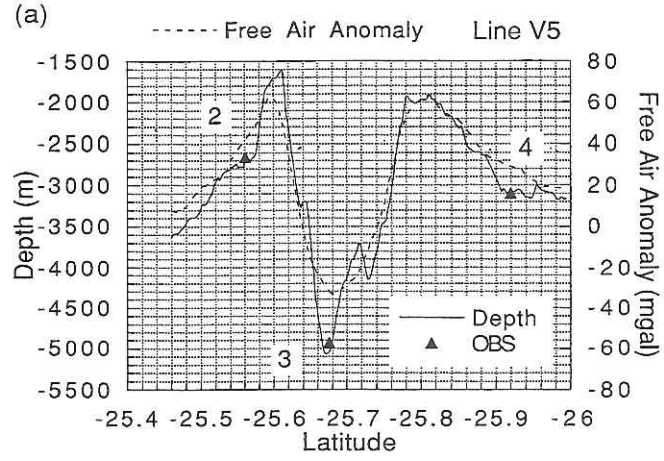

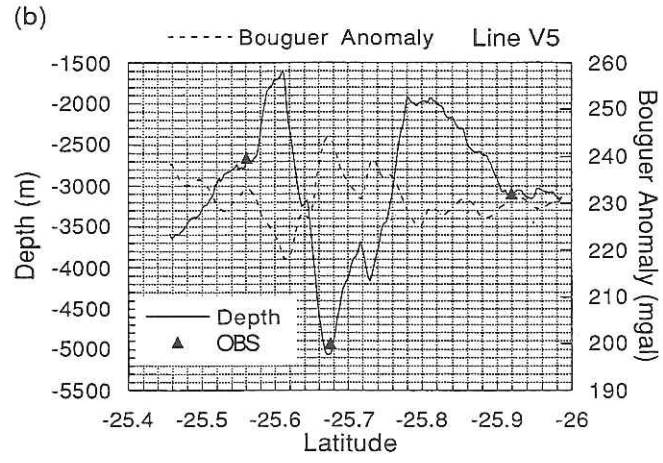

Fig. 4-10. Profiles of topography and gravity anomaly for Line V5.
(a) Depth and free air gravity anomaly.
(b) Depth and Bouguer anomaly where a density of 2.67 g cm^{-3} is assumed.

(a)

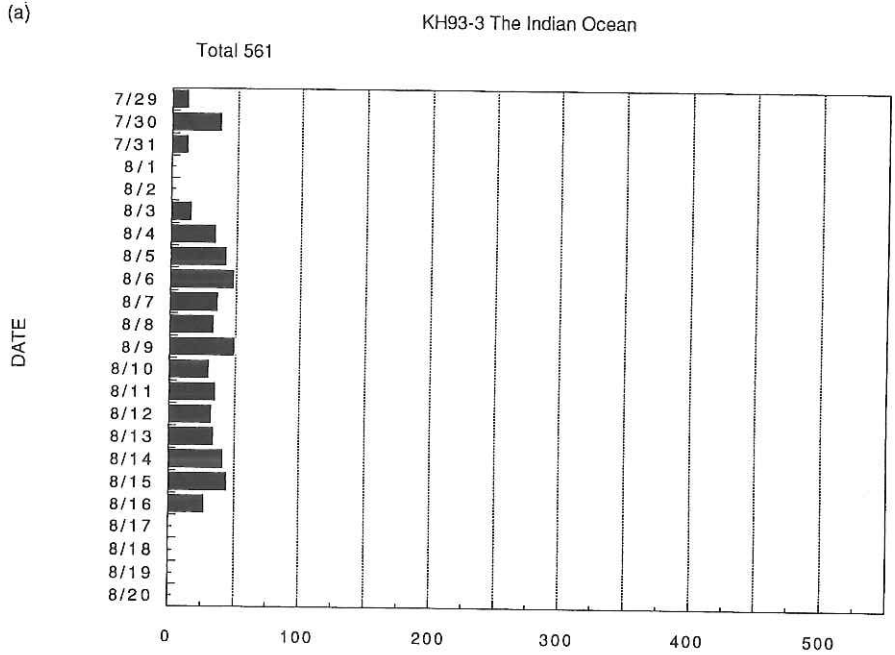

Fig. 4-11(a). Daily number of events. Events during airgun-shooting (7/31 600-8/3 930 GMT) are not included. The first and last days of each station are less than 24hrs.

(b)

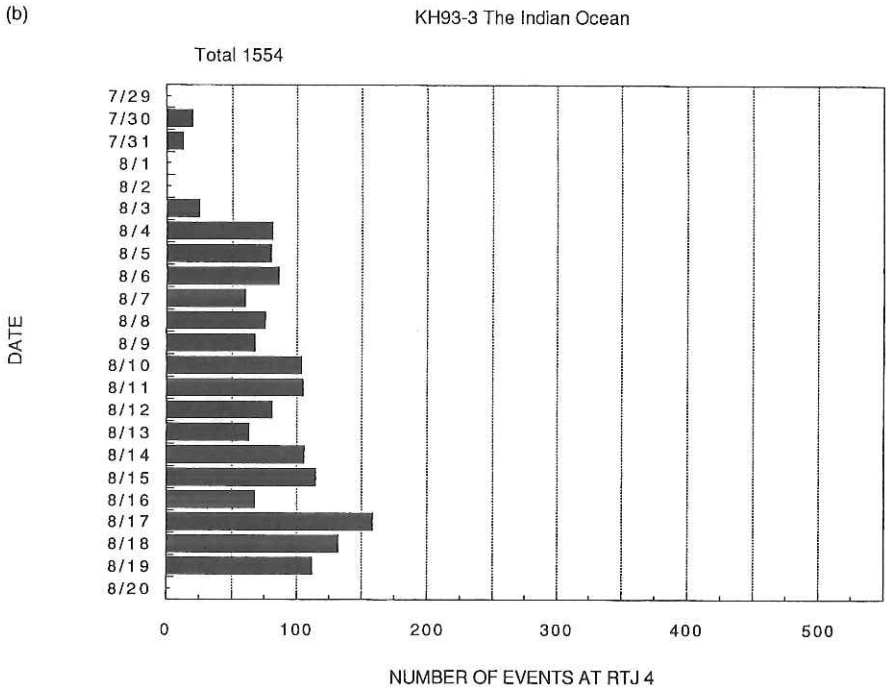

Fig. 4-11(b). Daily number of events. Events during airgun-shooting (7/31 600-8/3 930 GMT) are not included. The first and last days of each station are less than 24hrs.

(c)

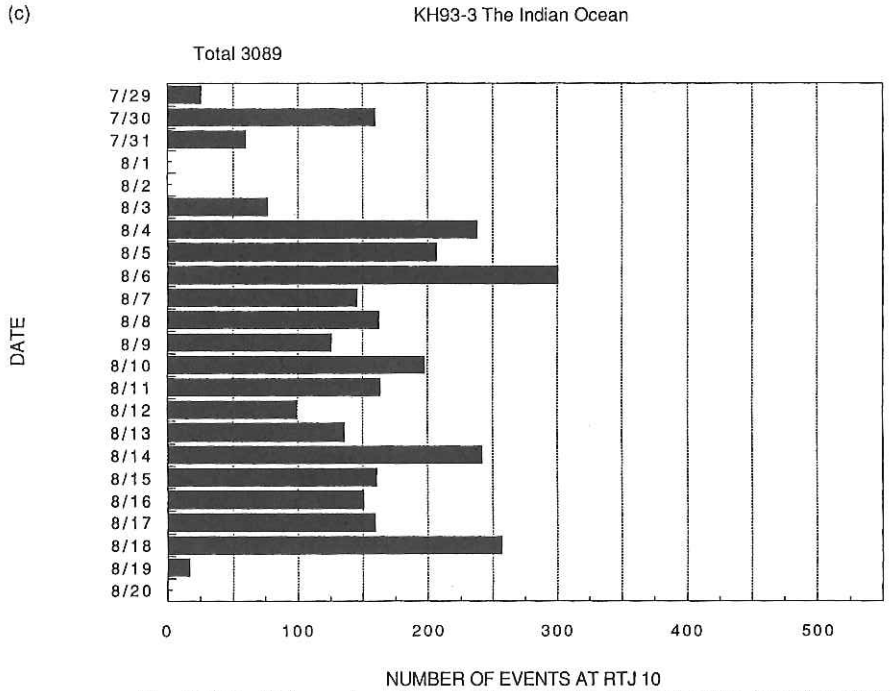

Fig. 4-11(c). Daily number of events. Events during airgun-shooting (7/31 600-8/3 930 GMT) are not included. The first and last days of each station are less than 24hrs.

(d)

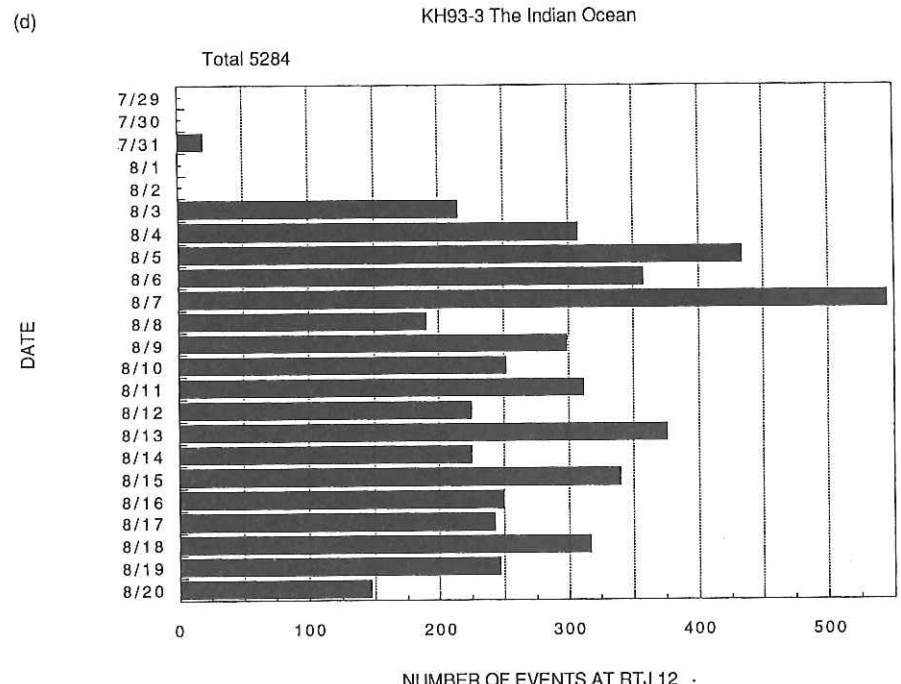

Fig. 4-11(d). Daily number of events. Events during airgun-shooting (7/31 600-8/3 930 GMT) are not included. The first and last days of each station are less than 24hrs.

(e)

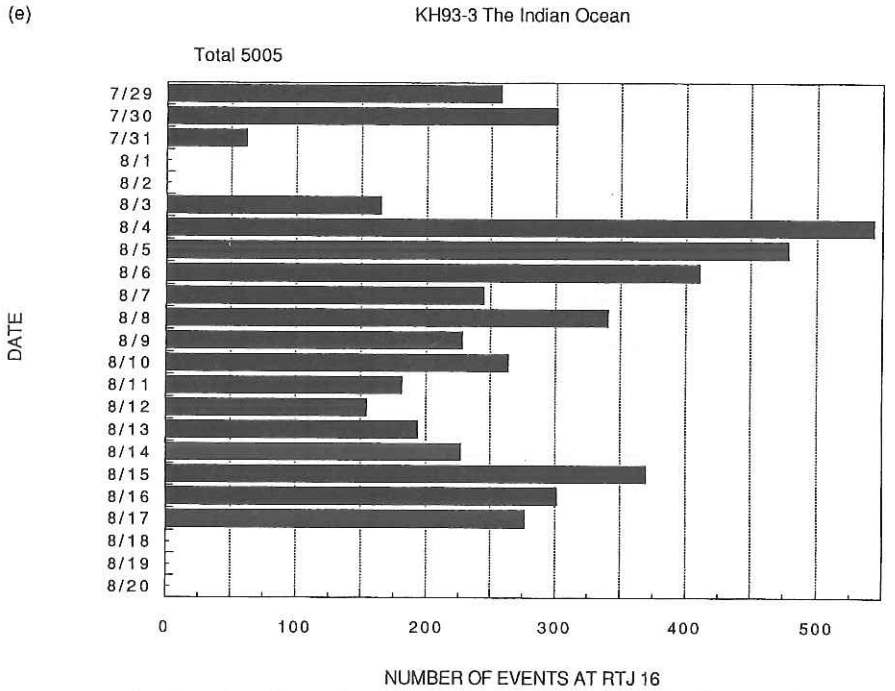

Fig. 4-11(e). Daily number of events. Events during airgun-shooting (7/31 600-8/3 930 GMT) are not included. The first and last days of each station are less than 24hrs.

(f)

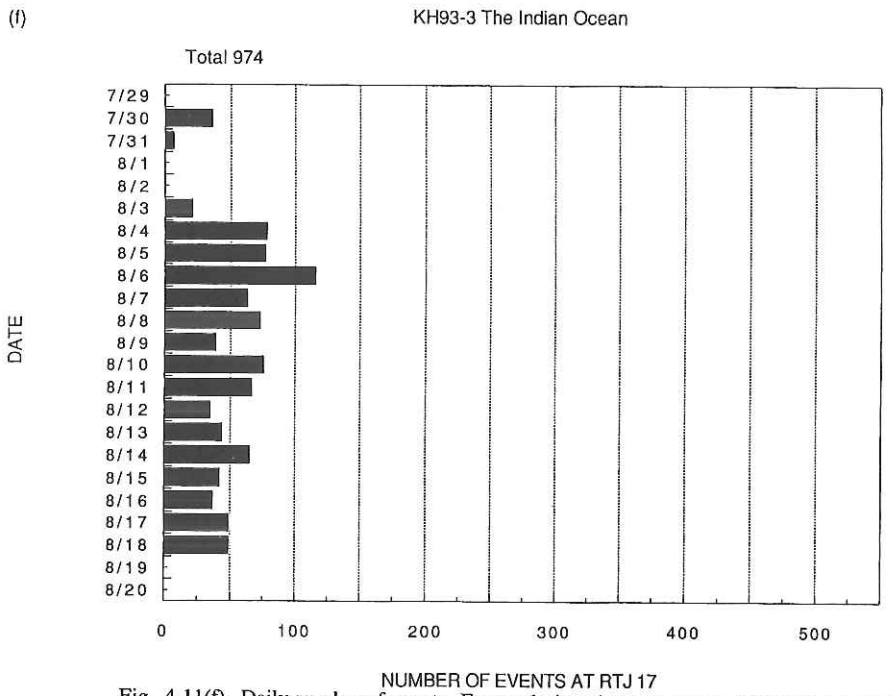

Fig. 4-11(f). Daily number of events. Events during airgun-shooting (7/31 600-8/3 930 GMT) are not included. The first and last days of each station are less than 24hrs.

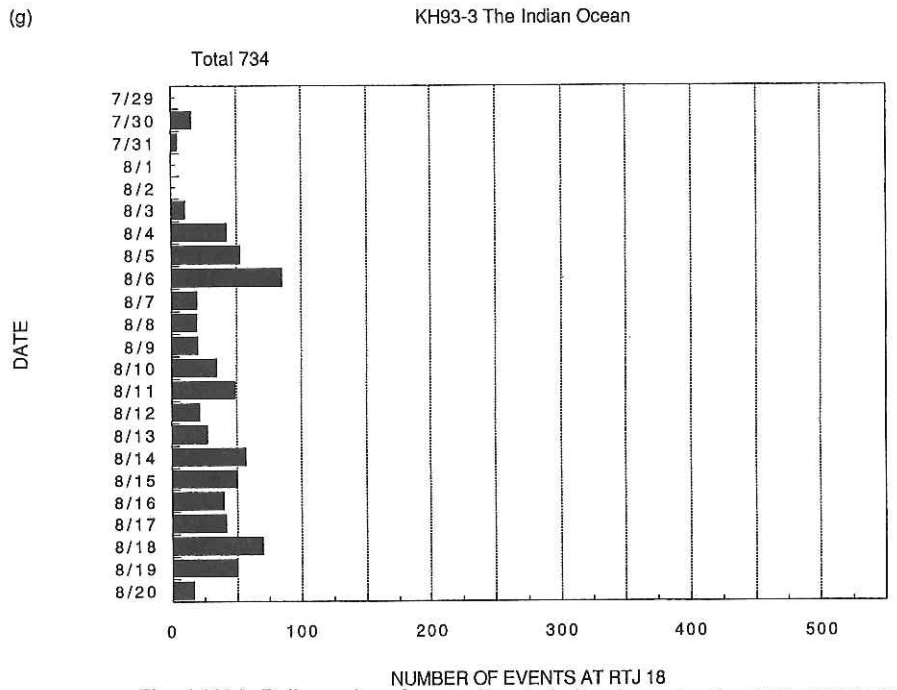

Fig. 4-11(g). Daily number of events. Events during airgun-shooting (7/31 600-8/3 930 GMT) are not included. The first and last days of each station are less than 24hrs.

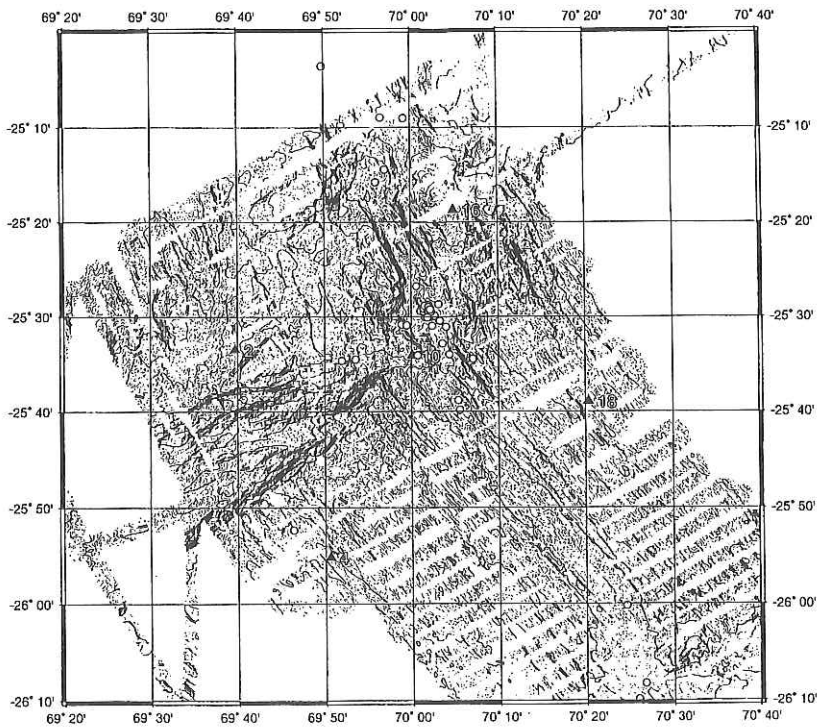

Fig. 4-12. Epicenter distributions. Events are indicated by open circles. The OBSs used for estimation are indicated by triangles.

5. Petrological sampling at the Rodriguez Triple Junction in the Indian Ocean

Toshitsugu FUJII[1], Shigeru YAMASHITA[1], Teruaki ISHII[2], Yoshiaki TAINOSHO[3], Charles H. LANGMUIR[4], Setsuya NAKADA[5], Satoshi MATSUMOTO[6], Yasushi HARADA[7], Narumi TAKAHASHI[8], and Kei HIROSE[9]

[1]*Earthquake Research Institute, University of Tokyo*
[2]*Ocean Research Institute, University of Tokyo*
[3]*Faculty of Human Development, Kobe University*
[4]*Lamont Doherty Earth Observatory, Columbia University, U.S.A.*
[5]*Department of Earth and Planetary Sciences, Faculty of Science, Kyushu University*
[6]*Department of Geology, Osaka City University*
[7]*Department of Earth and Planetary Physics, University of Tokyo*
[8]*Department of Earth Science, Faculty of Science, Chiba University*
[9]*Geological Institute, University of Tokyo*

1. Objective

The Rodriguez Triple Junction is one of the best exposed R-R-R triple junctions, which has been controlling the evolution of the major portion of the Indian Ocean. The three ridges with different spreading rates, the Central Indian Ridge, Southwest Indian Ridge, and the Southeast Indian Ridge, meet at the junction, and the topographic features of the three rift valleys are quite different, suggesting either the difference in the thermal structure of the mantle beneath each ridge or the difference in the crustal thickness.

The main purpose of our petrology group is to clarify the thermal structure of the mantle beneath each ridge system from the nature of magmas and to understand the relationship between the spreading rate and the thermal structure of the upper mantle. It is also expected that the thermal condition of the mantle just beneath the triple junction could be different from those of any normal ridges, and it must be reflected on the composition of magmas released at the triple junction. Therefore, our sampling strategy is designed to recover the most recent volcanic rocks at or near the junction and from the typical portions of the three different ridges. The sampling from the typical portion of a ridge system should cover at least a whole range of a single segment because intra-segment variation could be expected. To make the above-mentioned comparative study of the different ridges, it is necessary to have samples representing the present-day ridge system. For this purpose, samples from the very point of the spreading center, i.e., samples from the neo-volcanic zone are desired. The Rock Core sampling could be the most suitable method for this purpose because the samples recovered by this method represent those from a pin point. Even when the dredge haul is suitable to get samples rather than the Rock Core, only short distance of on-bottom dredge haul is planned to certify the location of the samples represents the neo-volcanic zone, and to exclude samples from the surrounding older portion.

Based on this strategy, several tens of locations were selected as the sampling sites. Most of the locations represent the summit areas of submarine volcanoes (approximately 100-200 m high and several miles diameter) of the neo-volcanic zone within the rift valley, and some represent the saddles between submarine volcanoes, which may represent the most recent

spreading center.

The locations of dredge haul or Rock Core sampling were showin in Figures 1 and 2, and listed in Table 1. Among the attempted 41 locations, we have recovered fresh basalt at 23 sites (11 of Dredge and 12 of Rock Core). Brief descriptions of the recovered samples are given in Tables 2 and 3.

2. Instrumentation of rock sampling and operation

Dredge system used in this cruise consists of a main chain bag dredge, and two pipe dredges with different sizes and weights. These are connected with a heavy chain (16 mm diameter and 10 m long); chain bag at the end and two pipes in the middle. The top of the heavy chain was weighted with approximately 200 kg of iron. A pinger was set on wire 40 m above the heavy chain top, 51 m above the main bag. The main chain bag dredge has iron mouse (60 cm wide, 45 cm high, and 20 cm deep), iron bucket (60 cm wide, 26 cm high, and 50 cm deep), and fish-netting chain (80 cm long with meshes of 6 x 4 cm) between the mouse and box. Fish-netting chain has small shackles, designed to be opened when rocks are taken out. Iron and stainless pipe dredges have sizes of 50 cm long with diameter of 26 cm (60 kg), and 60 cm long with diameter of 16 cm (50 kg), respectively. Total weight of the dredge system including chain and pipes reaches 400 kg.

Rock coring technique was initiated at the EPR, Venture Leg. 1, and the MAR, Atlantis II 127 legs (Langmuir et al., 1992). Rock Core used here has the weight of 250 kg in Leg 2 (350 kg in Leg 3). A large stainless disc with diameter of 25 cm was set at the head of 1.4 m-long, 10 cm-across stainless pipe, and four lead-plates of 200 kg in Leg 2 (6 plates of 300 kg in Leg 3) was in the middle. The stainless head are partitioned into 8 sectors and a center hole (each 8 cm deep), all open to the head surface. Wax was attached as thick as a few cm on the head. Wax was also attached outside of the stainless disc. A stainless collar (belt) with 19 cylinder pipes (each 5 cm long with 4.5 cm diameter) was set surrounding the lead-plate in the middle of Rock Core. Collar pipes are removable for sample treatment and were designated to be set perpendicular to Rock Core axis. Collar pipes were designed to catch glass chips when Rock Core lies down after hitting rock surface with the head. The upper half of the collar pipe was filled with wax. A small hole was made through the center of every wax parts in the head and pipes in order to trap glass tips and sediment inside with sea-water. Pinger was installed 50 m above Rock Core.

After Rock Core returned to deck, the head and collar pipes were detatched. We assessed carefully whether they certainly hit the bottom or not. When the head and pipes have glass, rock pieces, or sediments on and in wax, the pieces or sediments were scratched out with wax. New wax was attached on the remaining wax in the head and collar pipes. Or else, wax should be replaced wholly; we found out a few gram of glasses or sediments behind wax at several sites, which probaby flowed in through the hole digged in wax. During this cruise, however, we did not have enough time to replace whole wax before arriving the next target site, so that we did not recover glasses and sediments behinde wax.

Wax including glass and rock pieces was put into a glass beaker with water to be soaked with a boiled water; glass beaker was put in a micro-wave oven for five to ten minutes. Boiling was a way to clean up waxed samples; glass and rock pieces sink into the beaker bottom and wax floats. The beaker was put into supersonic-wave washing bath after boiling for complete separation of samples from wax.

3. Procedure of onboard sample classification

Dredged samples from each location were classified into several groups based on the macroscopic features; degree of alteration, phenocryst assemblage, morphology of lava etc. At least one sample (usually several samples) was selected from each group, labeled (A-1,A-2, B-1, B-2,...) and described in macroscopically detail. These selected samples were treated as "working samples", stored in the Earthquake Research Institute and/or Ocean Research Institute, University of Tokyo (Table 4). If any glass portion was preserved, glass chips are separated for the future analyses; the chips labeled with G code at the end of the sample numbers. If sample was wholly glassy such as glass rind of pillow, it was directly labeled with G code. These G samples are also "working samples", and stored in the Earthquake Research Institute.

Rock Core samples were taken out from wax carefully, repeatedly soaking in hot water. All glass chips recovered with Rock Core were treated as "working samples". Chips in wax attached to the Rock Core head was labeled with H code, while the collar pipes with C code. The average weight of glass or rock chips recovered with Rock Core is 21 g; the maximum is 60 g. All Rock Core samples stored in the Earthquake Research Institute (Table 5)

4. Description of recovered samples

Fresh glassy basalts were discovered from the summit of volcanic cones running along the ridge axis and saddle between two cones except SWIR. Mn-coated basalts with glassy rinds (relatively young) were recovered from off-axis volcanic cones (DR9, 15, and 18) in RTJ. From SWIR, relatively young basalts with glass rinds were dredged together with strongly altered (weakly metamorphosed) intrusive/extrusive rocks (DR10). Strongly altered extrusive/intrusive rocks were also found at two other sites in SWIR (DR11 and 18) and at two sites in RTJ (DR9 and 8). Serpentinite pebbles were dredged at DR5. Thickly Mn-coated basalts without glassy rinds (relatively old, slightly altered basalts) were also recovered from SWIR (DR12, 13, and 14). At a saddle on the eastern extension of SWIR valley (DR17), volcanic sand and cobbles of lava were dredged. No or few recovery with dredge haul was at the sites DR26 and 27 in RTJ, and DR22 in SEIR. Only mudy sediment was dredged at DR22 in SEIR. The peak at DR22 may not be volcanic cone but a tectonic peak at a transform zone between the first and second segments in SEIR. No recovery of basalt glass with Rock Core was at two sites, RC8 and RC10. Manganese particles, approximately 2 g, were attached on the surface of wax. However, it is difficult to say that these sites are inactive.

Basaltic glasses are commonly plagiolcase porphyritic. Olivine phenocryst also occurs in some specimens. Glassy rinds of pillows commonly have wavy surface and small protrusions like tears. Several film layers of reddish brown-colored oxidation ("rust") develop in vitric rind, up to a few cm inside of pillows. Exfoliation, up to a few mm thick, sometimes occurs along the oxidation film; the exfoliated surface is not glassy but rugged. Hydrothermally alteration occurs partly inside of pillow, even in fresh basalt. Crusts of hollowed pillows and sheet flows, approximately a few cm thick, were recovered. Walls between vacant chambers remain on the reverse side of the crust. The back surface is dark reddish, losing glassy luster. Glassy surface of pillow is sometimes coated with very thin layer of Mn, even in samples recovered from the active volcanic cones in SEIR and CIR.

5. Chemical features of the recovered samples

Glass chips separated from glassy rind of basalts dredged during Leg 2 were analyzed with EPMA of the Geological Institute, University of Tokyo. The analyzed samples do not cover whole the samples recovered during these legs, and the following discussions should be tentative. The chemical compositions of the glass chips are shown in Table 6. Each analysis represents one glass chip; three points were analyzed and the average was listed.

Basalt glasses analyzed here range in MgO contents from 7.2 wt.% to 8.8 wt.%. Basalt glasses from RTJ are less than 8.0 wt.% MgO, while those from SEIR and SWIR cover the wide range. Glasses from CIR are less than 8.5 wt.%, showing much scattering in MgO-variation diagrams (Figures 2 and 3). Two glass chips dredged at DR7 have the compositions extremely different from each other (7.2 and 8.8 wt.%). Assuming differentiation trends in MgO-diagrams, RTJ glasses are the most enriched in FeO* and TiO2, and the most impoverished in CaO and MgO. Samples in DR1 are most enriched in K_2O.

Basalts from SWIR are similar to those of SEIR and CIR. The basalts, dredged at DR10 where metamorphosed rocks were recovered together with them, have thin Mn-crust and show faint alteration. According to Price et al. (1986), basalt glasses from the active SWIR are more enriched in Al_2O_3 and Na_2O than those from RTJ, and poorer in FeO*. These facts probably indicate that the basalts dredged at DR10 are basalts formed by the old activity at SEIR and CIR. Volcanic activity of SWIR has not occurred yet in the segment nearest to RTJ.

The latitude-chemical composition plots (Figure 4), which show chemical variations along axis, reveal that MgO content of basalts decreases toward RTJ from both CIR and SEIR. Al_2O_3 content decreases in this way, while FeO* increases. These variations indicate that basalts in RTJ differentiated in higher degree than in SEIR and CIR. The manner of decreasing MgO contents toward the junction of two segments is similar to that shown in EPR by Sinton et al. (1991), where MgO contents decrease regularly toward the propagation head in a segment. More analyses of samples in this cruise will make the detailed chemical feature clear.

6. Summary

High-density rock-sampling around RTJ was attempted in order to clarify the thermal structure of mantle beneath RTJ, which controls the R-R-R type spreading. As a result, fresh glassy basalts were recovered from 23 sites among 41 sites. Relatively old basaltic rocks with relatively thick Mn-coat were recovered from the SWIR and the periphery of RTJ. Highly altered (weakly metamorphosed) basalts, dolerites, and gabbros were found along steep fault scarps in SWIR and RTJ. These metamorphosed igneous rocks probably represent the constituents of the oceanic crust once formed at the ancient SWIR/CIR.

Rock sampling results show that volcanism is active in both CIR and SEIR, while inactive in SWIR. Although neovolcanoes are also distributed in RTJ, tectonic movement in RTJ is complex such that crustal constituents and surpentinite expose on fault scarps. The propagation of CIR (in RTJ) against SEIR is associated with young volcanism. On the other hand, volcanism seems to have stopped on the northern extension of the ridge in SEIR (DR26). Volcanism has not occurred at the propagation terminate of SWIR against RTJ (DR17), where only splitting of oceanic crust has occurred.

Basalt glasses analyzed preliminarily range in MgO from 7.2 to 8.8 wt.%. Basalts in RTJ have differentiated composition in comparison with those in CIR and SEIR. A little older basalt glasses from SWIR have the composition similar to fresh glasses in CIR and SEIR.

REFERENCES

Langmuir, S. H., G. Klinkhammer, and H. Bougault, Evaluation of the relationships among segmentation, hydrothermal activity and petrological diversity on the Mid-Atlantic Ridge. Cruise report of FAZAR (R/V Atralntis II 127), Lamont-Doherty Geological Observatory of Columbia University, Technical Report No. LDGO-92-3, Palisades, New York, 1992.

Price, R.C., A.K. Kennedy, M. Riggs-Sneeringer, and F.A. Frey, Geochemistry of basalts from the Indian Ocean triple junction: implications for the generation and evolution of Indian Ocean ridge basalts. Earth Planet. Sci. Lett, 78, 379-396, 1986.

Shinton, J., S. Smaglik, and J. Mahoney, Magmatic processes at superfast spreading mid-Ocean Ridges: Glass compositional variations along the East Pacific Rise 13-23¡S. Jour. Geophys. Res., 96, 6133-6155, 1991.

Table 5-1. List of dredge haul and Rock Core sampling

		Time(GMT)	Position on bottom				Time(GMT)	Position off bottom			
Station ID	Day	on bottom	latitude(S)	longitude(E)	depth(m)	Wire out(m)	off bottom	latitude(S)	longitude(E)	depth(m)	Wire out(m)
DR1	7/29/93	8:05	25°22.87'	69°58.84'	3886	3930	8:57	25°22.02'	69°59.48'	4166	4045
DR2	7/30/93	21:55	25°33.21'	70°03.55'	4199	4220	22:44	25°33.56'	70°03.32'	4170	4170
DR3	8/4/93	1:55	25°14.11'	69°54.71'	4100		2:57	25°14.08'	69°54.48'	4086	
DR4	8/4/93	13:28	25°27.34'	69°59.65'	4170	4221	14:17	25°27.82'	69°59.88'	4171	4180
DR5	8/4/93	16:32	25°28.76'	69°59.99'	4260	4333	17:18	25°29.34'	70°00.17'	4170	4270
DR6	8/5/93	8:59	25°48.14'	70°13.21'	3604	3663	9:47	25°48.64'	70.13.52'	3682	3534
DR7	8/6/93	5:28	25°38.49'	70°03.97'	3753	3848	5:59	25°38.87'	70°04.21'	3788	3855
DR8	8/6/93	13:29	25°33.25'	70°00.62'	3227	3228	14:22	25°33.44'	69°59.97'	3200	2979
DR9	8/6/93	16:45	25°30.56'	70°01.65'	4050	4084	17:20	25°29.86'	70°01.60'	4111	3890
DR10	8/7/93	5:20	25°40.77'	69°42.04'	5047	5111	7:12	25°39.25'	69°41.34'	3446	4596
DR11	8/7/93	10:37	25°44.99'	69°35.80'	3397	3584	11:42	25°44.87'	69°35.60'	3800	3441
DR12	8/7/93	14:09	25°46.54'	69°38.96'	3700	3789	14:25	25°46.77'	69°39.09'	3849	3761
DR13	8/7/93	21:08	25°53.67'	69°22.36'	3926	3938	21:35	25°54.04'	69°22.32'	3997	3910
DR14	8/8/93	0:52	25°54.15'	69°14.82'	4018	4059	1:39	25°53.97'	69°13.99'	4015	4095
DR15	8/18/93	22:59	25°31.18'	70°00.74'	4042	4109	23:31	25°31.15'	70°00.39'	4104	4040
DR16	8/19/93	2:01	25°34.03'	69°59.29'	3404	3397	2:26	25°34.27'	69°59.06'	3496	3384
DR17	8/19/93	6:49	25°35.93'	69°55.15'	3773	3803	7:17	25°36.24'	69°54.74'	3864	3800
DR18	8/19/93	12:08	25°41.93'	69°40.26'	4436	4537	12:58	25°42.45'	69°40.60'	4439	4300
DR19	8/19/93	16:53	25°40.43'	69°43.03'	5062	5120	18:03	25°40.06'	69°43.75'	5039	5163
DR20	8/20/93	20:47	25°53.40'	70°17.61'	3680	3719	21:08	25°53.61'	70°17.83'	3755	3688
DR21	8/21/93	4:20	26°01.57'	70°23.80'	3706	3754	4:52	26°01.83'	70°24.01'	3798	3671
DR22	8/21/93	7:13	26°07.53'	70°24.59'	3824	3865	7:42	26°07.82'	70°24.79'	3874	3870
DR23	8/22/93	12:40	26°02.00'	71°18.65'	3722	3740	12:51	26°02.13'	71°18.76'	3876	3670
DR24	8/22/93	17:21	26°07.29'	70°48.44'	4133	4169	17:33	26°07.04'	70°48.36'	4204	4090
DR25	8/23/93	4:55	25°34.73'	70°03.37'	4261	4262	5:31	25°35.09'	70°03.66'	4280	4299
DR26	8/23/93	7:39	25°35.39'	70°00.62'	3399	3406	7:52	25°35.16'	70°00.92'	3501	3397
DR27	8/23/93	11:04	25°28.75'	69°59.95'	4306		12:20	25°27.37'	69°59.69'	4165	4558

		Time(GMT)	Position on bottom			
Station ID	Day	on bottom	latitude(S)	longitude(E)	depth(m)	Wire out (m)
RC1	7/29/93	5:27	25°23.92'	69°59.90'	4135	4068
RC2	7/30/93	5:52	25°45.42'	70°10.33'	3594	3640
RC3	7/31/93	2:40	25°45.42'	70°12.36'	3490	3496
RC4	8/3/93	18:57	25°19.89'	69°56.78'	3930	3952
RC5	8/3/93	23:11	25°17.40'	69°55.04'	3865	3920
RC6	8/4/93	10:51	25°27.24'	70°01.72'	3891	3898
RC7	8/4/93	0:29	25°41.87'	70°06.38'		3717
RC8	8/5/93	5:56	25°43.19'	70°08.41'		3620
RC9	8/6/93	8:29	25°38.23'	70°02.97'	3726	3763
RC10	8/6/93	10:56	25°36.55'	70°03.55'	3783	3775
RC11	8/20/93	14:24	25°47.86'	70°11.56'	3501	3483
RC12	8/20/93	18:24	25°51.09'	70°14.58'	3662	3702
RC13	8/20/93	23:09	25°54.26'	70°17.60'	3678	3655
RC14	8/21/93	1:40	25°57.10'	70°20.05'	3634	3769

Table 5-2. List of dredging sites and recovered materials

Station ID	Bottom signature	Recovery_materials	Recovery_amounts
DR1	Western slope of blocky seamount, axial volcanic zone of the first CIR segment	Fresh pillows and thin sheet flows with glassy rinds (aphyric); thin Mn and rust on the pieces; brownish mud attached on the rock surface	ca 100 kg
DR2	Axial deep, one of the miniature RTJ segments	Fresh glass pieces (sparsely Pl-phyric); thin Mn and rust on the pieces	a few tens kg
DR3	Flank of seamount, axial volcanic zone of the first CIR segment	Pillows and sheet flows with glassy rinds (sparsely Pl-phyric); thin Mn and rust on the pieces	> 100 kg
DR4	Axial deep, one of the miniature RTJ segments	Fresh glass rind pieces; brownish mud also in the dredge	a few tens g
DR5	Axial deep, one of the miniature RTJ segments	Serpentinite pieces; olive greenish sand also in dredge	a few tens g
DR6	Top of seamount, axial volcanic zone of the first SEIR segment	Fresh glass rind pieces and glassy lava bud (highly to moderately Pl-phyric); some rust on the pieces; mud also attached on the pieces	a few kg
DR7	Saddle between two conical seamounts, axial volcanic zone of the first SEIR segment	Fresh glass pieces (Pl-phyric)	a few tens g
DR8	Eastern flank of blocky seamount between the SWIR propagator and the miniature RTJ segment	Moderately to highly altered lavas, dolerites, gabbros, and hyaloclastites; brownish mud also in the dredge	ca 800 kg
DR9	Eastern slope of axial deep, one of the miniature RTJ segments	Pillows and sheet flows with glassy rinds (sparsely Pl-phyric); thick Mn on the pieces; some rust on the glassy top; brownish mud attached on the rocks	ca 100 kg
DR10	Northern slope of E-W trending deep, the first SWIR segment	Varyingly altered pillow and lava fragments (highly to sparsely Ol+Pl-phyric), dolerites, and gabbros; some pieces are well rounded; relatively fresh pillows preserve glassy rinds; thin Mn coating on the rocks; brownish mud also in the dredge	ca 300 kg
DR11	Top of seamount, one of the E-W trending ridges, the first SWIR segment	Moderately to highly altered lavas and dolerites	ca 100 kg
DR12	Top of seamount, one of the E-W trending ridges, the first SWIR segment	Moderately altered lava cobbles (sparsely Pl-phyric); thick Mn on the pieces; brownish mud also in dredge	a few kg
DR13	Top of seamount, one of the E-W trending ridges, the first SWIR segment	Moderately altered lava fragments (moderately Ol+Pl-phyric to aphyric); thick Mn on the pieces; brownish mud also in dredge	ca 20 kg
DR14	Top of seamount, one of the E-W trending ridges, the first SWIR segment	Moderately altered lava cobbles; thick Mn on the pieces; brownish mud also in dredge	a few tens g
DR15	Small topographic high binding axial deeps of the miniature RTJ segments	Slightly to moderately altered pillows and lava fragments (moderately Ol+Pl-phyric), dolerites, and hyaloclastites; relatively fresh pillow preserve glassy rinds; some Mn on the pieces; brownish mud with olive greenish sandy portions also in the dredge	ca 100 kg
DR16	Top of topographic high between SWIR propagator and the blocky tectonic high immediately west of RTJ	Pillows and lava fragments (sparsely Ol+Pl-phyric); some pieces preserve glassy rind; thick Mn on the pieces	ca 50 kg
DR17	Axial deep of SWIR propagator	Moderately altered lava cobbles (moderately Ol+Pl-phyric) in olive greenish volcanic sand (altered rocky pieces, glass shards, plagioclase, olivine, and fossils); thick Mn on the lava cobbles	ca 2 kg
DR18	Conical high lying on the southern slope of axial deep, the first SWIR segment	Moderately to highly altered pillows, lava fragments, dolerite, and hyaloclastites; thin Mn on the pieces	ca 500 kg
DR19	Axial deep, the first SWIR segment		No recovery
DR20	Top of conical seamount, axial volcanic zone of the first SEIR segment	Fresh glass rind pieces (moderately Pl-phyric); thin Mn and rust on the pieces	ca 1 kg
DR21	Top of conical seamount, axial volcanic zone of the first SEIR segment	Fresh pillows and hollowed pillows with glassy rinds (highly Pl-phyric); thin Mn and rust on the pieces	ca 10 kg
DR22	Top of seamount, axial volcanic zone(?), the southern offset in the first SEIR segment	Brownish mud (no rock recovery)	ca 2 kg
DR23	Top of conical seamount, axial volcanic zone of the northern end of the third SEIR segment	Fresh glass rind pieces (moderately Pl-phyric); thin Mn and rust on the pieces	ca 1 kg
DR24	Top of conical seamount, axial volcanic zone of the second SEIR segment	Fresh glass rind pieces (aphyric); thin Mn and rust on the pieces	ca 1 kg
DR25	Axial deep, one of the miniature RTJ segments	Fresh hollowed pillows with glassy rinds (sparsely Pl-phyric to aphyric); thin Mn and rust on the pieces; brownish mud also in the dredge	a few kg
DR26	Top of small topographic high lying on the northern extension of axial volcanic zone of the first SEIR segment	A few glass pieces in WAX on the dredge; thick Mn on the pieces	ca 1 g
DR27	Axial deep, one of the miniature RTJ segments	Brownish mud with olive greenish sand (no rock recovery)	ca 500 g

Table 5-3. List of Rock Core sampling sites and recovered materials

Station ID	Bottom signature	Recovery_materials	Recovery_amounts
RC1	Top of conical seamount, axial volcanic zone of the first CIR segment	Fresh glass pieces (Pl-phyric); rust on some pieces	1 g
RC2	Top of conical seamount, axial volcanic zone of the first SEIR segment	Fresh glass pieces; rust on some pieces; mud beyond WAX	63 g
RC3	Top of conical seamount, axial volcanic zone of the first SEIR segment	Fresh glass pieces (Pl-phyric); rust on some pieces	6 g
RC4	Top of conical seamount, axial volcanic zone of the first CIR segment	Fresh glass pieces (Pl-phyric); rust on some pieces	22 g
RC5	Top of conical seamount, axial volcanic zone of the first CIR segment	Fresh glass pieces;(Pl-phyric); rust on some pieces	6 g
RC6	Top of conical seamount, southern extension of axial volcanic zone of the first CIR segment	Fresh glass pieces (Pl-phyric); rust coating on some pieces	60 g
RC7	Top of conical seamount, axial volcanic zone of the first SEIR segment	Fresh glass pieces (Pl-phyric); rust on some pieces	19 g
RC8	Top of conical seamount, axial volcanic zone of the first SEIR segment	Manganese materials (few glass pieces)	2 g
RC9	Top of conical seamount, axial volcanic zone of the first SEIR segment	Fresh glass pieces (Pl-phyric); rust on some pieces	36 g
RC10	Top of conical seamount, eastern side of axial volcanic zone of the first SEIR segment	Manganese materials (few glass pieces)	2 g
RC11	Top of conical seamount, axial volcanic zone of the first SEIR segment	Fresh glass pieces (Pl-phyric); thin Mn and rust on some pieces	16 g
RC12	Top of conical seamount, axial volcanic zone of the first SEIR segment	Fresh glass pieces (Pl-phyric); thin Mn and rust on some pieces	27 g
RC13	Top of conical seamount, axial volcanic zone of the first SEIR segment	Fresh glass pieces (Pl-phyric); thin Mn and rust on some pieces; brownish mud attached on the core head	16 g
RC14	Top of conical seamount, axial volcanic zone of the first SEIR segment	Fresh glass pieces (Pl-phyric); rust on some pieces; brownish mud attached on the core head	24 g

Table 5-4. List of dredged working samples

Station ID	Sample ID	Size (cm)	Rock type	Others	Glass separation
DR1	A1	7*7*5	Pillow with glass rind	Aphyric; tiny Mn spots on surface	Done; labeled by A1G
DR1	A2	7 in long. dim.	Pillow with glass rind	Aphyric	Done; labeled by A2G
DR1	B1	16 in long. dim	Sheet flow with glass rind	Aphyric	Done; labeled by B1G
DR1	C1	23*15*12	Pillow with glass rind	Aphyric; moderately vesiculated; partly covered with thin Mn spots	Done labeled by C1G
DR1	D1	12 in long. dim.	Lava with fragmented glass rind	Aphyric; moderately altered; some Mn coating; surface covered with fragmented glass	Done; labeled by D1G
DR1	E1	24*16*16	Lava with glass rind	Aphyric; some surface is covered with Mn	Done; labeled by E1G
DR1	F1	30*20*17	Pillow with glass rind	Aphyric; this piece has another glass layer in it; surface partly covered with Mn; this piece is probably derived from the same flow as Group E; discrimination from Group E was made simply because this piece looks like almost whole pillow block	Done; labeled by F1G
DR2	A1	6*4*1.5	Glass rind	Sparsely Pl-phyric; rust coating covered with thin Mn	Done; labeled by A1G
DR2	A2	5*3*1	Glass rind	Sparsely Pl-phyric; rust coating covered with thin Mn	Done labeled by A2G
DR2	B1	7*2*3	Lava piece	Sparsely Pl-phyric; relatively thick Mn coating on some surface	No glass
DR3	A1	25*25*20	Pillow with glass rind	Rust coating covered with thin Mn spots on top	Done; labeled by A1G
DR3	A2	12*12*12	Pillow with glass rind	Rust coating covered with thin Mn spots on top	Done; labeled by A2G
DR3	A3	20*10*12	Pillow with glass rind	Rust coating covered with thin Mn spots on top	Done; labeled by A3G
DR3	B1	5*10*4	Sheet flow with glass rind	2 mm-thick Mn on external rocky surface; rust coating on glassy top	Done; labeled by B1G
DR3	B2	4*10*8	Sheet flow with glass rind	Some Mn on external rocky surface; rust coating on glassy top; half piece taken to LDGO	Done; labeled by B2G
DR3	B3	7*8*9	Sheet flow with glass rind	Thick glass rinds at both top and bottom; some Mn and rust coating on both sides	Done; labeled by B3aG(top glass) and B3bG(bottom glass)
DR3	C1	3*4*1	Sheet flow with glass rind	Some Mn coating on bottom	Done; labeled by C1G
DR3	D1	3*5*6	Composite sheet flow	No glass rind on external surface; one internal glass layer exists; some Mn coating	
DR3	D2	4*5*6	Composite sheet flow	No glass rind on external surface; one internal glass layer exists; some Mn coating	
DR3	E1	7*10*1.5	Sheet flow with glass rind	Thin Mn on top; thicker Mn on bottom	Done; labeled by E1G
DR3	E2	5*10*1.5	Sheet flow with glass rind	Thin Mn on top; thicker Mn on bottom	Done; labeled by E2G
DR4	A1G	4*3*2	Glass rind	Aphyric	
DR4	A2G	3*2*1.5	Glass rind	Aphyric	
DR4	A3G	2*4*2	Glass rind	Aphyric; half piece taken to LDGO	
DR5	A1	7*6*3	Serpentinite	Full piece taken to ORI	No glass
DR6	A1	22*14*9	Lava bud with glass rind	Moderately Pl-phyric	Done; labeled by A1G
DR6	A2	16*10*10	Sheet flow with glass rind	Moderately Pl-phyric	Done; labeled by A2G
DR6	B1G	5*4*1	Glass rind	Highly Pl-phyric; rust coating on top	
DR6	C1G	5*3*1	Glass rind	Moderately Pl-phyric	
DR7	A1G	3*2*0.5	Glass rind	Sparsely Pl-phyric; some Pele's tears and hairs preserved on top	
DR7	Pipe Dredge	av. 0.1 mm	Glass chips	These chips were founded in pipe dredges; two relatively large chips (10*10*0.5 mm) included	
DR8	A11	20*8*15	Lava	Moderately Pl-phyric; highly altered with common pyrites	No glass
DR8	A17	18*4*4	Lava	Highly Pl-phyric; moderately altered; no obvious pyrite precipitation	No glass
DR8	B11	12*4*4	Dolerite	Moderately altered	No glass
DR8	C3	15*14*8	Fine-grained gabbro	Moderately altered	No glass
DR8	C11	7*4*3	Fine-grained gabbro	Moderately altered	No glass
DR8	C13	10*6*4	Fine-grained gabbro	Moderately altered	No glass
DR8	D1	8*4*3	Breccia	Highly altered; angular lava fragments in basaltic(?) matrix	
DR9	A1	8*8*8	Pillow with glass rind	Sparsely Pl-phyric; rust on glassy surface; thick Mn on all external surface	Done; labeled by A1G
DR9	A2	12*8*7	Pillow with glass rind	Aphyric; thick Mn coating; sample of Mn coating and some glass pieces taken to LDGO	Done; labeled by A2G
DR9	B1	5*4*4	Pillow bud with glass rind	Aphyric	Done; labeled by B1G
DR9	C1	25*25*26	Sheet flow	Aphyric; glass rind has gone; external surface totally coated with thick Mn	No glass
DR9	D1	5*7*4	Sheet flow with glass rind	Sparsely Pl-phyric; rust on top; thick Mn coating on bottom; half piece taken to LDGO	Done; labeled by C1G
DR9	E1	4*5*1	Sheet flow with glass rind	Sparsely Ol+Pl-phyric; thick Mn coating on bottom; pahoehoe texture preserved	Done; labeled by E1G
DR9	E2	1*5*5	Sheet flow with glass rind	Aphyric; thick Mn coating on both top and bottom	Done; labeled by E2G
DR9	F1	20*15*15	Pillow with glass rind	Whole small pillow; some glass pieces taken to LDGO	Done; labeled by F1G
DR9	G1	20*10*10	Glassy extrusion	Sparsely Pl-phyric	Done; labeled by G1G
DR9	G2	?	Glassy extrusion	Sparsely Pl-phyric; one fragment taken to LDGO	Done; labeled by G2G
DR10	A1	10*10*8	Pillow with glass rind	Moderately Ol+Pl-phyric; rust on glassy top; thin Mn coating	Done; labeled by A1G
DR10	A2	7*6*5	Pillow with glass rind	Moderately Ol+Pl-phyric; rust on glassy top; thin Mn coating	Done; labeled by A2G
DR10	A3	5*5*5	Pillow with glass rind	Moderately Ol+Pl-phyric; rust on glassy top; thin Mn coating	Done; labeled by A3G
DR10	A4	6*3*3	Pillow with glass rind	Moderately Ol+Pl-phyric; rust on glassy top; thin Mn coating	Done; labeled by A4G
DR10	B1	5*6*7	Pillow with glass rind	Highly Ol+Pl-phyric	Done; labeled by B1G
DR10	C1	5*5*3	Lava cobble	Moderately Ol+Pl-phyric; rounded shape; some extents of alteration	Done; labeled by C1G
DR10	D1	12*8*8	Pillow with glass rind	Moderately Ol+Pl-phyric; some extents of alteration	Done; labeled by D1G
DR10	E1	9*8*6	Lava	Moderately Ol+Pl-phyric; slightly altered	No glass

DR10	E2	10*7*5	Lava	Moderately Ol+Pl-phyric; slightly altered	No glass
DR10	F1	13*8*5	Lava	Highly Ol+Pl-phyric; slightly altered	No glass
DR10	F2	8*5*4	Lava	Highly Ol+Pl-phyric; moderately altered	No glass
DR10	G1	11*6*5	Lava	Highly Pl+Ol-phyric; slightly altered; thin Mn coating on external surface	No glass
DR10	H1	16*11*9	Dolerite	Highly altered; thin Mn coating	No glass
DR10	I1	?	Fine-grained gabbro	Highly altered; thin Mn coating	No glass
DR10	J1	14*9*7	Lava	Highly altered with common quartz veins and pyrites; the following Group J samples were taken to assess the nature of the alteration (metamorphism) at this location; J1-5 were taken in the order of decreasing extents of the alteration	No glass
DR10	J2	12*9*4	Lava	Highly altered with some quartz veins and tiny pyrites; moderately Pl-phyric	No glass
DR10	J3	10*8*4	Lava	Highly altered with tiny pyrites; moderately Pl-phyric	No glass
DR10	J4	10*9*5	Lava	Moderately altered with sparse tiny pyrites; sparsely Pl-phyric	No glass
DR10	J5	14*10*4	Lava	Only slightly altered; moderately Ol+Pl-phyric; close to Groups A, B, D, E, F, and G in the extent of alteration	No glass
DR11	A3	14*10*8	Lava	Moderately Pl-phyric; moderately altered	No glass
DR11	A4	20*11*10	Lava	Moderately Pl-phyric; moderately altered	No glass
DR11	B2	25*15*7	Breccia	Aphyric lava fragments in fine matrix; highly altered	No fresh glass
DR11	B3	20*12*11	Breccia	Aphyric lava fragments in fine matrix; highly altered	No fresh glass
DR11	C1	9*6*5	Lava	Highly altered with ore deposits	No glass
DR11	C2	9*6*2	Lava	Highly altered with ore deposits	No glass
DR12	A1	2*2*2	Lava cobble	Moderately Ol+Pl-phyric; totally coated with thick (1-2 mm) Mn; thin glass layer at one side beneath Mn coating	
DR12	A2	3*2*1	Lava cobble	Moderately Ol+Pl-phyric; totally coated with thick Mn	No glass
DR12	A3	2*2*1	Lava cobble	Moderately Ol+Pl-phyric; totally coated with thick Mn; some extent of alteration	No glass
DR12	A4	2*2*1	Lava cobble	Moderately Ol+Pl-phyric; totally coated with thick Mn; one fragment taken to LDGO	No glass
DR12	A5	1*1*2	Lava cobble	Moderately Ol+Pl-phyric; totally coated with thick Mn	No glass
DR12	A6	2*1*1	Lava cobble	Moderately Ol+Pl-phyric; totally coated with thick Mn	No glass
DR13	A1	10*9*5	Lava	Moderately Ol+Pl-phyric; totally coated with thick (1 mm) Mn	No glass
DR13	B1	10*10*6	Lava	Aphyric; highly altered; totally coated with thick Mn; half piece taken to LDGO	No glass
DR13	B2	10*7*5	Lava	Aphyric; highly altered; totally coated with thick Mn	No glass
DR13	C1	10*8*4	Lava	Aphyric; coarse-grained; highly altered; totally coated with thick Mn	No glass
DR14	A1	5*5*2	Lava cobble	Aphyric; moderately altered; totally coated with thick Mn; this piece is actually two pieces connected each other with Mn	No glass
DR14	B1	4*3*2	Lava cobble	Aphyric; coarse-grained; moderately altered; totally coated with thick (~ 3 mm) Mn	No glass
DR15	A1	11*10*8	Pillow with glass rind	Moderately Ol+Pl-phyric; some extent of alteration; thin glass rind preserved on top; totally coated with thin Mn	Done; labeled by A1G
DR15	A2	15*12*11	Pillow with glass rind	Moderately Ol+Pl-phyric; thin glass rind preserved on top; totally coated with thin Mn	Done; labeled by A2G
DR15	A3	8*6*4	Pillow with glass rind	Moderately Ol+Pl-phyric; some extent of alteration; thin glass rind preserved on top; totally coated with thin Mn	Done; labeled by A3G
DR15	B1	15*10*5	Lava	Moderately Ol+Pl-phyric; some extent of alteration; totally coated with thin Mn	No glass
DR15	C1	17*16*16	Dolerite	Totally coated with thin Mn	No glass
DR15	E1	11*10*8	Hyaloclastite	Pl-phyric lava fragments in fine matrix; some relatively fresh glass chips preserved in matrix; external surface totally coated with thin Mn	Done; labeled by E1G
DR16	A1	40*40*25	Pillow with glass rind	Sparsely Ol+Pl-phyric; rust coating on glass; external surface totally coated with thick Mn	Done; labeled by A1G
DR16	A2	13*13*8	Pillow with glass rind	Sparsely Ol+Pl-phyric; rust coating on glass; external surface totally coated with thick Mn	Done; labeled by A2G
DR16	B1	12*8*8	Lava	Sparsely Ol+Pl-phyric; external surface totally coated with thick Mn	No glass
DR17	A1	4*3*2	Lava cobble	Moderately Ol+Pl-phyric; moderately altered; totally coated with thin Mn	No glass
DR17	A2	4*3*2	Lava cobble	Moderately Ol+Pl-phyric; moderately altered; totally coated with thin Mn	No glass
DR17	B		Volcanic sand	Olive greenish in color; sandy sediment consisting of greenish rocky pieces, plagioclase, olivine, glass shards, and fossils	
DR18	A1	9*9*8	Pillow	Glassy rind totally altered to paragonitic clay	No fresh glass
DR18	A2	8*6*5	Pillow bud	Glassy rind totally altered to paragonitic clay; some Mn spots	No fresh glass
DR18	B1	17*14*8	Lava	Sparsely Pl-phyric; moderately altered; totally coated with thin Mn	No glass
DR18	B2	15*10*8	Lava	Sparsely Pl-phyric; moderately altered; totally coated with thin Mn	No glass
DR18	C1	14*7*4	Hyaloclastite	Highly altered; totally coated with thin Mn	No fresh glass
DR20	A1G	13*8*3	Glass rind	Moderately Pl-phyric; thin Mn on top; some Pele's tears still preserved	
DR20	A2G	7*7*3	Glass rind	Moderately Pl-phyric; thin Mn on top; some Pele's tears still preserved	
DR20	A3G	8*5*2	Glass rind	Moderately Pl-phyric; rust coating on top	
DR20	A4G	4*4*1	Glass rind	Moderately Pl-phyric; rust coating on top	

DR20	A5G	8*4*0.5	Glass rind	Moderately Pl-phyric; thin Mn coating	
DR21	A1	28*27*17	Pillow	Highly Pl-phyric; rust on top; thin Mn on all external surface	Done; labeled by A1G
DR21	B1	13*11*3	Hollowed pillow	Highly Pl-phyric; rust on top; thin Mn on all external surface	Done; labeled by B1G
DR21	B2	8*6*2	Hollowed pillow	Highly Pl-phyric; rust on top; thin Mn on all external surface	Done; labeled by B2G
DR23	A1G	9*5*3	Glass rind	Moderately Pl-phyric; rust on top; thin Mn coating	
DR23	A2G	7*5*1	Glass rind	Moderately Pl-phyric; rust on top; thin Mn coating; ropy texture on top	
DR23	A3G.	5*4*12	Glass rind	Moderately Pl-phyric; some Pele's tears still preserved	
DR23	A4G	4*3*1	Glass rind	Moderately Pl-phyric; rust on top; thin Mn spots; some Pele's tears still preserved	
DR24	A1G	5*4*3.5	Glass rind	Aphyric; rust on top; thin Mn on all external surface	
DR24	A2G	5*3*2	Glass rind	Aphyric; rust on top; thin Mn on all external surface	
DR24	A3G	6*4*2	Glass rind	Aphyric; rust on top; thin Mn on all external surface	
DR24	A4G	4.5*4*0.8	Glass rind	Aphyric; topmost layer has gone	
DR25	A1	18*14*3	Hollowed pillow with glass rind	Aphyric; rust on top; thin Mn on bottom; some Pele's tears on top surface	Done; labeled by A1G
DR25	A2	15*6*4	Hollowed pillow with glass rind	Sparsely Pl-phyric; rust on top; thin Mn on bottom	Done; labeled by A2G
DR25	A3	10*6*3	Hollowed pillow with glass rind	Aphyric; rust on top; thin Mn on bottom; some Pele's tears on top surface	Done; labeled by A3G
DR26	WAX on pipe		Glass chips	Almost sandy size except for two chips (2-3 mm); thick Mn coating	

Table 5-5. List of Rock Core working samples

Station ID	H code sample (g)	C code sample (g)	Total recovery (g)
RC1	0.5	0.3	0.8
RC2	57	1	,58
RC3	4.5	1.3	5.8
RC4	20	2	22
RC5	4	1.5	5.5
RC6	51	9	60
RC7	16	3	19
RC8			2
RC9	28	8	36
RC10			2
RC11	10	6	16
RC12	20	7	27
RC13	12	4	16
RC14	20	4	24

Table 5-6. Microprobe analyses of glasses of basalts from the Indian Ridges

	Dredge#	SiO2	Al2O3	TiO2	FeO*	MnO	MgO	CaO	Na2O	K2O	Cr2O3	NiO	Total
CIR	DR3 A1	50.47	15.38	1.31	8.77	0.17	8.08	11.25	2.74	0.07	0.04	0.01	98.29
CIR	DR3 A2	50.42	15.27	1.30	8.46	0.13	8.18	11.39	2.82	0.05	0.07	0.01	98.10
CIR	DR3 A3	50.99	15.40	1.33	8.94	0.19	8.24	11.35	2.79	0.09	0.04	0.01	99.37
CIR	DR3 B1	50.93	15.29	1.38	8.68	0.17	8.15	11.27	2.78	0.09	0.04	0.03	98.81
CIR	DR3 B2	50.48	15.21	1.30	8.72	0.27	7.87	11.47	2.73	0.08	0.04	0.00	98.17
CIR	DR3 B3A	50.91	15.49	1.31	8.43	0.20	7.91	11.36	2.65	0.07	0.04	0.00	98.37
CIR	DR3 B3B	50.72	15.43	1.35	8.52	0.20	8.11	11.45	2.78	0.08	0.09	0.01	98.74
CIR	DR3 C1	50.54	15.56	1.31	8.80	0.21	8.05	11.45	2.72	0.06	0.08	0.07	98.85
CIR	DR3 chain	50.34	15.27	1.28	8.86	0.20	7.82	11.18	2.66	0.08	0.07	0.01	97.77
CIR	DR3 E1	50.96	15.47	1.38	8.80	0.18	8.00	11.28	2.83	0.06	0.07	0.02	99.05
CIR	DR3 E2	50.65	15.30	1.29	8.69	0.17	8.13	11.48	2.67	0.09	0.06	0.03	98.56
CIR	DR1 A1	51.01	15.86	1.39	8.25	0.14	7.92	11.24	2.96	0.18	0.08	0.01	99.04
CIR	DR1 A2	51.46	15.73	1.29	8.13	0.17	7.93	11.29	2.84	0.15	0.02	0.03	99.04
CIR	DR1 B1	50.92	15.80	1.28	8.25	0.11	7.95	11.19	2.82	0.19	0.06	0.03	98.60
CIR	DR1 B2	50.46	15.75	1.32	8.50	0.15	7.90	11.28	3.00	0.17	0.06	0.05	98.64
CIR	DR1 C1	50.86	15.71	1.29	8.13	0.16	7.98	11.31	2.90	0.14	0.08	0.01	98.57
CIR	DR1 D1	51.09	15.75	1.17	8.30	0.16	7.64	11.26	2.83	0.15	0.04	0.00	98.39
CIR	DR1 E1	50.69	15.70	1.21	8.66	0.17	7.93	11.11	3.01	0.19	0.04	0.01	98.72
CIR	DR1 F1-1	50.73	15.79	1.22	8.42	0.17	8.03	11.16	2.97	0.19	0.05	0.02	98.75
CIR	DR1 F1-2	51.19	15.38	1.24	8.75	0.21	7.67	11.21	3.02	0.19	0.15	0.00	99.01
TRJ	DR4 A1	51.21	14.73	1.61	9.75	0.18	7.46	10.48	3.07	0.12	0.03	0.04	98.68
TRJ	DR4 A2	50.85	14.72	1.68	9.88	0.26	7.42	10.66	2.99	0.10	0.02	0.00	98.58
TRJ	DR4 A3	50.76	14.80	1.60	9.55	0.20	7.45	10.57	3.02	0.12	0.02	0.05	98.14
TRJ	DR9 A1	50.47	14.44	1.65	10.32	0.14	7.22	10.72	2.99	0.11	0.03	0.02	98.11
TRJ	DR9 A2	50.92	14.61	1.58	10.23	0.19	7.20	10.71	2.97	0.09	0.00	0.05	98.55
TRJ	DR9 B1	50.65	14.47	1.60	9.87	0.26	7.16	10.76	2.97	0.11	0.03	0.01	97.89
TRJ	DR9 D1	50.39	14.34	1.67	10.17	0.23	7.30	10.58	3.02	0.10	0.06	0.04	97.90
TRJ	DR9 E1	50.65	14.58	1.54	9.95	0.17	7.21	10.76	3.00	0.09	0.05	0.01	98.01
TRJ	DR9 E2	50.58	14.58	1.58	10.11	0.21	7.39	10.80	3.00	0.10	0.06	0.03	98.44
TRJ	DR9 F1	50.78	14.70	1.66	9.88	0.15	7.41	10.70	2.98	0.10	0.05	0.05	98.46
TRJ	DR9 G1	50.27	14.54	1.61	9.89	0.18	7.34	10.72	2.93	0.09	0.02	0.01	97.60
TRJ	DR9 G2	50.73	14.63	1.56	10.39	0.23	7.37	10.75	2.87	0.13	0.06	0.04	98.76
TRJ	DR2 A1	50.28	14.84	1.60	9.53	0.18	7.83	10.88	2.77	0.08	0.03	0.06	98.08
TRJ	DR2 A2	50.25	15.02	1.51	9.51	0.19	7.85	10.89	2.86	0.11	0.06	0.01	98.26
TRJ	DR2 A3	50.67	15.05	1.53	9.61	0.20	7.89	10.98	2.83	0.12	0.02	0.07	98.97
SEIR	DR7 A1	50.83	16.00	0.89	8.05	0.14	8.76	12.36	2.31	0.05	0.07	0.01	99.47
SEIR	DR7 pipe	51.23	14.60	1.38	9.19	0.11	7.17	10.98	2.98	0.12	0.08	0.03	97.87
SEIR	DR6 A1	50.11	15.66	1.27	8.75	0.17	8.05	11.21	3.13	0.08	0.06	0.01	98.50
SEIR	DR6 A2	50.21	15.63	1.28	8.77	0.16	7.82	11.37	2.99	0.10	0.03	0.04	98.40
SEIR	DR6 A3	50.20	15.64	1.27	8.86	0.18	7.80	11.02	3.09	0.08	0.03	0.01	98.18
SEIR	DR6 B1	50.67	15.76	1.09	8.17	0.16	8.22	11.89	2.74	0.09	0.08	0.03	98.90
SEIR	DR6 B2	50.66	15.83	1.02	7.85	0.16	8.35	11.79	2.66	0.08	0.05	0.08	98.53
SEIR	DR6 C1	50.61	15.65	1.11	8.36	0.11	8.23	11.64	2.92	0.08	0.08	0.01	98.80
SEIR	DR6 C2	50.44	16.04	1.13	8.07	0.15	8.11	11.09	2.78	0.08	0.12	0.00	98.01
SWIR	DR10 A1	50.83	15.07	1.30	8.63	0.20	7.90	11.34	2.88	0.10	0.05	0.03	98.33
SWIR	DR10 A2	50.87	14.68	1.67	9.64	0.17	7.53	10.79	2.99	0.11	0.10	0.05	98.60
SWIR	DR10 A3	50.85	15.98	1.27	8.02	0.19	7.99	11.37	2.97	0.11	0.08	0.01	98.84
SWIR	DR10 A4	50.84	14.72	1.65	9.52	0.20	7.45	10.70	3.02	0.12	0.05	0.02	98.29
SWIR	DR10 B1	50.90	15.59	1.18	8.53	0.17	8.16	11.71	2.67	0.12	0.03	0.02	99.08
SWIR	DR10 B2	50.11	14.89	1.47	9.56	0.20	7.75	11.16	2.61	0.09	0.05	0.06	97.95
SWIR	DR10 C1	49.87	15.94	1.12	8.07	0.12	8.64	11.67	2.69	0.07	0.07	0.01	98.27
SWIR	DR10 D1	50.88	15.29	1.40	9.17	0.18	7.64	11.14	2.67	0.11	0.03	0.07	98.58

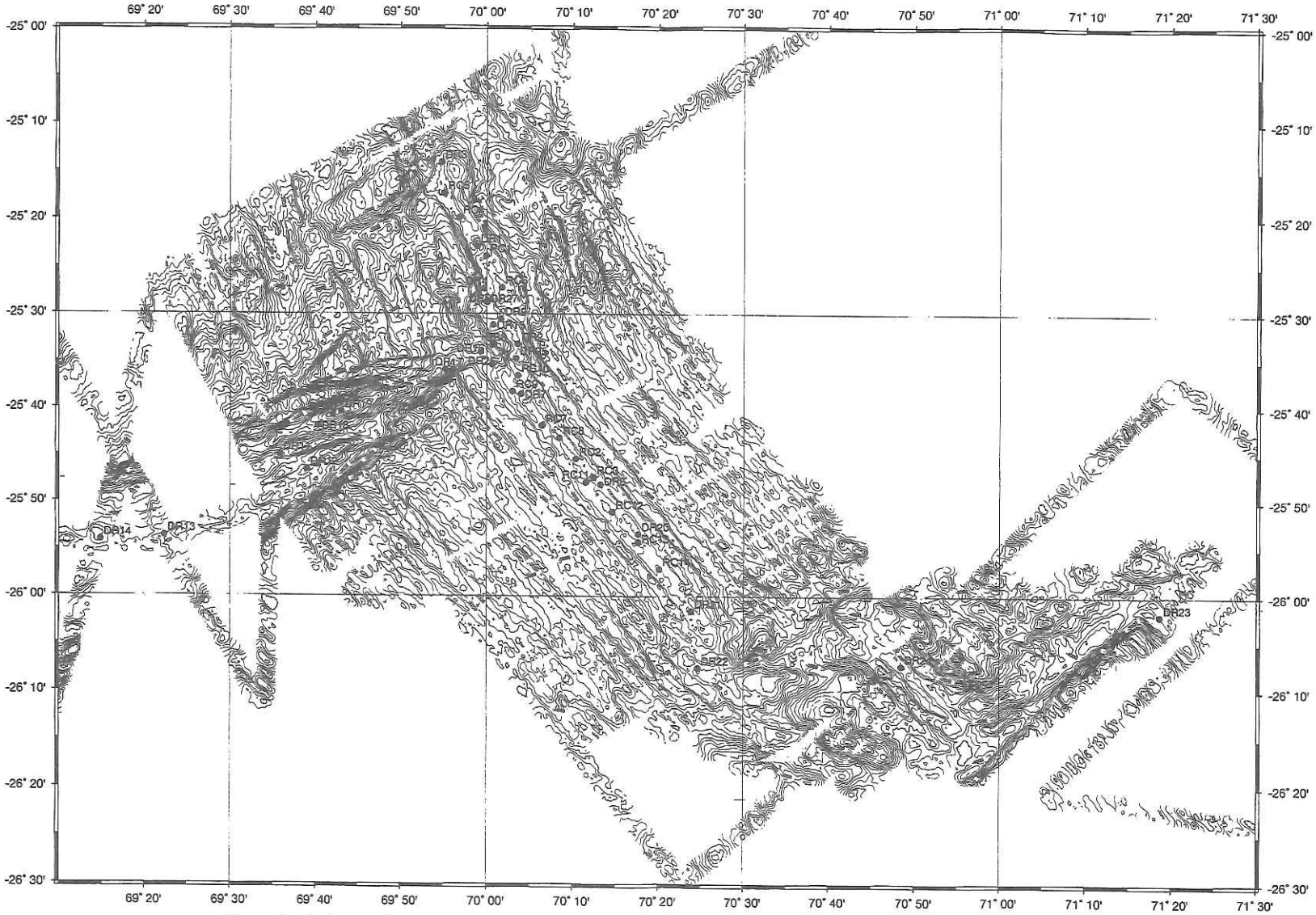

Figure 1. Bathymetric map of the Indian ridges showing all locations of dredge hauls and Rock Core sites.

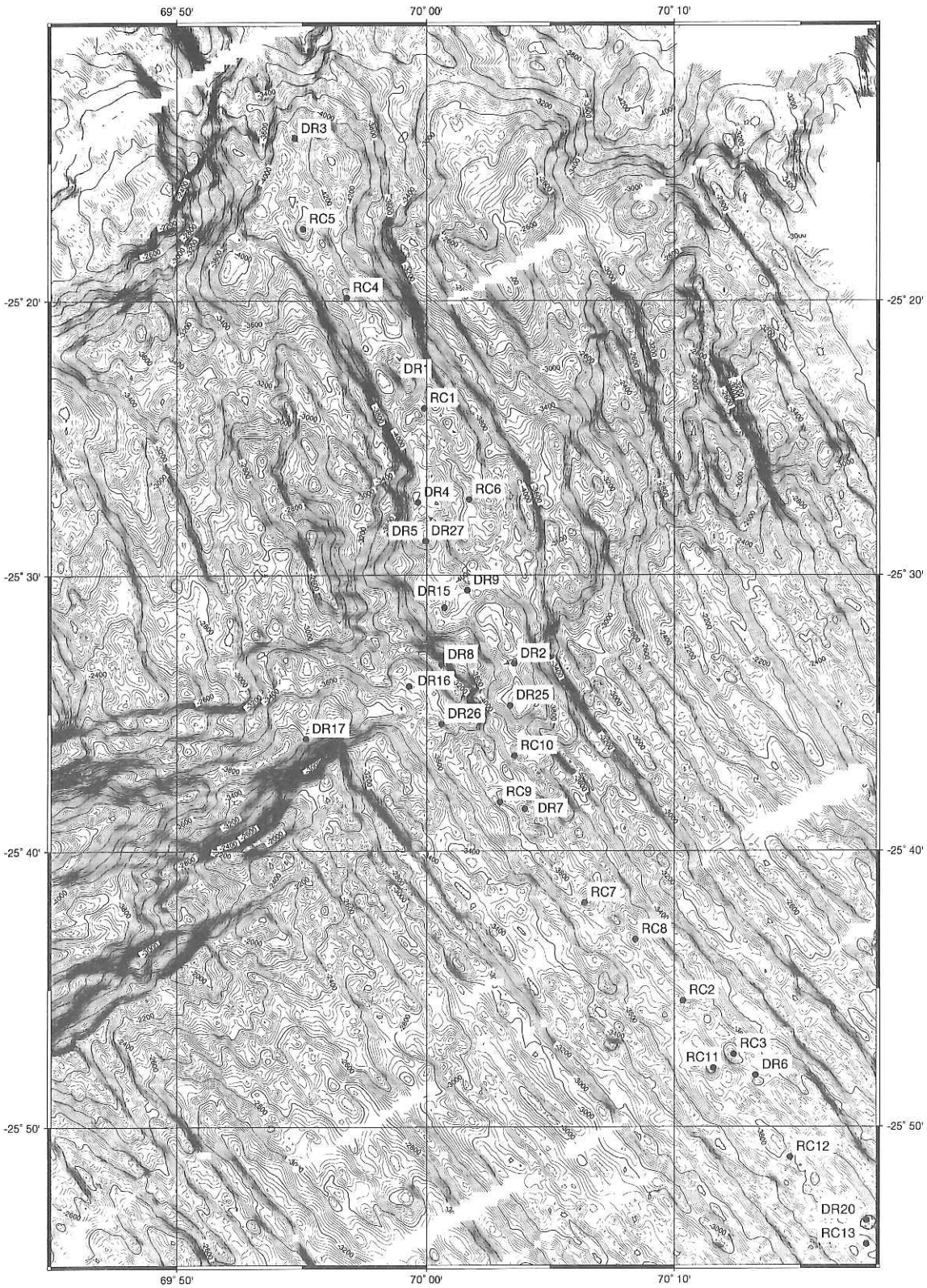

Figure 2a. Bathymetric map showing all locations of dredge hauls and Rock Core sites in the Rodriguez Triple Junction area.

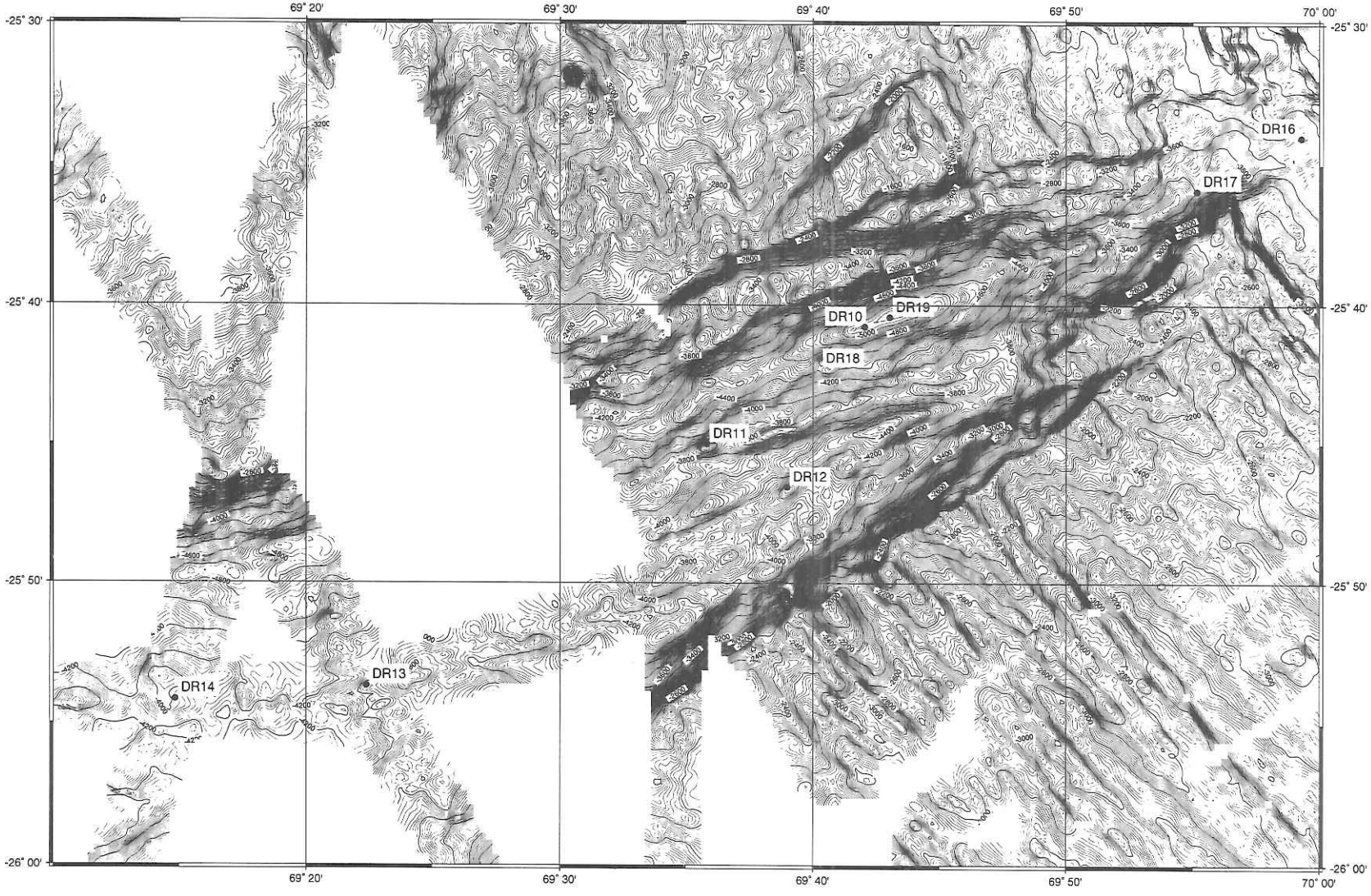

Figure 2b. Bathymetric map showing locations of dredge hauls in the Southwestern Indian Ridge.

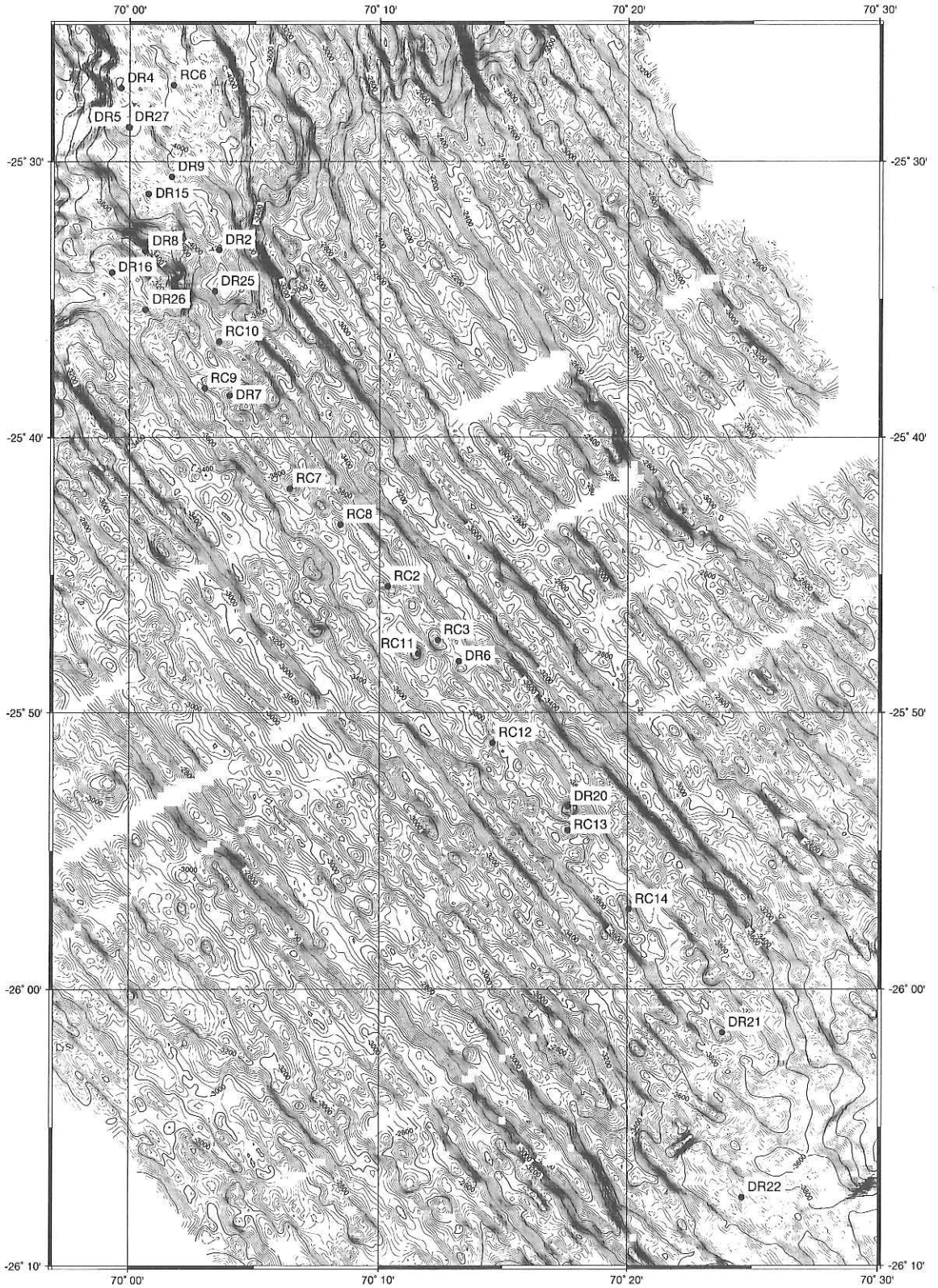

Figure 2c. Bathymetric map showing locations of dredge hauls and Rock Core sites in the Southeastern Indian Ridge near the Rodriguez Triple Junction.

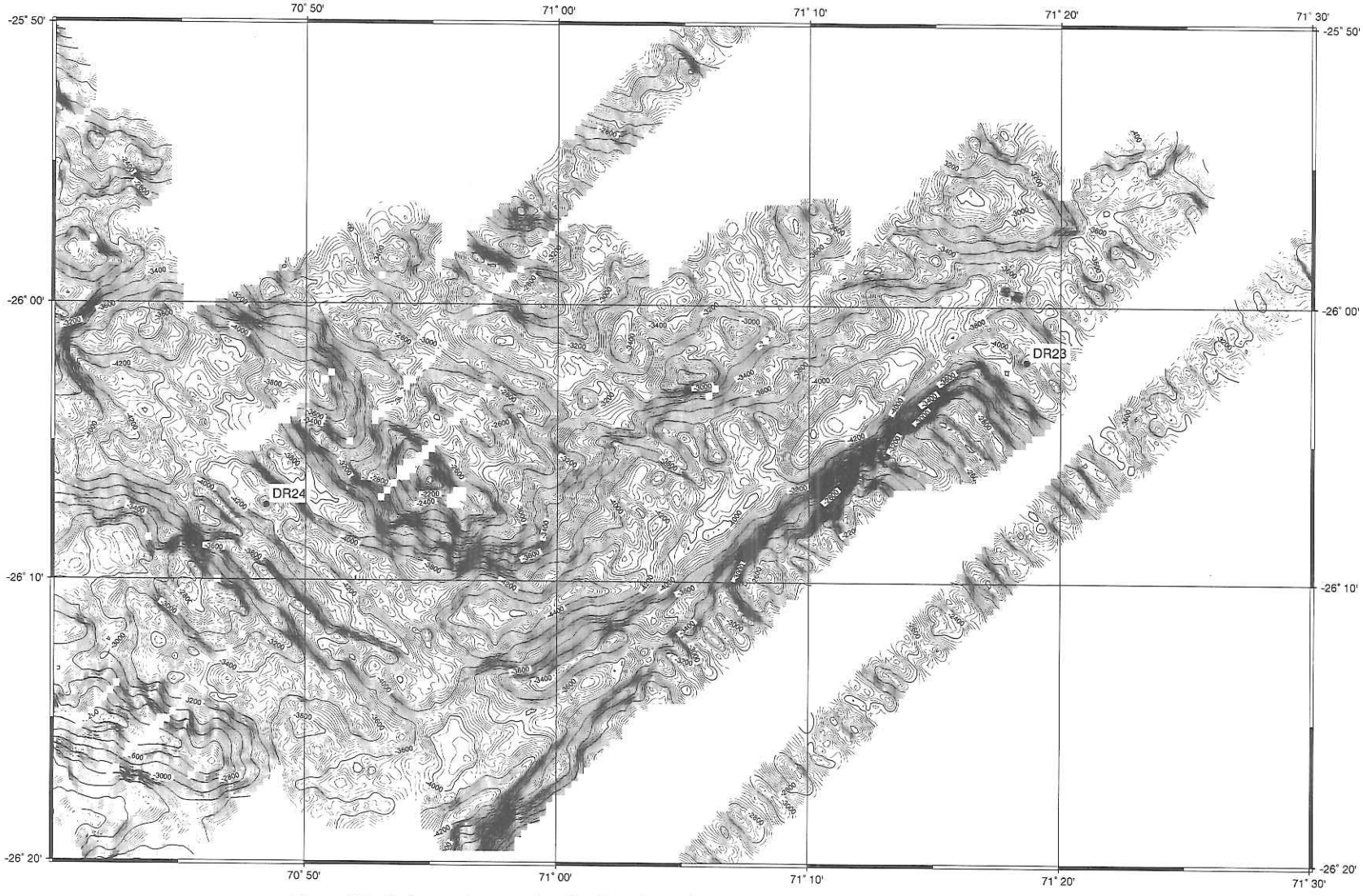

Figure 2d. Bathymetric map showing locations of dredge hauls in the Southeastern Indian Ridge.

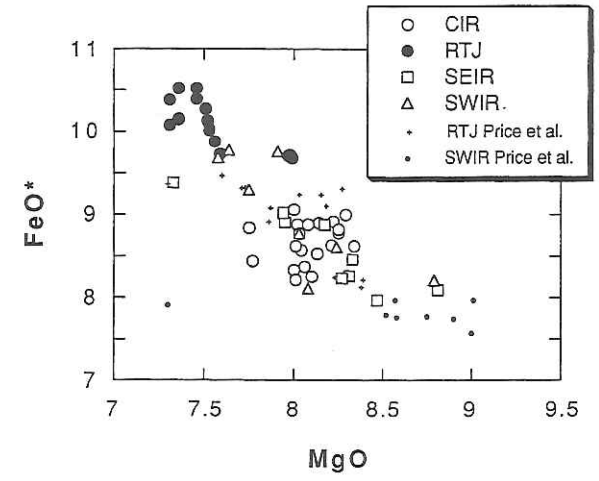

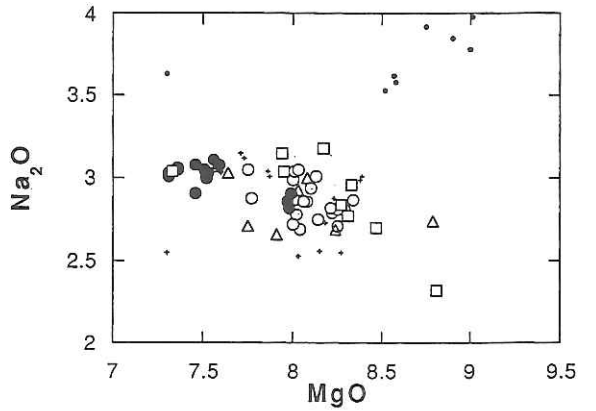

Fig. 5-3a. MgO-FeO* (total iron as FeO) and MgO-Na_2O plots of basalt glasses in the Indian Ridges. Data for the Triple Junction and Southwest Indian Ridge (Price et al. ,1986) are also shown for comparison. CIR = Central Indian Ridge, RTJ = Rodriguez Triple Junction, SEIR = Southeast Indian Ridge, SWIR = Southwest Indian Ridge.

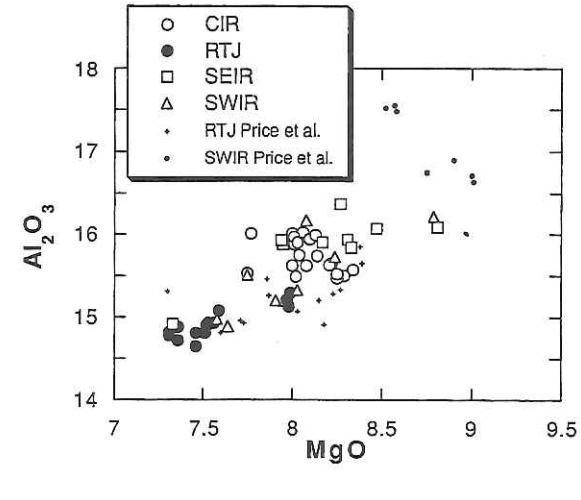

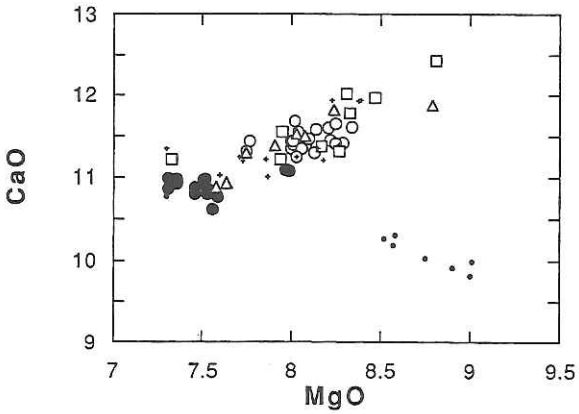

Fig. 5-3b. MgO-Al_2O_3 and MgO-CaO plots of basalt glasses in the Indian Ridges.

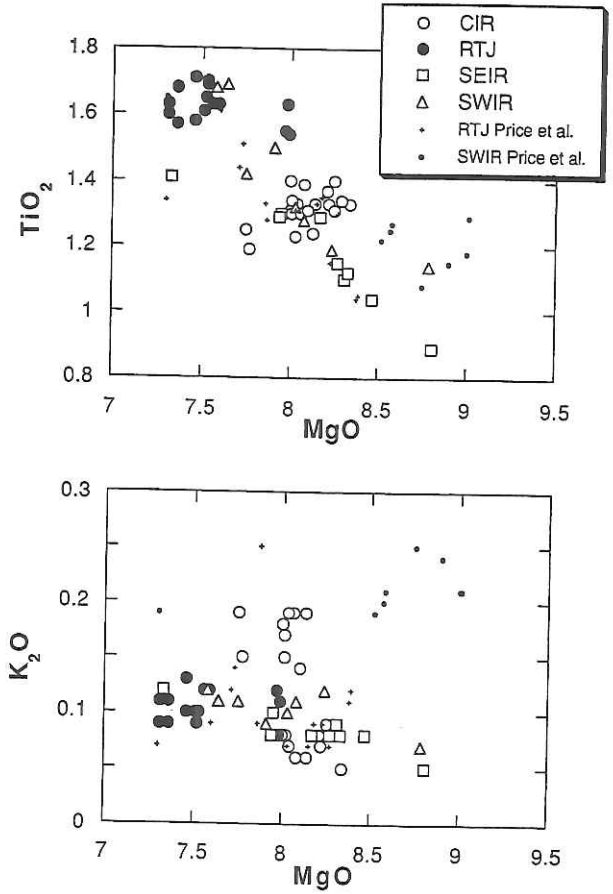

Fig. 5-3c. MgO-TiO_2 and MgO-K_2O plots of basalt glasses in the Indian Ridges.

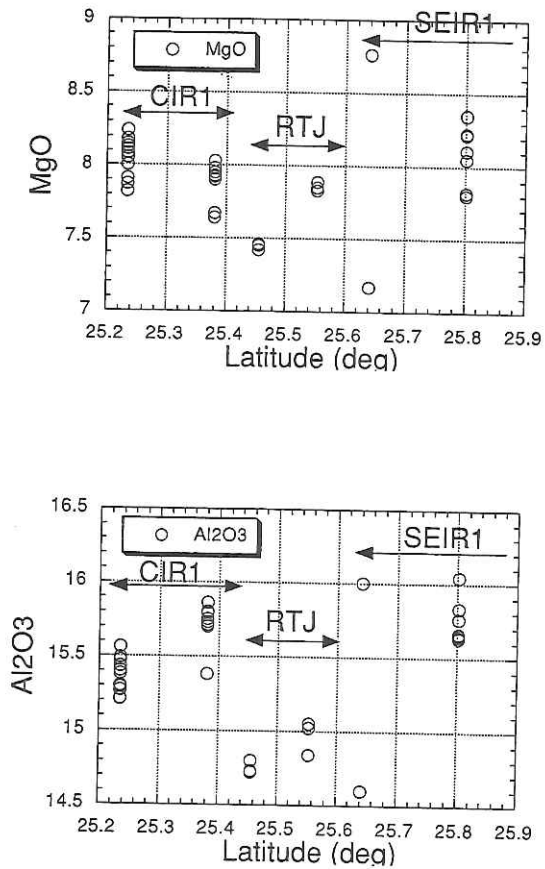

Fig. 5-4. Along-ridge variations in MgO and Al_2O_3 of basalt glasses in the Central and Southeast Indian ridges.

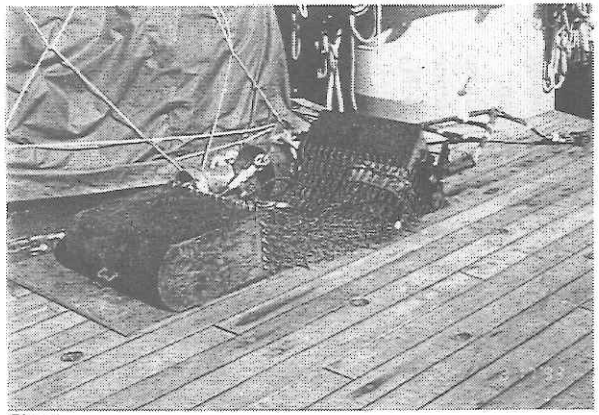

Plate 1
Dredge system used in KH-93-3 cruise. The system consists of a large chain bag with fish-netting chain in the middle, two dredge pipes, 200 kg iron weight, and a heavy chain connecting them.

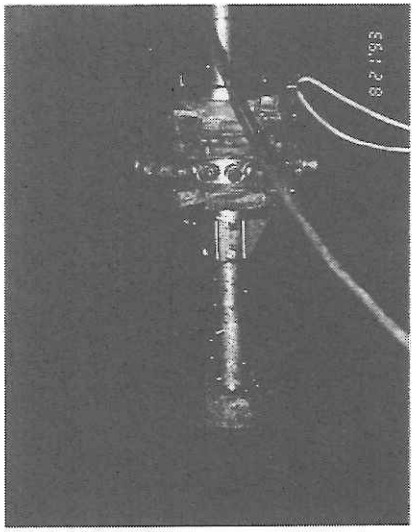

Plate 2
Rock.Core sampling system used in KH-93-3 cruise. Wax was attached thickly on the head (bottom) of the system and in small 19 pipes (collar pipes) on a belt surrounding lead plates (weight) in the middle.

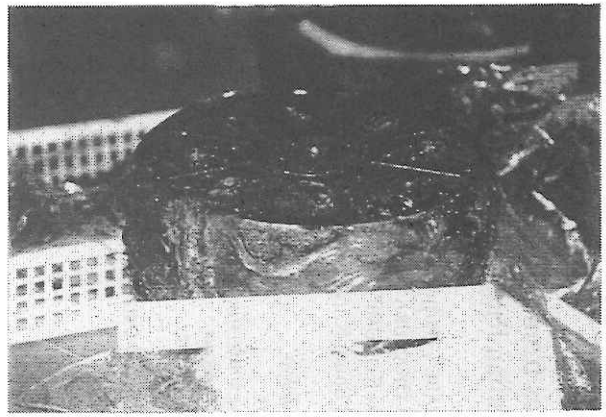

Plate 3
Tips of basalt glasses in wax attached on the Rock Core head (site RC13).

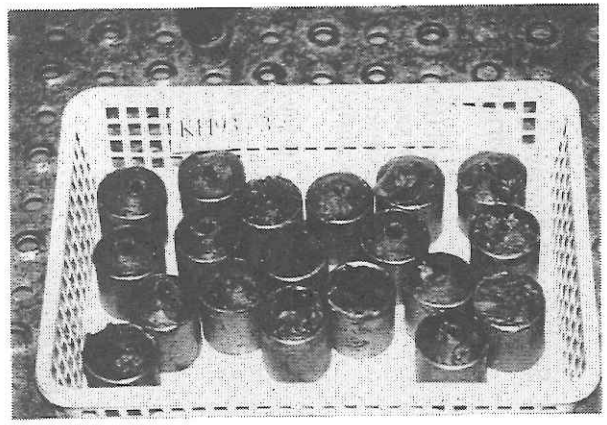

Plate 4
Tips of basalt glasses in wax in collar pipes (site RC13).

6. Search and discovery of hydrothermal plumes from water chemistry at the Rodriguez Triple Junction, Indian Ridge.

Toshitaka GAMO[1], Hiroshi HASUMOTO[1], Masaharu WATANABE[1], Harumi KOBAYASHI[1], Eiichiro NAKAYAMA[2], Hajime OBATA[2], Kei OKAMURA[2], Kenji ISSHIKI[3], Tamotsu OOMORI[4], Takayuki KOIZUMI[4], Kiminori SHITASHIMA[5], Satoshi MATSUMOTO[6], and Shinji KANAYAMA[7]

[1]*Ocean Research Institute, University of Tokyo*
[2]*Faculty of Science, Kyoto University*
[3]*Department of Applied Science, Kochi Women's University*
[4]*Department of Chemistry, University of the Ryukyus*
[5]*Central Research Institute of Electric Power Industry*
[6]*Department of Geology, Osaka City University*
[7]*Department of Earth Science, Faculty of Science, Yamagata University*

1. Introduction

In efforts to locate and characterize ocean bottom hydrothermal systems, water column distributions of various chemical components give us much information. Although submarine hydrothermal activity is a very localized phenomenon at sea bottom, it usually accompanies hydrothermal plumes, cloud-like widely dispersing water masses, which are the mixture of hydrothermal end members and ambient bottom seawater. Areal extent of hydrothermal plumes can be traced from water column anomalies of chemical components such as methane, manganese, helium-3, which are particularly enriched in hydrothermal solutions (e.g. Klinkhammer et al., 1985; Horibe et al., 1986; Gamo et al., 1987; Nojiri et al., 1989; Charlou et al., 1991a,b; Gamo et al., 1993). Detailed mapping of hydrothermal plumes from research vessels could give a conclusive clue to locate the very point of hydrothermal discharge, being indispensable for direct observations by ROV and/or manned submersibles as the next step.

Such geochemical surveys in the Indian Ocean have been quite few compared to those in the Pacific Ocean and the Atlantic Ocean. Herzig and Plüger (1988) showed the existence of hydrothermal activity at 21.5°S and 23°S areas along the Central Indian Ridge using CH_4 and Mn profiles. Plüger et al. (1990) found a more significant hydrothermal plume at 24°S. Jean-Baptiste et al. (1992) reported hydrothermal anomalies of δ^3He and Mn at 19° 29′S. However, these previous works are all restricted in the Central Indian Ridge north of the Rodriguez Triple Junction (25° 35′S, 70° 00′E); no geochemical survey has been done yet at the triple junction and more southern areas.

One of the principal objectives of this cruise is to locate hydrothermally active sites along the ridge axes centered at the Rodriguez Triple Junction. We conducted CTDT(a package of Conductivity, Temperature, Depth, and Light Transmission sensors) + RMS (Rosette Multi-Sampling system) observations along the rift valleys of the Indian Ridge in order to detect anomalies of temperature, salinity and light transmission. At the same time, seawater samples were collected at various depths to measure methane, manganese, iron, and aluminum on board the ship almost in real-time. Such shipboard analyses have a great advantage for effective survey of hydrothermal plumes, because we could modify the sampling sites and depths as promisingly as possible, judging from the updated analytical data.

2. Instruments and methods

2.1 CTD system

The CTDTRMS used during this cruise consists of the following instruments (see Fig.6-1)
CTD fish (Seabird, Model 9plus, 6800m) with a DO sensor
Light transmissometer (SeaTech, 25cm light path, 5000m)
Rosette sampling system (General Oceanics, Model 101524)
Lever-action Niskin samplers (General Oceanics, 12-liter type)
Niskin samplers (General Oceanics, 12-liter type)
Pinger (Benthos, Model 2216)
Transponder (Oki Electronics, Model SB-1009, U-402)

The CTDTRMS, attached at the end of the titanium armored cable (8mm o.d.) from the No.2 winch of R.V. Hakuho Maru, was controlled on board the ship by a CTD deck unit (Seabird, Model 11plus) connected with an IBM compatible desktop computer (Proside, Model MSH 486-66Dx2). The rosette array frame has usually a capability to hold 24 water samplers. During this cruise, however, 22 samplers were attached because the space for the rest two samplers was shared by the transponder, which is indispensable to locate the CTDTRMS by SSBL (super short baseline) subnavigation system. In addition, a pinger was installed inside the frame to monitor the distance between the CTDTRMS and the bottom.

The CTDTRMS was operated in either of the following two modes: (i) the usual vertical mode and (ii) the tow-yo mode. During the former operation, the ship stays at a fixed position, where the system is lowered to a depth of $\sim$ 10 m above the bottom. Water samples are taken by triggering the samplers at appropriate depths when the system is coming up to the surface. For contrast, the latter operation moves the ship slowly at a speed of 0.5 to 1 knot toward a pre-fixed direction, where the system is towed repeating upward and downward movements several times (the system traces a zig-zag pattern) to take multiple vertical profiles along the ship track. Water samples can be taken at any time during the tow-yo operation.

2.2 Water samplers

Two kinds of water samplers were installed to the CTDTRMS system: lever-action Niskin samplers (14 bottles) and ordinary Niskin samplers (8 bottles). The former (Fig.6-2) was main and the latter was supplementary, because we had found that the lever-action Niskin sampler is much more free from iron contamination than the ordinary Niskin sampler, when we compared them on trial in the south Pacific Ocean during the *Hakuho-Maru* Cruise KH92-4. In order to reduce the contamination level as low as possible, 12 lever-action Niskin samplers and all of the Niskin samplers had been thickly coated with teflon paint on their inside walls by San-giken Kogyo Ltd. before the cruise. The other two lever-action Niskin samplers had been already teflon-coated by General Oceanics and no additional coating was performed. Although the coating by General Oceanics is much thinner than that by San Giken Kogyo, there was no significant difference of Mn and Fe contamination level among all the lever-action Niskin samplers.

On board the ship, the samplers were cleaned thoroughly using 2% Extran MA01 (Merck) solution and Milli-Q pure water just before use. In spite of these treatments, the Niskin bottles were found still to suffer significant Fe contamination. The seawater samples were therefore collected only by the lever-action Niskin samplers at almost stations. Since we found the thermometer rotating mechanism of the lever-action sampler to be unreliable, the Niskin

samplers with reversing thermometers were paired with the lever-action Niskin samplers, in order to check whether the samplers were actuated at correct depths.

2.3 DESMOS hydrocast

DESMOS has 6 Niskin-type samplers (volume: 2 liters). These samplers (except for the No.2 sampler) were coated with teflon paint in the same manner as the rosette samplers mentioned above. Although it was not necessarily examined in detail to what extent the DESMOS samplers are free from contamination, it is supposed to be in a similar level as the 12-liter Niskin samplers attached to the CTDTRMS. During the DESMOS operation, the samplers were triggered one after another at any desired moment.

2.4 Chemical analyses

The following chemical components were measured on board the ship. Table 6-1 is the list of the responsible persons for these analytical works.

2.4.1 Salinity

Salinity was measured with a salinometer (Autosal, Model 8400A) in the usual way. IAPSO standard seawater (Ocean Scientific International Ltd., Batch: P121, Date: 08-Sep-92) was used for calibration.

2.4.2 Dissolved Oxygen

Dissolved oxygen was measured with an automatic titrator (Hirama, Model ART-3), which was calibrated by using CSK Standard of 0.0100N Potassium Iodate solution (WAKO Pure Chemical Industries, Ltd.). An oxygen bottle with a volume of 100 cm3 was used commonly for sampling and titration in order to avoid I2 vaporization loss.

2.4.3 pH

Seawater samples were collected in 100 cm^3 polyethylene bottles, and 40 cm^3 of the sample was analyzed by using high precision pH meter (model PHM93, Radiometer Analytical A/S) with a glass closed cell at a constant temperature of 25°C. Analysis time is 15 min per sample.

2.4.4 Titration alkalinity

Samples were collected in 250 cm^3 polyethylene bottles, and an aliquot of 50 cm^3 was used for analysis. Alkalinity was measured by the inflection point titration method using TitraLabTM (Radiometer Analytical A/S) system at a constant temperature (25°C) with an analysis time of less than 10 minutes.

2.4.5 Total inorganic carbon

Total CO_2 was measured by coulometric titration method using a Carbon Coulometer (UIC Inc.). The sample was collected in a 100 cm^3 glass vial bottle with sufficient overflow, and 0.05 cm^3 of 50% saturated $HgCl_2$ solution was added before sealing in order to restrict bacterial activity. An aliquot of 30 cm^3 of the sample was introduced to the reaction vessel, to which 2 cm^3 of phosphoric acid was added. The mixed solution was heated at about 60° C for 15 min in order to extract CO_2 gas, which was transferred to a coulometric titration cell for CO_2 measurement.

2.4.6 Methane

Dissolved CH_4 in seawater was measured with a FID gas chromatograph; the analytical method is principally similar to that by Gamo et al. (1987). Seawater samples were sealed in 100 cm^3 glass vial bottle, 0.05 cm^3 of 50% saturated $HgCl_2$ solution being added to stop biological activity. The samples were kept in a refrigerator and analyzed within a day after

sampling. Methane was measured with the Automated Methane Analyzing system (Denki Kagaku Keiki Corp., GAS-10(S) and GAS-10L) followed by the FID gas chromatograph (Shimadzu Corp., GC-6AM). Dissolved gases in seawater (40 cm^3) were extracted for 5.5 minutes by helium gas bubbling at a flow rate of 60 cm^3 min^{-1}, passed through a silica gel drying column, and collected by a U-trap (SUS 4x3, 16cm long) packed with active carbon (60/80 mesh). Then the trap was heated to $\sim$ 120° C and the trapped gases were injected to the gas chromatograph. All the procedures (gas extraction, trapping, injection and calculation of peak area) were controlled by an automatic data analyzer (Shimadzu, Chromatopac CR-6A). The analysis time was about 40 min per sample. Analytical conditions of the gas chromatograph were as follow: (1) separation column: SUS4x3, 5m long, packed with Porapak Q (60/80 mesh), (2) column temperature: 50°C, (3) carrier gas: nitrogen, with a flow rate of 40 cm^3 min^{-1}, (4)detector: flame ionization detector (Shimadzu, FID-6M), and (5) analytical error of CH_4: –0.2 nM estimated from replicate analyses.

2.4.7 Manganese

Manganese was determined on board by the automated-Mn analysis system which is based on the column electrolysis preconcentration and the chemiluminescence(CL) detection (Nakayama et al., 1989). In brief, 50 cm^3 of unfiltered seawater adjusted at pH 5.0 by adding ammonium acetate buffer solution is introduced to the system. Mn in the sample is adsorbed onto glassy carbon column electrode. The column is rinsed with the cleaning solution (pure water), and then hydrogen peroxide solution adjusted to pH 4 with ammonium acetate buffer solution is passed through the column. The eluent is mixed with alkaline luminol solution and the mixture is introduced into the CL cell through the mixing coil. Finally, Mn is determined by measurement of the CL intensity. Mn determined with this system is called "total adsorbable Mn", which contains Mn(II) ion and part of colloidal Mn. The relative standard deviation for five replicate measurements at 3.6 nM is 3.2 % and the determination limit(3s) is 0.14 nM for the typical analysis condition. The total throughput of analysis is 8 samples per hour. In addition to the measurement of total adsorbable Mn, total Mn was determined in the following manner: the samples were heated to boil with a microwave oven after adding hydrogen peroxide to decompose inert colloidal and particulate Mn. After this pretreatment, Mn was determined in the same manner as total adsorbable Mn.

2.4.8 Iron

Iron(III) in seawater was determined on board automatically in a closed flow system using chelating resin concentration and chemiluminescence detection (Obata et al., 1993). 125 cm^3 of unfiltered seawater was adjusted at pH 3.0 with 5 M formic acid-ammonium formate buffer solution. The sample solution filtered through a 0.22 m in-line filter was passed through the chelating resin column (MAF-8HQ, 8-quinolinol-immobilized fluoride containing metal alkoxide glass). Then the column was rinsed with cleaning solution (pure water), and the eluent (0.3 M hydrochloric acid) was passed through the column. The eluent was mixed with alkaline luminol solution, solution of hydrogen peroxide and 0.6 M aqueous ammonia, and the mixture was introduced into the CL cell through the mixing coil. The Fe(III) was determined by measurement of CL intensity. The column was washed with 1M hydrochloric acid after elution and washed with pure water not to remain hydrochloric acid. The relative standard deviation was 1.2% for 5 replicate measurements of purified seawater containing 1 nM Fe(III). Detection limit (3s) is 0.06 nM. Total Fe could also be determined by using this system after addition of hydrochloric acid and heating to boil with a microwave oven.

2.4.9 Aluminum

The dissolved and acid-leachable Al were determined by fluorimetric method of lumogallion-Al complex using Hitachi MPF-4 fluorescence spectrophotometer. The acid leachable Al is the sum of dissolved Al and particulate Al which is decomposed into dissolved form by heating seawater for an hour at pH 2. Since minerals can not be decomposed under this condition, the particulate Al measured in this study is thought to be Al-hydroxide derived from hydrothermal activity. Seawater samples were collected in 25 cm^3 teflon bottles. The samples were divided into two aliquots (10 cm^3 each) for dissolved Al and acid-leachable Al measurements. Nitric acid was added to the latter aliquot to adjust the pH to 2, and heated at 120°C for an hour. After cooling, 250 μl of 20 mM acetate buffer (pH:8) was added. Then, 1 $cm^3$of 20% acetate buffer (pH:5) and 200 μl of 0.01% lumogallion were added to the two aliquots and heated at 80° C for an hour. After cooling, Al concentrations were measured with the fluorescence spectrophotometer.

3. Observations

As shown in Table 6-2, we conducted 19 CTDTRMS observations (CTD-1 to -18 with a test operation: CTD-test), which include 5 tow-yo operations (CTD-9, 11, 15, 16, and 17). CTD-2 to -16 were performed in the main survey area close to Rodriguez Triple Junction (see Chapter A), and CTD-17 and -18 were the revisits to the SONNE Hydrothermal Plume Site, about 80 miles northward from the main survey area. We call thereafter these two survey areas "RTJ area" and "SONNE area". Detailed description about the SONNE area will be given in section 6-5. Figure 6-3 shows the locations of the CTD stations in RTJ area. CTD-1 is a control station, more than 250 miles northeastward from the main survey area. The location of the CTD-1 is almost the same as the GEOSECS station 453, where detailed chemical measurements were done in 1978 by the US geochemical group (Weiss et al., 1982).

At the beginning of the CTD observation, we planed to survey extensively the following three segments centered at the Rodriguez Triple Junction: the Central Indian Ridge (CIR), the Southeastern Indian Ridge (SEIR), and the Southwestern Indian Ridge (SWIR), in order to find hydrothermally active sites anywhere in these segments. As we proceeded with the surveys, however, our interest was gradually focused on the CIR as shown in Table 6-2, because significant hydrothermal plumes were observed only in the CIR, particularly in its northern area. This is the reason why four of the five tow-yo operations were concentrated at the northern CIR.

Figure 6-4 is a simplified section showing the tow-yo operation at CTD-9 together with the bottom topography. As shown in Fig. 6-4, the deep and the shallow turning points of the CTDTRMS are successively called B1, B2,...., and S1, S2,...., respectively, and the downward and upward observations are numbered as Down-1, Down-2,.... , and Up-1, Up-2, ..., respectively. The tracks of the CTDTRMS during the tow-yo observations in RTJ area (CTD-9, 11, 15, and 16) are shown in Figs. 6-5 to 6-8, where the locations of some turning points are also shown.

4. Results and discussion (1) : Rodriguez Triple Junction area

4.1 Hydrocast data

Tables 6-3 to -18 summarize the data of chemical analyses for the water samples collected at the CTDTRMS stations. For convenience, we will sometimes call the station name

"KH-93-3, CTD-**" simply "IR**", which is the abbreviation of "Indian Ridge". Some abbreviations in the Tables 6-3 to -18 are as follow. Bottle type N: Niskin, type L: Lever-action Niskin, TA-Mn: total adsorbable Mn, T-Mn: Total Mn, alk: alkalinity, and concentration nM: nmol l-1. Depth was calculated from P(pressure) and latitude using a universal equation. T(Temperature) data were those by the T-sensor of the CTD. S(Salinity) data were those measured by the salinometer on board the ship. No water sample was available at station CTD-5 (IR05) due to troubles of the sampling system. As to the water samples collected during the tow-yo operations, operation numbers, such as Down-2 or Up-3, are shown in the lower part of the Tables 6-10, 6-13, 6-17, and 6-18 together with the sampling bottle numbers to specify the locations of the samples. There are some bad samples with unreasonable salinity and oxygen values, probably due to water exchange through incompletely closed lids. Data from these samples are shaded in the Tables for caution. Data for the DESMOS hydrocasts are shown in Table 6-19.

4.2 Anomaly of light transmission

The light transmissiometer, which was employed for the first time in R.V. Hakuho Maru, offered us much useful information on the areal distribution of hydrothermal plumes, not only because the sensitivity of light transmission is high enough to detect water column turbidity due to hydrothermal plumes, but also because the anomaly can be detected in real time on board the ship.

Light transmission anomaly was first detected at station CTD-5 in the northern part of the CIR segment (Fig. 6-3). About half a day later, CTD vertical hydrocast was performed at almost the same location (CTD-6). Figure 6-7 shows the vertical profile of light transmission, together with those of potential temperature, salinity and sigma-theta at CTD-6, where a negative anomaly of light transmission probably due to a hydrothermal plume was clearly recognized at about 2250 m depth. As mentioned later, anomalies of CH_4, Mn, Fe, and Al were also detected consistently at this depth. It should be noted that this depth almost corresponds to a sudden change of density gradient, which may act as a barrier against more upward dispersion of the hydrothermal plume. It is somewhat curious that the plume appeared at remarkably shallow depth, about 1800 m above the bottom. It was only in the northeastern area of the CIR segment that significant light transmission anomaly was observed during this cruise. The other stations CTD-2, 3, 4, 7, 8, 10, 12, 13 and 14 along the ridge axes showed little anomaly of light transmission.

The CTDTRMS tow-yo observations were performed four times (CTD-9, 11, 15, and 16) around stations CTD-5 and 6 (Fig.6-3) for more detailed investigation of this hydrothermal plume. Stations CTD-15 and 16 were located in the northeastern off-axis area. As shown in Figures 6-8 to 6-11, light transmission anomaly at 2200 - 2350 m depth was commonly observed with some variations. The strong anomaly observed during CTD-9 (Fig.6-8) on August 6-7 was not identified during CTD-11 (Fig.6-9) on August 17, suggesting short term variations of the plume.

4.3 Anomalies of chemical components

Vertical profiles of CH_4, Mn (TA-Mn), Fe, and Al are shown in Figures 6-15 to 6-22. It should be first noted that, except for the control station (IR01), the whole water columns below $\sim$ 2000 m depth in the CIR, SEIR, and SWIR segments showed high concentrations of Mn, Fe and Al compared to those at the control station, strongly suggesting the effect of hydrothermal activity somewhere along the ridge axes.

In the northeastern area of the CIR segment including off-axis zone (stations IR06, 09, 11, 15, and 16), a significant hydrothermal plume was detected as big anomalies of CH_4 (Figure 6-15), Mn (Figure 6-17), and Fe (Figure 6-19) at 2200-2400 m depth, completely in accordance with the light transmission anomaly mentioned above. Profiles of acid-leachable Al (Fig.6-19) also showed slight anomaly at this depth range.

For contrast, any hydrothermal plume with a combination of CH_4, Mn, Fe, and Al anomalies was not observed in the SEIR and SWIR segments as shown in Figs. 6-13, 6-15, 6-17, and 6-20. Although it is suspected that station CTD-10 in the SWIR segment may have a moderate hydrothermal plume at 3700 m depth from the Fe profile(Fig.6-17), there was little corresponding anomaly in the Mn and CH_4 profiles over the same depth range (Figs.6-13 and 6-15).

4.4 Suggested source of hydrothermal discharge

Judging from the above results obtained during this cruise, it is suggested that hydrothermal vent sites should exist somewhere close to the northeastern area of the CIR segment. It is noteworthy that the plume appeared at a remarkably shallow depth, 1800 m above the bottom at IR05 and 06 located on the rift valley. The height of the plume above the bottom is extremely high compared to the previous data:~ 700 m above the bottom in the Mariana Trough (Horibe et al., 1986) and ~ 1000 m above the bottom in the eastern Manus Basin (Gamo et al., 1993).

Although it is common that hydrothermally active sites are located within the rift valleys as observed in the Mid-Atlantic Ridge (Klinkhammer et al., 1985; Rona et al., 1986), we would suggest that the source of hydrothermal fluids in the northern CIR may exist not on the bottom of the rift valley but on shallower off-axis wall or axial high from the following two reasons. (i) It seems unreal that hydrothermal plumes discharged from the rift valley of more than 4000 m depth comes up as many as 1800 m to reach a depth of 2200-2400 m. (ii) Anomalies of light transmission and chemical tracers are significant in the northeastern off-axis zone, while the observations performed in the northern rift valley (IR12, 14, and 02 as well as DESMOS-2) failed to detect any indication of hydrothermal plumes. Hydrothermal activities apart from the center of rift valley have ever been observed in SONNE area of the central Indian Ridge (Plüger et al., 1990) and in the eastern Manus backarc basin (Gamo et al., 1993).

5. Results and discussion (2) : SONNE hydrothermal Plume Site

5.1 Previous works

Plüger et al.(1990) reported that a hydrothermal plume was observed at (24° 00.3′S, 69° 39.6′E) of the eastern wall of the Central Indian Ridge rift valley (SONNE Hydrothermal Plume Site), during the cruise GEMINO-3 by R.V. SONNE in 1988. Although they also found a water column temperature anomaly of 0.05° C and hydrothermally altered rocks near the SONNE Site, they could not locate the source of the plume by camera/video towing.

5.2 Additional information by KH-93-3 cruise

With the assumption that the hydrothermal plume observed in 1988 by Plüger et al.(1990) was still active, two CTDTRMS stations were occupied close to the SONNE Site: one of them was a vertical mode operation (CTD-18) and the other is a tow-yo operation (CTD-17). The purposes of CTD-17 and -18 are: (1) to locate hydrothermal vent sites more closely, (2) to elucidate temporal variations, if any, of the hydrothermal plume since 1988, and (3) to compare chemical characteristics of hydrothermal plumes between the SONNE area and the RTJ area.

The locations of CTD-17 and 18 are listed in Table 6-2. Figure 6-21 is a SEABEAM map of the SONNE area by *Hakuho Maru*, where the track of CTD-17 is plotted. The SONNE Hydrothermal Plume Site, which is almost the same as the starting point of CTD-17, locates at the western wall of a small depression with a maximum depth of ~ 3420m, neighboring to the eastern axial high as shown in Fig. 6-21. Since it was unknown whether the source of the plume is inside the depression or in the eastern wall of the rift valley, the CTD-17 tow-yo was performed westward from the SONNE Site toward the rift valley in order to investigate an areal distribution of the hydrothermal plume along the track. After the tow-yo observations at CTD-17, water samples were collected at various depths during the ascent (Up-5) of the CTDTRMS between (24° 00.3′S, 69° 38.1′E) and (24° 00.3′S, 69° 37.1′E). The purpose of CTD-18 was to compare the characteristics of the plume between 1988 and 1993. Data of the two hydrocasts (CTD-17 and 18) are listed in Tables 6-20 and 6-21.

Figure 6-22 shows vertical profiles of light transmission observed during the CTD-17 tow-yo operation. There are two types of anomalies: (i) a broad anomaly centered at ~ 2900 m depth which was commonly observed in all the profiles and (ii) a sharp anomaly at 2500 m depth observed only near the axial high. The first type negative anomaly between the depression and the axial high (B1~B3) seems to extend to the bottom with no minimum point in contrast to that in the western side of the axial high (B4~B5). The axial high (minimum depth: ~ 2880m) may behave as a topographic barrier to restrict westward dispersion of low transmission characteristic from the eastern side of the axial high. The second type anomaly suggests a local discharge of hydrothermal fluids somewhere close to the axial high.

The anomalies of CH_4, Mn, and Fe at CTD-17 and 18 were apparently more significant than those at the RTJ area as shown in Figure 6-23, 24 and 25. The profiles of these tracers are basically similar to those of light transmission; the peak shape at CTD-18 is broader than those at CTD-17. The maximum values of CH4 and Mn at CTD-18 were 5.7 nM and 10.2 nM, respectively, which are slightly lower than the values of 9.0 nM and 23 nM observed in the SONNE Site in 1988. The characteristics of CH_4 and Fe profiles are similar to each other, showing higher concentrations at CTD-18 than CTD-17 (Figs.6-22 and 23). On the other hand, Mn shows higher values at CTD-17 (Fig.6-24). This discrepancy made it difficult to locate the source of the hydrothermal plume. More observations are necessary. It is of interest that, though the reason is unclear, the profile of the acid-leachable Al was significantly high compared to that of dissolved Al only at CTD-17 as shown in Fig. 6-26. There may be some difference in behaviors of particulate matter between IR17 and IR18.

6. Summary of the on board studies

The works on water geochemistry were conducted almost perfectly with great success. There was little failure of the CTDTRMS operation and little trouble of analytical instruments. The only problem was the lack of time for more detailed surveys. The conclusions obtained on board the ship can be summarized as follow.

(1) In the Rodriguez Triple Junction area, Mn, Fe and Al show significantly higher concentrations than the background values outside the ridge system, suggesting the existence of hydrothermal activity somewhere along the ridge axes.

(2) A distinct hydrothermal plume was detected for the first time in the Central Indian Ridge segment close to RTJ. The center of the plume was in a shallow depth of ~ 2200 m, about 1800 m higher than the bottom of the rift valley. Judging from the areal distribution of the plume, its source is suggested to be somewhere at the eastern off-axis area.

(3) It was confirmed that the SONNE Hydrothermal Plume Site had maintained its activity since 1988. The source area of the plume could not be fixed due to a complexity of areal distribution of plumes.

7. Future works

The following studies are planned by the on board scientists in shorebased laboratories using collected samples during the cruise. Some of them will be cooperative works with scientists other than the cruise participants.

7.1 Trace element analyses (by K. Shitashima)

Seawater samples were stored in 500ml acid cleaned high density polyethylene bottle (Nalgen^{TM}), and 2.5ml of nitric acid was added in order to adjust the pH to 2. Several trace metals (Al, Fe, Mn, Cu, Zn, Cd, Co, Pb, Ni, Mo and V) will be extracted and concentrated from sea water by using chelating resin extraction method or solvent extraction method, and measured on GFAAS or ICP-MS.

7.2 Minor and trace element analyses (by T. Oomori)

Seawater samples (ca. 200 bottles with each 300 cm^3) were collected by the CTD hydrocasts at the Rodriguez Triple Junction area. These samples will be used for analyzing the minor and trace elements, which are related to the submarine hydrothermal activity. Ga-APDC coprecipitation technique and ICP-MS connected with ETV will be employed for the analysis of small amount of trace elements.

7.3 Measurements of Ra isotopes in Indian surface sea water (by T. Oomori)

Mn-coated resin has been developed originally by our group for the purpose of rapid adsorption of radioactive nuclides such as Ra etc. from sea water. Ra in surface sea water are adsorbed on this Mn-coated resin at 10 sites of the Indian Ocean from Port Louis to Penang. The distribution and the behavior of Ra isotopes in the Indian Ocean will be studied.

7.4 Studies on general trace metals, vanadium, and arsenic (by E. Nakayama, H. Obata, K. Okamura and K. Isshiki)

For measuring general trace metals, 500 ml of seawater was filtered through a Millipore Omnipore filter(0.22 μm) and was passed through the column packed with 8-quinolinol-immobilized on silica gel(MAF-8HQ). The trace metals adsorbed on the resin were eluted with 5 ml of 1 M hydrochloric acid. The determination of Cu, Zn, Pb, Ni, Cd et al. will be done with a inductively-coupled plasma atomic mass spectrometer. For vanadium, 100 ml of seawater was filtered through a Nuclepore filter(0.22 μm). Vanadium(IV) and vanadium (V) will be determined separately by the catalytic method using Bindschedler's green leuco base. For arsenic, 600 ml of seawater was filtered through a Nuclepore filter(0.45 μm). Arsenic(III) was preconcentrated by solvent extraction from 500 ml of seawater. Arsenic will be determined by hydride generation-atomic absorption spectrometry. Total arsenic(arsenic(III), arsenic(V) and organoarsenic species) in 50 ml seawater sample will be determined by the same method as arsenic(III) without further pretreatment.

7.5 $d^{13}C$ of SCO_2 in seawater (by T. Gamo et al.)

Every water samples collected by the CTD hydrocasts were sealed in 100 cm^3 vial bottles with adding 0.05 cm^3 of 50% saturated $HgCl_2$ solution and stored in a refrigerator. After the cruise, SCO_2 will be extracted and its $d^{13}C$ will be measured by stable isotope mass spectrometry. Besides the CTD samples, surface seawaters were collected almost every day during the ship transits from Singapore to Port Louis, from Port Louis to Penang, and from Penang to Tokyo (Table 6-22). The samples were taken from a faucet of research seawater in No.6 laboratory, being stored in the same way as the CTD samples, except that 0.5 cm^3 of saturated $HgCl_2$ solution was added to each sample. The surface seawaters will be analyzed by T. Nakazawa et al. (Faculty of Science, Tohoku University) as a cooperative study.

7.6 Helium isotope measurements (by T. Gamo et al.)

Helium isotope ratio ($^3He/^4He$) is known to be a good indicator of hydrothermal plumes because helium of magmatic origin has higher $^3He/^4He$ ratio than that of crustal origin. For the measurement of the helium isotope ratio, seawater samples with no air contamination were sealed in copper tubing (9.52 mm O.D. with a thickness of 1.2 mm, 100 cm long) by pinching the both ends of the tubing. Table 6-23 shows a list of the He samples. In laboratories on land, helium gas will be extracted and purified to measure $^3He/^4He$ ratio by helium isotope mass spectrometry.

7.7 Measurements of Po, Pb, and rare earth elements in seawater (by T. Gamo et al.)

Seawater samples for Po and Pb analyses were taken in 3-liter large-mouthed polyethylene bottles. 2 cm^3 of conc.HCl (WAKO, special grade) was added to each sample before storage. Seawater samples for rare earth elements were taken in 3-liter small-mouthed polyethylene bottles. 2 cm^3 of 6N HCl (TAMAPURE) was added to each sample before storage. Table 6-24 is a list of these samples.

8. Papers to be published

T. Gamo and all chemistry members, Chemical characteristics of hydrothermal plumes due to off-axis hydrothermal activity near the Rodriguez Triple Junction, Indian Ridge.
T. Gamo et al., The distribution of Helium-3 in the hydrothermal plumes near the Rodriguez Triple Junction, Indian Ridge.
T. Gamo et al., Revisit to the SONNE Hydrothermal Plume Site in the Indian Ridge: comparison of chemical anomalies between 1988 and 1993.
E. Nakayama et al., Vertical distributions of manganese and iron in the western Indian Ocean.
E. Nakayama et al., Behavior of vanadium and arsenic in seawater in hydrothermally active sites of the Central Indian Ridge.
T. Oomori et al., Determination of minor and trace elements in seawater at the Rodriguez Triple Junction by ICP-MS.
T. Oomori et al., Ra isotopes in surface waters of the Indian Ocean.
K. Shitashima et al., Aluminum and other trace metals as indicators of hydrothermal activity.

9. Acknowledgments

The water chemistry group wishes sincerely to thank the co-chief scientists of this cruise, Profs. K. Takami and H. Fujimoto, for their outstanding leadership to carry out the surveys as effectively as possible. Prof. S. Ohta and Mr. K. Shimizu kindly helped us to take water samples during the DESMOS operations. Dr. J. Ishibashi allowed us to use the Automatic CH_4 Analyzing system and made strenuous efforts to adjust the system properly. Topographic maps in this report were suitably arranged by Ms. C. Honsho.

REFERENCES

J.L. Charlou, H. Bougault, P. Apprio, T. Nelsen and P. Rona (1991a) Different TDM/CH4 hydrothermal plume signatures: TAG site at 26°N and serpentinized ultrabasic diapir at 15° 05′N on the Mid-Atlantic Ridge. Geochim. Cosmochim. Acta, 55, 3209-3222.

J.L. Charlou, H. Bougault, P. Appriou, P. Jean-Baptiste, J. Etoubleau and A. Birolleau (1991b) Water column anomalies associated with hydrothermal activity between 11° 40′ and 13°N on the East Pacific Rise: discrepancies between tracers. Deep-Sea Res., 38, 569-596.

T. Gamo, J. Ishibashi, H. Sakai and B. Tilbrook (1987) Methane anomalies in seawater above the Loihi submarine summit area, Hawaii. Geochim. Cosmochim. Acta, 51, 2857-2864.

T. Gamo, H. Sakai, J. Ishibashi, E. Nakayama, K. Isshiki, H. Matsuura, K. Shitashima, K. Takeuchi and S. Ohta (1993) Hydrothermal plumes in the eastern Manus Basin, Bismarck Sea: CH_4, Mn, Al and pH anomalies. Deep-Sea Res., in press.

P.M. Herzig and W.L. Plüger (1988) Exploration for hydrothermal activity near the Rodriguez Triple Junction, Indian Ocean. Canadian Mineralogist, 26, 721-736. Y. Horibe, K.-R. Kim and H. Craig (1986) Hydrothermal methane plumes in the Mariana back-arc spreading centre. Nature, 324, 131-133.

P. Jean-Baptiste, F. Mantisi, H. Pauwells, D. Grimaud, and P. Patriat (1992) Hydrothermal ^3He and manganese plumes at 19° 29′S on the Central Indian Ridge. Geophys. Res. Lett., 19, 1787-1790.

G.P. Klinkhammer, P. Rona, M. Greaves and H. Elderfield (1985) Hydrothermal manganese plumes in the Mid-Atlantic Ridge rift valley. Nature, 314, 727-731.

E. Nakayama, K. Isshiki, Y. Sohrin and H. Karatani (1989) Automated determination of manganese in seawater by electrolytic concentration and chemiluminescence detection. Anal. Chem., 61, 1392-1396.

Y. Nojiri, J. Ishibashi, T. Kawai, A. Otsuki and H. Sakai (1989) Hydrothermal plumes along the North Fiji Basin spreading axis. Nature, 342, 667-670.

H. Obata, H. Karatani and E. Nakayama (1993) Automated determination of iron in seawater by chelating resin concentration and chemiluminescence detection. Anal. Chem., 65, 1524-1528.

W.T. Plüger, P.M. Herzig, K.P. Becker, G. Deissmann, D. Schöps, J. Lange, A. Jenisch, H.H. Richnow, T. Schulze, and W. Michaelis (1990) Discovery of hydrothermal fields at the Central Indian Ridge. Marine Mining, 9, 73-86.

P.A. Rona, G. Klinkhammer, T.A. Nelsen, J.H. Trefry, and H. Elderfield (1986) Black smokers, massive sulphides and vent biota at the Mid-Atlantic Ridge. Nature, 321, 33-37.

R.F. Weiss et al. (1982) GEOSECS Indian Expedition, Vol.5, U. S. Government Printing Office.

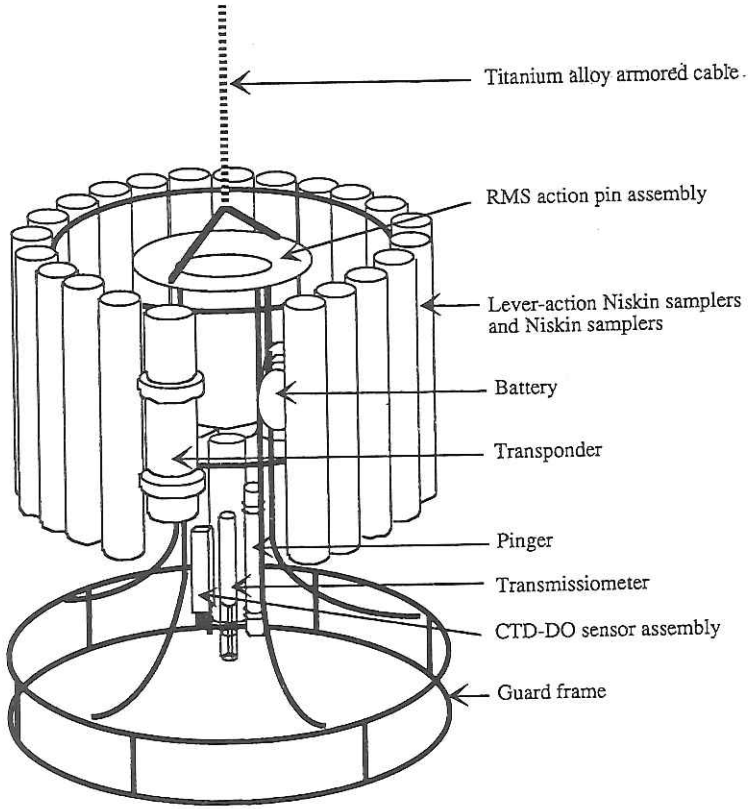

Fig. 6-1. The CTDTRMS system used during KH-93-3 cruise.

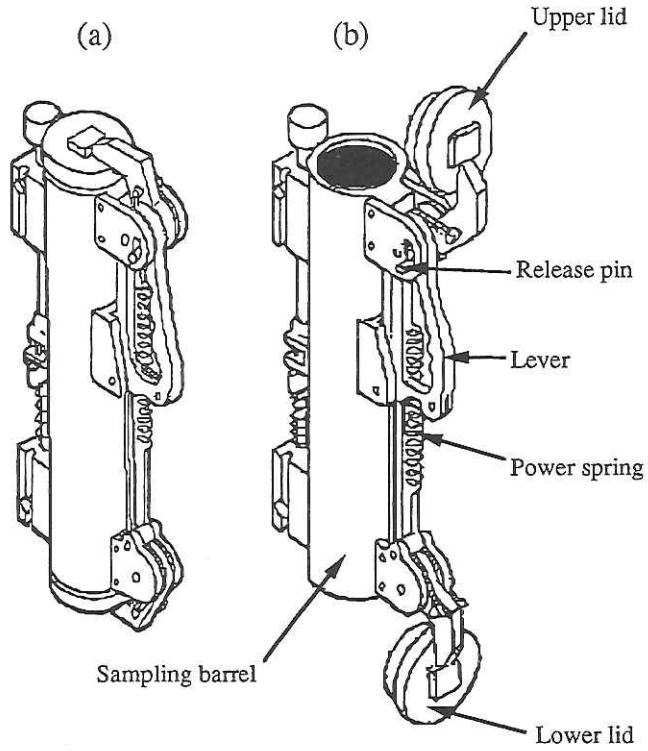

Fig. 6-2. Lever action Niskin sampler, closed (a) and open (b).

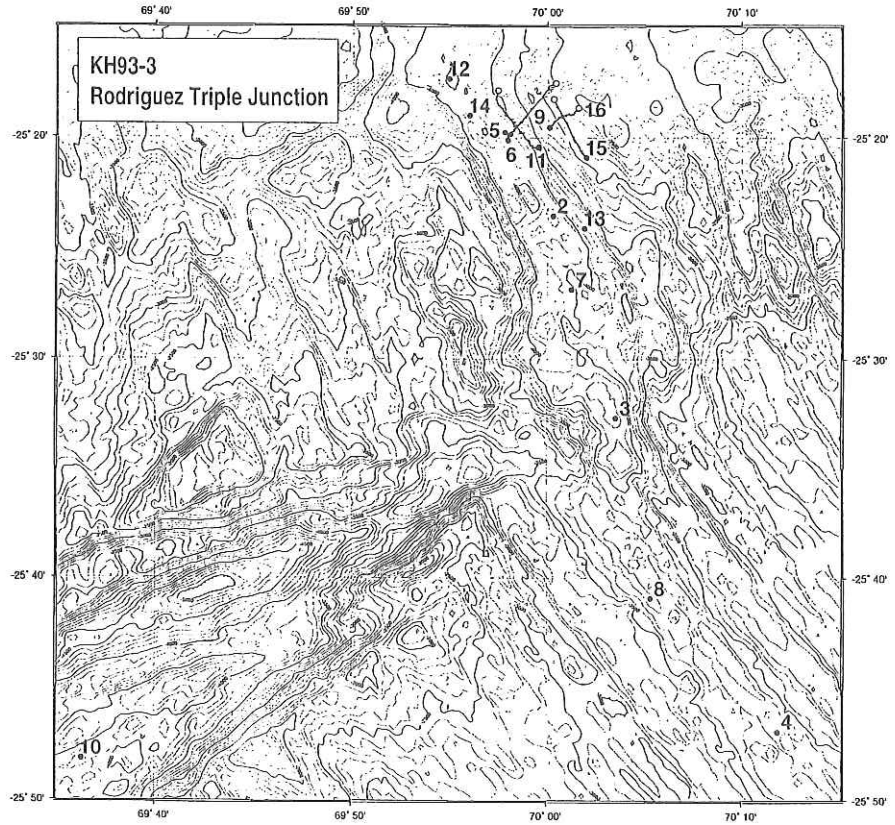

Fig. 6-3. Map showing the locations of CTD stations near to the Rodriguez Triple Junction.

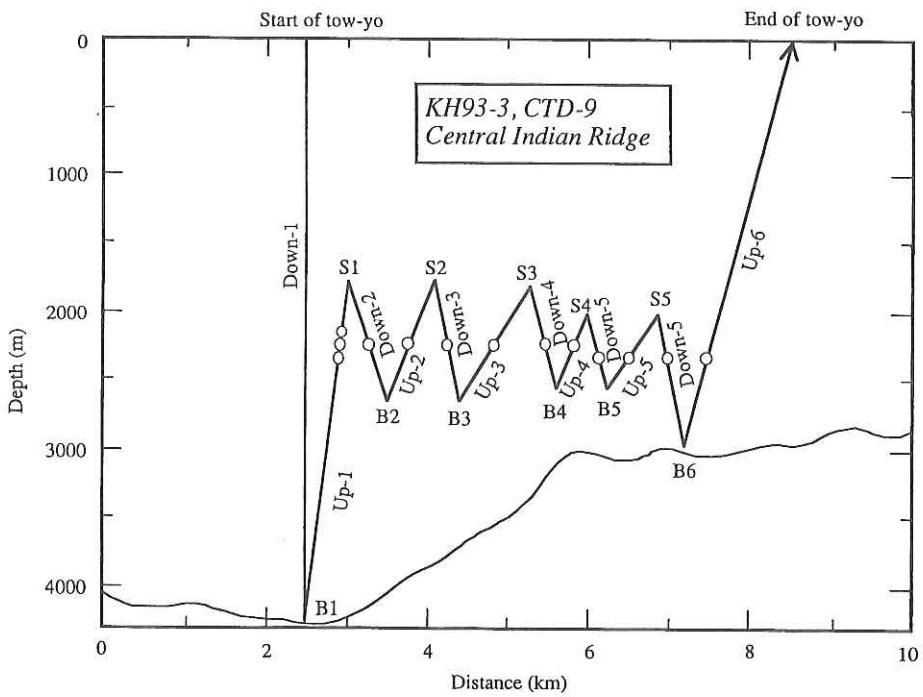

Fig. 6-4. Vertical section of the CTD-9 tow-yo observation.

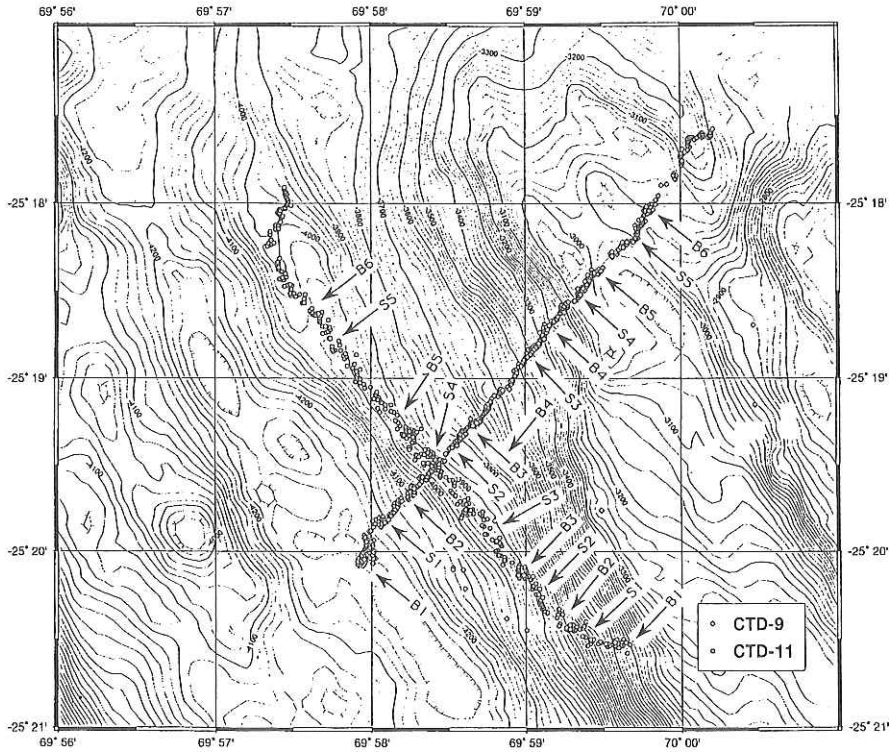

Fig. 6-5. Topographic map showing the tow-yo tracks of the CTDTRMS at CTD-9 and 11.

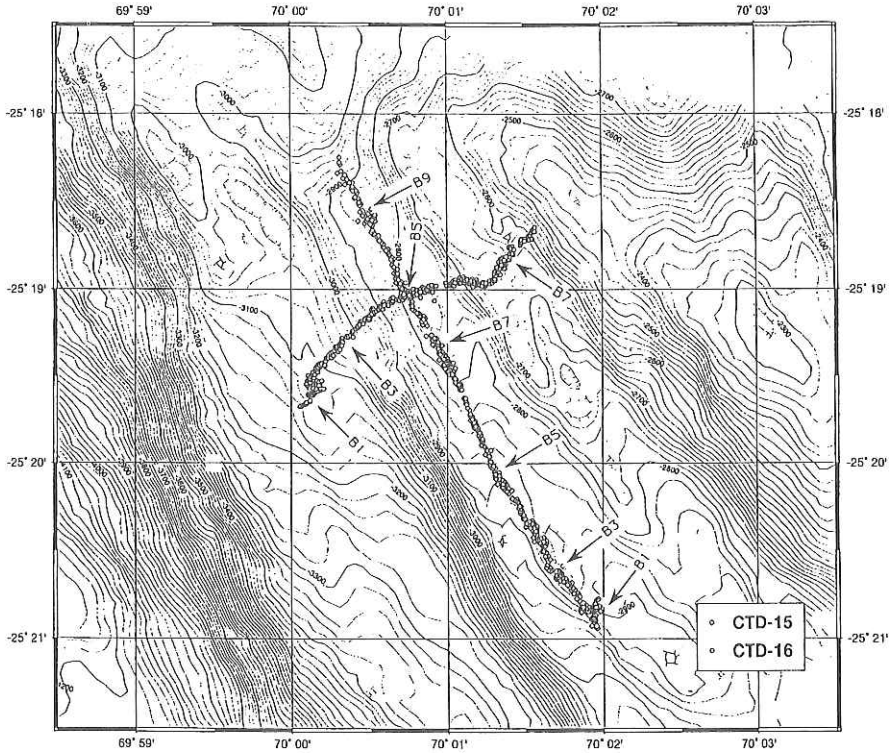

Fig. 6-6. Topographic map showing the tow-yo tracks of the CTDTRMS at CTD-15 and 16.

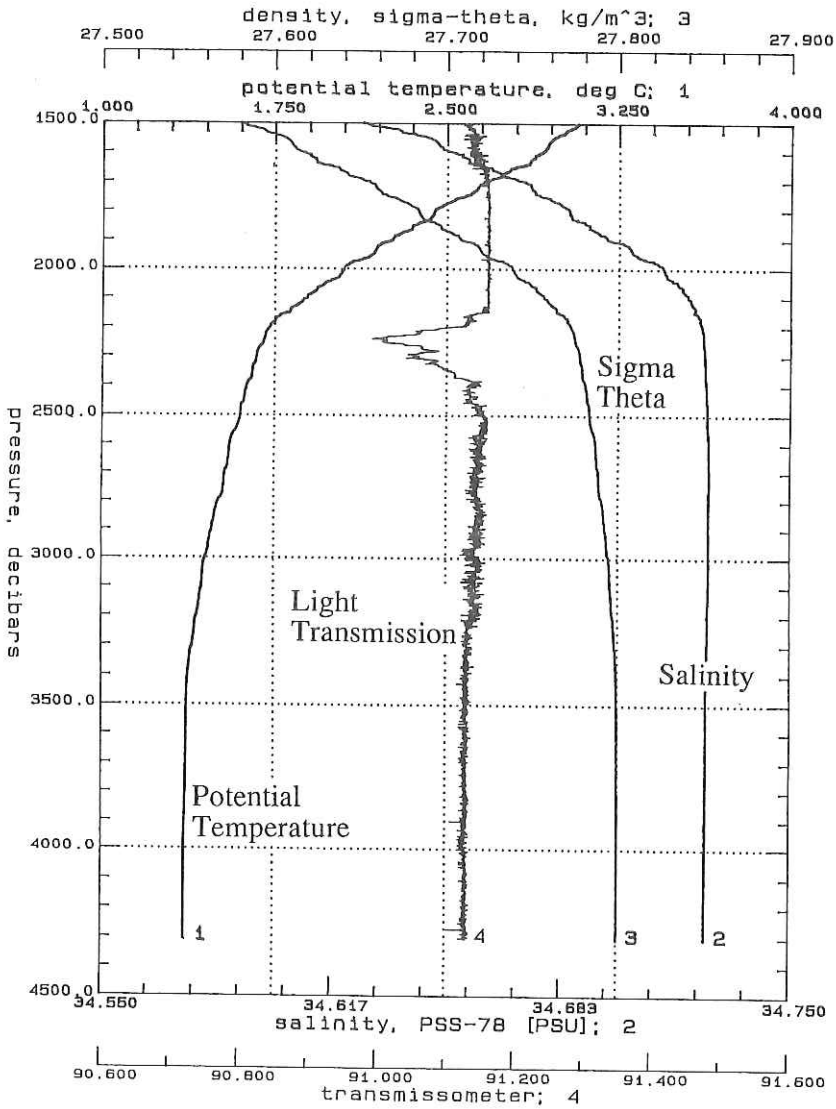

Fig. 6-7. Vertical profiles of potential temperature, salinity, potential density (sigma theta), and light transmission at station CTD-6.

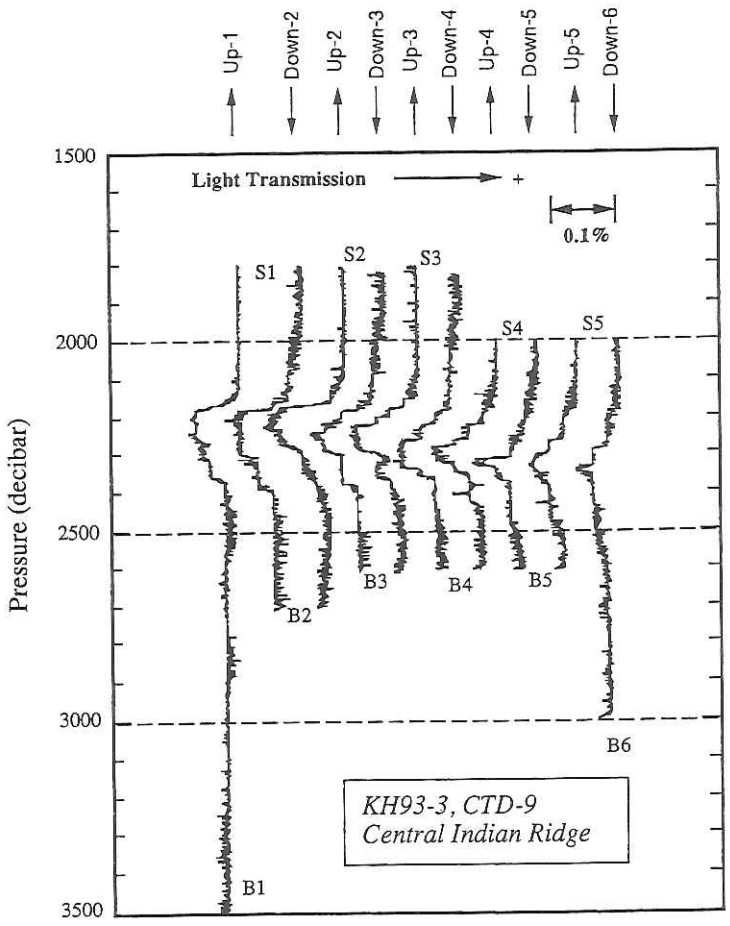

Fig. 6-8. Vertical profiles of light transmission observed during the CTD-9 tow-yo operation, which are arbitrarily offset for convenience.

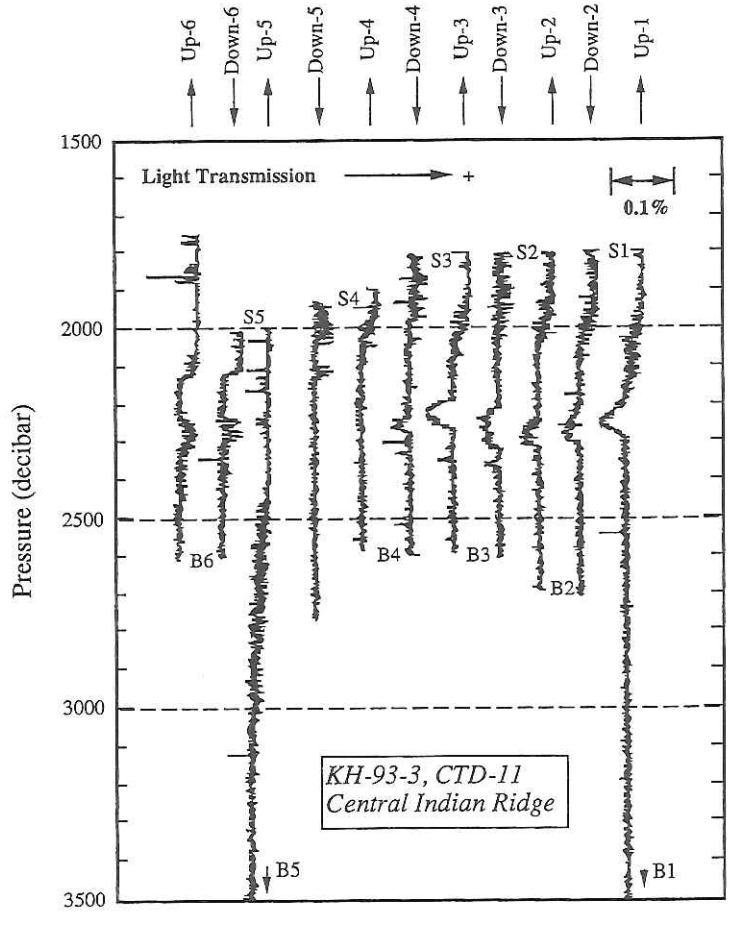

Fig. 6-9. Vertical profiles of light transmission observed during the CTD-11 tow-yo operation, which are arbitrarily offset for convenience.

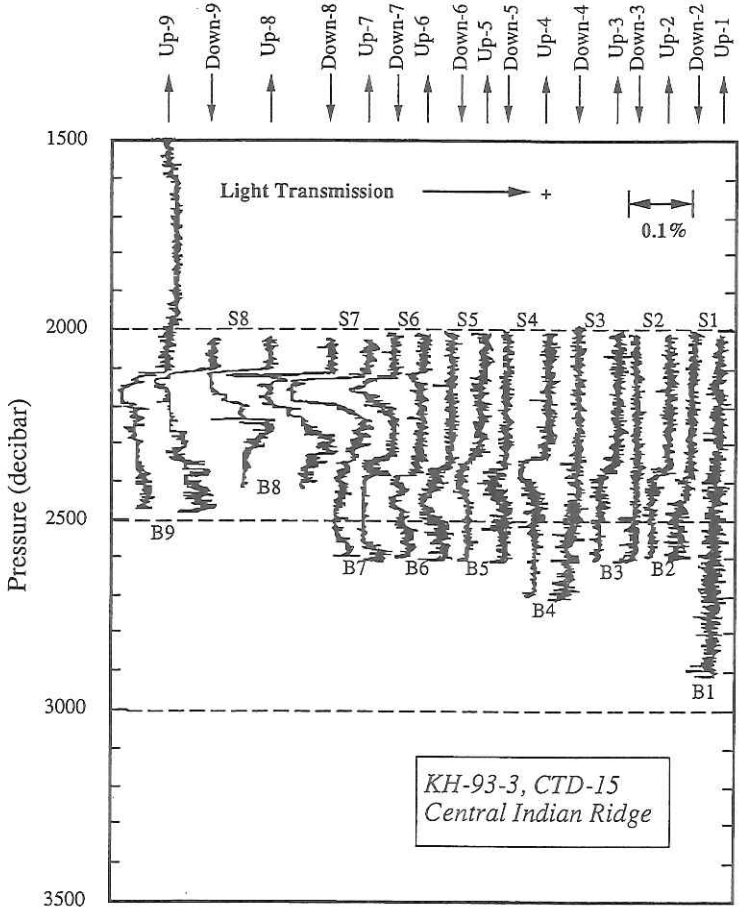

Fig. 6-10. Vertical profiles of light transmission observed during the CTD-15 tow-yo operation, which are arbitrarily offset for convenience.

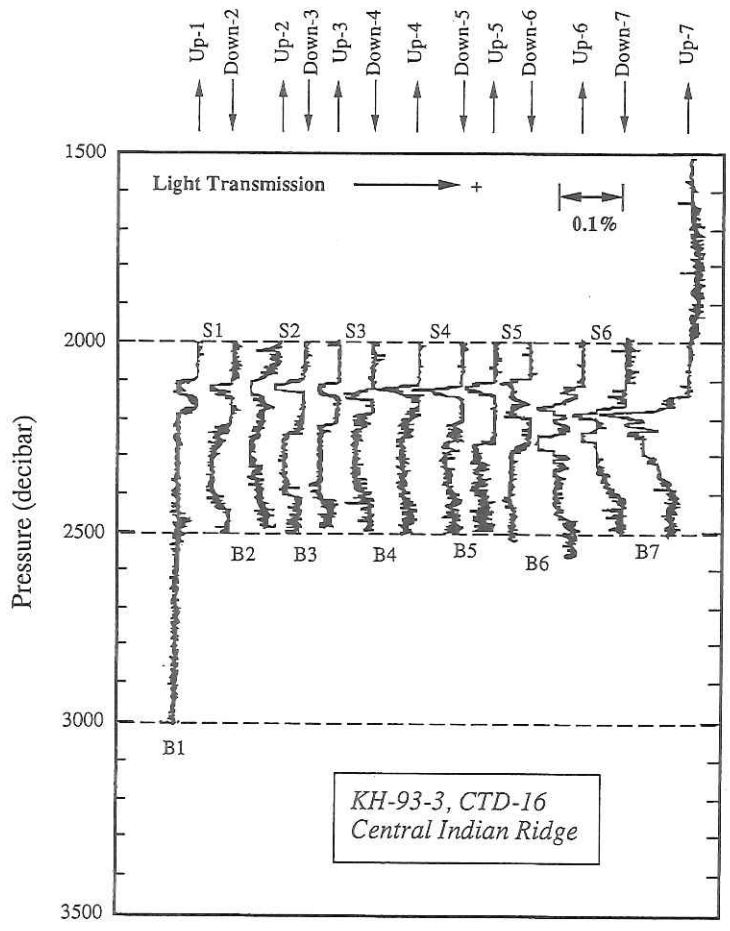

Fig. 6-11. Vertical profiles of light transmission observed during the CTD-16 tow-yo operation, which are arbitrarily offset for convenience.

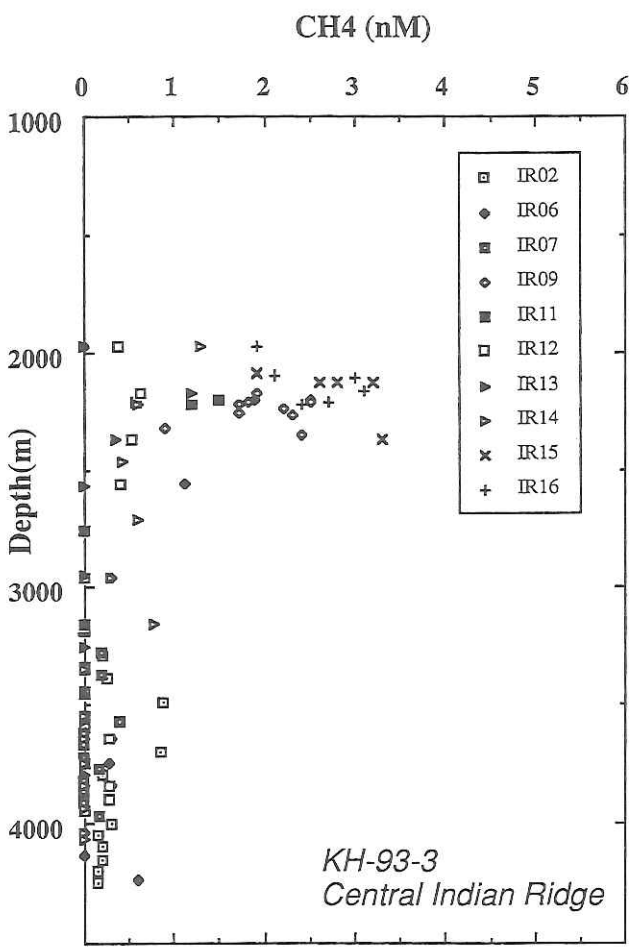

Fig. 6-12. Vertical profiles of dissolved CH_4 in the Central Indian Ridge segment.

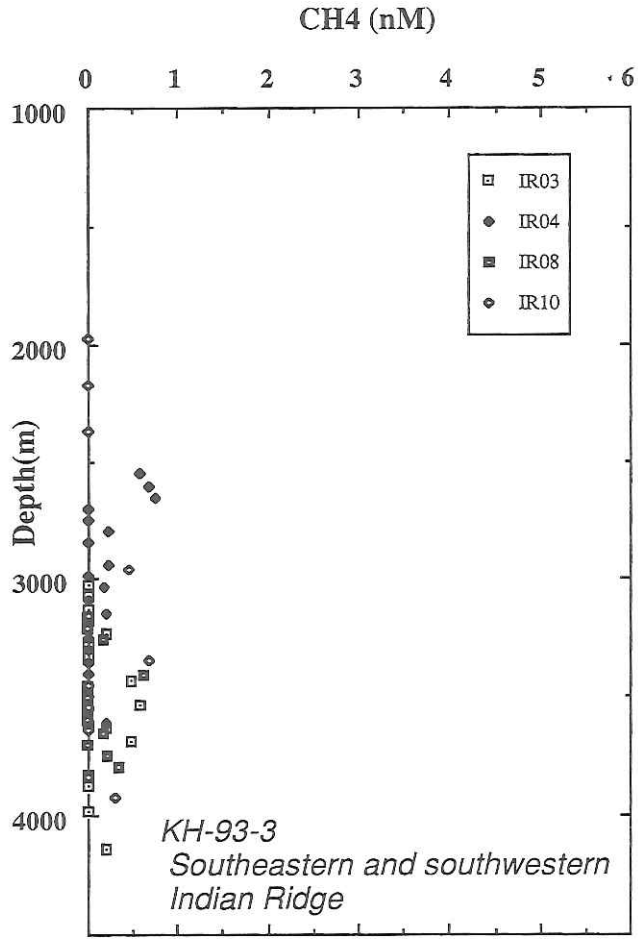

Fig. 6-13. Vertical profiles of dissolved CH_4 in the Southeastern and Southwestern Indian Ridge segments.

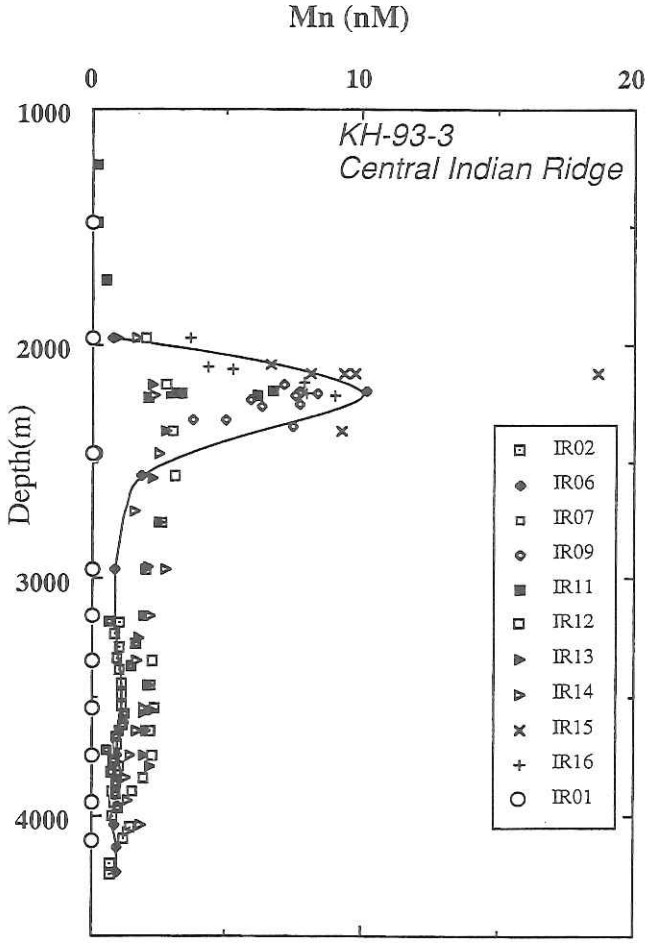

Fig. 6-14. Vertical profiles of total adsorbable manganese in the Central Indian Ridge segment.

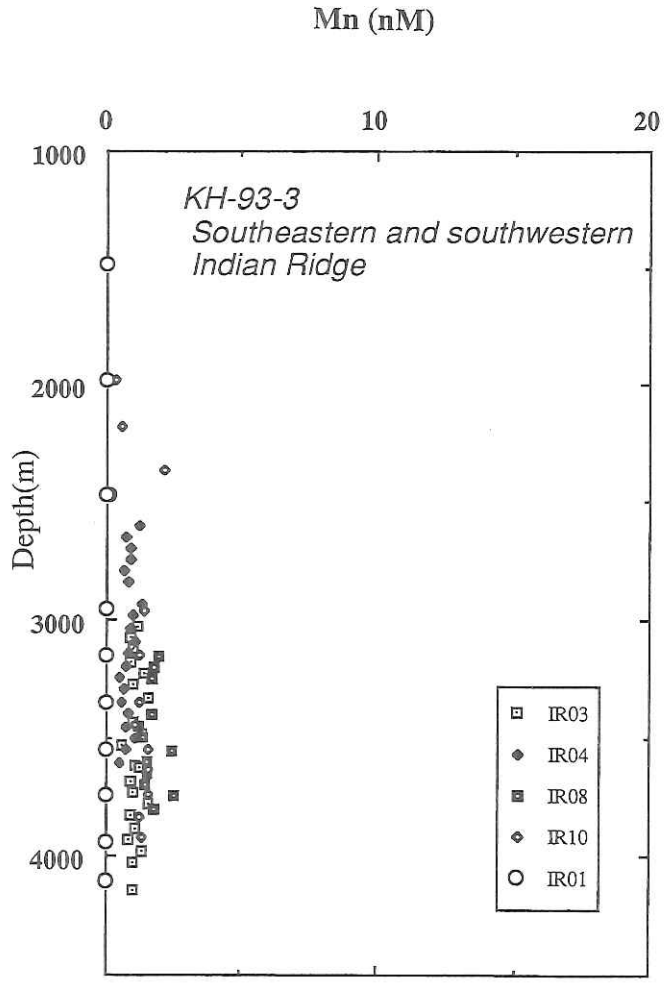

Fig. 6-15. Vertical profiles of total adsorbable manganese in the Southeastern and Southwestern Indian Ridge segments.

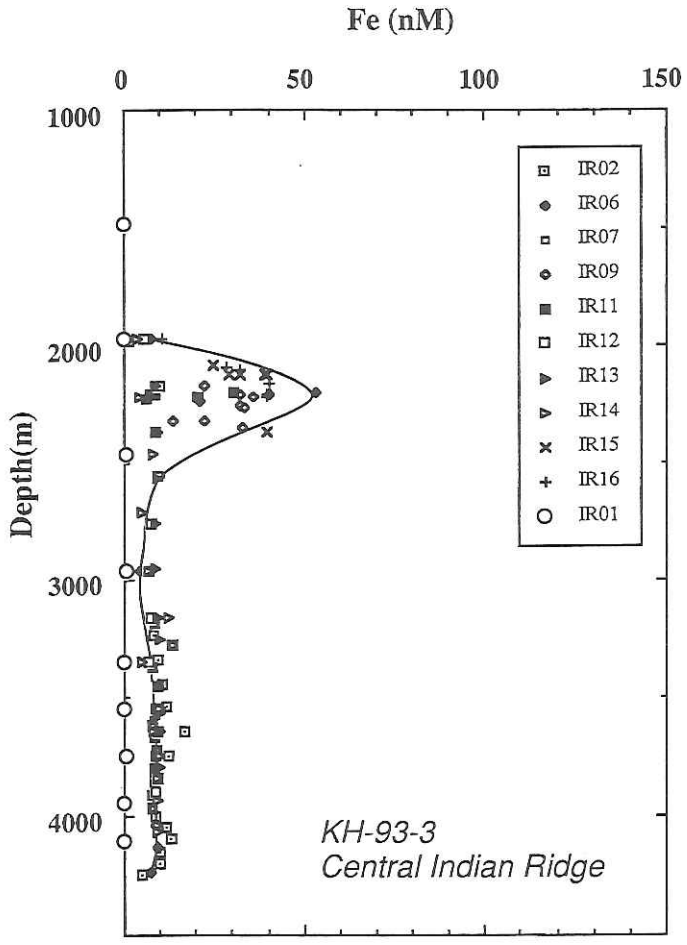

Fig. 6-16. Vertical profiles of iron(III) in the Central Indian Ridge segment.

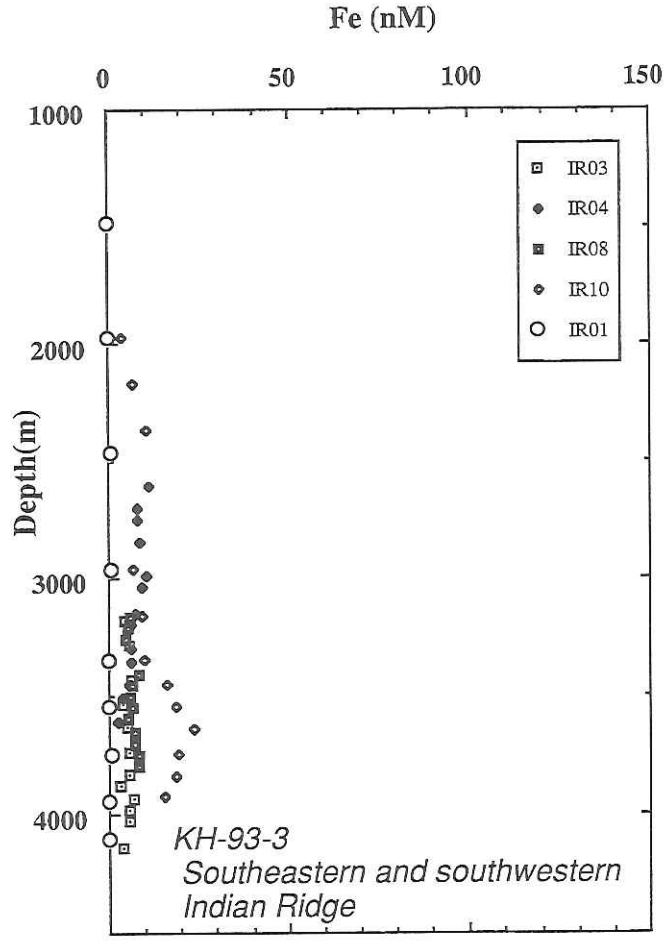

Fig. 6-17. Vertical profiles of iron(III) in the Southeastern and Southwestern Indian Ridge segments.

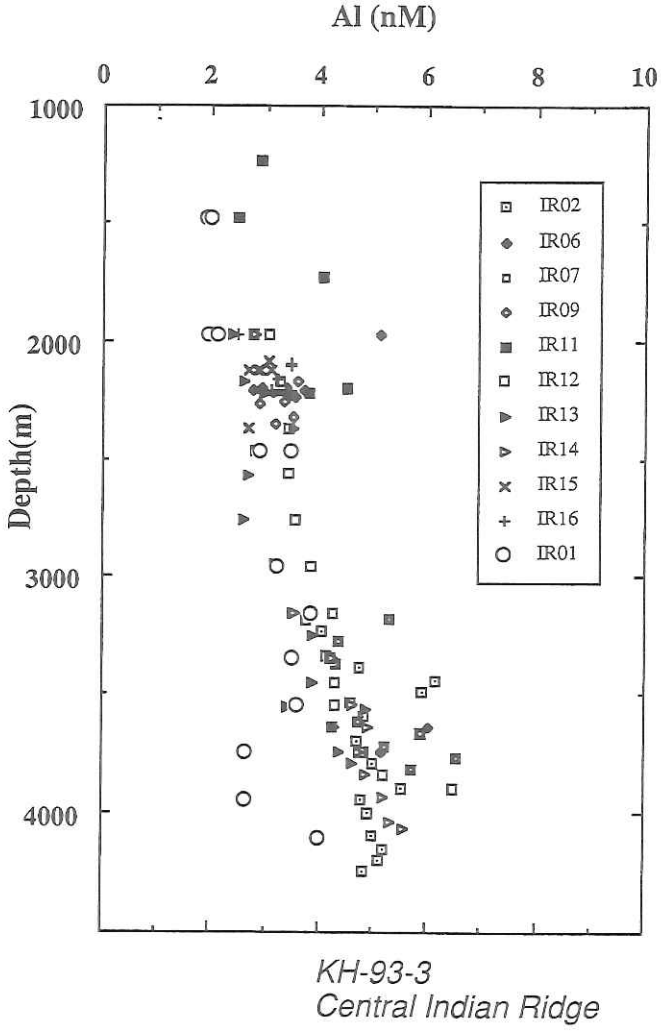

Fig. 6-18. Vertical profiles of aluminum in the Central Indian Ridge segment.

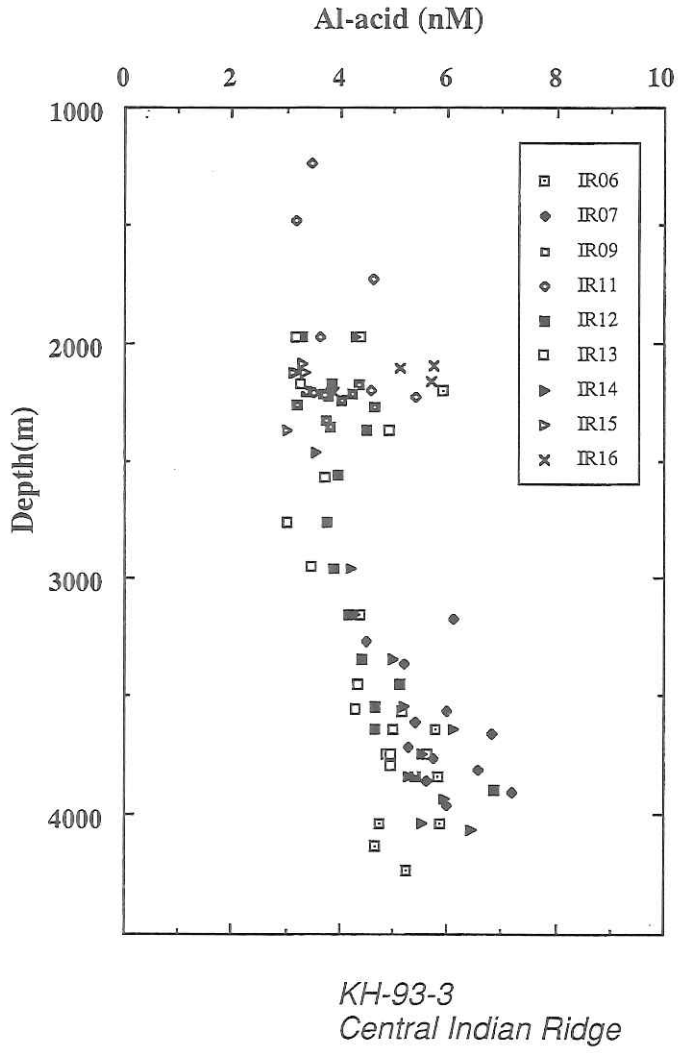

Fig. 6-19. Vertical profiles of aluminum (dissolved + acid-reachable fraction) in the Central Indian Ridge segment.

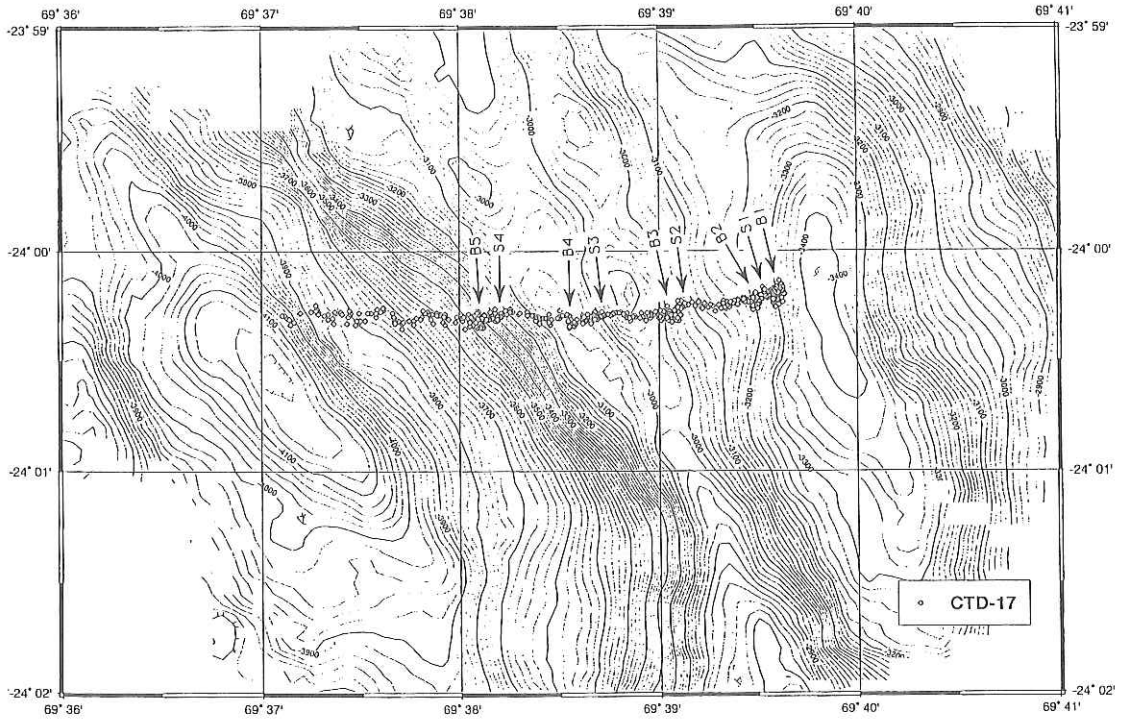

Fig. 6-21. Topographic map near the SONNE Hydrothermal Plume Site (24°00.3′ S, 69°39.6′ E) together with the tow-yo track of the CTDTRMS at CTD-17.

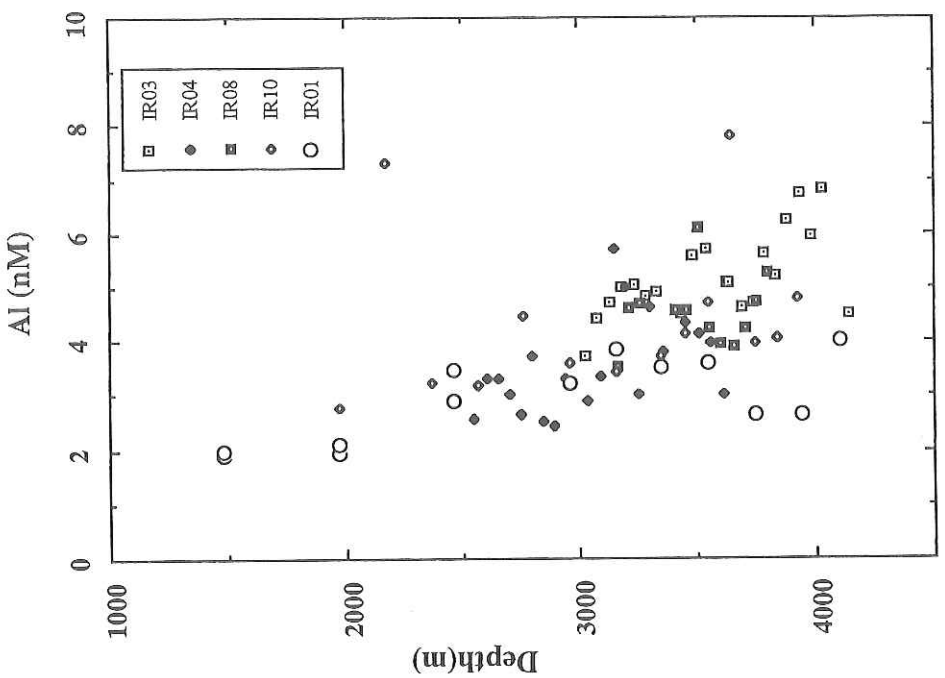

Fig. 6-20. Vertical profiles of aluminum in the Southeastern and Southwestern Indian Ridge segments.

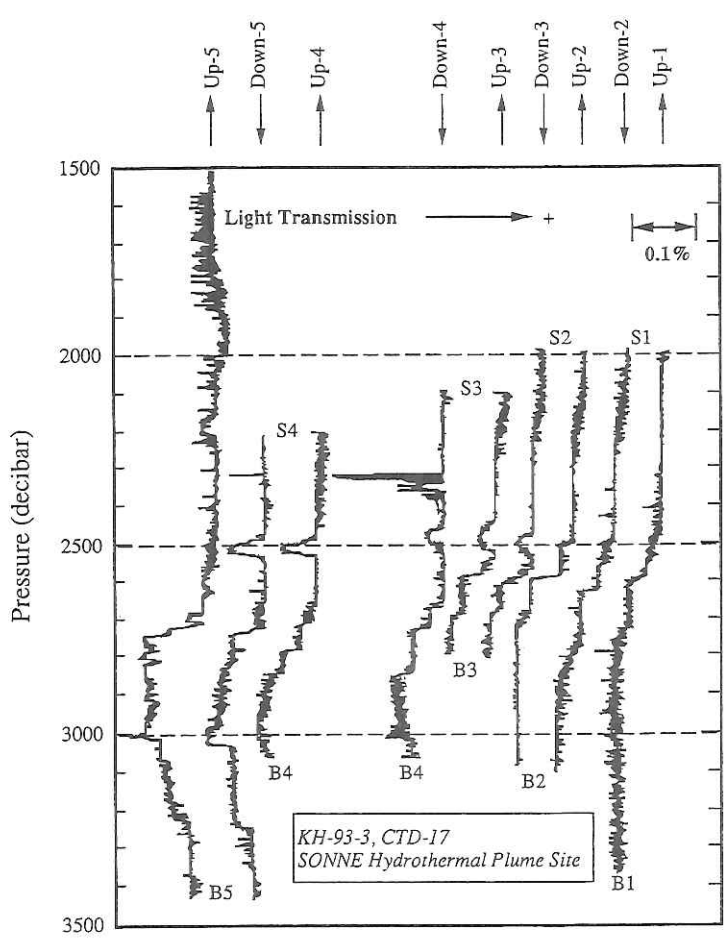

Fig. 6-22. Vertical profiles of light transmission observed during the CTD-17 tow-yo operation, which are arbitrarily offset for convenience.

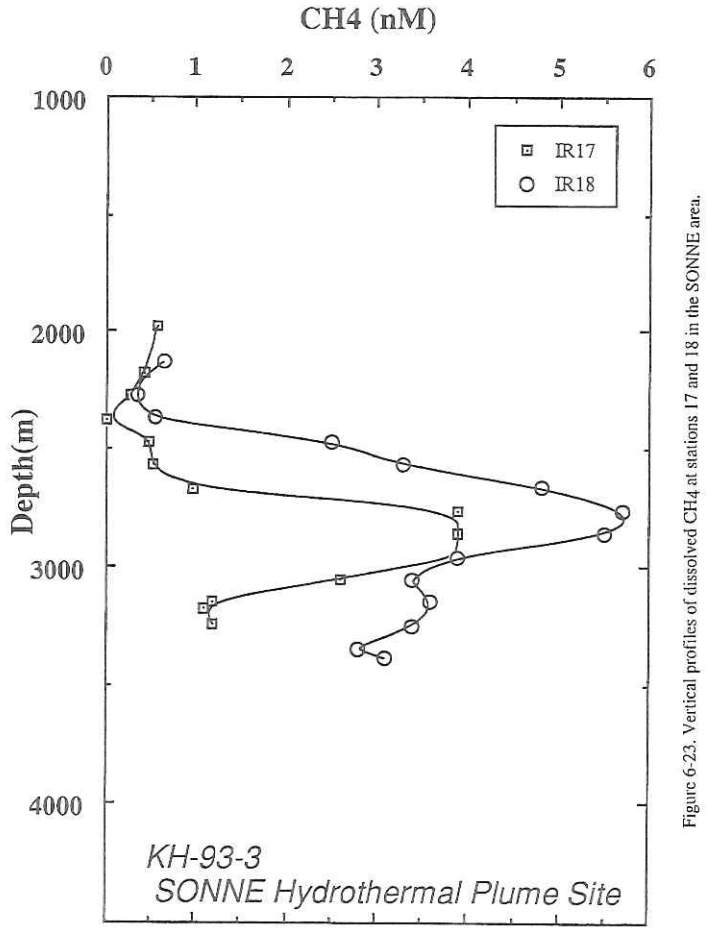

Fig. 6-23. Vertical profiles of dissolved CH_4 at stations 17 and 18 in the SONNE area.

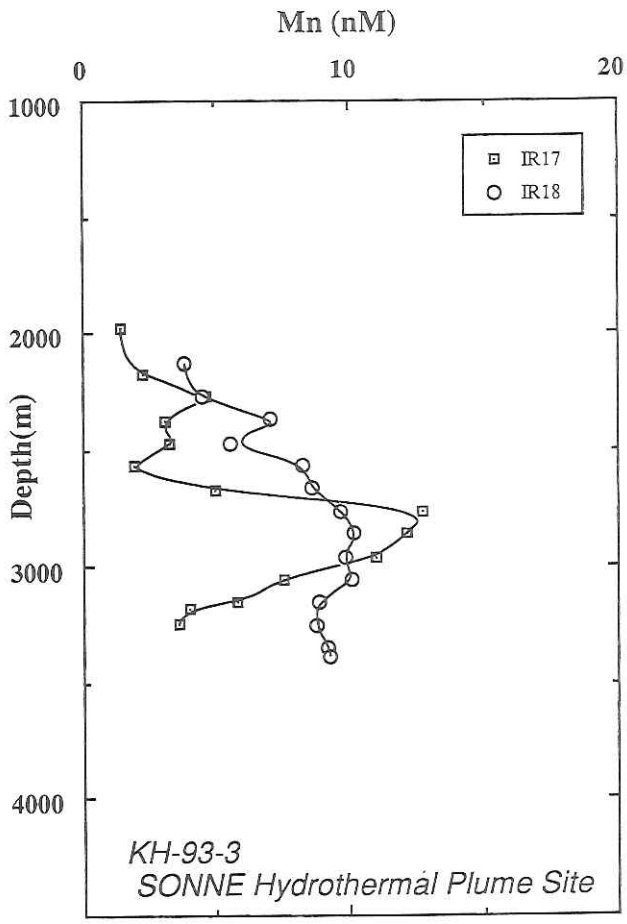

Fig. 6-24. Vertical profiles of total adsorbable Mn at stations 17 and 18 in the SONNE area.

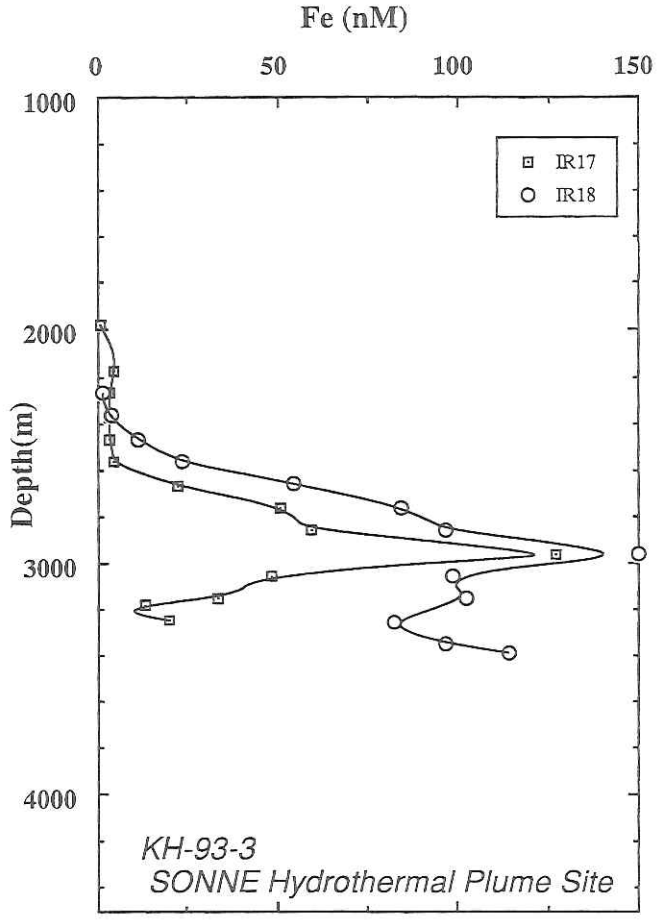

Fig. 6-25. Vertical profiles of Fe(III) at stations 17 and 18 in the SONNE area.

Table 6-1. Division of the shipboard works by the chemistry group

Items	2nd leg	3rd leg
Superintendent	T. Gamo	T. Gamo
Salinity	H. Hasumoto E. Nakayama H. Obata	H. Obata K. Okamura
Dissolved oxygen	T. Gamo	S. Matsumoto
pH, alkalinity	T. Koizumi	T. Koizumi
Total CO2	K. Shitashima H. Kobayashi	T. Oomori K. Shitashima
Methane	S. Kanayama	S. Kanayama
Manganese	E. Nakayama	K. Okamura K. Isshiki
Iron	H. Obata	H. Obata
Aluminum	K. Shitashima	K. Shitashima
CTD operation and data administration	H. Hasumoto M. Watanabe H. Kobayashi T. Gamo	H. Hasumoto K. Isshiki H. Kobayashi T. Gamo

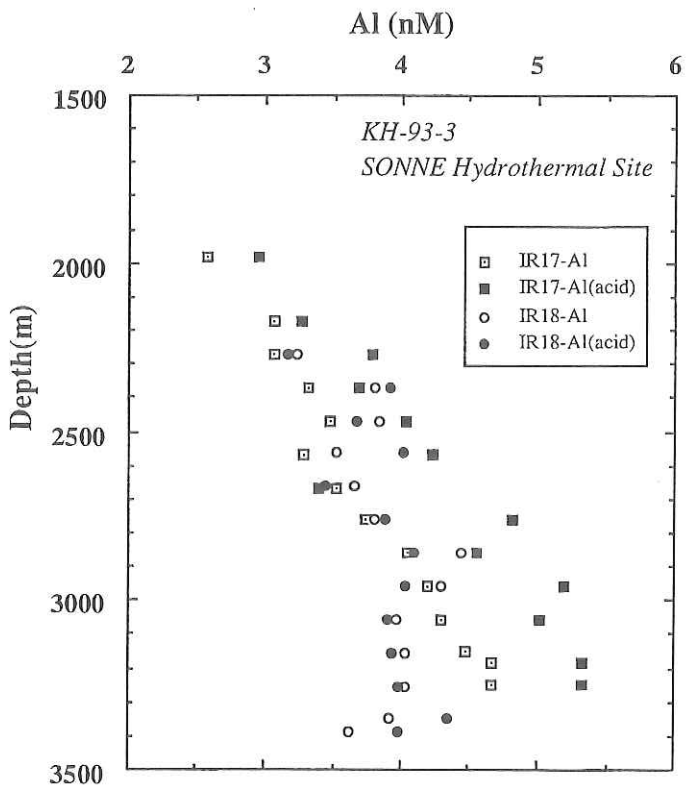

Fig. 6-26. Vertical profiles of dissolved Al and acid-leachable Al at stations 17 and 18 in the SONNE area.

Table6-2. Locations of the CTD stations.

Leg	Station No.	Depth (m)	Area	Date	Location		Remarks
					Latitude	Longitude	
1	CTD-1	4,128	(Control station)	93.7.28	22°59.97'S	74°00.04'E	
1	CTD-2	4,202	Central Indian Ridge	93.7.29	25°23.52'S	70°00.27'E	
1	CTD-3	4,132	Rodriguez Triple Junction	93.7.29	25°32.69'S	70°03.49'E	
1	CTD-4	3,618	Southeastern Indian Ridge	93.7.30	25°46.91'S	70°11.81'E	
1	CTD-5		Central Indian Ridge	93.8.03	25°19.75'S	69°57.83'E	No water sample
1	CTD-6	4,218	Central Indian Ridge	93.8.04	25°19.85'S	69°58.10'E	
1	CTD-7	4,111	Central Indian Ridge	93.8.04	25°26.86'S	70°01.23'E	
1	CTD-8	3,773	Southeastern Indian Ridge	93.8.05	25°40.93'S	70°05.26'E	
1	CTD-9	3,099~4,254	Central Indian Ridge	93.8.06~07	25°20.12'S	69°57.97'E	Start of Tow-yo
					25°17.53'S	70°00.41'E	End of Tow-yo
1	CTD-10	3,924	Southwestern Indian Ridge	93.8.07	25°48.15'S	69°36.31'E	
2	CTD-test	4,465	Central Indian Ridge	93.8.16	25°43.96'S	69°34.82'E	
2	CTD-11	3,652~3,992	Central Indian Ridge	93.8.17	25°20.41'S	69°59.54'E	Start of Tow-yo
					25°17.87'S	69°57.49'E	End of Tow-yo
2	CTD-12	3,925	Central Indian Ridge	93.8.17	25°17.34'S	69°54.95'E	
2	CTD-13	3,725	Central Indian Ridge	93.8.18	25°24.08'S	70°01.88'E	
2	CTD-14	4,074	Central Indian Ridge	93.8.18	25°19.01'S	69°56.03'E	
2	CTD-15	2,926~3,191	Central Indian Ridge	93.8.23	25°20.89'S	70°01.96'E	Start of Tow-yo
					25°17.52'S	69°59.62'E	End of Tow-yo
2	CTD-16	2,536~3,097	Central Indian Ridge	93.8.23~24	25°19.53'S	70°00.08'E	Start of Tow-yo
					25°18.64'S	70°01.56'E	End of Tow-yo
2	CTD-17	3,353~4,058	SONNE Hydrothermal site	93.8.24	24°00.25'S	69°39.63'E	Start of Tow-yo
					24°00.13'S	69°36.19'E	End of Tow-yo
2	CTD-18	3,397	SONNE Hydrothermal site	93.8.25	24°00.29'S	69°39.90'E	

Table 6-3. Summarized chemical data at station CTD-1

Bottle		Sample	P	Depth	T	S	O2	CH4	TA-Mn	T-Mn	Fe	Al	Al(acid)	pH	Alk	∑CO2	P	T	S	O2	Trans.	∑-t	P.temp
No.	type	No.	db	m	°C	psu	ml/l	nM	nM	nM	nM	nM	nM		mM	mM	db	°C	psu	ml/l	%		°C
0		0	0	0	21.9	35.321	5.02	1.42						8.225	2.424		2	21.68	35.299	4.19	89.1	24.54	21.677
22	L																10	21.68	35.299	4.16	89.5	24.54	21.679
21	N																20	21.68	35.300	4.16	89.9	24.54	21.676
20	L																30	21.69	35.300	4.09	90.0	24.54	21.679
19	N																50	21.69	35.302	3.93	90.0	24.54	21.681
18	L																75	21.55	35.419	3.82	90.0	24.66	21.539
17	N																100	21.45	35.492	3.75	90.1	24.75	21.428
16	L																125	20.50	35.607	3.57	90.2	25.09	20.479
15	N	15	1498	1484	3.411	34.670	3.17		<0.14	0.74		1.92		7.689	2.464	2.337	150	19.62	35.707	3.45	90.4	25.40	19.597
14	L	14	1498	1484	3.411	34.684	3.18		<0.14	<0.14	0.11	1.99		7.703	2.463	2.324	175	19.03	35.744	3.43	90.6	25.58	19.002
13	N	13	1995	1973	2.457	34.723	3.67		<0.14	0.41		1.96		7.718	2.477	2.339	200	18.11	35.768	3.49	90.7	25.84	18.071
12	L	12	1995	1973	2.457	34.724	3.66		<0.14	<0.14	0.12	2.12		7.718	2.479	2.352	300	15.50	35.575	3.76	90.7	26.31	15.449
11	N	11	2500	2470	1.830	34.735	4.22		<0.14	1.39		2.88		7.741	2.476	2.327	501	11.49	35.009	4.18	90.7	26.69	11.424
10	L	10	2500	2470	1.830	34.766	4.19		<0.14	0.52	0.60	3.46		7.768	2.477	2.311	750	8.69	34.632	4.03	90.7	26.88	8.605
9	N	9	2997	2957	1.540	34.737	4.40		<0.14	0.78				7.783	2.478	2.329	1000	5.02	34.439	3.33	90.8	27.23	4.933
8	L	8	2997	2957	1.540	34.736	4.40		<0.14	<0.14	0.37	3.21		7.758	2.477	2.326	2000	2.51	34.718	2.46	91.1	27.70	2.367
7	N	7	3198	3154	1.470	34.734	4.39		<0.14	0.73		3.83		7.755	2.482	2.334	2500	1.86	34.730	2.82	91.2	27.77	1.684
6	L	6	3397	3349	1.437	34.733	4.38		<0.14	0.29	0.20	3.52		7.754	2.481	2.346	3100	1.51	34.733	2.95	91.2	27.80	1.286
5	L	5	3600	3547	1.426	34.730	4.33		<0.14	0.34	0.21	3.60		7.761	2.493	2.344	3200	1.48	34.732	2.93	91.3	27.80	1.247
4	L	4	3796	3739	1.442	34.727	4.28		<0.14	0.23	0.38	2.64		7.758	2.493	2.353	3300	1.46	34.731	2.91	91.3	27.80	1.211
3	L	3	4000	3938	1.450	34.798	4.29	0.20	<0.14	0.21	0.15	2.66		7.804	2.478	2.323	3400	1.44	34.730	2.90	91.3	27.80	1.185
2	L	2	4166	4100	1.450	34.740	4.27	0.20	<0.14	0.25	0.22	3.99		7.773	2.495	2.358	3500	1.43	34.729	2.87	91.3	27.80	1.169
1	L																3600	1.43	34.728	2.85	91.3	27.80	1.156
																	3700	1.42	34.727	2.84	91.3	27.80	1.136
																	3800	1.42	34.727	2.81	91.3	27.80	1.126
																	3900	1.43	34.726	2.80	91.3	27.80	1.119
																	4000	1.43	34.726	2.80	91.3	27.80	1.116
																	4100	1.44	34.726	2.77	91.3	27.80	1.115

Table 6-4. Summarized chemical data at station CTD-2

Bottle		Sample	P	Depth	T	S	O2	CH4	TA-Mn	T-Mn	Fe	Al	Al(acid)	pH	Alk	ΣCO2	P	T	S	O2	Trans.	Σ-t	P.temp
No.	type	No.	db	m	°C	psu	ml/l	nM	nM	nM	nM	nM	nM		mM	mM	db	°C	psu	ml/l	%		°C
0		0	0	0	20.9												2	20.74	35.571	4.29	89.9	25.00	20.739
22	L																10	20.74	35.569	4.28	89.9	25.00	20.741
21	N	21	3231	3186	1.674	34.729	4.19	<0.2	0.96			3.74		7.732	2.486	2.343	30	20.74	35.572	4.20	89.9	25.00	20.737
20	L	20	3282	3236	1.667	34.728	4.22		0.83	1.37	8.25	4.05		7.733	2.483	2.364	50	20.73	35.577	4.05	89.9	25.01	20.725
19	N	19	3335	3288	1.658	34.728	4.22	0.20	1.01					7.733	2.485	2.347	75	20.69	35.598	3.92	90.0	25.04	20.671
18	L	18	3387	3338	1.652	34.728	4.21	<0.20	0.87	2.02	9.00	4.12		7.733	2.486	2.383	100	20.67	35.610	3.88	90.0	25.05	20.648
17	N	17	3438	3388	1.650	34.728	4.19	0.26	1.02			4.77		7.740	2.490	2.366	200	16.86	35.680	3.80	90.5	26.07	16.830
16	L	16	3490	3439	1.649	34.728	4.19	<0.20	1.06	1.26	10.80	6.16		7.741	2.486	2.347	300	14.05	35.383	4.01	90.6	26.47	14.008
15	N	15	3541	3489	1.652	34.728	4.22	0.87	1.06			5.90		7.744	2.486	2.346	500	11.85	35.058	4.16	90.6	26.66	11.787
14	L	14	3592	3539	1.654	34.729	4.20		1.11	1.31	12.00	4.57		7.733	2.489	2.338	750	9.14	34.683	4.04	90.7	26.85	9.055
13	N	13	3644	3590	1.659	34.729	4.18	<0.20	1.13			4.83		7.735	2.484	2.342	1000	5.32	34.430	3.48	90.8	27.19	5.239
12	L	12	3696	3640	1.663	34.729	4.18		0.97	1.06	16.80			7.734	2.485		1500	3.22	34.626	2.43	90.9	27.57	3.105
11	N	11	3749	3692	1.667	34.725	4.20	0.85	0.94			4.72		7.734	2.484		2000	2.18	34.714	2.82	91.0	27.73	2.038
10	L	10	3800	3742	1.671	34.725	4.18		0.83	0.84	12.70	4.84		7.734	2.485		2500	1.78	34.726	2.82	91.0	27.77	1.602
9	N	9	3852	3793	1.675	34.730	4.19	0.20	1.01			4.99		7.735	2.484		3000	1.71	34.727	2.79	91.1	27.78	1.483
8	L	8	3956	3894	1.685	34.730	4.18		0.75	1.20		5.54		7.735	2.486		3100	1.68	34.727	2.78	91.1	27.78	1.448
7	N	7	4009	3946	1.691	34.730	4.19	<0.20	0.81			4.78		7.737	2.484		3200	1.67	34.727	2.78	91.1	27.78	1.430
6	L	6	4060	3996	1.697	34.730	4.19	0.29	0.78	0.83	8.92	4.90		7.738	2.485		3300	1.66	34.727	2.78	91.1	27.78	1.411
5	L	5	4111	4045	1.702	34.730	4.20	<0.20	1.38	0.83	11.60			7.735	2.488		3400	1.65	34.726	2.77	91.1	27.78	1.392
4	L	4	4164	4097	1.708	34.731	4.22	0.20	1.18	0.91	13.00	4.99		7.736	2.487		3500	1.65	34.726	2.75	91.1	27.78	1.381
3	L	3	4216	4148	1.714	34.738	4.19	0.20		0.79	9.97	5.20		7.740	2.482		3600	1.66	34.726	2.76	91.1	27.78	1.376
2	L	2	4267	4197	1.720	34.732	4.20	<0.20	0.65	0.90	10.20	5.14		7.737	2.493		3700	1.67	34.726	2.74	91.1	27.78	1.373
1	L	1	4319	4248	1.726	34.725	4.24	<0.20	0.65	1.04	5.17	4.83		7.735	2.488		3800	1.67	34.726	2.72	91.1	27.78	1.370
																	3900	1.68	34.726	2.73	91.1	27.78	1.367
																	4000	1.69	34.726	2.70	91.1	27.78	1.366
																	4100	1.70	34.726	2.71	91.1	27.78	1.365
																	4200	1.71	34.726	2.70	91.1	27.77	1.365
																	4300	1.72	34.726	2.70	91.1	27.77	1.364
																	4319	1.73	34.726	2.69	91.1	27.77	1.364

Table 6-5. Summarized chemical data at station CTD-3

Bottle		Sample	P	Depth	T	S	O2	CH4	TA-Mn	T-Mn	Fe	Al	Al(acid)	pH	Alk	ΣCO2	P	T	S	O2	Trans.	Σ-t	P.temp
No.	type	No.	db	m	°C	psu	ml/l	nM	nM	nM	nM	nM	nM		mM	mM	db	°C	psu	ml/l	%		°C
0		0	0	0	20.3												2	20.32	35.64	4.38	89.7	25.17	20.314
22	L																10	20.32	35.64	4.34	89.8	25.17	20.318
21	N	21	3069	3027	1.698	34.726	4.20	<0.20	1.13	1.87		3.72		7.741	2.482	2.407	30	20.33	35.64	4.27	89.9	25.17	20.322
20	L	20	3118	3075	1.678	34.727	4.20	<0.20	0.91	1.36		4.43		7.739	2.481	2.403	50	20.33	35.66	4.10	89.9	25.18	20.315
19	N	19	3170	3126	1.659	34.726	4.23	<0.20	0.98	1.88		4.73		7.740	2.482	2.394	75	20.06	35.72	3.98	90.0	25.30	20.044
18	L	18	3222	3177	1.652	34.726	4.21	0.20	0.90	1.14	4.56	5.02		7.739	2.486	2.431	100	19.94	35.75	3.96	90.0	25.35	19.917
17	N	17	3274	3228	1.641	34.726	4.24	<0.20	1.43	2.19		5.03		7.741	2.485	2.357	150	19.19	35.76	3.98	90.2	25.56	19.167
16	L	16	3327	3280	1.641	34.725	4.24	<0.20	0.98	1.39	5.41	4.83		7.740	2.500	2.355	200	16.38	35.65	3.88	90.6	26.16	16.348
15	N	15	3380	3331	1.642	34.726	4.23	<0.20	1.56	1.75		4.93		7.744	2.481		300	13.92	35.37	4.11	90.6	26.49	13.878
14	L	14	3484	3433	1.650	34.726	4.23	0.48	1.03	1.57	6.14	4.49		7.747	2.466	2.356	500	11.97	35.08	4.19	90.6	26.65	11.903
13	N	13	3535	3483	1.654	34.725	4.22		1.35	1.80		5.58		7.744	2.475	2.382	750	9.38	34.71	4.10	90.7	26.83	9.294
12	L	12	3587	3534	1.659	34.726	4.22	0.57	0.61	1.20	3.81	5.69		7.745	2.463	2.353	1000	5.35	34.43	3.56	90.7	27.18	5.262
11	N	11	3673	3618	1.663	34.726	4.22	<0.20	1.08	1.65		5.10		7.746	2.482	2.383	1500	3.22	34.62	2.49	90.8	27.56	3.108
10	L	10	3687	3632	1.667	34.730	4.24	0.20	1.21	1.24	4.81	5.09		7.748	2.474	2.344	2000	2.20	34.71	2.81	91.0	27.73	2.063
9	N	9	3739	3682	1.670	34.726	4.19	0.48	0.92	1.57		4.63		7.747	2.476	2.347	2500	1.78	34.73	2.81	91.0	27.77	1.599
8	L	8	3789	3731	1.675	34.726	4.23		1.00	1.11	5.30	4.73		7.746	2.478	2.345	3000	1.71	34.73	2.79	91.1	27.78	1.492
7	N	7	3839	3780	1.680	34.723	4.20		1.56	1.62		5.60		7.748	2.489	2.337	3100	1.69	34.73	2.78	91.1	27.78	1.456
6	L	6	3890	3830	1.685	34.727	4.19	<0.20	0.90	1.07	5.75	5.20		7.749	2.478	2.343	3200	1.65	34.73	2.79	91.1	27.78	1.414
5	L	5	3941	3879	1.689	34.727	4.18	<0.20	1.06	1.02	2.88	6.23		7.749	2.483	2.347	3300	1.64	34.73	2.78	91.1	27.78	1.394
4	L	4	3993	3930	1.693	34.728	4.18		0.85	1.06	6.80	6.74		7.768	2.486	2.341	3400	1.65	34.73	2.78	91.1	27.78	1.385
3	L	3	4044	3980	1.699	34.737	4.23	<0.20	1.29	0.99	5.71	5.96		7.760	2.483	2.341	3500	1.65	34.73	2.77	91.1	27.78	1.383
2	L	2	4094	4029	1.703	34.728	4.19		1.00	0.93	5.35	6.83		7.753	2.429	2.342	3600	1.66	34.73	2.77	91.1	27.78	1.380
1	L	1	4204	4136	1.719	34.736	4.14	0.20	0.98	0.99	3.70	4.52		7.754	2.482	2.329	3700	1.67	34.73	2.75	91.1	27.78	1.376
																	3800	1.68	34.73	2.75	91.1	27.78	1.374
																	3900	1.69	34.73	2.73	91.1	27.78	1.372
																	4000	1.70	34.73	2.72	91.1	27.78	1.370
																	4100	1.71	34.73	2.71	91.1	27.78	1.369
																	4200	1.72	34.73	2.69	91.1	27.77	1.369
																	4204	1.72	34.73	2.70	91.1	27.77	1.368

Table 6-6. Summarized chemical data at station CTD-4

Bottle		Sample	P	Depth	T	S	O2	CH4	TA-Mn	T-Mn	Fe	Al	Al(acid)	pH	Alk	ΣCO2	P	T	S	O2	Trans.	Σ-t	P.temp
No.	type	No.	db	m	°C	psu	ml/l	nM	nM	nM	nM	nM	nM		mM	mM	db	°C	psu	ml/l	%		°C
0		0	0	0	20.5												3	20.42	35.601	4.01	89.9	25.11	20.415
22	N	22	2589	2556	1.785	34.727		0.57				2.58		7.733	2.479		10	20.42	35.601	4.00	89.9	25.11	20.416
21	L	21	2637	2604	1.771	34.726	4.12	0.66	1.26	1.80	11.20	3.32		7.734	2.471	2.382	20	20.42	35.602	4.01	89.9	25.11	20.414
20	N	20	2686	2652	1.760	34.725	4.13	0.74	0.74			3.30		7.736	2.481	2.416	30	20.42	35.602	4.02	89.9	25.11	20.414
19	L	19	2736	2701	1.750	34.723	4.13	<0.20	0.89	1.47	7.79	3.00		7.737	2.477	2.394	50	20.19	35.653	4.00	89.9	25.21	20.180
18	L	18	2784	2748	1.737	34.723	4.13	<0.20	0.89	1.36	7.83	2.66		7.739	2.478	2.397	75	19.76	35.735	3.87	89.6	25.39	19.744
17	N	17	2832	2795	1.736	34.721	4.14	0.23	0.70			3.70		7.739	2.476	2.446	100	18.89	35.742	3.78	90.0	25.62	18.873
16	L	16	2879	2841	1.729	34.721	4.15	<0.20	0.84	1.41	8.98	2.54		7.739	2.484	2.387	125	18.17	35.734	3.78	90.3	25.79	18.147
15	L	15	2928	2889	1.723	34.860	4.37	1.35	0.72	1.52	8.21	2.45		7.821	2.465	2.368	150	17.24	35.700	3.80	90.4	26.00	17.213
14	N	14	2946	2936	1.713	34.721	4.17	0.23	1.29			3.29		7.743	2.481	2.411	175	16.21	35.632	3.83	90.6	26.19	16.177
13	L	13	3027	2986	1.701	34.720	4.20	<0.20	0.96	6.08	10.50			7.744	2.478	2.361	200	15.56	35.570	3.81	90.6	26.29	15.526
12	L	12	3079	3037	1.686	34.721	4.20	<0.20	0.93	1.72	9.36	2.90		7.745	2.477	2.360	300	13.69	35.336	4.01	90.6	26.51	13.649
11	N	11	3136	3093	1.675	34.722	4.24	<0.20	1.06			3.34		7.747	2.475	2.366	500	11.71	35.037	4.13	90.6	26.67	11.643
10	L	10	3190	3146	1.669	34.756	4.26	0.20	0.86	1.86	7.15	5.69		7.763	2.475	2.337	750	9.27	34.697	3.98	90.7	26.84	9.187
9	L	9	3242	3196	1.660	34.722	4.21	<0.20	0.74	1.38	6.43	5.02		7.760	2.484	2.351	1000	5.22	34.427	3.46	90.8	27.20	5.132
8	N	8	3296	3249	1.646	34.729	4.26	<0.20	0.53			3.03		7.750	2.468	2.351	1500	3.21	34.618	2.47	90.9	27.56	3.098
7	L	7	3347	3299	1.645	34.722	4.24	<0.20	0.69	0.96	6.25	4.61		7.751	2.471	2.345	2000	2.22	34.712	2.80	91.0	27.72	2.077
6	L	6	3400	3351	1.645	34.723	4.23	<0.20	0.58	1.15	6.25	3.82		7.751	2.480	2.376	2500	1.79	34.726	2.80	91.0	27.77	1.609
5	N	5	3452	3402	1.644	34.723	4.25	<0.20	0.86					7.753	2.483	2.342	3000	1.71	34.726	2.78	91.1	27.78	1.490
4	L	4	3505	3454	1.648	34.724	4.23		0.74	0.98	5.84	4.32		7.765	2.474	2.339	3100	1.69	34.726	2.78	91.1	27.78	1.457
3	L	3	3556	3503	1.654	34.753	4.25		1.08	1.08	3.82	4.13		7.756	2.480	2.331	3200	1.67	34.727	2.80	91.1	27.78	1.431
2	N	2	3609	3555	1.660	34.724	4.24	<0.20	0.74			3.97		7.752	2.482	2.338	3300	1.65	34.726	2.79	91.1	27.78	1.398
1	L	1	3662	3607	1.667	34.723	4.13	0.20	0.53	1.10	2.22	3.27		7.753	2.475	2.340	3400	1.65	34.726	2.79	91.1	27.78	1.387
																	3500	1.65	34.726	2.79	91.1	27.78	1.378
																	3600	1.66	34.726	2.78	91.1	27.78	1.378

Table 6-7. Summarized chemical data at station CTD-6

Bottle		Sample	P	Depth	T	S	O2	CH4	TA-Mn	T-Mn	Fe	Al	Al(acid)	pH	Alk	ΣCO2	P	T	S	O2	Trans.	Σ-t	P.temp
No.	type	No.	db	m	°C	psu	ml/l	nM	nM	nM	nM	nM	nM		mM	mM	db	°C	psu	ml/l	%		°C
0		0	0	0	20.5												2	20.26	35.625	4.13	89.9	25.17	20.260
22	N		2000	1978	2.191												10	20.26	35.625	4.13	90.0	25.17	20.257
21	L	14	1999	1977	2.191	34.713	4.19	<0.20	0.76	1.71	7.20	5.14	4.39	7.745	2.484	2.340	30	20.26	35.625	4.12	90.0	25.17	20.259
20	L	13	2225	2199	1.866	34.712	4.17	1.88	10.15	9.26	53.00	2.93	5.91	7.740	2.475	2.327	50	20.26	35.628	4.07	90.0	25.17	20.251
19	N		2598	2565	1.743												75	20.24	35.636	3.96	90.0	25.18	20.227
18	L	12	2598	2565	1.742	34.771	4.26	1.12	1.78	1.78	10.00	3.12	3.99	7.777	2.470	2.317	100	19.69	35.763	3.94	90.2	25.43	19.668
17	L	11	2999	2959	1.671	34.771	4.41	0.29	0.86	0.69	4.57	3.66	4.17	7.873	2.474	2.275	150	18.11	35.727	3.73	90.4	25.80	18.083
16	N		3400	3351	1.639												200	15.66	35.580	3.88	90.6	26.27	15.626
15	L	10	3400	3351	1.639	34.917	4.39	<0.20	0.88	1.26	6.53	4.15	4.85	7.858	2.470	2.299	300	13.55	35.317	4.07	90.6	26.53	13.508
14	L	9	3498	3447	1.644	35.605	5.24	<0.20	1.03	1.31	1.16			8.210	2.431		500	11.81	35.051	4.21	90.6	26.67	11.741
13	N		3599	3546	1.653												750	8.96	34.665	4.01	90.7	26.86	8.880
12	L	8	3600	3547	1.653	35.603	5.23	1.41	0.71	1.32	1.50			8.209	2.431		1000	5.26	34.428	3.48	90.8	27.19	5.175
11	L	7	3699	3643	1.662	34.710	4.20	0.29	1.03	1.17	8.68	6.04	5.79	7.760	2.485	2.351	1500	3.20	34.623	2.46	90.9	27.57	3.090
10	N		3800	3742	1.672												2000	2.16	34.714	2.82	91.0	27.73	2.022
9	L	6	3800	3742	1.672	34.712	4.21	0.27	0.88	1.08	8.75	5.17	5.63	7.756	2.485	2.359	2500	1.78	34.726	2.82	91.1	27.77	1.605
8	L	5	3899	3839	1.679	34.715	4.22	0.29	1.10	0.94	8.53		5.84	7.760	2.483	2.334	3000	1.68	34.726	2.78	91.1	27.78	1.462
7	N		4001	3938	1.687												3100	1.67	34.726	2.78	91.1	27.78	1.434
6	L	4	4100	4035	1.697	34.712	4.17	<0.20	0.81	1.03	8.46		5.86	7.758	2.495	2.340	3200	1.66	34.726	2.78	91.1	27.78	1.415
5	L	3	4099	4034	1.697	34.711	4.18	<0.20	0.79	0.99	8.68		4.74	7.758	2.487	2.339	3300	1.65	34.726	2.78	91.1	27.78	1.396
4	N		4202	4134	1.709												3400	1.64	34.726	2.77	91.1	27.78	1.381
3	L	2	4202	4134	1.709	34.712	4.18	<0.20	0.88	1.19	9.16		4.67	7.763	2.489	2.339	3500	1.65	34.726	2.76	91.1	27.78	1.376
2	N		4303	4232	1.722												3600	1.65	34.726	2.76	91.1	27.78	1.373
1	L	1	4304	4233	1.723	34.712	4.18	0.59	0.93	1.27	7.13		5.25	7.758	2.492	2.340	3800	1.67	34.726	2.74	91.1	27.78	1.369
																	3900	1.68	34.726	2.73	91.1	27.78	1.367
																	4000	1.69	34.726	2.73	91.1	27.78	1.363
																	4100	1.70	34.726	2.71	91.1	27.78	1.362
																	4200	1.71	34.726	2.71	91.1	27.78	1.362
																	4204	1.71	34.726	2.71	91.1	27.77	1.362

Table 6-8. Summarized chemical data at station CTD-7

Bottle		Sample	P	Depth	T	S	O2	CH4	TA-Mn	T-Mn	Fe	Al	Al(acid)	pH	Alk	ΣCO2	P	T	S	O2	Trans.	Σ-t	P.temp
No.	type	No.	db	m	°C	psu	ml/l	nM	nM	nM	nM	nM	nM		mM	mM	db	°C	psu	ml/l	%		°C
0		0	0	0	19.8												3	20.25	35.606	5.12	89.4	25.16	20.245
22	N		3219	3174	1.647												10	20.26	35.607	4.55	89.7	25.16	20.253
21	L	14	3219	3174	1.646	34.718	4.18	<0.20	0.69		8.46	5.32	6.11	7.743	2.483	2.360	20	20.25	35.607	4.43	89.9	25.16	20.249
20	L	13	3318	3271	1.642	34.718	4.22	0.20	1.69	1.97	13.40	4.38	4.51	7.748	2.478	2.336	30	20.26	35.607	4.35	89.9	25.16	20.249
19	N		3419	3370	1.646												50	20.26	35.608	4.17	89.9	25.16	20.251
18	L	12	3418	3369	1.646	34.719	4.23	0.20	1.46	1.54	8.26	4.33	5.22	7.747	2.475	2.338	75	20.22	35.651	4.00	89.9	25.20	20.208
17	L	11	3519	3468	1.652	34.938	4.39	0.29	0.61	0.96	3.17	5.28	5.66	7.858	2.465	2.309	100	19.26	35.736	3.83	89.9	25.52	19.245
16	N		3568	3515	1.654												125	18.34	35.735	3.80	90.2	25.75	18.322
15	L	10	3568	3515	1.654	34.952	4.37	1.22	0.81	1.27	3.66		5.22	7.866	2.466	2.282	150	17.25	35.692	3.83	90.5	25.99	17.224
14	L	9	3619	3565	1.658	34.719	4.23	0.40	1.26	2.08	8.69		5.99	7.749	2.478	2.363	175	16.47	35.642	3.85	90.5	26.13	16.438
13	N		3669	3614	1.662												200	15.59	35.566	3.94	90.6	26.28	15.554
12	L	8	3669	3614	1.662	34.719	4.21	<0.20	1.13	2.88	7.88	4.77	5.43	7.752	2.481	2.354	300	13.43	35.305	4.20	90.6	26.54	13.390
11	L	7	3718	3662	1.665	34.720	4.20	<0.20	0.90	2.39	8.46	5.89	6.82	7.750	2.480	2.362	500	11.64	35.026	4.22	90.6	26.68	11.576
10	N		3769	3712	1.670												750	9.23	34.693	4.04	90.7	26.84	9.147
9	L	6	3768	3711	1.670	34.719	4.19	<0.20	0.61	1.30	9.02	5.25	5.28	7.795	2.480	2.377	1000	5.18	34.426	3.45	90.7	27.20	5.098
8	L	5	3819	3761	1.674	34.728	4.21	<0.20	0.85	1.43	8.55	6.57	5.75	7.757	2.480	2.377	1500	3.17	34.625	2.45	90.8	27.57	3.064
7	N		3871	3811	1.680												2000	2.17	34.714	2.81	91.0	27.73	2.033
6	L	4	3870	3810	1.679	34.721	4.19	<0.20	0.73	1.41	8.53	5.73	6.55	7.754	2.484	2.339	2500	1.81	34.726	2.82	91.0	27.77	1.632
5	L	3	3920	3859	1.685	34.722	4.20	<0.20	0.94	1.24	8.49		5.63	7.748	2.483	2.338	3000	1.70	34.726	2.78	91.0	27.78	1.478
4	N		3969	3907	1.690												3100	1.68	34.726	2.78	91.0	27.78	1.444
3	L	2	3968	3906	1.690	34.721	4.19	<0.20	0.90	1.71	8.29		7.20	7.753	2.478	2.343	3200	1.65	34.726	2.79	91.0	27.78	1.413
2	N		4020	3957	1.696												3300	1.64	34.726	2.80	91.0	27.78	1.390
1	L	1	4020	3957	1.696	34.723	4.18	<0.20	0.97	1.70	8.34		5.99	7.757	2.480	2.360	3400	1.64	34.726	2.79	91.1	27.78	1.384
																	3500	1.65	34.726	2.77	91.1	27.78	1.381
																	3600	1.66	34.726	2.76	91.1	27.78	1.378
																	3700	1.67	34.726	2.76	91.1	27.78	1.373
																	3800	1.67	34.726	2.74	91.1	27.78	1.370
																	3900	1.68	34.726	2.74	91.1	27.78	1.369
																	4000	1.69	34.726	2.73	91.1	27.78	1.369
																	4020	1.70	34.726	2.73	91.1	27.78	1.369

Table 6-9. Summarized chemical data at station CTD-8

Bottle		Sample	P	Depth	T	S	O2	CH4	TA-Mn	T-Mn	Fe	Al	Al(acid)	pH	Alk	ΣCO2	P	T	S	O2	Trans.	Σ-t	P.temp
No.	type	No.	db	m	°C	psu	ml/l	nM	nM	nM	nM	nM	nM		mM	mM	db	°C	psu	ml/l	%		°C
0		0	0	0	19.8												2	19.68	35.705	5.40	89.8	25.39	19.675
22	N		3200	3155	1.676												10	19.68	35.709	4.58	89.5	25.39	19.678
21	L	14	3199	3154	1.674	34.714	4.21	<0.20	1.99	3.14	6.36	3.55	4.12	7.749	2.470	2.331	20	19.68	35.709	4.54	89.7	25.39	19.681
20	L	13	3248	3202	1.661	34.734	4.22	<0.20	1.82	3.29	5.76	4.63	4.09	7.748	2.470	2.329	30	19.69	35.709	4.46	89.9	25.39	19.681
19	N		3298	3251	1.656												50	19.70	35.709	4.26	89.9	25.38	19.688
18	L	12	3298	3251	1.655	34.715	4.25	<0.20	1.77	1.86	4.90	4.72	4.06	7.752	2.474	2.333	75	19.57	35.816	4.12	89.9	25.50	19.555
17	L	11	3349	3301	1.655	34.938	4.46	0.42	0.77	2.61	1.34	4.04	3.65	7.857	2.467	2.288	100	19.39	35.836	4.10	90.0	25.56	19.372
16	N		3400	3351	1.652												125	19.11	35.845	4.06	89.9	25.64	19.091
15	L	10	3399	3350	1.652	34.942	4.39	0.62	1.16	1.52	2.70	3.38	3.95	7.868	2.461	2.281	150	16.92	35.673	4.00	90.3	26.05	16.897
14	L	9	3449	3399	1.650	34.718	4.25		1.77	2.67	8.51	4.59	4.77	7.765	2.472	2.334	175	15.78	35.589	3.99	90.5	26.25	15.757
13	N		3500	3449	1.653												200	15.02	35.508	3.96	90.7	26.36	14.992
12	L	8	3500	3449	1.653	34.716	4.23	<0.20	1.24	2.69	6.61	4.57	6.93	7.761	2.474	2.331	300	13.37	35.296	4.27	90.6	26.55	13.325
11	L	7	3550	3498	1.658	34.715	4.23	<0.20	1.38	3.25	6.46	6.10	6.88	7.760	2.409	2.335	500	11.69	35.033	4.20	90.6	26.67	11.625
10	N		3600	3547	1.664												750	8.77	34.644	3.94	90.7	26.88	8.689
9	L	6	3600	3547	1.663	34.715	4.24	<0.20	2.46	1.97	6.69	4.27	4.69	7.749	2.479	2.336	1000	5.44	34.428	3.43	90.7	27.17	5.350
8	L	5	3650	3595	1.670	34.738	4.28	<0.20	1.53	1.29	5.69	3.98	4.36	7.758	2.471	2.333	1500	3.19	34.617	2.45	90.8	27.56	3.083
7	N		3701	3645	1.675												2000	2.18	34.714	2.79	90.9	27.73	2.038
6	L	4	3700	3644	1.675	34.715	4.22	<0.20	1.60	2.49	7.73	3.92		7.758	2.478	2.338	2500	1.79	34.726	2.81	91.0	27.77	1.617
5	L	3	3753	3696	1.681	34.717	4.23	<0.20	1.46	2.40	7.27	4.25	5.57	7.751	2.481	2.337	3000	1.70	34.726	2.83	91.0	27.78	1.480
4	N		3801	3743	1.687												3100	1.69	34.726	2.82	91.0	27.78	1.455
3	L	2	3799	3741	1.686	34.716	4.23	0.23	2.55	1.78	8.64	4.77	7.11	7.755	2.469	2.337	3200	1.67	34.726	2.83	91.0	27.78	1.431
2	N		3853	3794	1.692												3300	1.66	34.727	2.84	91.0	27.78	1.408
1	L	1	3853	3794	1.692	34.717	4.25	0.35	1.80	5.24	8.88	5.29	5.60	7.762	2.490	2.337	3400	1.65	34.726	2.84	91.0	27.78	1.392
																	3500	1.66	34.726	2.84	91.0	27.78	1.387
																	3600	1.67	34.726	2.83	91.0	27.78	1.386
																	3700	1.68	34.726	2.82	91.0	27.78	1.384
																	3800	1.69	34.726	2.82	91.0	27.78	1.384
																	3853	1.69	34.726	2.81	91.0	27.78	1.384

Table 6-10. Summarized chemical data at station CTD-9

Bottle		Sample	P	Depth	T	S	O2	CH4	TA-Mn	T-Mn	Fe	Al	Al(acid)	pH	Alk	ΣCO2	P	T	S	O2	Trans.	Σ-t	P.temp
No.	type	No.	db	m	°C	psu	ml/l	nM	nM	nM	nM	nM	nM		mM	mM	db	°C	psu	ml/l	%		°C
0		0	0	0	20.4												2	20.26	35.609	4.51	89.3	25.16	20.255
22	N		1000	991	5.088												10	20.25	35.609	4.37	89.6	25.16	20.251
21	L	14	1000	991	5.055	34.424	4.28	0.59	<0.14	3.37		2.72	4.55	7.785	2.398	2.247	30	20.26	35.609	4.28	89.7	25.16	20.259
20	L	13	2348	2321	1.825	34.723	4.13	0.89	3.71	4.67	13.7	3.53		7.759	2.471	2.324	50	20.14	35.638	4.10	89.8	25.21	20.133
19	N		2352	2314	1.811												75	19.66	35.728	4.02	89.9	25.41	19.648
18	L	12	2350	2322	1.808	34.724	4.15	0.89	4.99	5.75	22.5	3.51	3.77	7.762	2.473	2.321	100	19.59	35.764	3.97	89.9	25.45	19.576
17	L	11	2313	2286	1.840	34.860	4.30	1.20	2.56	2.76	12.4	3.02	3.91	7.840	2.460	2.284	125	19.33	35.771	3.94	89.9	25.53	19.307
16	N		2315	2288	1.831		4.15										150	18.01	35.716	3.71	90.2	25.82	17.982
15	L	10	2385	2357	1.832	34.723		2.40	7.46	7.96	32.7	3.19	3.84	7.763	2.474	2.332	175	16.91	35.677	3.76	90.4	26.06	16.885
14	L	9	2268	2242	1.854	34.726	4.17	2.20	5.88	6.55	21.1	3.57	4.06	7.764	2.470	2.325	200	15.81	35.585	3.83	90.5	26.24	15.775
13	N		2281	2254	1.827												300	13.75	35.348	4.12	90.5	26.51	13.710
12	L	8	2280	2254	1.825	34.724	4.17	1.70	7.65	8.02	32.0	3.36	3.23	7.764	2.474	2.330	500	11.76	35.044	4.18	90.5	26.67	11.691
11	L	7	2228	2205	1.841	34.725	4.16	2.50	7.65	7.81		3.38	3.37	7.769	2.472	2.326	750	9.18	34.687	4.01	90.6	26.85	9.091
10	N		2237	2210	1.845												1000	5.19	34.426	3.47	90.7	27.20	5.103
9	L	6	2239	2213	1.846	34.723	4.13	2.50	8.37	8.52	40.0	3.72	3.73	7.764	2.472	2.327	1500	3.21	34.620	2.47	90.8	27.56	3.101
8	L	5	2216	2191	1.849	34.793	4.25	1.60	5.15	5.52	23.5	3.18	4.09	7.807	2.461	2.303	2000	2.13	34.716	2.85	90.9	27.73	1.992
7	N		2236	2210	1.844												2500	1.77	34.726	2.85	90.9	27.77	1.595
6	L	4	2235	2209	1.844	34.723	4.15	1.80	7.65	7.85	32.1	2.76	4.25	7.770	2.468	2.328	3000	1.69	34.726	2.81	91.0	27.78	1.464
5	L	3	2200	2175	1.855	34.723	4.15	1.90	7.10	7.25	22.4	3.60	4.38	7.768	2.472	2.326	3100	1.67	34.726	2.81	91.0	27.78	1.440
4	N		2248	2222	1.829												3200	1.65	34.726	2.81	91.0	27.78	1.407
3	L	2	2250	2224	1.828	34.722	4.15	1.70	7.52	7.26	36.2	3.15	3.82	7.770	2.473	2.327	3300	1.65	34.726	2.81	91.0	27.78	1.397
2	N		2294	2247	1.856												3400	1.65	34.726	2.79	91.0	27.78	1.386
1	L	1	2295	2267	1.806	34.724	4.16	2.30	6.28	7.34	33.7	2.90	4.69	7.771	2.473	2.325	3500	1.65	34.726	2.78	91.0	27.78	1.378
			1	Up-6	7	Down-5	13	Down-3	19	Up-1							3600	1.65	34.726	2.78	91.0	27.78	1.374
			2	Up-6	8	Down-5	14	Down-3	20	Up-1							3700	1.66	34.726	2.77	91.0	27.78	1.372
			3	Up-6	9	Up-4	15	Up-2	21	Up-1							3800	1.67	34.726	2.76	91.0	27.78	1.371
			4	Down-6	10	Down-4	16	Down-2	22	Up-1							4000	1.69	34.726	2.75	91.0	27.78	1.368
			5	Down-6	11	Down-4	17	Down-2									4200	1.71	34.726	2.74	91.0	27.78	1.363
			6	Up-5	12	Up-3	18	Up-1									4319	1.73	34.726	2.73	91.0	27.77	1.363

Table 6-11. Summarized chemical data at station CTD-10

Bottle		Sample	P	Depth	T	S	O2	CH4	TA-Mn	T-Mn	Fe	Al	Al(acid)	pH	Alk	ΣCO2	P	T	S	O2	Trans.	Σ-t	P.temp
No.	type	No.	db	m	°C	psu	ml/l	nM	nM	nM	nM	nM	nM		mM	mM	db	°C	psu	ml/l	%		°C
0		0	0	0	19.6												6	19.78	35.714	4.94	89.3	25.37	19.779
22	N		1999	1977	2.193												10	19.78	35.714	4.79	89.4	25.37	19.778
21	L	14	1999	1977	1.189	34.716	4.00	<0.20	0.34	2.21	3.8	2.78		7.740	2.463	2.324	20	19.78	35.715	4.62	89.6	25.37	19.778
20	L	13	2199	2173	1.958	34.721	4.03	<0.20	0.57	2.88	7.0		3.72	7.750	2.473	2.334	30	19.78	35.715	4.52	89.7	25.37	19.777
19	N		2399	2370	1.804												50	19.78	35.715	4.30	89.7	25.37	19.773
18	L	12	2399	2370	1.804	34.724	4.09	<0.20	2.11	3.45	10.4	3.23		7.759	2.478	2.334	75	19.78	35.715	4.13	89.8	25.37	19.763
17	L	11	2600	2567	1.760	34.859	4.29	1.50	1.91	6.77	9.9	3.17	3.42	7.822	2.469	2.298	100	19.74	35.718	4.07	89.9	25.38	19.724
16	N		2800	2764	1.740	34.724	4.13							7.765	2.479		125	18.54	35.739	3.96	90.0	25.71	18.513
15	L	10	2800	2764	1.739	34.898	4.35	<0.20	1.21	2.78	10.2	4.46	5.10	7.847	2.465	2.334	150	17.53	35.708	3.97	90.3	25.93	17.503
14	L	9	3000	2960	1.714	37.726	4.17	0.44	1.44	2.05	6.9	3.58	3.99	7.762	2.476	2.333	175	16.20	35.621	4.06	90.4	26.18	16.169
13	N		3200	3155	1.700												200	15.57	35.564	3.99	90.5	26.28	15.539
12	L	8	3199	3154	1.670	34.724	4.16	<0.20	1.28	4.73	9.1	3.44	3.94	7.760	2.479	2.334	300	13.45	35.303	4.19	90.5	26.54	13.407
11	L	7	3399	3350	1.682	34.728	4.20	0.66	1.28	3.14	10.1	3.72	3.39	7.772	2.478	2.333	500	11.87	35.059	4.26	90.5	26.66	11.800
10	N		3498	3447	1.657												750	9.05	34.677	4.08	90.6	26.86	8.964
9	L	6	3499	3448	1.656	34.724	4.18	<0.20	1.11	5.01	16.3	4.14		7.762	2.481	2.336	1000	5.27	34.415	3.58	90.6	27.18	5.182
8	L	5	3600	3547	1.641	34.731	4.20	<0.20	1.60	2.07	18.8	4.71	5.19	7.768	2.482	2.337	1500	3.12	34.624	2.55	90.7	27.58	3.007
7	N		3697	3611	1.632												2000	2.17	34.709	2.79	90.9	27.73	2.031
6	L	4	3696	3640	1.632	34.734	4.21	<0.20	1.57	7.57	23.4		5.60	7.762	2.482	2.337	2500	1.79	34.726	2.79	90.9	27.77	1.615
5	L	3	3801	3743	1.635	34.722	4.20		1.57	3.39	19.1	3.96	4.10	7.763	2.483	2.338	3000	1.72	34.726	2.78	90.9	27.77	1.495
4	N		3900	3839	1.640												3100	1.71	34.726	2.78	90.9	27.78	1.474
3	L	2	3900	3839	1.640	34.722	4.19	<0.20	1.28	2.60	18.9	4.04	5.40	7.763	2.483	2.339	3200	1.70	34.726	2.79	90.9	27.78	1.460
2	N		3983	3920	1.654												3300	1.70	34.726	2.79	90.9	27.78	1.447
1	L	1	3983	3920	1.645	34.722	4.21	0.29	1.34	3.25	15.7	4.80	5.74	7.761	2.488	2.336	3400	1.69	34.726	2.79	90.9	27.78	1.424
																	3500	1.67	34.726	2.79	90.9	27.78	1.396
																	3600	1.64	34.726	2.79	90.9	27.78	1.360
																	3700	1.64	34.725	2.78	90.9	27.78	1.345
																	3800	1.64	34.725	2.77	90.9	27.78	1.334

Table 6-12. Summarized chemical data at station CTD-test

Bottle		P	Depth	T	S	O2	CH4	TA-Mn	Fe	Al	Al(acid)	pH	Alk	ΣCO2	P	T	S	O2	Trans.	Σ-t	P.temp
No.	type	db	m	°C	psu	ml/l	nM	nM	nM	nM	nM		mM	mM	db	°C	psu	ml/l	%		°C
0		0	0	20.1											4	19.90	35.690	4.15	89.7	25.32	19.904
22	N	203	201	14.589	35.453	5.16									10	19.91	35.694	4.11	89.7	25.32	19.903
21	L	203	201	14.580	35.455	5.11									20	19.72	35.722	4.11	89.7	25.39	19.717
20	L	198	196	14.596	35.450	5.16									30	19.68	35.733	4.07	89.7	25.41	19.673
19	N	201	199	14.585	35.451	5.17									50	19.36	35.806	3.94	89.6	25.55	19.348
18	L	203	202	14.577	35.468	5.13									75	18.95	35.826	3.82	89.4	25.67	18.937
17	L	203	201	14.569	35.451	5.17									100	17.64	35.743	3.78	89.8	25.93	17.625
16	N	200	198	14.597	35.450	5.15									125	16.49	35.656	3.77	90.2	26.14	16.472
15	L	199	197	14.589	35.450	5.13									150	15.93	35.606	3.77	90.3	26.23	15.910
14	L	203	201	14.583	35.261	5.14									175	15.30	35.538	3.77	90.4	26.32	15.270
13	N	296	293	13.156	35.259	5.23									200	14.59	35.454	3.76	90.4	26.41	14.562
12	L	299	296	13.158	35.259	5.25									300	13.16	35.260	3.80	90.5	26.56	13.115
11	L	299	296	13.138	35.305	5.24									400	12.25	35.118	3.82	90.5	26.63	12.192
10	N	299	297	13.162	35.260	5.25									500	11.38	34.988	3.84	90.5	26.70	11.315
9	L	299	297	13.131	35.258	5.23															
8	L	397	394	12.172	35.144	5.29															
7	N	402	399	12.160	35.105	5.30															
6	L	397	394	12.157	35.138	5.29															
5	L	400	397	12.138	35.107	5.30															
4	N	500	496	11.36	34.986	5.34															
3	L	501	497	11.36	34.986	5.37															
2	N	499	495	11.37	34.986	5.34															
1	L	501	497	11.36	35.220	5.27															

Table 6-13. Summarized chemical data at station CTD-11

Bottle		Sample	P	Depth	T	S	O2	CH4	TA-Mn	T-Mn	Fe	Al	Al(acid)	pH	Alk	ΣCO2	P	T	S	O2	Trans.	Σ-t	P.temp
No.	type	No.	db	m	°C	psu	ml/l	nM	nM	nM	nM	nM	nM		mM	mM	db	°C	psu	ml/l	%		°C
0		0	0	0	20.3												2	20.14	35.654	4.34	89.3	25.22	20.144
22	N	14	43	43	19.671	35.729	5.23		1.30	1.97		3.57	4.69	8.206	2.434	2.065	10	20.15	35.654	4.29	89.3	25.22	20.147
21	L		42	42	19.668												50	19.65	35.746	4.12	89.8	25.43	19.639
20	L	13	99	98	19.018	35.828	5.23		0.96	4.03		4.69		8.190	2.449	2.086	100	18.71	35.754	3.89	89.7	25.67	18.695
19	N		501	497	11.343												200	14.76	35.472	3.88	90.5	26.39	14.730
18	L	12	501	497	11.344	34.971	5.31		<0.14	2.64		3.58	4.28	7.999	2.382	2.156	300	13.18	35.264	4.00	90.5	26.56	13.136
17	L	11	750	744	8.758	34.921	5.04		0.41	0.72		3.17	3.18	7.988	2.395	2.162	400	12.16	35.106	4.05	90.5	26.64	12.108
16	N		999	990	4.863												500	11.39	34.993	4.09	90.6	26.70	11.322
15	L	10	999	990	4.857	34.604	4.48		0.15	0.68		3.44	3.40	7.841	2.401	2.230	600	10.61	34.877	4.13	90.6	26.75	10.533
14	L	9	1248	1236	3.585	34.517	3.62		0.19	0.93		2.91	3.47	7.724	2.455	2.305	700	9.38	34.706	4.06	90.6	26.83	9.297
13	N		1501	1486	3.096												800	8.40	34.605	3.87	90.6	26.90	8.312
12	L	8	1500	1485	3.102	34.624	3.47		0.14	1.87		2.48	3.18	7.718	2.455	2.325	900	6.42	34.472	3.63	90.6	27.08	6.340
11	L	7	1750	1731	2.604	34.787	3.96		0.46	2.57		4.04	4.62	7.807	2.457	2.314	1000	5.03	34.417	3.48	90.6	27.21	4.945
10	N		2004	1982	2.071												1100	4.25	34.436	3.21	90.6	27.31	4.166
9	L	6	2001	1979	2.081	34.713	4.09		2.22	6.27		2.76	3.64	7.760	2.467	2.322	1200	3.77	34.497	2.89	90.7	27.41	3.678
8	L	5	2253	2227	1.844	34.731	4.13		2.08	4.91	6.10	3.46	5.43	7.772	2.472	2.327	1300	3.45	34.539	2.75	90.7	27.48	3.353
7	N		2236	2210	1.873	34.724											1400	3.32	34.606	2.54	90.7	27.54	3.215
6	L	4	2236	2210	1.873	34.724	4.16		3.33	7.88	7.20	3.29	3.50	7.771	2.477	2.328	1500	3.16	34.632	2.47	90.7	27.58	3.051
5	L	3	2239	2213	1.870	34.721	4.11	0.57	2.91	3.76	8.40	3.17	3.74	7.768	2.473	2.332	1600	2.97	34.652	2.48	90.7	27.61	2.857
4	N		2223	2197	1.856												1700	2.66	34.676	2.59	90.8	27.66	2.540
3	L	2	2223	2197	1.857	34.723	4.15	1.50	6.70	10.59	30.10	4.49	4.57	7.769	2.472	2.328	1800	2.49	34.691	2.67	90.8	27.68	2.365
2	N		2246	2220	1.844												2000	2.14	34.716	2.79	90.9	27.73	1.997
1	L	1	2246	2220	1.845	34.724	4.17	1.20	6.14	10.37	20.50	3.81	3.72	7.770	2.476	2.328	2200	1.87	34.724	2.81	90.9	27.76	1.716
																	2400	1.80	34.725	2.80	90.9	27.77	1.633
			1	Up-1	7	Down-6	13	Up-6	19	Up-6							2600	1.74	34.726	2.78	90.9	27.77	1.558
			2	Up-1	8	Up-6	14	Up-6	20	Up-6							2800	1.73	34.727	2.78	90.9	27.77	1.524
			3	Up-3	9	Up-6	15	Up-6	21	Up-6							3000	1.70	34.727	2.76	90.9	27.78	1.478
			4	Up-3	10	Up-6	16	Up-6	22	Up-6							3200	1.68	34.727	2.77	90.9	27.78	1.442
			5	Up-5	11	Up-6	17	Up-6									3400	1.66	34.726	2.75	90.9	27.78	1.403
			6	Down-6	12	Up-6	18	Up-6									3500	1.66	34.726	2.75	90.9	27.78	1.392

Table 6-14. Summarized chemical data at station CTD-12

Bottle		Sample	P	Depth	T	S	O2	CH4	TA-Mn	T-Mn	Fe	Al	Al(acid)	pH	Alk	ΣCO2	P	T	S	O2	Trans.	Σ-t	P.temp
No.	type	No.	db	m	°C	psu	ml/l	nM	nM	nM	nM	nM	nM		mM	mM	db	°C	psu	ml/l	%		°C
0		0	0	0	20.5												2	20.48	35.555	4.91	89.1	25.06	20.475
22	N		1999	1977	2.101												10	20.54	35.541	4.67	89.5	25.03	20.533
21	L	14	1998	1977	2.100	34.729	4.12	0.36	1.96	5.83	5.72	3.05	3.30	7.738	2.453	2.324	50	19.73	35.725	4.31	89.7	25.39	19.721
20	L	13	2198	2172	1.862	34.725	4.13	0.63	2.76	12.12	9.82	3.25	3.85	7.740	2.474	2.331	100	18.80	35.836	4.13	89.6	25.71	18.781
19	N		2397	2368	1.786												200	15.46	35.555	4.02	90.4	26.30	15.427
18	L	12	2398	2369	1.782	34.726	4.14	0.52	2.94	4.18	8.51	3.45	4.50	7.744	2.477	2.332	300	13.48	35.304	4.08	90.5	26.53	13.434
17	L	11	2598	2565	1.746	34.747	4.17	0.40	3.04	3.49	9.44	3.45	3.95	7.754	2.472	2.327	400	12.30	35.128	4.18	90.5	26.63	12.248
16	N		2797	2761	1.725												500	11.53	35.009	4.21	90.5	26.69	11.462
15	L	10	2799	2763	1.725	34.728	4.21	<0.20	2.56	4.86	7.30	3.54	3.77	7.749	2.477	2.331	600	10.31	34.832	4.27	90.5	26.77	10.241
14	L	9	2997	2957	1.694	34.733	4.21	<0.20	1.99	2.20	7.12	3.84	3.90	7.748	2.481	2.334	700	9.35	34.705	4.13	90.5	26.83	9.267
13	N		3199	3154	1.658												800	7.96	34.577	3.90	90.5	26.95	7.875
12	L	8	3200	3155	1.658	34.726	4.21	<0.20	1.90	5.02	7.30	4.25	4.17	7.749	2.484	2.335	900	6.03	34.455	3.68	90.6	27.12	5.949
11	L	7	3398	3349	1.648	34.725	4.20	<0.20	2.25	3.33	6.98	4.20	4.41	7.748	2.478	2.337	1000	4.91	34.419	3.50	90.6	27.23	4.832
10	N		3498	3447	1.656												1200	3.78	34.496	2.89	90.6	27.41	3.691
9	L	6	3498	3447	1.656	34.725	4.20	<0.20	2.17	3.99	9.48	4.30	5.11	7.748	2.482	2.338	1400	3.30	34.605	2.52	90.7	27.54	3.197
8	L	5	3599	3546	1.664	34.727	4.20	<0.20	2.30	4.58	8.62	4.28	4.69	7.750	2.481	2.338	1600	2.94	34.657	2.49	90.7	27.62	2.827
7	N		3699	3643	1.675												1800	2.54	34.689	2.66	90.8	27.68	2.417
6	L	4	3699	3643	1.675	34.725	4.25	0.27	2.17	3.14	8.99	4.27	4.69	7.753	2.482	2.338	2000	2.20	34.713	2.83	90.8	27.73	2.056
5	L	3	3798	3740	1.680	34.726	4.18	<0.20	2.24	5.65	8.96	4.80	4.89	7.751	2.483	2.337	2200	1.89	34.725	2.86	90.8	27.76	1.737
4	N		3901	3840	1.691												2400	1.80	34.726	2.85	90.9	27.77	1.627
3	L	2	3899	3839	1.691	34.726	4.17	0.27	1.93	3.86	9.25	5.19	5.40	7.753	2.483	2.337	2600	1.75	34.726	2.83	90.9	27.77	1.562
2	N		3955	3893	1.690												2800	1.73	34.727	2.82	90.9	27.77	1.523
1	L	1	3954	3892	1.690	34.726	4.20	0.27	1.50	3.24	8.79	6.49	6.84	7.754	2.491	2.330	3000	1.70	34.727	2.81	90.9	27.78	1.479
																	3200	1.67	34.727	2.79	90.9	27.78	1.431
																	3400	1.65	34.726	2.79	90.9	27.78	1.389
																	3600	1.67	34.726	2.77	90.9	27.78	1.384
																	3800	1.68	34.726	2.76	90.9	27.78	1.378
																	3900	1.69	34.726	2.75	90.9	27.78	1.376

Table 6-15. Summarized chemical data at station CTD-13

Bottle		Sample	P	Depth	T	S	O2	CH4	TA-Mn	T-Mn	Fe	Al	Al(acid)	pH	Alk	ΣCO2	P	T	S	O2	Trans.	Σ-t	P.temp
No.	type	No.	db	m	°C	psu	ml/l	nM	nM	nM	nM	nM	nM		mM	mM	db	°C	psu	ml/l	%		°C
0		0	0	0	20.1												4	19.95	35.689	5.32	89.8	25.30	19.953
22	N		1999	1977	2.056												10	19.96	35.689	5.00	89.8	25.30	19.960
21	L	14	2000	1978	2.055	34.719	4.04	<0.20	0.91	2.32	3.53	2.38	3.20	7.760	2.471	2.326	50	19.69	35.721	4.31	89.7	25.39	19.685
20	L	13	2200	2174	1.905	34.723	4.08	1.20	2.20	6.05	8.56	2.61	3.26	7.762	2.478	2.332	100	19.17	35.793	4.11	89.4	25.59	19.153
19	N		2398	2369	1.807												200	15.15	35.523	4.09	90.5	26.34	15.121
18	L	12	2398	2369	1.807	34.725	4.13	0.34	2.72	4.85	9.03	3.50	4.93	7.760	2.467	2.332	300	13.30	35.281	4.19	90.5	26.55	13.259
17	L	11	2600	2567	1.760	34.759	4.18	<0.20	2.23	4.02	9.15	2.70	3.71	7.782	2.474	2.323	400	12.18	35.114	4.26	90.5	26.64	12.123
16	N		2800	2764	1.733												500	11.16	34.962	4.31	90.5	26.72	11.096
15	L	10	2799	2763	1.732	34.785	4.18	<0.20	2.46	2.80	8.97	2.62	3.00	7.789	2.469	2.326	600	10.31	34.833	4.32	90.6	26.77	10.234
14	L	9	2990	2950	1.683	34.738	4.18	<0.20	2.04	5.05	8.92	3.19	3.49	7.774	2.476	2.334	700	9.21	34.686	4.15	90.6	26.84	9.131
13	N		3197	3152	1.648												800	8.02	34.576	3.93	90.6	26.94	7.940
12	L	8	3199	3154	1.648	34.727	4.21	<0.20	1.99	8.88	9.60	3.50	4.39	7.766	2.477	2.336	900	6.56	34.475	3.69	90.6	27.07	6.478
11	L	7	3298	3251	1.650	34.725	4.20	<0.20	1.76	2.90	9.97	3.87		7.772	2.476	2.337	1000	5.15	34.430	3.46	90.6	27.21	5.065
10	N		3399	3350	1.649												1200	3.76	34.499	2.89	90.6	27.41	3.669
9	L	6	3400	3551	1.649	34.726	4.19	<0.20	2.21	3.61	9.49	3.45	4.31	7.771	2.473	2.339	1400	3.32	34.606	2.53	90.7	27.54	3.213
8	L	5	3500	3449	1.652	34.737	4.23	<0.20	2.09	7.88	9.42	3.87	4.35	7.777	2.476	2.341	1600	2.82	34.668	2.53	90.8	27.64	2.707
7	N		3600	3567	1.695												1800	2.44	34.695	2.74	90.8	27.69	2.310
6	L	4	3600	3567	1.660	34.725	4.16	<0.20	1.89	4.75	9.92	4.86	5.16	7.768	2.479	2.342	2000	2.12	34.716	2.82	90.9	27.73	1.985
5	L	3	3699	3643	1.668	34.726	4.17	<0.20	1.95	4.43	9.68	4.28	4.99	7.776	2.479	2.347	2200	1.91	34.723	2.82	90.9	27.76	1.754
4	N		3802	3744	1.680												2400	1.81	34.726	2.82	90.9	27.77	1.636
3	L	2	3800	3742	1.680	34.725	4.20	<0.20	1.93	2.61	9.01	4.37	4.96	7.771	2.478	2.344	2600	1.76	34.726	2.81	90.9	27.77	1.570
2	N		3850	3791	1.686												2800	1.73	34.726	2.80	90.9	27.77	1.523
1	L	1	3849	3790	1.686	34.726	4.18	<0.20	2.16	7.93	9.76	4.62	4.95	7.774	2.486	2.346	3000	1.69	34.727	2.81	90.9	27.78	1.464
																	3200	1.65	34.726	2.83	90.9	27.78	1.408
																	3400	1.65	34.726	2.83	90.9	27.78	1.389
																	3600	1.66	34.726	2.83	91.0	27.78	1.381
																	3800	1.68	34.726	2.84	91.0	27.78	1.378

Table 6-16. Summarized chemical data at station CTD-14

Bottle		Sample	P	Depth	T	S	O2	CH4	TA-Mn	T-Mn	Fe	Al	Al(acid)	pH	Alk	ΣCO2	P	T	S	O2	Trans.	Σ-t	P.temp
No.	type	No.	db	m	°C	psu	ml/l	nM	nM	nM	nM	nM	nM		mM	mM	db	°C	psu	ml/l	%		°C
0		0	0	0	20.3												2	20.10	35.696	4.57	88.4	25.27	20.098
22	N		1998	1976	2.100												10	19.95	35.711	4.54	88.9	25.32	19.952
21	L	14	2000	1978	2.096	34.717	4.09	1.30	1.62	1.30	3.65	2.82	4.31	7.746	2.465	2.324	30	19.69	35.723	4.50	89.4	25.40	19.688
20	L	13	2247	2221	1.861	34.723	4.12	0.60	2.35	2.96	4.33	3.00		7.745	2.470	2.333	50	19.48	35.783	4.29	89.5	25.50	19.467
19	N		2501	2470	1.760												100	18.98	35.838	4.05	89.6	25.67	18.959
18	L	12	2499	2468	1.758	34.724	4.15	0.42	2.46	4.25	8.12	2.83	3.57	7.750	2.477	2.334	150	16.23	35.628	3.97	90.2	26.18	16.204
17	L	11	2748	2713	1.729	34.816	4.26	0.60	1.58	2.35	4.83	3.06		7.806	2.461	2.316	200	14.46	35.437	4.00	90.4	26.43	14.430
16	N		2998	2958	1.705												300	13.08	35.248	4.07	90.4	26.57	13.037
15	L	10	2999	2959	1.704	34.725	4.20	0.29	2.71	3.11	6.67	3.18	4.21	7.760	2.475	2.337	400	12.23	35.117	4.14	90.4	26.64	12.174
14	L	9	3198	3153	1.673	34.731	4.21	0.78	2.12	3.07	12.40	3.57	4.30	7.757	2.466	2.333	500	11.29	34.976	4.14	90.4	26.71	11.224
13	N		3399	3350	1.654												600	10.31	34.829	4.17	90.5	26.77	10.234
12	L	8	3398	3349	1.655	34.724	4.18	<0.20	1.62	3.53	4.80	4.27	4.98	7.759	2.477	2.340	800	7.61	34.551	3.88	90.5	26.98	7.531
11	L	7	3599	3546	1.657	34.724	4.20	<0.20	1.91	3.80	9.61	4.61	5.20	7.759	2.477	2.341	1000	5.11	34.418	3.47	90.6	27.20	5.024
10	N		3701	3645	1.663												1250	3.66	34.513	2.84	90.7	27.43	3.568
9	L	6	3698	3642	1.663	34.724	4.18	<0.20	1.64	3.70	8.28	4.92	6.11	7.754	2.481	2.339	1500	3.11	34.637	2.60	90.8	27.59	2.995
8	L	5	3798	3740	1.673	34.739	4.16	<0.20	1.39	5.24	9.93	4.75	5.53	7.764	2.477	2.340	1750	2.58	34.684	2.80	90.8	27.67	2.459
7	N		3895	3835	1.683												2000	2.11	34.717	3.00	90.8	27.74	1.975
6	L	4	3896	3836	1.683	34.725	4.15	<0.20	1.26	2.19	9.17	4.86	5.30	7.765	2.475	2.341	2200	1.90	34.724	3.01	90.8	27.76	1.745
5	L	3	3999	3936	1.693	34.725	4.15	<0.20	1.36	2.06	9.01	5.22	5.93	7.760	2.481	2.343	2400	1.80	34.726	3.02	90.9	27.77	1.631
4	N		4100	4035	1.705												2600	1.75	34.726	3.01	90.9	27.77	1.567
3	L	2	4098	4033	1.705	34.725	4.16	<0.20	1.84	4.21	9.47	5.35	5.55	7.759	2.479	2.342	2800	1.73	34.727	3.01	90.9	27.77	1.529
2	N		4134	4068	1.709												3000	1.71	34.727	3.01	90.9	27.78	1.490
1	L	1	4134	4068	1.709	34.725	4.15	<0.20	1.30	3.72	9.47	5.57	6.44	7.760	2.498	2.341	3200	1.68	34.726	2.99	90.9	27.78	1.437
																	3400	1.65	34.726	2.98	90.9	27.78	1.393
																	3600	1.66	34.726	2.96	90.9	27.78	1.377
																	3800	1.67	34.726	2.94	90.9	27.78	1.371
																	4100	1.71	34.726	2.91	90.9	27.78	1.369

Table 6-17. Summarized chemical data at station CTD-15

Bottle		Sample	P	Depth	T	S	O2	CH4	TA-Mn	T-Mn	Fe	Al	Al(acid)	pH	Alk	ΣCO2	P	T	S	O2	Trans.	Σ-t	P.temp
No.	type	No.	db	m	°C	psu	ml/l	nM	nM	nM	nM	nM	nM		mM	mM	db	°C	psu	ml/l	%		°C
0		0	0	0	20.4												2	20.14	36.031	4.24	88.5	25.51	20.142
22	N																10	20.15	35.681	3.77	89.0	25.24	20.145
21	L																30	20.07	35.699	4.32	89.4	25.28	20.063
20	L																50	20.05	35.706	4.12	89.6	25.29	20.040
19	N																100	18.91	35.786	3.93	89.4	25.65	18.890
18	L																200	14.62	35.464	3.88	90.5	26.42	14.585
17	L																300	13.12	35.251	4.08	90.4	26.57	13.073
16	N																400	12.12	35.102	4.14	90.4	26.65	12.071
15	L																500	11.28	34.974	4.13	90.4	26.70	11.220
14	L																600	10.28	34.827	4.12	90.4	26.77	10.209
13	N																700	9.31	34.701	4.02	90.4	26.83	9.232
12	L																800	7.83	34.567	3.77	90.5	26.96	7.747
11	L																900	6.08	34.449	3.62	90.5	27.11	5.997
10	N		2149	2124	1.868												1000	4.91	34.422	3.38	90.5	27.23	4.827
9	L	6	2149	2124	1.868	34.724	4.10	2.60	18.64	19.70	29.20	2.86	3.36	7.758	2.471	2.331	1100	4.37	34.485	2.95	90.6	27.34	4.281
8	L	5	2402	2373	1.814	34.727	4.09	3.30	9.29	10.39	39.90	2.68	3.01	7.757	2.472	2.331	1200	3.84	34.505	2.79	90.6	27.41	3.748
7	N		2401	2373	1.814												1300	3.49	34.537	2.68	90.6	27.47	3.396
6	L	4	2150	2125	1.860	34.727	4.11	3.20	9.79	9.81	39.70	3.09	3.18	7.748	2.472	2.332	1400	3.19	34.579	2.62	90.6	27.53	3.091
5	L	3	2149	2124	1.849	34.728	4.14	2.80	8.11	8.92	39.10	2.69	3.33	7.764	2.472	2.331	1500	2.92	34.618	2.65	90.7	27.59	2.810
4	N		2148	2123	1.847												1600	2.82	34.657	2.60	90.7	27.63	2.710
3	L	2	2116	2092	1.833	34.729	4.10	1.90	6.65	7.19	24.80	3.07	3.29	7.758	2.473	2.333	1700	2.71	34.672	2.61	90.7	27.65	2.588
2	N		2151	2126	1.853												1800	2.41	34.696	2.74	90.7	27.69	2.287
1	L	1	2152	2127	1.854	34.727	4.10	3.20	9.36	8.12	32.50	2.88	3.15	7.761	2.473	2.324	1900	2.28	34.707	2.80	90.8	27.71	2.144
																	2000	2.10	34.717	2.83	90.8	27.74	1.961
			1	Down-7	7	Down-8	13		19								2100	1.93	34.723	2.85	90.8	27.76	1.786
			2	Down-7	8	Up-8	14		20								2200	1.85	34.724	2.85	90.8	27.76	1.701
			3	Down-7	9	Up-9	15		21								2400	1.79	34.725	2.85	90.8	27.77	1.626
			4	Down-7	10	Up-9	16		22								2600	1.76	34.726	2.84	90.8	27.77	1.576
			5	Up-7	11		17										2800	1.73	34.727	2.83	90.8	27.77	1.522
			6	Down-8	12		18										2900	1.68	34.727	2.83	90.9	27.78	1.467

Table 6-18. Summarized chemical data at station CTD-16

Bottle		Sample	P	Depth	T	S	O2	CH4	TA-Mn	T-Mn	Fe	Al	Al(acid)	pH	Alk	ΣCO2	P	T	S	O2	Trans.	Σ-t	P.temp
No.	type	No.	db	m	°C	psu	ml/l	nM	nM	nM	nM	nM	nM		mM	mM	db	°C	psu	ml/l	%		°C
0		0	0	0	20.4												3	20.18	35.657	3.87	89.7	25.22	20.180
22	N																10	20.18	35.655	3.88	89.7	25.22	20.180
21	L	14															30	20.05	35.705	3.90	89.7	25.29	20.048
20	L	13															50	20.03	35.709	3.90	89.7	25.30	20.023
19	N																100	18.70	35.791	3.92	89.6	25.70	18.682
18	L	12															150	16.22	35.634	3.96	90.4	26.19	16.199
17	L	11															200	14.75	35.481	3.93	90.5	26.40	14.722
16	N																300	13.04	35.241	4.18	90.4	26.57	12.998
15	L	10															400	12.12	35.100	4.28	90.4	26.65	12.063
14	L	9															500	11.26	34.970	4.35	90.4	26.71	11.198
13	N																600	10.52	34.860	4.35	90.4	26.75	10.442
12	L	8															700	9.27	34.696	4.25	90.4	26.84	9.194
11	L	7															800	7.80	34.563	4.00	90.5	26.96	7.716
10	N		1998	1976	2.111												900	6.07	34.447	3.83	90.6	27.11	5.992
9	L	6	1998	1976	2.110	34.720	4.06	1.90	3.65	4.41	10.30	2.49		7.752	2.459	2.321	1000	4.97	34.420	3.58	90.6	27.22	4.884
8	L	5	2184	2159	1.850	34.730	4.10	3.10	7.82	8.29	40.20	3.21	5.71	7.761	2.472	2.328	1100	4.34	34.487	3.08	90.6	27.34	4.254
7	N		2241	2215	1.790												1200	3.93	34.511	2.90	90.6	27.41	3.835
6	L	4	2241	2215	1.790	34.730	4.11	2.70	7.97	8.76	39.90	2.76	3.87	7.758	2.470	2.332	1300	3.47	34.538	2.82	90.7	27.47	3.375
5	L	3	2242	2216	1.784	34.730	3.97	2.40	9.02	9.27	39.90	2.90		7.761	2.473	2.330	1400	3.14	34.581	2.77	90.7	27.54	3.042
4	N		2120	2096	1.861												1500	2.98	34.608	2.75	90.7	27.57	2.874
3	L	2	2120	2096	1.861	34.736	4.11	2.10	4.29	5.09	28.40	3.49	5.76	7.760	2.468	2.331	1600	2.87	34.659	2.68	90.7	27.63	2.759
2	N		2127	2103	1.876												1700	2.56	34.682	2.78	90.8	27.67	2.441
1	L	1	2127	2103	1.873	34.729	4.11	3.00	5.18	6.18	32.30	3.47	5.14	7.762	2.469	2.330	1800	2.39	34.697	2.86	90.8	27.70	2.259
																	1900	2.23	34.710	2.92	90.8	27.72	2.098
			1	Down-5	7	Up-7	13		19								2000	2.07	34.718	2.94	90.8	27.74	1.928
			2	Down-5	8	Up-7	14		20								2200	1.84	34.725	2.94	90.9	27.76	1.688
			3	Down-6	9	Up-7	15		21								2400	1.80	34.726	2.93	90.9	27.77	1.628
			4	Down-6	10	Up-7	16		22								2600	1.75	34.726	2.92	90.9	27.77	1.563
			5	Up-6	11		17										2800	1.72	34.727	2.92	90.9	27.77	1.521
			6	Up-7	12		18										3000	1.72	34.727	2.92	90.9	27.77	1.500

Table 6-19. Summarized chemical data by the DESMOS hydrocast. At DESMOS-4, No.6 bottle was not closed in spite of the trigger command. At DESMOS-5, No.1~4 bottles were closed although the trigger commands sent 3 times

Bottle		P	Depth	T	S	O2	CH4	TA-Mn	Fe	Al	Al(acid)	ΣCO2
No.		db	m	°C	psu	ml/l	nM	nM	nM	nM	nM	mM
DESMOS-2 (25°24.30'S, 70°00.07'E to 25°22.16'S, 69°58.76'E; Depth 4151-3967m; 93.08.18)												
6		2197	2171	1.895	34.727	4.19		3.87	8.42		7.60	2.337
5		2236	2210	1.888	34.726	4.22		1.89	14.50	8.41		2.335
4		3923	3862	1.717	34.725	4.20		2.52	26.70		8.47	2.342
3		3889	3829	1.712	34.725	4.18		4.26	38.50	6.86	8.32	2.339
2		3970	3908	1.722	34.724	4.18		8.34	10.40		8.41	2.335
1		4251	4182	1.752	34.724	4.18		1.94	8.35	6.54	7.50	2.343
DESMOS-3 (25°48.06S, 70°11.14'E to 25°47.31'S, 70°12.88'E; Depth 3724-3591m; 93.08.22-23)												
6		490	485	11.3	34.733	4.07		6.78	6.33			
5		991	982	5.211	34.731	4.08		5.21	7.00			
4		1492	1477	3.088	34.720	4.08		3.60	6.06			
3		1988	1966	2.126	34.732	4.08		4.72	7.69			
2		2300	2273	1.886	34.728	4.10		7.62	8.34			
1		2491	2460	1.793	34.730	4.11		4.20	6.70			
DESMOS-4 (25°19.14'S, 70°00.61'E to 25°19.79'S, 70°00.66'E; Depth 2895-3096m; 93.08.24)												
6		2090	2066	1.97								
5		2192	2167	1.907	34.725	4.13	2.40	3.15				
4		2288	2261	1.870	34.728	4.10	2.30	8.34				
3		2390	2360	1.823	34.729	4.16	2.30	5.08				
2		2791	2755	1.779	34.728	4.16	0.99	5.59				
1		2793	2756	1.771	34.729	4.15	1.40	2.43				
DESMOS-5 (24°00.45'S, 69°40.03'E to 23°59.24'S, 69°38.73'E; Depth 3385-3082m; 93.08.24-25)												
6												
5												
4								13.50	80			
3		2989	2949	1.792				10.90	20			
2		2910	2872	1.790				13.70	40			
1		2905	2867	1.792				2.89	6			

Table 6-20. Summarized chemical data at station CTD-17

Bottle		Sample	P	Depth	T	S	O2	CH4	TA-Mn	T-Mn	Fe	Al	Al(acid)	pH	Alk	ΣCO2	P	T	S	O2	Trans.	Σ-t	P.temp
No.	type	No.	db	m	°C	psu	ml/l	nM	nM	nM	nM	nM	nM		mM	mM	db	°C	psu	ml/l	%		°C
0		0	0	0	20.4												3	21.21	35.419	4.91	89.4	24.76	21.211
22	N		2003	1981	1.993												10	20.97	35.460	4.71	89.4	24.86	20.964
21	L	14	2002	1980	1.994	34.720	4.12	0.56	1.37	7.95	0.70	2.58	2.95	7.796	2.453	2.307	50	20.69	35.505	4.24	89.4	24.96	20.683
20	L	13	2201	2175	1.868	34.727	4.11	0.41	2.21	8.04	4.60	3.06	3.27	7.767	2.470	2.331	100	20.24	35.626	4.10	89.6	25.18	20.223
19	N		2300	2273	1.820												200	17.89	35.724	3.89	90.3	25.86	17.852
18	L	12	2301	2274	1.820	34.728	4.09	0.28	4.60	8.51	3.00	3.06	3.79	7.760	2.473	2.333	300	14.62	35.455	4.04	90.5	26.41	14.578
17	L	11	2400	2371	1.804	34.728	4.10	0.00	3.03	5.40	2.80	3.31	3.69	7.762	2.476		400	13.10	35.248	4.25	90.4	26.57	13.041
16	N		2499	2468	1.789												500	12.13	35.101	4.27	90.5	26.64	12.068
15	L	10	2498	2467	1.789	34.728	4.09	0.48	3.23	7.01	3.10	3.48	4.03	7.764	2.476	2.336	600	11.01	34.932	4.28	90.5	26.72	10.938
14	L	9	2601	2568	1.761	34.728	4.13	0.52	1.86	4.59	4.60	3.28	4.23	7.763	2.475	2.336	700	9.76	34.758	4.23	90.5	26.80	9.681
13	N		2702	2667	1.751												800	8.68	34.640	4.04	90.5	26.89	8.594
12	L	8	2702	2667	1.749	34.728	3.98	0.97	4.97	8.28	22.40	3.52	3.39	7.763	2.474	2.333	900	6.83	34.501	3.80	90.6	27.05	6.745
11	L	7	2800	2764	1.744	34.728	4.15	3.90	12.76	8.97	50.70	3.73	4.82	7.763	2.476	2.337	1000	5.36	34.441	3.54	90.6	27.19	5.272
10	N		2899	2861	1.747												1100	4.41	34.472	3.07	90.6	27.32	4.320
9	L	6	2899	2861	1.747	34.727	4.13	3.90	12.16	10.48	59.40	4.05	4.55	7.763	2.477	2.337	1200	3.95	34.502	2.89	90.6	27.40	3.859
8	L	5	3000	2960	1.752	34.728	4.15	3.90	10.96	8.53	127.00	4.20	5.19	7.765	2.478	2.335	1300	3.60	34.562	2.67	90.7	27.48	3.506
7	N		3099	3057	1.755												1400	3.32	34.597	2.60	90.7	27.53	3.217
6	L	4	3100	3058	1.755	34.726	4.14	2.60	7.50	9.78	48.30	4.30	5.01	7.765	2.477	2.335	1500	3.07	34.625	2.63	90.7	27.58	2.963
5	L	3	3197	3153	1.760	34.726	4.15	1.20	5.77	7.62	33.50	4.47		7.766	2.480	2.334	1600	2.85	34.660	2.66	90.8	27.63	2.737
4	N		3294	3247	1.766												1700	2.65	34.677	2.73	90.8	27.66	2.533
3	L	2	3294	3247	1.766	34.725	4.17	1.20	3.55	6.48	19.60	4.68	5.32	7.767	2.479	2.335	1800	2.39	34.696	2.83	90.8	27.70	2.267
2	N		3224	3179	1.777												1900	2.18	34.711	2.89	90.9	27.73	2.050
1	L	1	3225	3180	1.777	34.725	4.17	1.10	3.95	6.19	13.10	4.68	5.33	7.766	2.476	2.333	2000	2.00	34.719	2.91	90.9	27.75	1.862
																	2200	1.88	34.722	2.93	90.9	27.76	1.731
			1	Up-5	7	Up-5	13	Up-5	19	Up-5							2400	1.83	34.725	2.93	90.9	27.77	1.658
			2	Up-5	8	Up-5	14	Up-5	20	Up-5							2600	1.78	34.726	2.93	90.9	27.77	1.595
			3	Up-5	9	Up-5	15	Up-5	21	Up-5							2800	1.75	34.727	2.92	90.9	27.77	1.550
			4	Up-5	10	Up-5	16	Up-5	22	Up-5							3000	1.76	34.727	2.90	90.9	27.77	1.536
			5	Up-5	11	Up-5	17	Up-5									3200	1.78	34.727	2.88	90.9	27.77	1.532
			6	Up-5	12	Up-5	18	Up-5									3300	1.78	34.727	2.88	90.9	27.77	1.531

Table 6-21. Summarized chemical data at station CTD-18

Bottle		Sample	P	Depth	T	S	O2	CH4	TA-Mn	T-Mn	Fe	Al	Al(acid)	pH	Alk	ΣCO2	P	T	S	O2	Trans.	Σ-t	P.temp
No.	type	No.	db	m	°C	psu	ml/l	nM	nM	nM	nM	nM	nM		mM	mM	db	°C	psu	ml/l	%		°C
0		0	0	0	20.9												4	20.74	35.493	5.05	89.1	24.94	20.740
22	N		2153	2128	1.874												10	20.74	35.492	4.94	89.2	24.94	20.735
21	L	14	2152	2127	1.874	34.806	4.22	0.64	3.77	5.10		3.22	3.41	7.818	2.455	2.297	30	20.75	35.493	4.62	89.4	24.94	20.741
20	L	13	2299	2272	1.841	34.724	4.10	0.34	4.46	5.78	1.26	3.23	3.17	7.755	2.469	2.331	50	20.73	35.495	4.30	89.5	24.95	20.718
19	N		2399	2370	1.821												100	20.16	35.651	4.05	89.5	25.22	20.140
18	L	12	2399	2370	1.818	34.724	4.10	0.54	7.06	7.99	3.45	3.80	3.92	7.759	2.466	2.333	150	19.77	35.707	4.04	89.9	25.36	19.743
17	L	11	2499	2468	1.797	34.723	4.14	2.50	5.56	7.14	11.10	3.83	3.68	7.763	2.471	2.335	200	18.63	35.742	3.90	90.2	25.68	18.599
16	N		2598	2566	1.782												300	14.82	35.478	4.05	90.4	26.38	14.772
15	L	10	2597	2565	1.782	34.724	4.15	3.30	8.30	10.00	23.30	3.53	4.01	7.756	2.466	2.335	400	13.08	35.244	4.26	90.4	26.57	13.024
14	L	9	2695	2661	1.768	34.726	4.13	4.80	8.59	9.10	54.30	3.65	3.44	7.765	2.469	2.336	500	12.10	35.095	4.31	90.4	26.64	12.034
13	N		2798	2762	1.754												600	11.19	34.956	4.33	90.4	26.71	11.109
12	L	8	2798	2762	1.754	34.726	4.14	5.70	9.64	10.70	84.30	3.81	3.88	7.764	2.473	2.334	700	9.78	34.761	4.28	90.4	26.80	9.701
11	L	7	2897	2859	1.758	34.727	4.14	5.50	10.20	11.00	96.70	4.45	4.10	7.769	2.472	2.336	800	8.56	34.630	4.07	90.5	26.90	8.472
10	N		3000	2960	1.763												900	6.54	34.485	3.82	90.5	27.08	6.454
9	L	6	3000	2960	1.762	34.727	4.12	3.90	9.80	10.71	150.00	4.30	4.04	7.765	2.470	2.335	1000	5.33	34.440	3.57	90.5	27.19	5.243
8	L	5	3099	3056	1.768	34.729	4.13	3.40	10.10	10.75	98.30	3.96	3.90	7.765	2.470	2.334	1100	4.37	34.473	3.14	90.5	27.33	4.280
7	N		3199	3155	1.776												1200	3.93	34.502	2.94	90.5	27.40	3.837
6	L	4	3199	3155	1.776	34.729	4.12	3.60	8.85	10.24	102.00	4.03	3.94	7.763	2.470	2.336	1400	3.33	34.597	2.65	90.6	27.53	3.228
5	L	3	3299	3253	1.786	34.730	4.16	3.40	8.77	9.70	82.30	4.03	3.99	7.769	2.471	2.333	1600	2.81	34.663	2.73	90.7	27.63	2.694
4	N		3398	3349	1.794												1800	2.42	34.695	2.85	90.7	27.69	2.295
3	L	2	3399	3350	1.794	34.730	4.14	2.80	9.18	10.08	96.70	3.92	4.34	7.765	2.479	2.335	2000	1.98	34.720	2.96	90.8	27.75	1.843
2	N		3436	3387	1.798												2200	1.88	34.722	2.96	90.8	27.76	1.728
1	L	1	3438	3389	1.799	34.731		3.10	9.23	10.07	114.00	3.62	3.99	7.769	2.475	2.333	2400	1.82	34.725	2.96	90.8	27.77	1.654
																	2600	1.79	34.726	2.97	90.8	27.77	1.600
																	2800	1.76	34.727	2.97	90.8	27.77	1.553
																	3000	1.76	34.727	2.96	90.8	27.77	1.539
																	3200	1.78	34.727	2.95	90.8	27.77	1.533
																	3400	1.79	34.727	2.93	90.8	27.77	1.530

Table 6-22. List of surface seawater samples collected during the ship transits (by T. Gamo)

Sample No.	Date & Time (Local)	Area	Position	Tempereture (°C)	Salinity-1	Salinity-2	Air Temp. (°C)
KH93-3, SW-1	July 24, 11:10	Indian Ocean	10°29.1'S, 97°42.5'E	28.1	34.47	35.396	23.9
KH93-3, SW-2	July 25, 11:10	Indian Ocean	13°44.9'S, 91°45.2'E	25.7	34.65	35.342	
KH93-3, SW-3	July 26, 14:40	Indian Ocean	17°21.1'S, 84°56.9'E	23.8	34.59	35.392	22.4
KH93-3, SW-4	July 27, 13:05	Indian Ocean	20°24.1'S, 79°05.1'E	22.0	35.17	35.206	20.3
KH93-3, SW-5	Aug. 27, 09:00	Indian Ocean	16°37.6'S, 76°03.5'E	24.2	35.71		23.2
KH93-3, SW-6	Aug. 28, 08:48	Indian Ocean	12°07.7'S, 79°51.4'E	25.3	35.65		24.6
KH93-3, SW-7	Aug. 29, 12:15	Indian Ocean	6°43.4'S, 84°19.8'E	27.2	37.31		27.0
KH93-3, SW-8	Aug. 30, 08:40	Indian Ocean	2°49.9'S, 87°43.8'E	28.0	36.87		27.2
KH93-3, SW-9	Aug. 31, 08:40	Indian Ocean	1°51.4'N, 91°34.7'E	28.6	36.13		27.5
KH93-3, SW-10	Sept. 1, 08:26	Andaman Sea	6°01.1'N, 94°46.7'E	28.3	35.77		27.1
KH93-3, SW-11	Sept. 8, 08:50	South China Sea	4°54.4'N, 106°42.2'E	28.9	33.11		27.4
KH93-3, SW-12	Sept. 9, 09:45	South China Sea	10°08.5'N, 111°16.3'E	28.5	32.50		29.2
KH93-3, SW-13	Sept. 10, 08:25	South China Sea	13°34.3'N, 116°28.3'E	28.5	33.61		26.5
KH93-3, SW-14	Sept. 11, 08:25	South China Sea	18°40.4'N, 120°33.1'E	29.0	33.13		26.8
KH93-3, SW-15	Sept. 12, 07:55	Philippine Sea	19°29.4'N, 127°07.9'E	28.5	34.58		27.5
KH93-3, SW-16	Sept. 13, 08:00	Philippine Sea	23°51.0'N, 127°04.0'E	27.8	34.76		27.6
KH93-3, SW-17	Sept. 14, 08:00	Philippine Sea	26°03.4'N, 128°12.2'E	28.2	34.68		27.1
KH93-3, SW-18	Sept. 15,	Philippine Sea					
KH93-3, SW-19	Sept. 16,	Philippine Sea					

Table 6-23. List of seawater samples sealed in copper tubing for He isotope analysis (by T. Gamo)

Station No.	IR01	IR02	IR03	IR04	IR06*	IR07	IR08	IR09	IR10	IR11	IR12	IR13	IR014	IR15	IR16	IR17	IR18
Sample No.																	
15	○																
14																	
13	○	○	○	○	○		○										
12						○											
11	○	○	○	○	○			○									
10							○										
9	○	○	○	○		○		○	○		○	○	○			○	○
8																	
7	○	○	○	○	○		○	○			○	○	○			○	○
6						○			○								
5	○	○	○	○				○			○	○	○			○	○
4							○							○			
3	○	○	○	○	○	○			○		○	○	○	○		○	○
2	○				○			○									
1		○	○	○	○	○	○		○		○	○	○			○	○
Remark	*IR06 samples have labels of "IR05" instead of "IR06" on the Cu tubings																

Table 6-24. List of seawater samples for the analyses of Po, Pb, and rare earth elements (by T. Gamo)

Sample No.	Sampler	Depth (m)	Po, Pb sample (large-mouth)	REE sample (small-mouth)	Remark
IR01-2	Lever-action N.	4100	○	○	
IR01-4	Lever-action N.	3739	○	○	
IR01-7	Niskin	3154	○	○*	HCl 1ml
IR01-9	Niskin	2957	○	○	
IR01-11	Niskin	2470	○	○	
IR01-13	Niskin	1973	○	○	
IR01-15	Niskin	1484	○	○	
IR03-1	Lever-action N.	4136	○	○	
IR03-5	Lever-action N.	3879	○	○	
IR03-10	Lever-action N.	3632	○	○	
IR03-15	Niskin	3331	○	○	
IR11-4	Lever-action N.	2210	○	○	
IR11-5	Lever-action N.	2227	○	○	
IR11-6	Lever-action N.	1979	○	○	
IR11-7	Lever-action N.	1731	○	○	
IR11-8	Lever-action N.	1485	○	○	
IR11-9	Lever-action N.	1236	○	○	
IR11-10	Lever-action N.	990	○	○	
IR11-11	Lever-action N.	744	○	○	
IR11-12	Lever-action N.	497	○	○	
IR11-13	Lever-action N.	98	○	○	
IR11-14	Niskin	43	○	○	

7. Bottom Observations Searching for Hydrothermal Vent Communities by the Deep Sea Multi-Monitoring System (DESMOS)

Suguru OHTA[1], Kenji SHIMIZU[1], Masaharu WATANABE[1], and Maki ITO[2]

[1]*Ocean Research Institute, University of Tokyo*
[2]*Department of Ocean Science and Technology, Tokai University*

Exploration of active spreading and hydrothermalism along the rift systems in the Indian Ocean has been conducted by the scientists of various disciplines of many countries. However, so far, location of active hydrothermal vents and vent-associated biological communities has not been realized. The prime objective of the biological participants was to find the active hydrothermal vents and vent organisms along the rift systems. Direct demonstration of the world-wide occurrence of vent communities, *per se*, is important, and also it is highly expected from the zoogeographical and genetic points of view.

Bottom surveys and observations were carried out using a deep-tow type bottom surveying system named "DESMOS" (deep-sea multi-monitoring system). During the third leg of KH93-3, five operations were devoted, in vain, to the exploration of the hydrothermalism and vent associated biological communities along the Central Indian Ridge (CIR) of the Rodriguez Triple Junction in the central Indian Ocean. The last operation was devoted, again in vain, to the location of the possible hydrothermalism in the "Sonne Field" on the CIR to the north of the present extensive survey area.

All operations were carried out in collaboration with chemical, geological and geophysical parties. The towing points were determined primarily on the basis of the results of ordinary and "tow-yo" modes of CTD-multi-rosette hydrocast which is equipped also a transmissiometer. Large anomalies of light transmission together with the plumes of high concentration of Mn, Fe and methane, especially in the layer between 2,200-2,300m deep suggested the nearby presence of the hydrothermal activities. Experts of chemistry, petrology, volcanology and geophysics were invited at any time to the main console of the DESMOS system to comment every features on the TV monitors.

Exploration of hydrothermal activities and vent-associated biological communities were not rewarded, and no slightest indication of vent activity was detected during the surveys. However, high quality bottom images afforded direct and best information of the biota and bottom features around the rift valley system.

1. Specifications and operations of the system

The underwater vehicle of the DESMOS is composed of a stereo-pair of color TV, a pair of stereo still cameras (up to 1,700 frames using 35mm, 100-foot long strip color negative films, CTD (Sea-Bird Electronics, Inc.: Model SBE 9/11, modified by Tsurumi Seiki Co. Ltd.), 6-bottle rosette water sampler (Niskin-type; 1.5 liter each) and a releasing clamp beside auxiliary instruments such as an acoustic altimeter, an inclinometer, an acoustic transponder and a chain suspended from the frame of the vehicle. Images illuminated by four 300 watt halogen lamps and measurement signals are conducted to the shipboard console via 6,000m

long, 14.4mm phi composite armored cable (consisting of 6 optical fibers, 4 signal wires and 6 power chords).

Taking photographs, water sampling and releasing of any kind of instruments are controlled by the operators based on the real-time information displayed on shipboard monitors. Vertical and horizontal CTD profiles were monitored on CRT, X-Y plotter and printer. Horizontal mode of the CTD profile is specially designed for the quick discrimination of thermal anomalies on analog graphics. Video images and essential LAN data are displayed on two monitor TV and recorded on S-VHS cassettes together with voice comments of the observers. The vehicle is not equipped with thrusters, simply hung on a tethered cable and maneuvered by up-down winch operations and surface ship's joy-stick dynamic positioning system.

A pendulum chain of 250cm long served as a distance cue for winch operation and dimensioning of the objects. When the tip of the chain touched the bottom, the rough estimation of the frame coverage was 2 by 2.5m on the bottom, as, in most cases, cameras were set perpendicular to the bottom and zooming was set as wide as possible. Detailed analysis and dimensioning and identification of photographed objects will be carried out in the laboratory on land. Note that the depth figures superimposed on video monitor was fed from Seabeam via LAN, and the time in GMT. True vehicle depth was recorded continuously on CTD graphic and floppy data.

Water samples were analyzed by chemical party and geological descriptions along several DESMOS tracks (Stations DESM02, DESM03 and DESM05) were made primarily by S. Nakada, T. Ishii and S. Yamashita. The detailed results will be described elsewhere in this report.

Trackings of the underwater vehicle together with surface ship were fixed and guided by means of a SSBL (super-short-base-line) acoustic transponder subnavigation system (OKI Electronic Company Ltd.). M. Watanabe and M. Ito were responsible for these operations. K. Shimizu improved the software of the SSBL operation on board. Geophysical party (especially C. Honsho) prepared for us the on-board Seabeam maps of the pertinent areas in due time. T. Matsumoto and S. Kanayama helped us in the grease up of the cable winch at the end of the last operation and they were rewarded special T-shirts.

The system was operated at 5 survey points (Stations DESM01, DESM02, DESM03, DESM04 and DESM05) and the preliminary observations were briefly summarized in the following. Date and time are expressed in GMT.

2. Brief resume of the video observations

Station DESM01 [see Fig. 7-1]

Location: A steep NE slope of the CIR axial rift valley
[ship] 25° 19.99′S; 69° 58.00′E (4,251m) - 25° 18.02′S; 69° 59.91′E (3,022m)
[desm] 25° 20.00′S, 69° 57.90′E (4,258m) - 25° 18.42′S, 69° 59.45′E (3,011m)
Date and time of operation: 10:20-15:36, Aug. 17, 1993
Duration of bottom observations: 11:42-14:45, Aug. 17, 1993
Span of the bottom observation track: 3,750m (horizontal projection)
Bottom still photos: ca. 600 frames (#2 camera only) [Konica XG400]
Video records: 2 pairs of S-VHS cassettes during 11:36-14:52
Water bottle sampled: none

Objectives and remarks: The prime objective of the DESMOS operation in this station was to explore and to locate the new vent fields along a steep NE inner slope of the CIR central rift valley, where CTD hydrocasts and "tow-yo" operations during Leg 2 and Leg 3 (Stations CTD-9 and CTD-11) told the strongest anomalies in the light transmission and water chemistry related to hydrothermal activities at a layer around 1,300m.

It turned against the expectation. No sign of present hydrothermal activity along the track with the exception of small inconsistent seeming "thermal anomalies". Sporadic "thermal anomalies" recorded on the continuous CTD record during horizontal tow can be considered to be artefacts due to 1) sediment cloud evoked by collision of the system to the bottom passed the sensor chamber (in this case, salinity shows erratic fluctuation synchronously), and 2) temperature sensor is bathed in water heated by the incandescent lamps of the DESMOS, because the "anomalies" were observed when the system hit the obstacles. Camera# 1 did not work due to a trouble in the take-up mechanism of the film.

Typical scenery: DESMOS climbed uphill the huge NE inner wall of the rift valley of the CIR from the base of the graben 4,250m deep to the top of the rift 3,022m deep. Principally the scenery of the scarp was the alternation of breccias and talus of not so fresh appearance. Around 2,500m just below the top, seemingly greenish altered basalt was observed.

Biota: The biota of the bare rock region was exceedingly poor both in species number and abundance. No organisms worthy of mention were seen except sporadic aristeinid swimming shrimps, slender gorgonians and sea anemones on the fresh basalts.

Station DESM02 [see Fig. 7-2]

Location:Two topographic highs in the rift axis of the CIR
[ship] 25° 24.31′S; 70° 00.06′E (4,152m) - 25° 22.15′S; 69° 58.77′E (3,970m)
[desm] 25° 24.30′S, 69° 59.98′E (4,162m) - 25° 22.45′S, 69° 59.85′E (3,918m)
Date and time of operation: 22:48 (Aug. 17) - 04:55 (Aug. 18, 1993)
Duration of bottom observations: 00:08-03:45, Aug. 18, 1993
Span of the bottom observation track: 3,950m (horizontal projection)
Bottom still photos: ca. 880 frames (#2 camera only) [Konica XG400]
Video records: 2 pairs of S-VHS cassettes during 00:05-03:49
Water bottle sampled: 6 bottles

Objectives and remarks: Possible hydrothermal vent fields were searched for around two large volcanic cones with different scales in the rift axis of the CIR. Chemical analysis during Leg 2 predicted moderate anomaly in Fe around this site (Station CTD-2).

Again the expectation and labor was not rewarded. Sporadic "thermal anomalies" recorded on the CTD record can be considered to be artefacts due to incandescent lamp of the DESMOS system.

Camera #1 did not work due to a trouble in the take-up mechanism of the film.

Typical scenery: The two volcanic cones consist principally of alternation of pillow lobe piles and of pillow breccias/hyaloclastites. The summit of the larger volcanic cone is occupied by sheet flow, while that of the smaller one by hyaloclastites. Sediment, a few cm thick, covers lavas on both volcanic cones. These volcanic cones are inactive, but nearly "zero-aged", because fresh, glassy surface remains and sediment cover is thin enough.

Biota: Extremely poor in larger living organisms as was observed in the preceding operation. Organisms to be mentioned were scarce occurrence of Hyalonema-type hyaline sponges.

Station DESM03 [see Fig. 7-3]

Location: Two small volcanoes in the central rift valley of the northernmost segment of the SEIR
[ship] 25° 48.07′S; 70° 11.14′E (3,718m) - 25° 47.31′S; 70° 12.87′E (3,584m)
[desm] 25° 48.15′S, 70° 11.05′E (3,712m) - 25° 47.37′S, 70° 12.15′E (3,543m)
Date and time of operation: 22:06 (Aug. 21)-02:35 (Aug. 22, 1993)
Duration of bottom observations: 23:16 (Aug. 21)-01:35 (Aug. 22, 1993)
Span of the bottom observation track: 2,725m (horizontal projection)
Bottom still photos: ca. 390 stereo pairs [Konica XG400]
Video records: 2 pairs of S-VHS cassettes during 23:12-01:43
Water bottle sampled: 6 bottles during ascent

Objectives and remarks: This station was established by the geological party to observe directly the development of two volcanic cones in the axial graben of the northernmost segment of the SEIR adjoining to the Rodriguez Triple Junction. Negative gravity anomaly was most pronounced around here.
Typical scenery: The two cones consisting pillow lavas and hyaloclastites stand on sheet-flow floors with different elevations. Each cone was cut by N-NE trending faults in both sides. Talus is widely distributed below fault scarps. The activity of faults occurred after the formation of these volcanic cones. However, very thin sediment cover and fresh glassy surface of lavas indicated that the volcanic cones are "zero-aged". Glittering black sunflower-like structure, indicating degassing from lava flows, was frequently observed on the surface of sheet flows.
Biota: Again and again, the biomass was extremely low, as is usual in the barren abyssal zone. Elasipod holothurians (possibly belonging to Psychropotinae), ophiuroids including the clinging member like *Asteronyx* and shrimp of the genus *Nematocarcinus*.

Station DESM04 [see Fig. 7-4]

Location:On a bench of the NE inner wall of the rift valley of the CIR
[ship] 25° 19.14′S; 70° 00.61′E (2,910m) - 25° 19.81′S; 70° 00.64′E (3,110m)
[desm] 25° 19.15′S, 70° 00.55′E (2,919m) - 25° 19.53′S, 70° 00.90′E (2,916m)
Date and time of operation: 01:10 - 05, Aug. 24, 1993
Duration of bottomobservations: 02:02 - 05:02, Aug. 24, 1993
Span of the bottom observation track: 3,210m (horizontal projection)
Bottom still photos: ca. 1,150 stereo pairs [Konica XG400]
Video records: 2 pairs of S-VHS cassettes during 01:59-05:10
Water bottle sampled: 6 bottles on the seafloor

Objectives and remarks: Chemical party surveyed new tow-yo tracks (Stations CTD-15 and CTD-16) only two miles to the east of the Stations CTD-9 and CTD-11, where the plume of largest anomaly of hydrothermal effluence around 1,300m layer was found. This station was established expecting that the possible spring responsible for the 1,300m layer plume may be located on the shallower portion of the NE inner wall of the CIR rift valley.

Except the artificial "thermal anomalies" on the CTD record, no indication at all was witnessed along the U-shaped track line of the DESMOS.
Typical scenery: The bottom of this station consists fundamentally of relatively old basalts, with the alteration of pleated sheet lava flows, lobate lavas, pillow breccias/hyaloclastites along

the depth gradient. The toes of steep scarps were skirted by talus of breccias and relatively flat floors were either covered by pleated sheet flows, sometimes with fissures trending N-S, or if blanketed with whitish, well oxygenated sediment, pebbles of glass were scattered. Occasional ripple marks in the pocket of large pillow lavas suggest relatively strong local bottom water movement. No signs of hydrothermal deposits, hydrothermally altered rocks and thermal anomalies were there.

Biota: Animal observed were ophiuroids of the genus Ophiuridae and phrynophiurids clinging to the stalks of hyaline sponges, nematocarcinid and aristeinid shrimps, holothurians belonging to the genus Benthodytes and Mesothuria (or*Pseudostichopus*), and fishes of the genus *Aldrovandia* (and/or *Halosaurus*), slender forms of ophidiids and *Ipnops*. All of them are ordinary constituents of the "normal" deep-sea floor inhabitants. Slightly higher abundance of the benthic organisms might be due to the shallower depth and more diverse bottom environment with sediment cover. However, the low density and dominancy of echinoderms (most of them are intolerant of hydrothermal atmosphere) suggest the vent fields are far away.

Station DESM05 [see Fig. 7-5]

Location:"Sonne Hydrothermal Field" on the eastern flank of the rift valley of the CIR
[ship] 24° 00.45′S; 69° 40.03′E (3,382m) - 23° 59.25′S; 69° 38.73′E (3,069m)
[desm] 24° 00.48′S, 69° 40.03′E (3,387m) - 23° 59.78′S, 69° 38.80′E (3,095m)
Date and time of operation: 19:04 (Aug. 24) - 11:33, Aug. 25, 1993
Duration of bottom observations: 20:13 (Aug. 24)-10:01, Aug. 25, 1993
Span of the bottom observation track: 16,725m (horizontal projection)
Bottom still photos: ca. 1,300 stereo pairs [Konica XG400]
Video records: 7 pairs of S-VHS cassettes during 20:07-10:05
Water bottle sampled: 3 bottles on the seafloor

Objectives and remarks: The operation aimed at relocation of the hydrothermal activity suggested by the German party on board Sonne in 1987. "Tow-yo" survey preceding DESMOS operation by our chemical party revealed salient transmission and chemical anomalies below 2,500m level which must be concomitant with hydrothermalism, strongly suggesting nearby occurrence of venting. The expectation was not realized through 16-hour observations of the DESMOS, No sign of the present-day hydrothermal activity was ascertained in terms of surface deposits, basalt rock features and biota along the track line. Sporadic "thermal anomalies" recorded on the CTD record can be considered to be artefacts due to incandescent lamp of the DESMOS system.

Typical scenery: The survey area situates in an off-axis graben trending N-S, bounded by faults. Flat bottom was blanketed with thick, grayish brown silty sediment (up to several tens of cm). Talus deposits exposed below fault scarps, while pillow lavas with hyaloclastites/breccias on the scarps. Pebbles of basalt glass scattered on sediment show the evidence of turbidity flows into the bottom.

Biota: Unusually thick sediment (considering the geological settings of the CIR) and weak bottom water movement characterized the benthic fauna. Detritus feeders utilizing scarce organic matter on the sediment dominated. Seemingly abundant biological activity is ascribed, in part, to the well preservation of the lebensspuren under the faint bottom current regime. Animals frequently observed are listed below in taxonomic order.

Protozoa: xenophyophores (abundant)

Porifera: *Hyalonema* spp.
Coelenterata: simple scleractinian corals, Umbellula sp., sea anemones, cerianthids and ctenophores
Echiura: star-shaped traces of echiuran worms (*Torbenwolffia*-type and others).
Mollusca: many meandering tracks of medium-sized gastropods
Macrura: *Nematocarcinus* spp., aristeinid shrimp (*Benthesicymus* spp.?)
Asteroidea: porcellanasterids?, 6-armed asteroids (Freyella oligobrachia)
Ophiuroidea: Ophiuridae
Echinoidea: lebensspuren of medium-sized spatangoids (abundant)
Holothurioidea: *Enypniastes eximia, Benthodytes* (*sanguinolenta*?)
Pisces: *Ipnops* spp., slender ophidiids and *Aldrovandia* sp.

3. Discussion and proposed future works

All the effort to locate active hydrothermal vents and special biological communities in the survey areas did not bear fruits. Although midwater plumes of chemical and light transmission anomalies suggest unequivocal activity of "nearby" hydrothermalism, bottom observations by DESMOS and rock samples collected by dredges together with the catches of bait traps gave rise to negative results. There must be some gap of "resolution power" between chemical survey and DESMOS observation to be filled with in near future.

Detailed root maps of the track lines of DESMOS and scrutiny of the rocks and gelology based on voluminous VTR records afford insights into the geology of the pertinent area. After the development of the films, bottom images and organisms of the two cameras will be analyzed stereoscopically and be investigated in detail on land to prepare the reports such as;

* Ohta, S., K. Shimizu and M. Watanabe: Deep-sea benthic life along the rift system of the central Indian Ocean revealed by a deep-tow observation platform DESMOS.
* K. Shimizu and S. Ohta: Ichnology and biological activities on the deep-sea floor of the Central Indian Region.
* Nakada, S., T. Ishii, S. Kinoshita, S. Ohta and K. Shimizu: Geological development of volcanic cones in the Indian Ridges.

4. Data storage and inquiries

S. Ohta (ORI) is responsible for the storage of original video and film records as well as DESMOS-CTD data on graphic charts and floppy disks, event records and subnavigation records on floppy disks. Data of water chemistry are supplied by T. Gamo. The chief scientists of the cruise, Drs. K. Tamaki and H. Fujimoto are in charge of the distribution and publicity of these data.

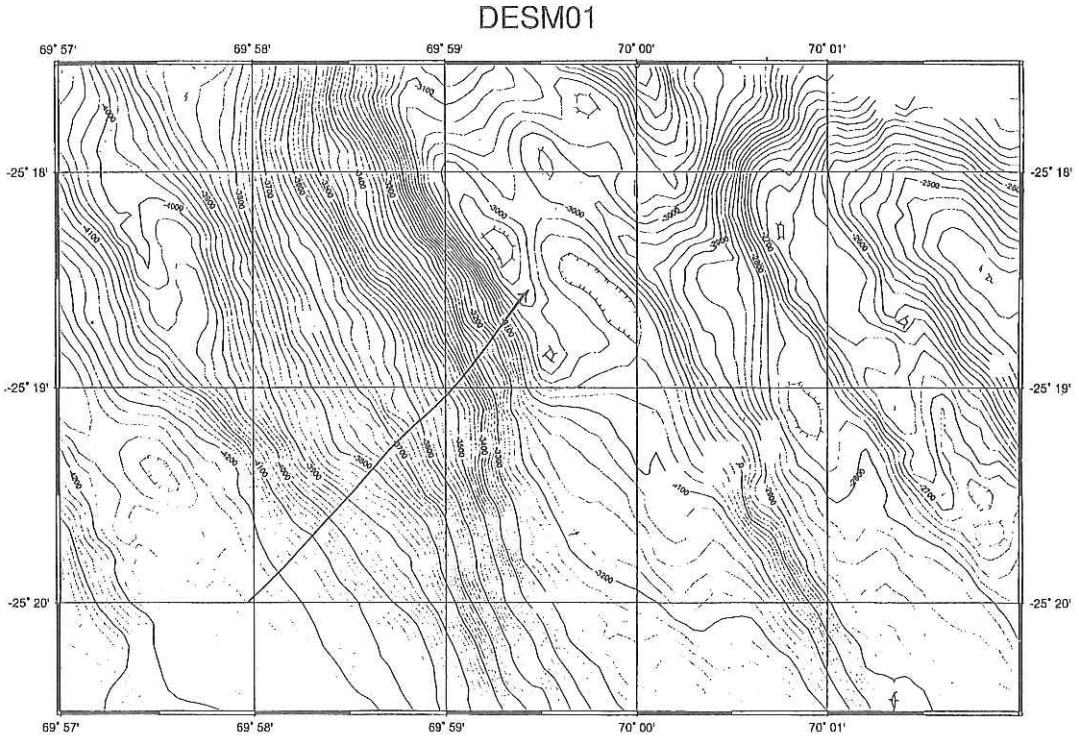

Fig. 7-1. Topography and track of the DESMOS vehicle at the Station DESM01

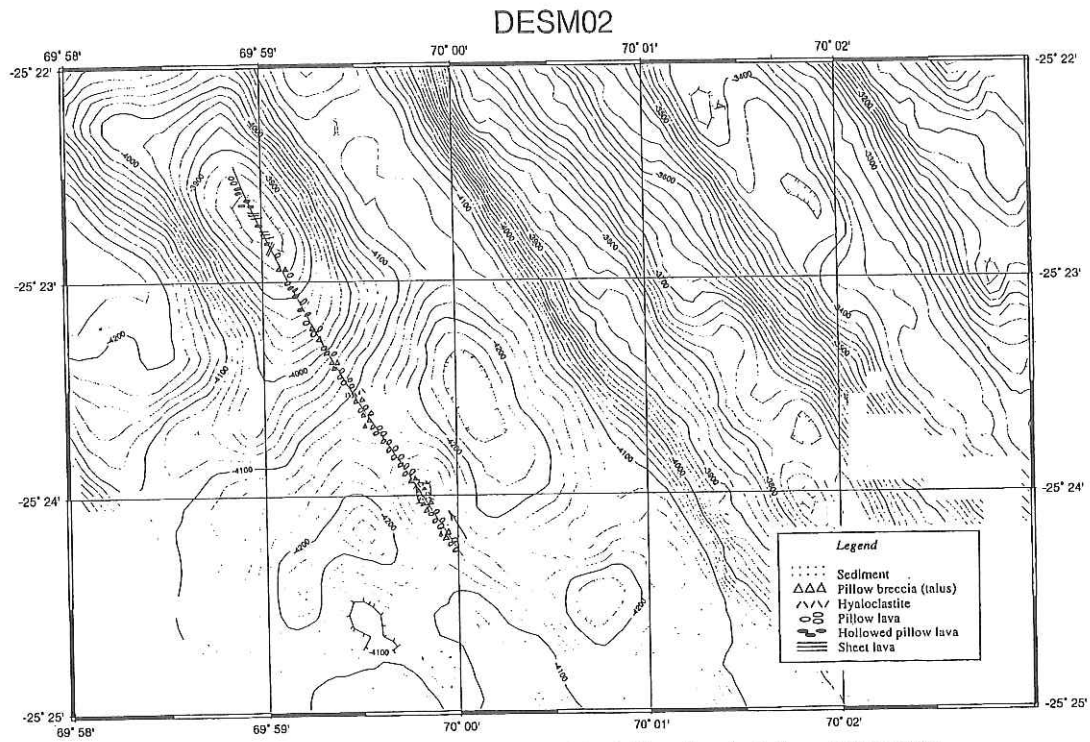

Fig. 7-2. Topography,track of the DESMOS vehicle and geological annotations (after S.Nakada) at the Station DESM02

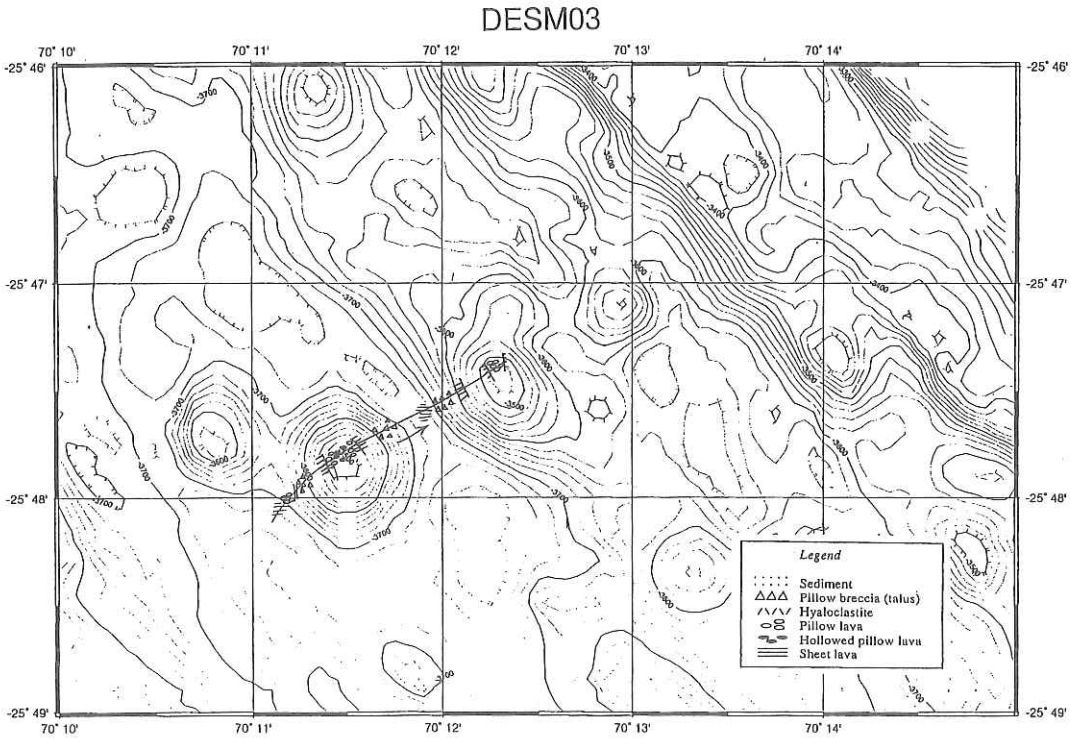

Fig. 7-3. Topography,track of the DESMOS vehicle and geological annotations (after S.Nakada) at the Station DESM03

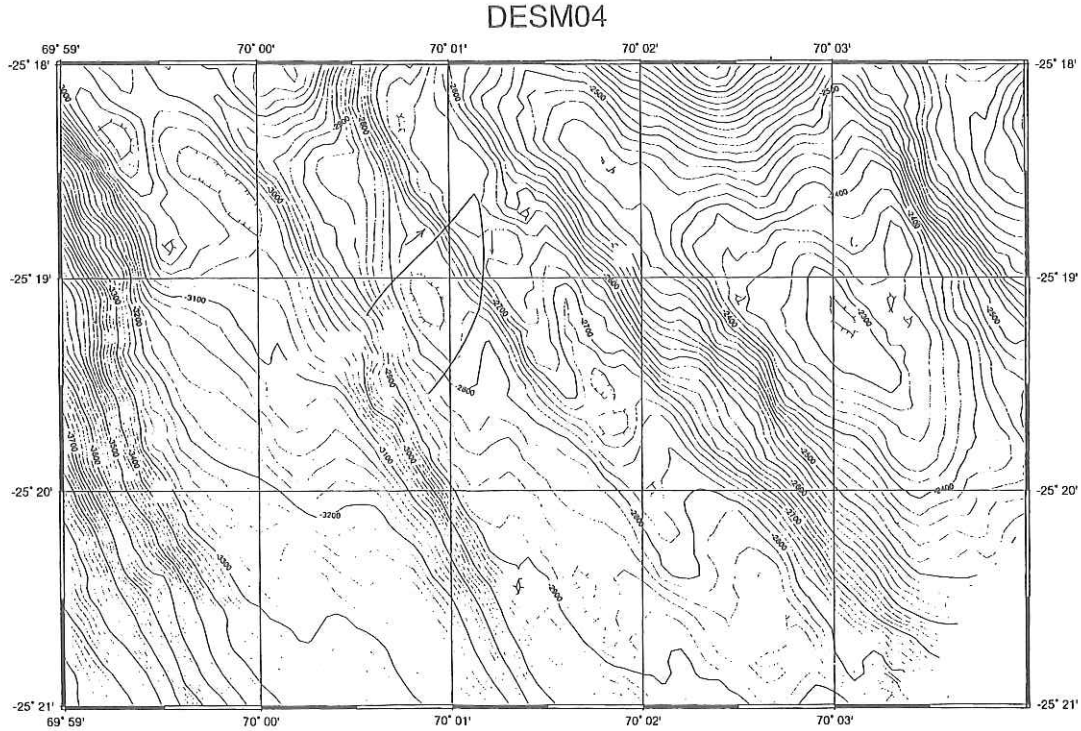

Fig. 7-4. Topography and track of the DESMOS vehicle at the Station DESM04

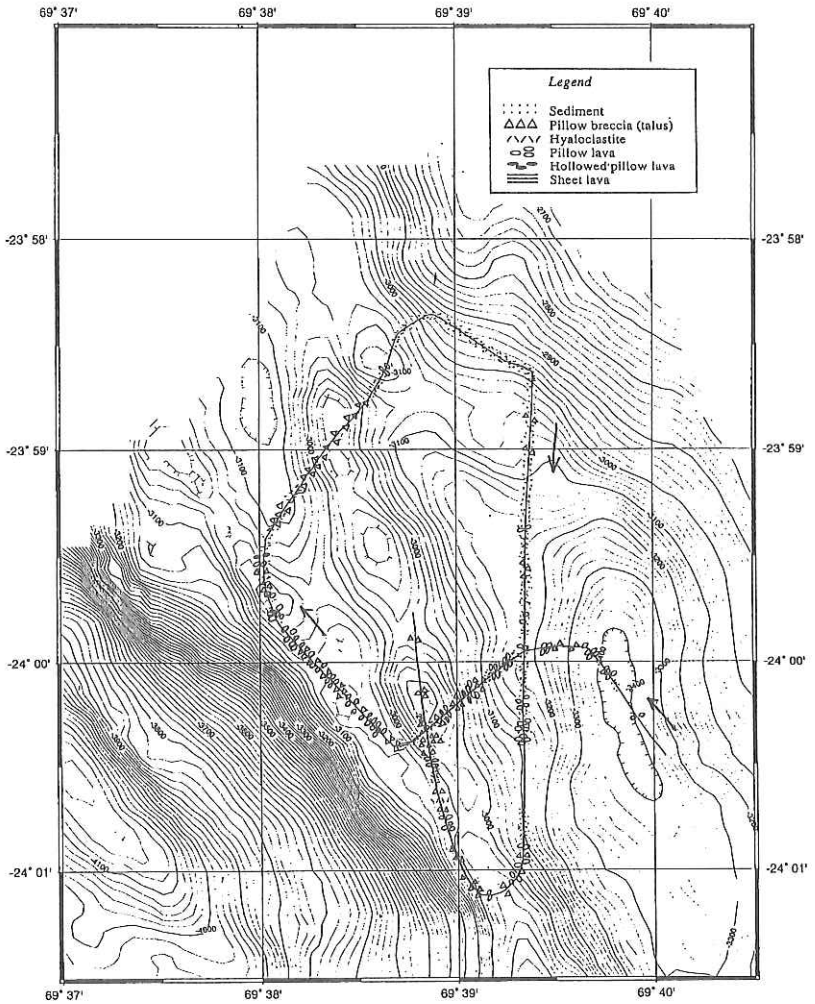

Fig. 7-5. Topography,track of the DESMOS vehicle and geological annotations (after S.Nakada) at the Station DESM05.

8. Geology of sea floor in the Central and Southeastern Indian Ridges by Deep-Sea Cameras

Setsuya NAKATA[1], Shigeru YAMASHITA[2], and Teruaki ISHII[3]

[1]*Department of Earth and Planetary Sciences, Faculty of Science, Kyushu University*
[2]*Earthquake Research Institute, University of Tokyo*
[3]*Ocean Research Institute, University of Tokyo*

1. Introduction

Geology in active ridge areas has not been known well, because of scarce opportunity to observe directly. It is much interest to know geological development among different ridges joining at a triple junction. Active and nearly active ridges (the Southeast and Central Indian ridges; SEIR and CIR, respectively) together with a less active ridge (the Southwestern Indian Ridge; SWIR) meet at the Rodriguez Triple Junction. Fresh and glassy basalts were recovered from both SEIR and CIR in this cruise, while relatively old basalt and weakly metamorphosed extrusive/intrusive rocks from SWIR.

Sea floor of CIR and SEIR was investigated with Deep-sea cameras installed in the Deep Sea Multi-Monitoring System (DESMOS; see Chapter 7 in this report). The DESMOS was towed in 5 courses (DESM01 - 05); one in SEIR, and four in CIR (see Chapter 7). Among the latter, the longest survey (DESM05) was done in the ZONNE area. We recorded geological aspects of three courses (DESM02, 03, and 05). Geological maps along the DESMOS towing routes (Figures 1, 2 and 3) and schematic cross-sections (Figures 4 and 5) are also shown. Geological logs are shown in Tables 1, 2 and 3. In this paper, we show the geological outline.

2. Geology of DESM02

Two volcanic cones with different scales (300 m and 80 m high) in a rift axis of CIR were investigated with DESMOS (Figure 1). No samples were taken directly from these cones, but samples from volcanic cones lining up the same volcano-alignment are fresh enough.

Two cones consist principally of alternation of pillow lobe piles and of pillow breccias/hyaloclastites (see Figure 4). The summit of the larger cone is occupied by a sort of sheet flow (aggregate of large and long lobes of hollowed pillow of more than 2 m across), while that of the smaller one by hyaloclastite. Sediment, a few cm to > 3 cm thick, covers lavas in both volcanoes. Sea animals and plants are scarce, probably implying no present hydrothermal activity around these volcanoes. These volcanic cones are inactive, but nearly "zero-aged", because fresh, glassy surface remains and sediment cover is thin.

3. Geology of DESM03 in the Southeastern Indian Ridge

Two volcanic cones (210 m and 120 m high) in the rift axis of SEIR were surveyed with DESMOS in order to investigate present volcanic activity and geological history of these volcanoes (Figure 2). This site is in the middle of the segment nearest to the Rodriguez Triple Junction, where the rift floor is the shallowest and the distribution density of volcanic cones is

the highest. Two volcanic cones investigated here belong to different alignments each other which overlap around this site. The eastern cone stands on a floor uplifted by a step-fault, approximately 90 m higher than the floor of the western cone. Fresh glassy samples were taken directly from the summit of these cones with Rock Core. These cones stand on the flat floor of sheet flows, and consist mainly of pile of pillow lobes and minor amount of hyaloclastite. The cones were cut by faults in the both sides; each peak is sandwiched by steep cliffs (see Figure 5). On the foots of two cones talus of pillow breccias are widely distributed. The activity of these several faults recently occurred after the formation of two volcanoes. This implies inactivity of these volcanoes. The facts that sediment cover is faint and that the lava surface looks fresh and glassy, however, indicate that the volcanoes are "zero-aged".

Ropy structure was evident in sheet flows at the foot of volcanic cones. Sunflower-like structure was frequently found on the surface of sheet flow. A round hole (crater; up to 5 cm diameter) in the center, several tens of radial ridges come radially from the rim of the crater. The diameter of the sunflower is about 1 m. Thin sediment on the surface made the structure visible clearly. This probably is a sort of pressure ridge due to degassing through the crater from lava's interior.

4. Geology of DESM05 in the SONNE area

In the SONNE area, signs of hydrothermal activity were reported by German Group (R/V SONNE). The studied area is a off-axis graben trending N-S, bounded by faults; the bottom of the graben reaches -3,400 m depth (Figure 3). The central axis at the same latitude is deeper than -4,000 m.

Thick sedimentary deposits of light-brown color cover the bottom of the graben. Talus deposits exposed on the foot of fault scarps, while pillow lavas with hyaloclastite/breccias on the scarps. The evidence for turbidity currents into the bottom is shown by pebbles of basalt glass scattered on sediment. Although lavas preserve perfect structure of pillow (corrugation, wrinkle, expanding crack, etc.), deposition of thick sediment (several tens of cm) indicates inactivity of volcanism in this area. The sign showing hydrothermal activity was not confirmed geologically in this area.

5. Summary

Geology of volcanic cones on the sea bottom of CIRRI and SEIR. Two towing courses (DESM02 and 03) with different directions (toward NW and NE) gave us general idea on the history of volcanic cones. The studied volcanic cones, which have the standard sizes in CIR and SEIR, consist of thick piles of pillow lavas with hyaloclastite and talus deposits (Figure 4). Principally volcanic cones stand on flat floors of sheet flow (Figure 5). Although hollowed pillows were sometimes observed at the summits of volcanic cones, lavas with the texture showing supply vent for sheet-flows of sea floor were not found. It is likely that volcanism at the Indian Ridges contains two stages; sea-floor stage and the following volcanic cone stage.

Table 8-1. Geological note of DESM02 in the Central Indian Ridge

DESM02
Bottom survey started at 25°24.3'S, 69°59.9'E (-4,140 m),
and ended at 25°22.5'S, 69°58.8'E (-3,860 m)
GMT 00:08 - 03:45 August 18, 1993

GMT	Depth (m)	
		vehicle
0008		Pillow lobes with fresh, glassy skin; lobe up to 1 m across, covered with thin sediment (c. 1cm thick). Typical structure of pillow lavas were recognized; corrugation, wrinkle, expanding crack.
0029		Partly pillow breccias and then changed into pile of pillow lobes.
0035		Hyaloclastite changing into pile of pillow lobes (up to 1 m across).
0042		Talus of pillow breccias; 30 to 60 cm across.
0045		Pillows on talus. Breccias in talus are angular to subangular, relatively sorted, changing into pile of pillow lobes (average size of pillow is 50 cm across, but up to 1 m).
0056		Pile of pillow lobes (lobes 1 to 0.5 m across) with breccias in spaces among lobes.
0100		Pile of pillow lobes (approximately 1 m across) covered with sediment (up to 2 cm thick) having ripple mark.
0105		Pillow breccias (30 - 50 cm across; sorted)
		--- summit of the first volcano ---
0107		Alternation of hyaloclastite to pillow breccias.
0110		Repeating of hyaloclastite and pillow breccias, but mainly hyaloclastite.
0113		Ill-sorted pillow breccias of 20 to 50 cm across.
0116		Pillow lavas (approximately 50 cm across) and breccias covered with thin sediment (<1 cm).
0123	4160	Flat surface of pillow lobes with breccias.
0128		Pillow lobes (30 - 50 cm across) with relatively thick sediment (2-3 cm) having ripple mark.
0135	3987	Pile of pillow lobes (up to 1 m across).
0140	3965	Pillow lobes (up to 50 cm across)
0146		Ill-sorted pillow breccias (20 to 60 cm across).
0151	4080	Flat surface of pillow breccias (angular to irregular; approximately 30 cm across) including perfect pillows.
0154		Sediment with ripple mark, like in temples' gardens in Kyoto.
0155		Pillow lobes of up to 1 m across with sediment cover; breccias in spaces among lobes.
0159		Hyaloclastite to breccias changing into pillow lobes.
0203	4100	Pillow lobes with fragments in space.
0210		Pillow lobes (approximately 1 m across) with sediment cover. Ripple mark on sediment is evident.
0215		Talus of pillow breccias (30 to 10 cm across).
0216		Pillow lobes on talus deposits, such that they tended to flow down from the top of talus slope. Alternation of layers of pillow breccias and of pillow lobes.
0218	4000	Pile of pillow lobes (0.5 - 1 m across)
0224	3980	Pillow lobes, partly breccias
0228		Pile of pillow lobes (0.5 - 1 m across) and sediment cover with ripple mark.
0234		Pillow breccias (20 - 50 cm across), angular to irregular shaped.
0235		Pillow lobes with fragments in space.
0237		Hollowed pillows with thick sediment cover.
0243	3890	Flat surface of pillow lobes with thick sediment cover.
0250	3875	Pile of crusts of hollowed pillows. Pillow size ranging 50 cm to 1 m across.
	3860	Hollowed pillow thickly covered with sediments; broken walls of pillows standing in sediment surface.
0254		Looks like sheet lava (large elongated lobes of hollowed pillows).
0257	3830	Pillow lobes with diameter more than 2 m.
0258		Subangular pillow breccias, 20 - 50 cm across, including perfect pillows of approx. 50 cm.
0259	3800	Pillow lobes (up to 50 cm across) with thick sediment cover.
0303	3820	N-S trending crack of 1 m wide.
0305	3820	Sheet-flow with thick sediment cover, changing into pile of fat pillow lobes.
0315		--- around summit ---
		Aggregation of crusts of hollowed pillows, probably sheet flows. Sediment of approximately 3 cm thick with ripple mark.
0323		Mound of hollowed pillow lobes or lava tubes (50 cm - 1m across). Aggregation of crusts of hollowed pillows.
0331		Pile of pillow lobes --- still summit area but north of summit in map ---
0337		Crusts of hollowed pillows, lava tubes, hollowed pillows.
0344		Aggregation of lava tubes, like roots of tree, probably one of eruption center.
0345	3860	Pillow lobes with subsidence structure on the surface, implying space in the interior (hollowed pillow). Relatively thick sediment cover (more than 3 cm) with ripple mark.

Table 8-2. Geological note of DESM03 in the Southeast Indian Ridge

DESM03
Bottom survey started at 23°48.2'S, 70°11.1'E (-3,721 m),
and ended at 23°47.4'S, 70°12.3'E (-3,400 m)
GMT 23:14 August 22, 1993 - 01:31 August 23, 1993

GMT	Depth (m) vehicle	
2314	3721	White-colored sediment on relatively flat lava surface, sometimes showing ropy structure (sometimes glassy, but probably not fresh enough).
2329	3704	Start to climb-- few centimeter across pebble-like protrusion on lava surface.
2332	3702	Flat but large lobes of pillow, still covered with white-colored sediment.
2337	3703	c. 2 m-width fissure, trending N-S. ---piling of fat lobes of pillow, probably a sort of sheet-flow---
2345	3695	Talus of pillow breccias. Angular to subangular, 50 cm to 1 m across without fine matrix.
2357	3600	Talus of pillow breccias.
2359	3589	Hyaloclastite layers, probably intercalated in talus deposits.
0000	3575	Talus of pillow breccias
0003	3537	Steep cliff; alternation of layer of pile of pillows and hyaloclastite on the cliff surface (each, approximately several meter thick). Pillows, approximately 1 m across.
0007	3474	Top of the cliff; pile of large pillow lobes.
0008	3464	Smooth surface of pillow lobes; white-colored sediments among the space of lobes.
0010	3459	Locally pillow breccias. Hollowed pillows. --nearest the summit—
0016	3465	Large pillow lobes (several m across), locally pillow breccias.
0034	3503	Top of steep cliff.
0039	3586	Talus of pillow breccias on the foot of cliff. Angular to subangular breccias.
0044	3645	Ill-sorted fragments of pillow lavas (up to 20 cm across), probably talus including hyaloclastite. ---reached flat floor---
0054	3730	Sheet-like flow covered with white-colored sediment. Ropy structure on the surface, convex westward. *Sunflower-like structure* on the surface of sheet flow (50 cm to 1 m across).
0106	3689	Talus of pillow breccias. Breccias of 0.5 to 1 m across.
0113	3599	Steep escarpment of pillow breccias, and then gentle slope of talus.
0116	3547	Steep cliff of closed packed pillow.
0119	3507	Talus of pillow breccias.
0125	3424	Steep cliff, pillow lava piling on the cliff surface (up to 50 cm across).
0129	3380	Top of the cliff, near the summit. Relatively flat surface of piled large pillows.
0131	3400	A steep cliff start just after the summit, trending N-E.

Table 8-3. Geological note of DESM05 in the SONNE area of the Central Indian Ridge

DESM05
Bottom survey started at 24°00.5'S, 69°40.0'E (-3,400 m),
and ended at 23°59.8'S, 69°38.4'E (-2,949 m)
GMT 20:20 August 24 - 10:00 August 25, 1993

GMT	Depth (m) vehicle	
2020	3400	Flat surface of thick, light-brown-colored sediment; rarely fragments of pillows in it.
2030		Black-colored pebbles (<5 cm across) on sediment.
2039	3390	--- vehicle N-heading --- No pebbles on sediment, many living fossils.
2046	3370	Ripple mark with about 50 cm wave length on sediment.
2049	3380	A few pillows (approximately 0.5 - 1 m across) in sediment.
2105		High density of basalt glass pebbles on sediment.
2108		Decreasing number of pebbles on sediment.
2111		A mound of pillow lava, partly hollowed pillows, and fragments, covered thickly with sediment having ripple mark.
2111	3415	Thick sediment without ripple mark and basalt glass pebbles. Some kinds of sea animals and living fossils.
2123		Pebbles of basalt glass (approximately up to 3 cm across).
2124		Pile of pillow lavas in the cliff, also covered with thick sediment.
	3391	Exposure of closed packed pillows in the cliff roughly trending E-W.
2125		Top of cliff (approximately 25 m height) covered with sediment, but still sparsely lava fragments.
2130	3373	Flat sediment surface containing pillows in part.
2136	3366	A mound of pillow breccias with perfect pillows, then changed into closed packed pillow on E-W trending cliff.
2140	3338	Ill-sorted pillow breccias on cliff (hyaloclastite?).
2142	3250	--- Vehicle of NE heading --- Cliffs of gentle slope, on which pillow breccias and pillow lavas expose, with steps thickly covered with sediment. Height of cliff reaches more than 50 m.
2157	3240	Flat surface of sediment without ripple mark nor basalt glass pebble, but rarely ripple mark with long wave length was observed.
2211		Repeating of outcrops of thickly-deposited sediment in which several pillows expose, pillow lava piles, and pillow breccias.
2220	3163	Flat sediment with many living fossils.
2224		Pillow lavas with pillow breccias. Some places were covered
-2233	3445	thickly with sediment.
2235	3110	Approximately 30 m-height cliff, trending NS. Pillow breccias of ill-sorted, angular to subangular (up to 20 cm across), and pillow lavas exposed.
2237	3080	Flat surface of sediment in which hollowed pillow and the breccias exposed. Sediment has ripple mark.
2041	3045	Cliff of pillow breccias, ill-sorted, angular to subangular (up to 50 cm across). Steps covered thickly with sediment. Pillow breccias are replaced with pillow lavas and hyaloclastite. Pillows size reach 2 m across. Hollow pillows are also contained. Sediment cover occasionally has ripple mark.
2307		--- Vehicle went downward --- Cliff of pillow breccias and hyaloclastite; both composed of ill sorted, irregular to angular fragments (up to 10 cm across).
2321	3050	--- Vehicle NW heading --- Continuation of talus.
2330	3060	--- Vehicle N heading --- Continuation of talus. Ill-sorted pillow breccias of angular to subangular, approximately 5 - 30 cm across.

2340	3040	Pillow lobes of approximately 50 cm - 1 m across, sediment in spaces among pillows. Occasionally ill-sorted pillow breccias (5 - 30 cm across) cover pillows.
0002	3053	Pillow lavas/pillow breccias covered with thin sediment.
0030		Pillow breccias and pillow lavas (pillows have the average diameter of 50 cm). Sediment deposited thickly in spaces among pillows. Pillow lavas principally consist of elongated pillow lobes.
0109		--- Vehicle heading NNE --- Talus deposits.
0112		Pillow lavas; up to 1 m across/pillow breccias.
0121	3076	Hollowed pillow.
0130	3110	Flat surface of sediment at bottom of a basin.
		--- Vehicle NE heading ---
0143	3107	--- Vehicle went upward on gentle slope --- Pillow breccias (talus).
0147	3062	Flat surface of sediment.
0204	2920	Pillow breccias covered with thin sediment. -- Went upward and then downward---
0225	2954	--- Went upward, SE heading, downward ---
0236	3111	Sediment plain, sometimes with basalt glass pebbles scattered on the surface.
0244		Pillow lavas exposed on a cliff trending N-S, then sediment with flat surface.
0257		Sediment occasionally with ripple mark and pebbles of basalt glass.
0302		--- Vehicle NE heading --- Sediment enriched in living fossils. Occasionally, angular lava fragments (up to 30 cm) and basalt glass pebbles in sediment.
0323	2941	Sedimentary flat surface with living fossils.
0340		--- Vehicle SE heading --- Still sediment plain.
0353	2968	Thick sediment partly with basalt glass sediment. --- Vehicle E heading then NE heading ---.
0415	2940	--- Vehicle N heading --- flat surface of sediment.
	2960	--- Vehicle W, then SW heading, downhill ---.
0428		--- Vehicle S heading
0439	3025	Flat surface of sediment without ripple mark; occasionally lava fragments in sediment.
0513	3065	Pillow breccias of irregular to subangular, up to 20 cm across, in sediment.
0516		Scarce amounts of basalt glass pebbles on sediment.
0543		Pillow breccias of subangular to rounded, containing perfect pillows of up to 1 m across. Soon changed into sediment dominated scenery.
0551		Frequent outcropping of pillow breccias in sediment. Breccias of ill-sorted, commonly much less than 50 cm across.
0602	3147	Sediments without ripple mark. Occasionally small amount of lava fragments and top of pillow lava mound appeared in sediments.
0626	3150	Cliff of pillow lava; height of approximately 30 m. Talus deposits of ill-sorted breccias.
0634	3130	Top end of cliff covered thickly with sediment. Several small cliffs of pillow lavas.
0711		Thick sediment with gently convex ridges, like the surface of sheet flows thickly covered with sediment.
0721		Pillow lava pile covered with talus deposits (pillow breccias and partly hyaloclastite). Pillow breccias of subangular to rounded, reach the size up to 50 cm across.
0726		--- Vehicle SW heading --- Cliff of hyaloclastite/pillow breccias. Some times pile of pillow lobes of less than 50 cm across.
0732		--- Vehicle W and then NW heading --- Hyaloclastite/pillow breccias.
0750		--- Vehicle NNW heading --- Steep cliff trending NW, right down.

0753	2952	--- Still down-going --- Pillow breccias/hyaloclastite/pillow lavas on cliff wall.
0759		--- Vehicle N heading, still steep cliff, but down in left ---
0810		E-W trending cliff, north up. Pillow breccias containing hyaloclastite and rare pillow lavas exposed on cliff. Thick sediment on steps in steep cliff.
0822		Talus deposits of pillow breccias; ill-sorted, subangular to surrounded, 10 to 50 cm across.
0826		Sediment with ripple mark, occasionally pillow lava pile in it.
0835		Pillow breccias and hyaloclastite exposed on small cliffs.
0850		Pillow breccias.
0932		Around here, relatively high density of sea animals.
0916		Pillow lavas
0952	2996	Sediment with heads of pillows on surface.
0958	2949	Pillow breccias covered with thick sediment, changed into sediments.

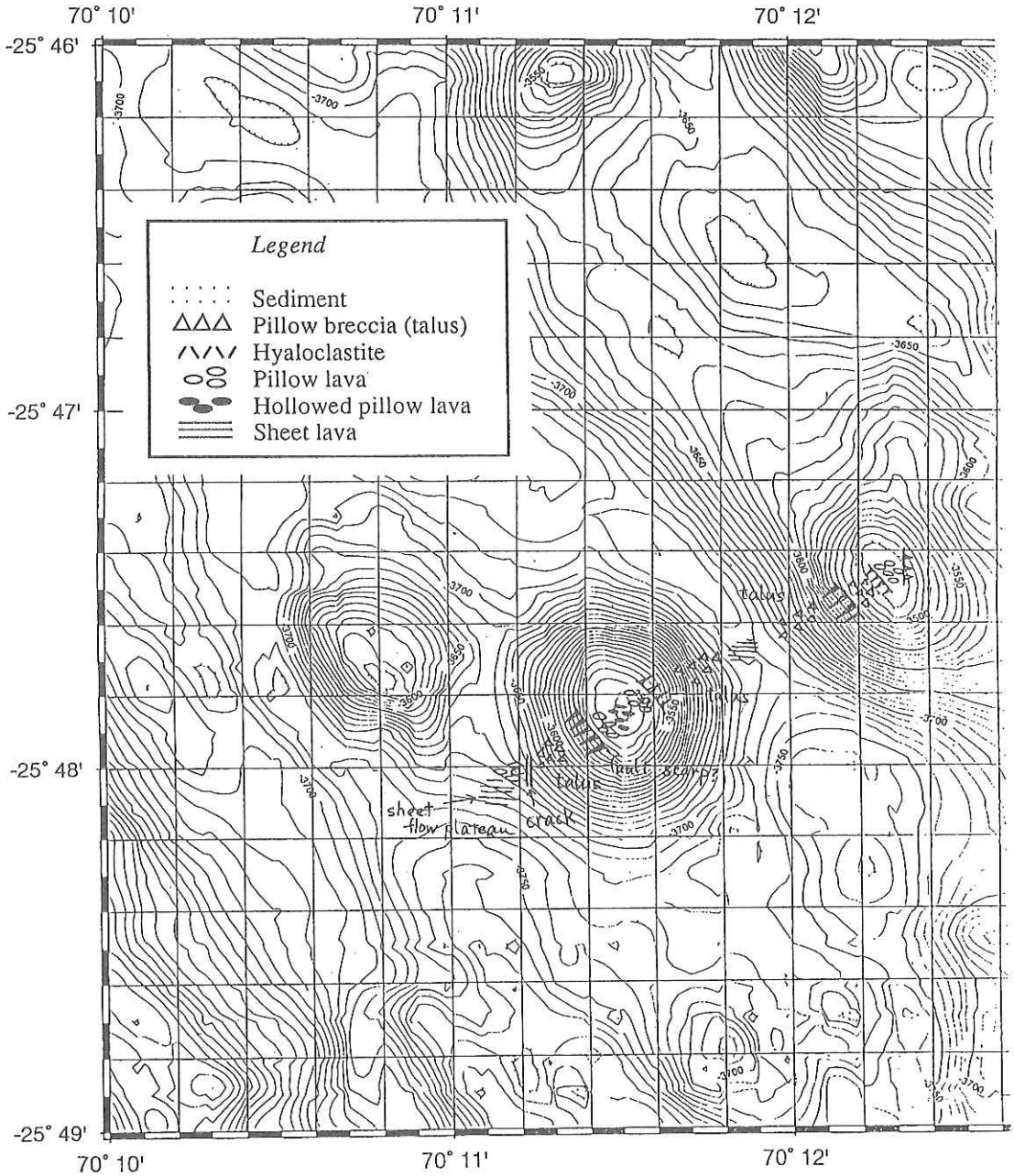

Fig. 8-1. Geological route map of DESM02.

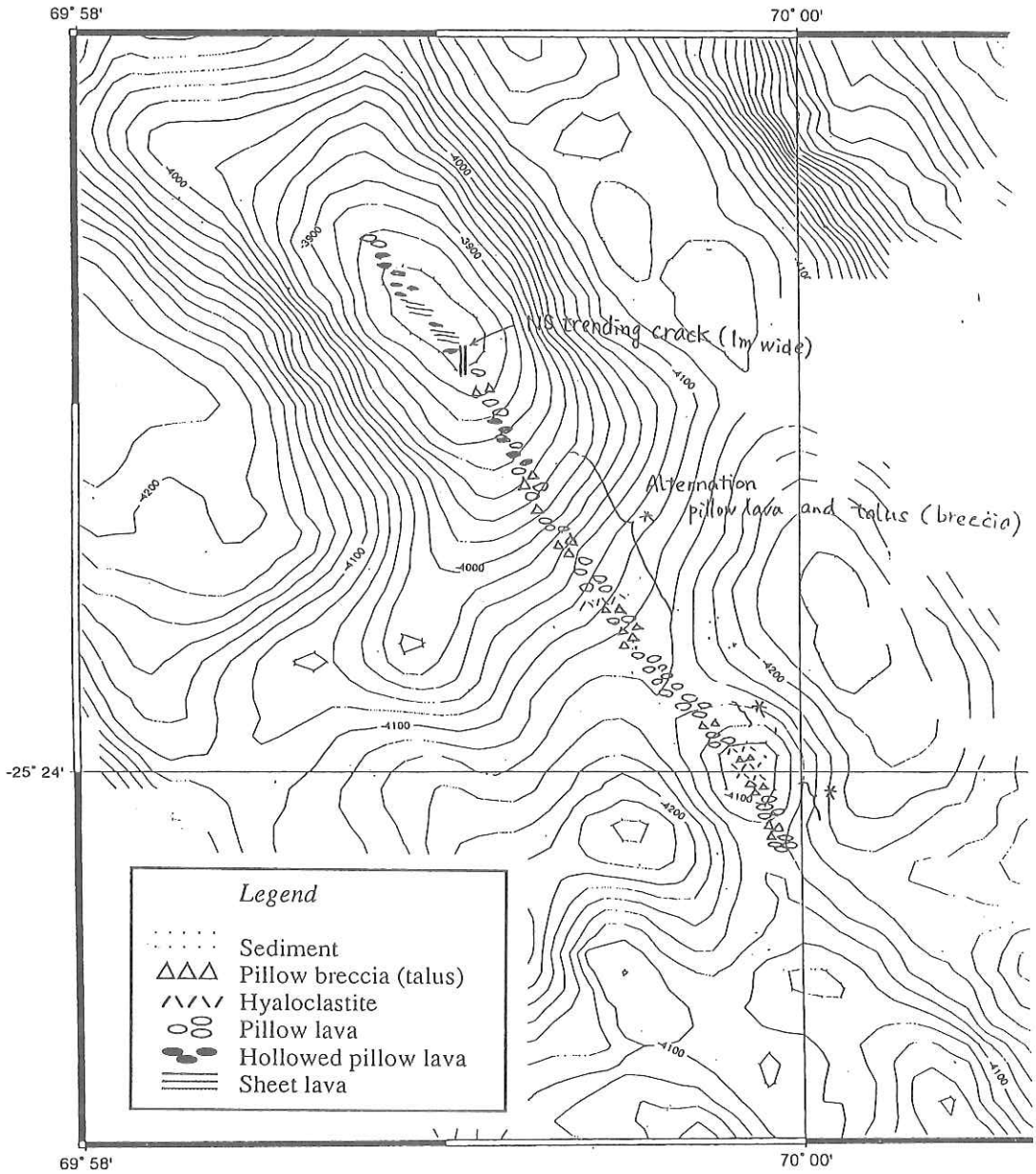

Fig. 8-2. Geological route map of DESM03.

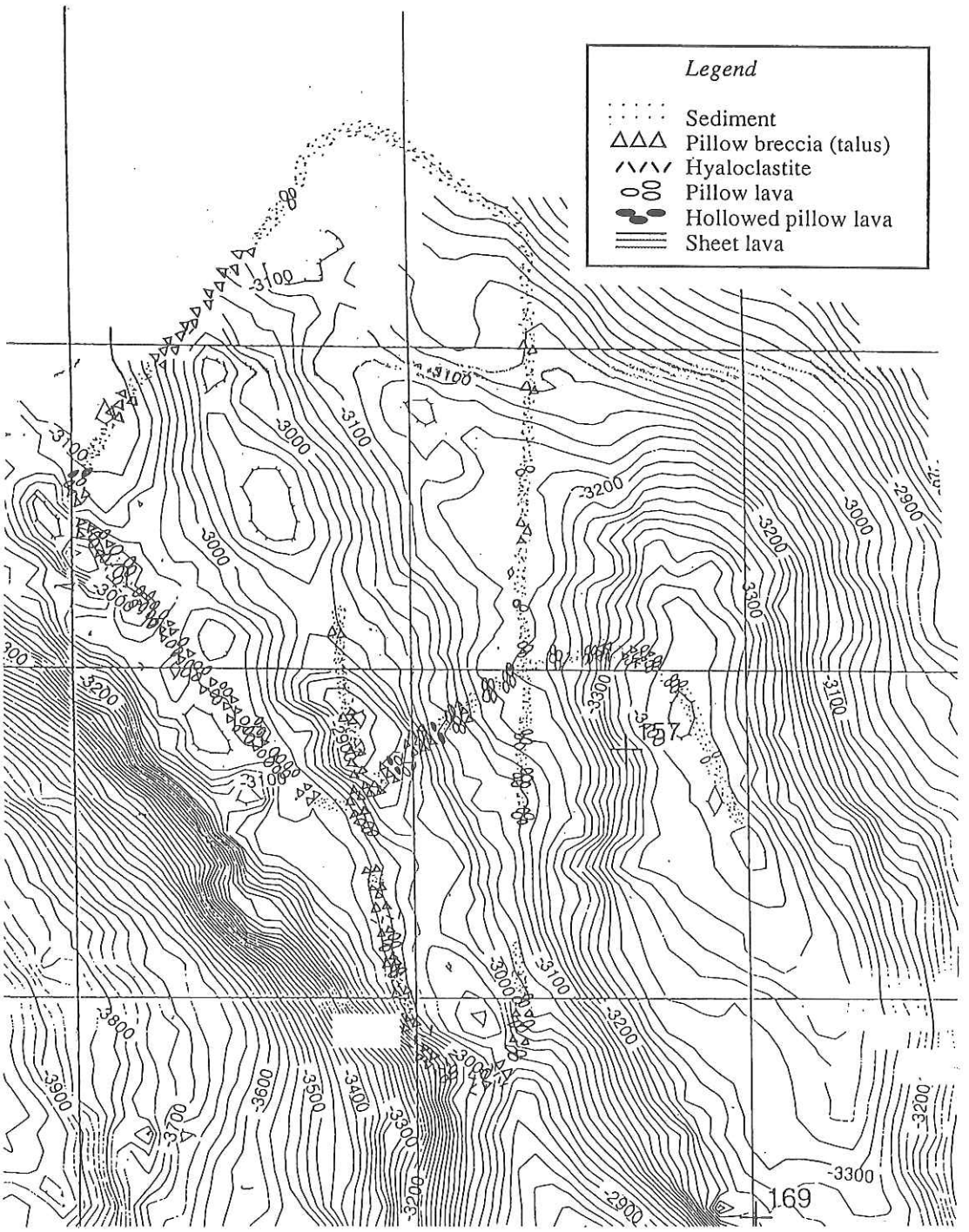

Fig. 8-3. Geological route map of DESM05.

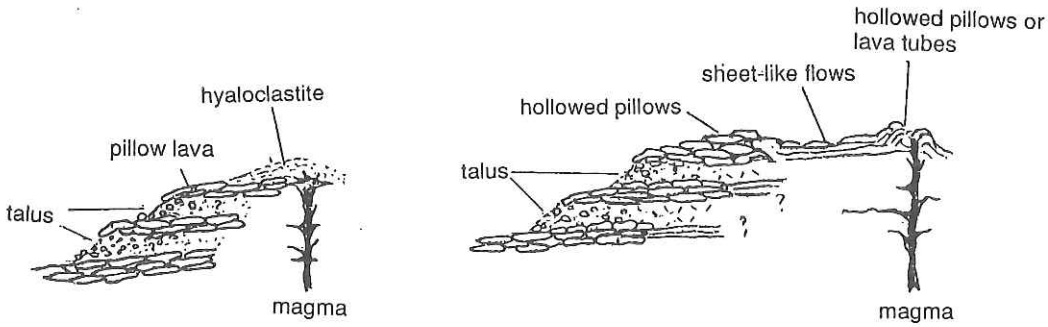

Fig.8-4. Cartoon showing geological cross-section of volcanic cones surveyed in DESM02 in the Central Indian Ridge. Talus deposits consist of pillow breccia and hyaloclastite.

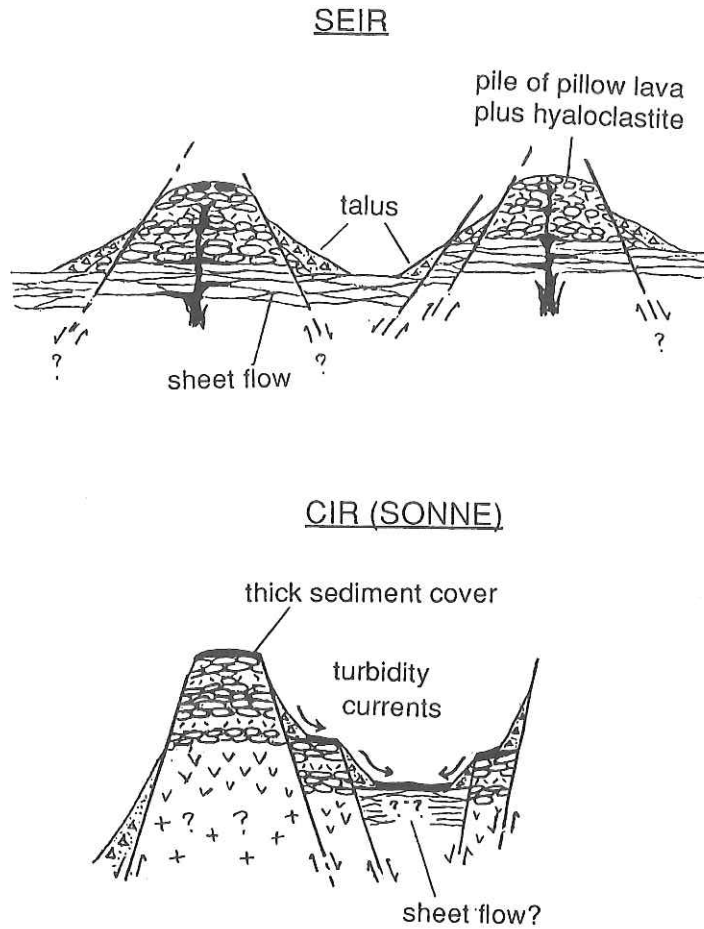

Fig. 8-5. Schematic geological cross-sections in the Southeastern Indian Ridge and SONNE area in the Central Indian Ridge.

9. Bait Trap Sampling of Deep-sea Benthos around the Rift System of the Indian Ocean

Suguru OHTA[1] and Kenji SHIMIZU[1]

[1] *Ocean Research Institute, University of Tokyo*

1. Objective

Ragged bottom on the rift system preclude ordinary biological sampling gears, such as trawl, dredge and grab sampler. Bait trap attract, in general, only the carnivores and scavengers, it has still an advantage of collecting intact specimens efficiently from vast areas within a limited time.

Bottom-moored bait traps were deployed twice to collect macro- and mega-benthos on the Central Indian Ridge (CIR) system. The main objectives are 1) to collect rarer organisms in this barren area, especially crustaceans to be analyzed taxonomically and genetically, 2) to facilitate the interpretation of the bottom observations using DESMOS, and 3) to judge indirectly the neighborhood to the hydrothermal vent fields.

2. Instrumentation and procedure

Three hemispherical cage traps (so-called crab cages) were attached to the bottom-moored, acoustic releasing system. The system consists of the following units;

1. main buoy unit: 4 Benthos 17 inch glass spheres (20kg x 4 net buoyancy)
2. ballast weight: 150kg iron block
3. acoustic releaser: Nichiyu Giken, Model L-1 (call code 1A)
4. retrieval facility: a flag, deep-sea submergence flasher and radio beacon (43.528 MHz: JS1012) attached to a pole of a signal buoy
5. trap cages: 150cmj hemispherical cage with an 150mmj cone orifice at a pole, netted by 15x15mm square mesh, baited with minced fish and the heads of bonitos. Small and medium bait cages were also set within the main cages to retain smaller creatures such as amphipods and isopods.

3. Basic data

Station BK1

Location: in the axial grabenof the Rodriguez Triple Junction

Deployment

date and time:	04:56′, Aug. 19, 1993
position:	25° 35.05′ S, 70° 00.32′ E; 3,385m
descending rate:	ca. 70m/min

Retrieval

release command:	07:26′, Aug. 23, 1993
popping up:	08:22′, Aug. 23, 1993

position: 25° 34.81′S, 70°00.77′E; 3,330m
ascending rate: ca. 60m/min
Duration of bottom mooring: 4d 1h 42m
Main catch
Munidopsis sp. 1 specimen
Rysianassid amphipods several hundreds

Station BK2
Location: Small trough on the eastern inner wall of the CIR rift valley, possible hydrothermal vent field in the "Sonne Field"
Deployment
date and time: 18:55′, Aug. 24, 1993
position: 24° 00.39′S, 69°40.02′E; 3,388m
descending rate: not monitored (probably 70m/min)
Retrieval
release command: 11:03′, Aug. 25, 1993
position: 23° 59.24′ S, 69° 39.27′ E; 3,169m
popping up: 12:00′, Aug. 25, 1993
ascending rate: ca. 60m/min
Duration of bottom mooring: 15h 20m
Main catch:
Rysianassid amphipods several tens

4. Results

A huge white galatheid, Munidopsis sp. was collected by the first trial. Small rysianassid amphipods swarmed on and among the bait, and the bonito heads were completely denuded.

Only rysianassid amphipods were attracted to the cage during the second trial. However, large amphipods were collected in the medium cage.

Half of the samples were preserved in a deep freezer for genetic investigation, and the remaining half were fixed in formalin and preserved in 70% ethanol for taxonomic scrutiny.

5. Discussion and future studies

Considering the duration of bottom mooring, the poor catch reflect the barren environment in terms of nutritional condition of the present field.

Empirically, large, motile members such as fishes, galatheids and crabs can be attracted from, say, 1 mile circumstances within a few days under ordinary bottom current regime. If the cages were located rather near the hydrothermal vent fields, they (encircling the dishes of the vent communities) must also be attracted to the cage. The poor catch of larger, motile members suggests that both sites were not in the neighborhood of the hydrothermal vent communities.

The data will be scrutinized later to be fruited, hopefully, as the papers that titled;

* Ohta, S., H. Watabe and K. Shimizu: A galatheid (Anomura, Crustacea) collected by bait traps on the Central Indian Ridge
* Ohta, S., K. Shimizu : Bait trap experiments on the Central Indian Ridge

10. Underway Geophysics

Kensaku TAMAKI[1], Hiromi FUJIMOTO[1], Chie HONSHO[1],
Kin-ichiro KOIZUMI[1], Maki ITO[2], Keiichi FURUYA[3],
Mayumi SEKINE[3], and Yasushi HARADA[4]

[1]*Ocean Research Institute, University of Tokyo*
[2]*Department of Ocean Science and Technology, Tokai University*
[3]*Department of Earth Science, Faculty of Science, Chiba University*
[4]*Department of Earth and Planetary Physics, University of Tokyo*

1. Objective

The target survey area of the KH-93-3 cruise, Rodriguez Triple Junction, is far away from Japan, and so the following underway geophysical observations during the transits were quite important: Sea Beam swath mapping, 3.5 kHz sub-bottom profiling, gravimetry, total force and three-component magnetic surveys. The objective is twofold: one is to get long geophysical profiles and the other is to carry out grid surveys at selected small boxes during the transits.

2. Philippine Sea and South China Sea

As is shown in Figure I-1, the Hakuho-maru cruised along the Nankai Trough and Ryukyu Trench and passed through the South China Sea during the Leg 1 and Leg 4. We selected the Ryukyu Trench as the most interesting target, and two small box areas on the Ryukyu Trench were surveyed as is shown in Figures 10-1 and 10-2. Figure 10-2 covers the area where thare is no detailed geophysical surveys on the Ryukyu Trench. The trench has been surveyed by Hydrographic Department of Japan in the northeastern part and by Japan Marine Science and Technology Center (JAMSTEC) in the western part. Detailed geophysical mapping along the trench axis has been completed with the survey shown in Figure 10-2.

Three lines of topographic highs running NE-SW are recognized in the seaward of the Ryukyu Trench in Figure 10-2. The westernmost one is on the trench axis and may be related to the bending of the Ryukyu Trench here. Several faults running NW-SE are observed to the southeast of these topographic highs.

The Typhoon No.15 was waiting the Hakuho-maru at Luzon Strait on her way back to Japan. That is why the ship's track is off the usual track line. Although ship time at the Ryukyu Trench was reduced, we could obtain a survey line in the northwestern part of the Philippine Sea. We found a seamount at 19°30'N, 12°09'E (Figure 10-3), which had not been well documented in the topographic maps. We also observed several small conical seamounts along the track.

In the South China Sea, we passed above the central part of a seamount at 10°6.5'N, 111°14'E. We planned to survey other seamounts, but we had to change the course due to the Typhoon mentioned above.

3. Indian Ocean

Most of ship time during Leg 2 and Leg 3 was spent in the Indian Ocean. As we tried to concentrate as much time as possible on the target area, we had no extra ship time for the surveys during the transits. An important target was the Ninety East Ridge, which is interpreted to be hot spot origin. Geophysical data of the ridge is fairly limited. We hoped to get E-W profiles across the ridge, but the ridge was so large that it required much more extra time to get E-W profiles. Anyway, we obtained geophysical profiles across the Ninety East Ridge at two different seafloor ages, which will be useful in future works.

Sea Beam swath mapping shows that seafloor topography of the basin in the Indian Ocean is quite flat. Although many small seamounts are observed near the Southwest and Central Indian Ridges, very few seamounts were observed in the basin area.

KH93-3 Leg1 Off Ishigaki

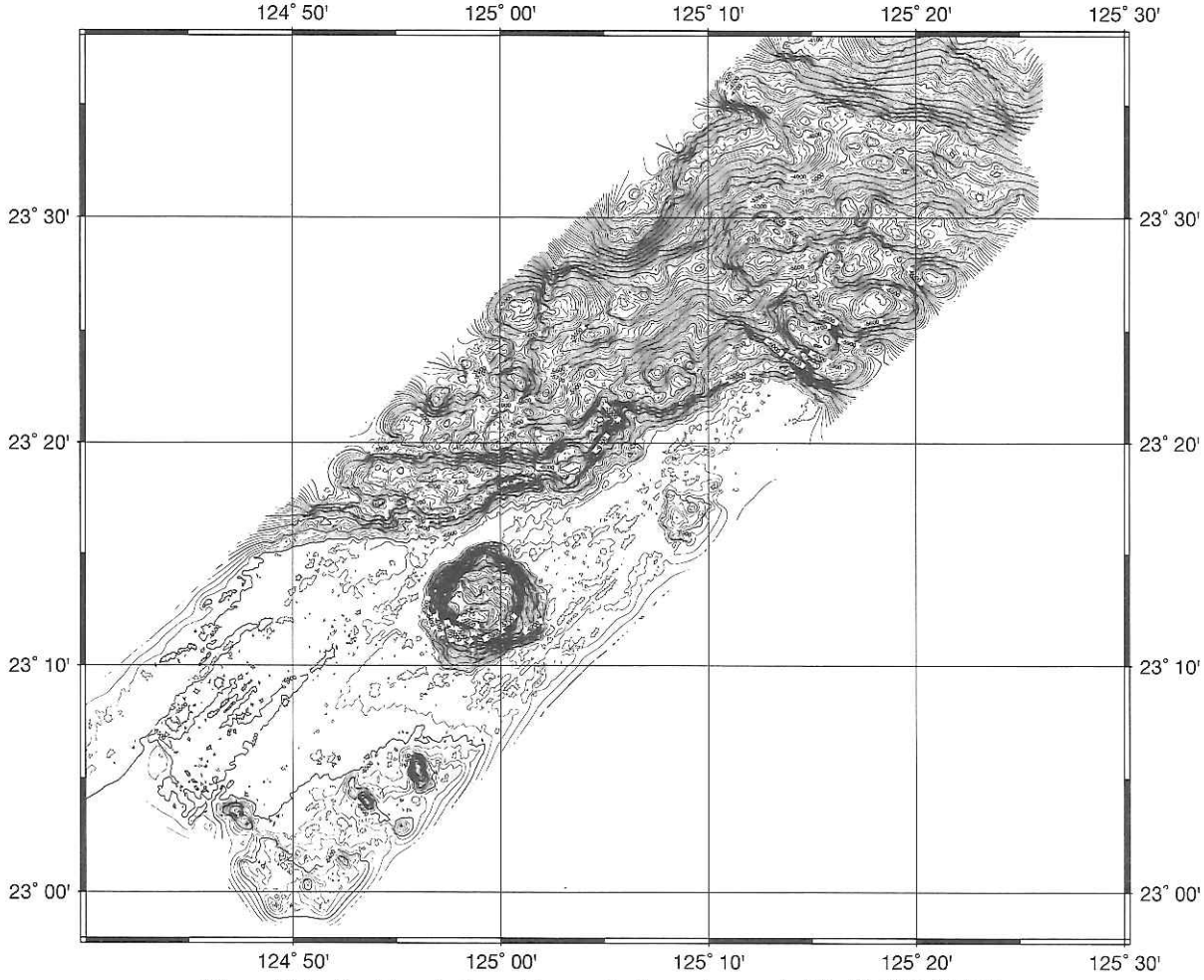

Figure 10-1. Sea Beam bathymetric map in the western part of the Rhykyu Trench.

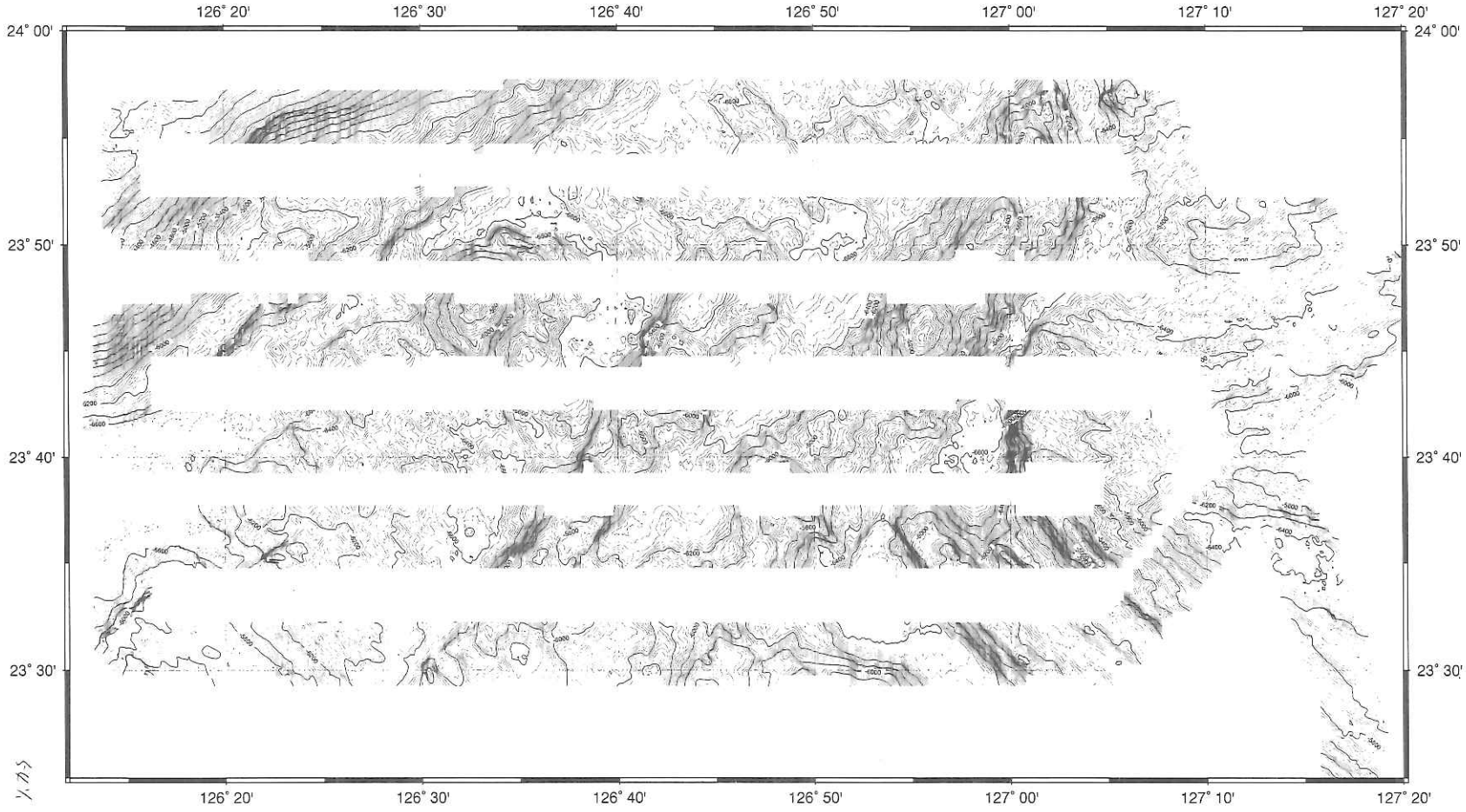

Figure 10-2. Sea Beam bathymetric map near a bending of the Rhykyu Trench.

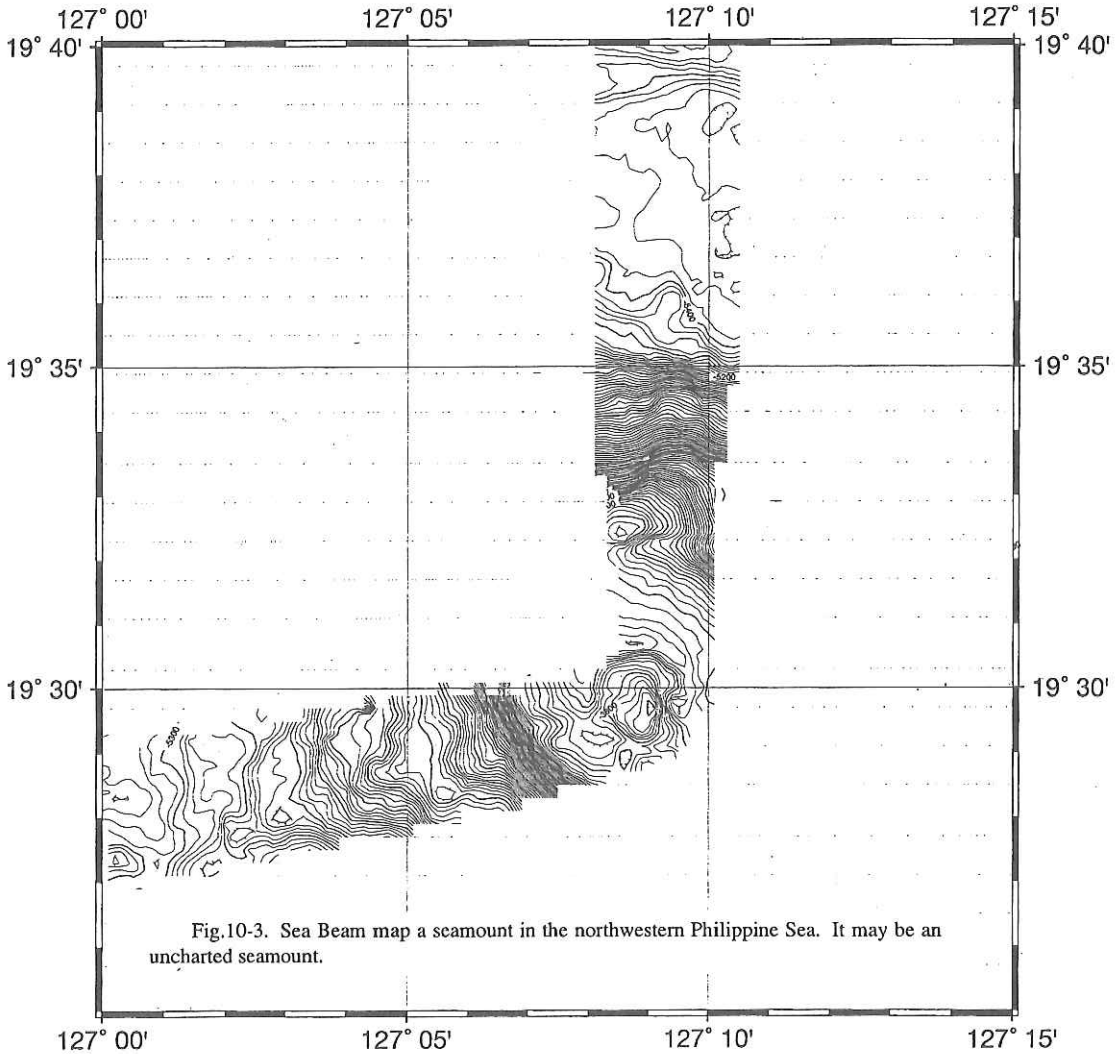

Fig.10-3. Sea Beam map a seamount in the northwestern Philippine Sea. It may be an uncharted seamount.

11. Studies on Zooplankton in the Subtropical and Tropical Waters of the Indian Ocean and the western North Pacific

Harumi KOBAYASHI[1], Hiroshi HASUMOTO[1], and Makoto TERASAKI[1]

[1] *Ocean Research Institute, University of Tokyo*

1. Objective: Composition and biomass of zooplankton

The oceanic zooplankton communities in subtropical and tropical waters are essentially different from those of the higher-latitude waters and coastal waters. In the former waters gelatinous plankton, such as jellyfishes, salps, doliolids and pteropods are known to be more common and abundant than in other waters. However, information on the biomass and composition of zooplankton in tropical and subtropical waters of the Indian Ocean is scarce and scattered. The main puropose of our plankton group is to examine distribution and biomass of the major taxonomic groups in the surveyed area.

2. Sampling and general procedures

Samples for each topic described below were collected by the following methods. Samples for the study of horizontal distributions of macroplankton and micronekton were collected by oblique towing of an ORI net with a mesh size of 0.69 mm. Along with the ORI net towing, zooplankton was collected by the surface towing the same net with mesh size of either 0.69 mm or 1mm. Surface smaller epipelagic plankton was collected by surface towing of Motoda horizontal nets (MTD nets) with mesh size of 0.33 mm. Smaller, epipelagic plankton was collected by vertical towing of a NORPAC-twin net (mesh size: 0.10 and 0.33 mm) from 200 m depth to the surface. The volume of water filtered by the ORI net or NORPAC-twin net was estimated with a Tsurumi flow meter attached to the mouth of the nets. Sampling depths and temperatures were measured with a Rigosha depth meter (RMD) and a Rigosha temperature meter, the latter occasionally being used only in ORI net.

Most of the samples were fixed and preserved in 70% ethanohol. Live specimen were occasionally sorted and used for experimental and/or histological studies. A part of the specimen was fixed and preserved in 4% formaldehyde/seawater solution buffered with sodium tetraborate for the examination of ultrastructure and gut contents with SEM.

3. Distribution and ecology of pelagic molluscus, especially pteropods

The identification and counting of the specimens were now in progress.The specimens were sorted into major taxonomic groups, their wet weights and individual number measured. The gastropods (Mollusca: Gastropoda) are distributed widely and abundantly in the aquatic environments in the world. Many species are essentially benthic, having close connection with the sea bottom. However, in the oceanic waters there exist a group of purely pelagic gastropods, which have no direct connection with the bottom. This study examines the taxonomy, morphology, geographical distribution and feeding habits of pelagic gastropods. Pteropods, heteropods and pelagic nudibranchs were sorted from the original samples.

Although identification and counting of the specimens are now in progress, a total of 25 species of thecosomatous pteropods were identified (Table 1) for the present. It includes one unreported species referable genus Limacina.

Table 11-1. Occurence of thecosomatous pteropods collected during KH-93-3

Station	PN-1	PN-2	PN-3	PN-4	PN-5	PN-6	PN-8	PN-10	PN-11	PN-12	PN-13	PN-14	PN-15	PN-16	PN-17	PN-18
Number of species	14	12	14	21	13	17	4	6	9	9	18	13	6	12	17	16
Order: Thecosomata																
Suborder: Euthecosomata																
Family: Limacinidae																
1 *Limacina inflata*	○	○		○	○	○				○	○	○			○	○
2 *Limacina bulimoides*					○	○					○					○
3 *Limacina leseuri*						○									○	
4 *Limacina sp.*											○					
Family: Cavoliniidae																
5 *Creseis acicula f. acicula*	○	○	○	○	○	○		○	○					○	○	○
6 *Creseis virgula f. conica*	○			○	○			○		○	○	○	○	○	○	○
Creseis virgula f. virgula	○			○											○	○
7 *Styliola subula*	○	○	○	○	○	○	○		○	○				○	○	○
8 *Hyalocylis striata*											○			○		
9 *Clio pyramidata f. lanceolata*	○	○	○	○		○			○	○	○	○		○	○	○
10 *Clio cuspidata*										○	○				○	○
11 *Cuvierina columnella f. columnella*	○	○	○	○	○	○	○		○	○	○	○	○			○
12 *Diacria trispinosa*	○	○	○	○	○	○		○				○			○	
13 *Diacria danae*	○	○	○	○	○	○	○	○	○		○	○	○	○	○	○
14 *Diacria quadridentata*			○	○	○	○						○				
15 *Diacria costata*											○	○	○	○		
16 *Cavolinia uncinata f. pulsata*	○		○	○								○	○		○	
17 *Cavolinia gibbosa*			○	○	○									○	○	
18 *Cavolinia globulosa*		○		○		○					○	○		○	○	○
19 *Cavolinia inflexa*	○	○	○	○	○	○	○		○	○	○			○	○	○
20 *Diacavolinia angulosa*						○				○	○	○	○	○	○	○
21 *Diacavolinia vanutrechti*		○	○	○							○	○			○	○
22 *Diacavolinia longirostris*																
Suborder: Pseudothecosomata																
Family: Peraclididae																
23 *Peraclis reticulata*	○		○	○					○		○	○		○	○	○
24 *Peraclis moluccensis*	○			○												
25 *Peraclis apicifulva*		○		○							○					○

(○: occurence)

Table 11-2-1. Plankton sampling record of the KH93-3 cruise

Station	Location				Date	Time		Type of Net	Mesh size	Towing	Wire Out	Sampling	*Vol. Water	Fixation	Remarks
	Net in		Net out			Net in	Net out		(mm)	Method	(m)	Layer (m)	Filtered (m^3)		
PN-1-1	20-06.550N	120-24.250E	20-05.860N	120-23.260E	12-Jul	23:24	0:11	ORI	0.69	Obl.	1000	No data	4926.6	ethanol	
PN-1-2	20-06.340N	120-23.980E	20-06.000N	120-23.510E	12-Jul	23:43	0:03	ORI	0.69	Hor.	0	surface		ethanol	
PN-2-1	16-26.010N	115-53.200E	16-25.040N	115-53.380E	13-Jul	23:18	23:57	ORI	0.69	Obl.	1000	665	4428.3	ethanol	
PN-2-2	16-25.910N	115-53.250E	16-25.420N	115-53.300E	13-Jul	23:23	23:42	ORI	0.69	Hor.	0	surface		ethanol	
PN-3-1	11-46.980N	112-11.150E	11-45.730N	112-10.340E	14-Jul	23:08	23:41	ORI	0.69	Obl.	800	414	4226.8	ethanol	
PN-3-2	11-46.860N	112-11.080E	11-46.150N	112-10.540E	14-Jul	23:11	23:30	ORI	0.69	Hor.	0	surface		ethanol	
PN-4-1	12-06.540S	094-43.760E	12-08.100S	094-44.890E	24-Jul	23:12	23:52	ORI	0.69	Obl.	900	No data	5724.6	ethanol	SSBL installed
PN-4-2	12-06.760S	094-43.900E	12-07.620S	094-44.500E	24-Jul	23:16	23:38	ORI	0.69	Hor.	0	surface		ethanol	
PN-5-1	24-05.680S	065-04.780E	24-05.620S	065-04.000E	8-Aug	23:03	23:30	ORI	0.69	Obl.	800	673	4008.2	ethanol	
PN-5-2	23-05.670S	065-04.650E	24-05.630S	065-04.070E	8-Aug	23:07	23:27	ORI	0.69	Hor.	0	surface		ethanol	
PN-6-1	21-24.710S	059-10.720E	21-24.610S	059-09.530E	9-Aug	20:33	21:09	ORI	0.69	Obl.	800	476	4520.6	ethanol	
PN-6-2	21-24.800S	059-10.620E	21-25.280S	059-09.960E	9-Aug	20:36	20:56	ORI	0.69	Hor.	0	surface		ethanol	
NOR-1-1	25-34.800S	069-34.690E			16-Aug	20:50	21:05	NORPAC-twin	0.13	Ver.	200+7	200	49.2	ethanol	
									0.33	Ver.	200+7	200	48.1	ethanol	
NOR-1-2						21:12	21:22	NORPAC-twin	0.13	Ver.	150+23	150	35.6	formaldehyde	for Hasumoto
									0.33	Ver.	150+23	150	36.2	formaldehyde	
NOR-1-3			25-43.410S	69-34.700E		21:22	21:40	NORPAC-twin	0.13	Ver.	200+10	200	46.1	formaldehyde	
									0.33	Ver.	200+10	200	45.9	formaldehyde	
PN-7-1	25-33.100S	069-39.910E	25-32.410S	069-40.290E	16-Aug	23:38	0:07	ORI	0.69	Obl.	800	359	3915.1	ethanol	
PN-7-2	25-33.010S	069-39.950E	25-32.180S	069-40.420E	16-Aug	23:40	0:00	ORI	0.69	Hor.	0	surface		ethanol	
PN-8-1	25-24.840S	069-54.140E	25-25.540S	069-53.910E	17-Aug	12:22	12:49	ORI	0.69	Obl.	750	461	3153.3	ethanol	
PN-8-2	25-24.980S	069-54.130E	25-25.350S	069-53.960E	17-Aug	12:27	12:43	ORI	0.69	Hor.	0	surface		ethanol	
NOR-2-1	25-18.690S	070-05.070E			18-Aug	1:03	1:12	NORPAC-twin	0.13	Ver.	150+14	150	30.1	formaldehyde	for Hasumoto
					18-Aug				0.33	Ver.	150+14	150	42.7	formaldehyde	
NOR-2-2					18-Aug	1:17	1:28	NORPAC-twin	0.13	Ver.	200+13	200	39.6	ethanol	sample lost
					18-Aug				0.33	Ver.	200+13	200	38.5	ethanol	
NOR-2-3			25-17.740S	070-05.160E	18-Aug	1:32	1:45	NORPAC-twin	0.13	Ver.	200+26	200	43.3	formaldehyde	
					18-Aug				0.33	Ver.	200+26	200	42.8	formaldehyde	

Table 11-2-2. Plankton sampling record of the KH93-3 cruise

Station	Location				Date	Time		Type of Net	Mesh size	Towing	Wire Out	Sampling	*Vol. Water	Fixation	Remarks
	Net in		Net out			Net in	Net out		(mm)	Method	(m)	Layer (m)	Filtered (m^3)		
NOR-3-1	25-29.240S	070-12.760E			18-Aug	21:10	21:20	NORPAC-twin	0.13	Ver.	200+4	200	39.6	ethanol	
					18-Aug				0.33	Ver.	200+4	200	37.9	ethanol	
NOR-3-2					18-Aug	21:25	21:35	NORPAC-twin	0.13	Ver.	150+3	150	31.4	formaldehyde	for Hasumoto
					18-Aug				0.33	Ver.	150+3	150	29.7	formaldehyde	
NOR-3-3			25-28.980S	070-12.360E	18-Aug	21:39	21:50	NORPAC-twin	0.13	Ver.	200+8	200	39.1	formaldehyde	
					18-Aug				0.33	Ver.	200+8	200	36.9	formaldehyde	
PN-9-1	25-41.440S	069-41.100E	25-41.140S	069-41.620E	19-Aug	19:15	19:48	ORI	0.69	Obl.	750	563	3008.8	ethanol	
PN-9-2	25-41.400S	069-41.140E	25-41.300S	069-41.340E	19-Aug	16:18	19:34	ORI	0.69	Hor.	0	surface		ethanol	
PN-10-1	25-42.140S	070-13.820E	25-43.020S	070-13.390E	20-Aug	12:54	13:27	ORI	0.69	Obl.	750	485	3670.2	ethanol	
PN-10-2	25-42.170S	070-13.810E	25-42.730S	070-13.530E	20-Aug	0:55	1:15	ORI	0.69	Hor.	0	surface		ethanol	
PN-11-1	25-50.670S	070-13.540E	25-50.750S	070-14.270E	20-Aug	21:01	21:35	ORI	0.69	Obl.	750	458	3399.1	ethanol	
PN-11-2	25-50.690S	070-13.570E	25-50.700S	070-14.030E	20-Aug	21:03	21:22	ORI	0.69	Hor.	0	surface		ethanol	
PN-12-1	13-59.100S	078-18.860E	13-59.710S	078-18.340E	27-Aug	22:02	22:32	ORI	0.69	Obl.	750	507	3297.2	ethanol	
PN-12-2	13-59.170S	078-17.910E	13-59.650S	078-18.250E	27-Aug	22:06	22:27	ORI	0.69	Hor.	0	surface		ethanol	
PN-13-1	09-34.310S	081-59.630E	09-34.970S	082-00.140E	28-Aug	22:03	22:31	ORI	0.69	Obl.	750	475	3334.1	ethanol	
PN-13-2	09-34.340S	081-59.710E	09-34.830S	082-00.030E	28-Aug	22:06	22:26	ORI	0.69	Hor.	0	surface		ethanol	
PN-14-1	04-43.430S	086-02.200E	04-44.370S	086-02.160E	29-Aug	22:02	22:31	ORI	0.69	Obl.	750	431	3243.9	ethanol	
PN-14-2	04-43.540S	086-02.180E	04-44.180S	086-02.120E	29-Aug	22:05	22:26	ORI	0.69	Hor.	0	surface		ethanol	
PN-15-1	03-41.220N	092-58.770E	03-41.890N	092-59.230E	31-Aug	20:13	20:40	ORI	0.69	Obl.	750	496	2954.3	ethanol	SSBL installed
PN-15-2	03-41.280N	092-58.810E	03-41.820N	092-59.170E	31-Aug	20:16	20:36	ORI	1	Hor.	0	surface		ethanol	oilballs removed
PN-16-1	23-01.550N	127-22.950E	23-01.310N	127-24.350E	12-Sep	21:50	22:23	ORI	0.69	Obl.	750	305	3989.7	ethanol	SSBL installed
PN-16-2	23-01.490N	127-23.180E	23-01.350N	127-24.050E	12-Sep	21:55	22:15	ORI	1	Hor.	0	surface		ethanol	
PN-17-1	29-09.020N	130-38.110E	29-10.180N	130-39.050E	14-Sep	21:33	22:06	ORI	0.69	Obl.	750	355	4025.6	ethanol	
PN-17-2	29-09.110N	130-38.160E	29-09.870N	130-38.820E	14-Sep	21:36	21:56	ORI	1	Hor.	0	surface		ethanol	
PN-18-1	33-33.570N	136-37.000E	33-34.010N	136-38.240E	15-Sep	21:33	22:10	ORI	0.69	Obl.	850	456	3694.0	ethanol	
PN-18-2	33-33.620N	136-37.090E	33-33.910N	136-37.840E	15-Sep	21:36	21:57	ORI	1	Hor.	0	surface		ethanol	

* Estimated from the data of the flowmeter calibrations performed during this cruise.

Fig.11-1. Map showing the position of plankton sampling station

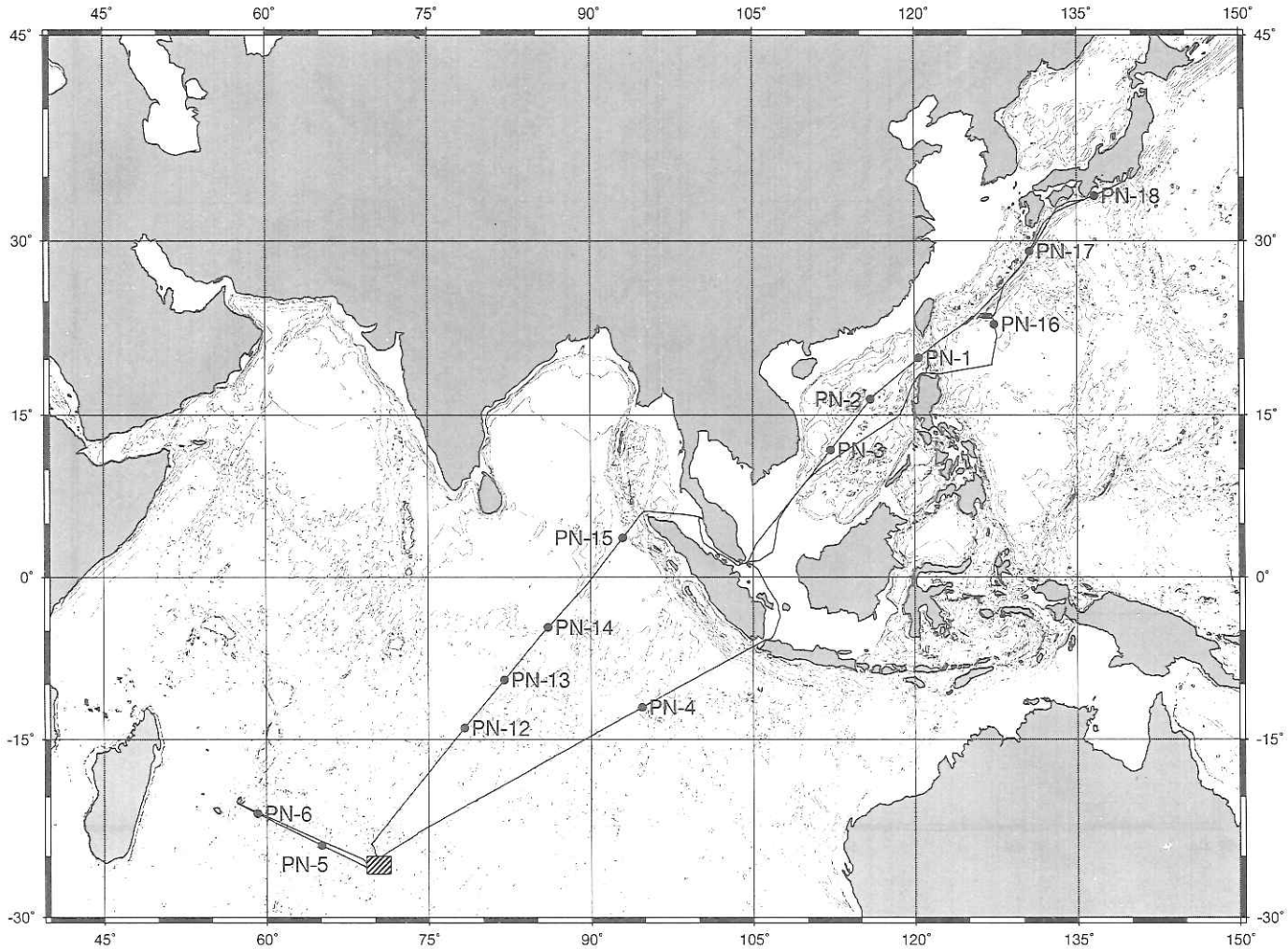

Fig.11-2. Map showing the position of plankton sampling station in the Rodriguez Triple Junction

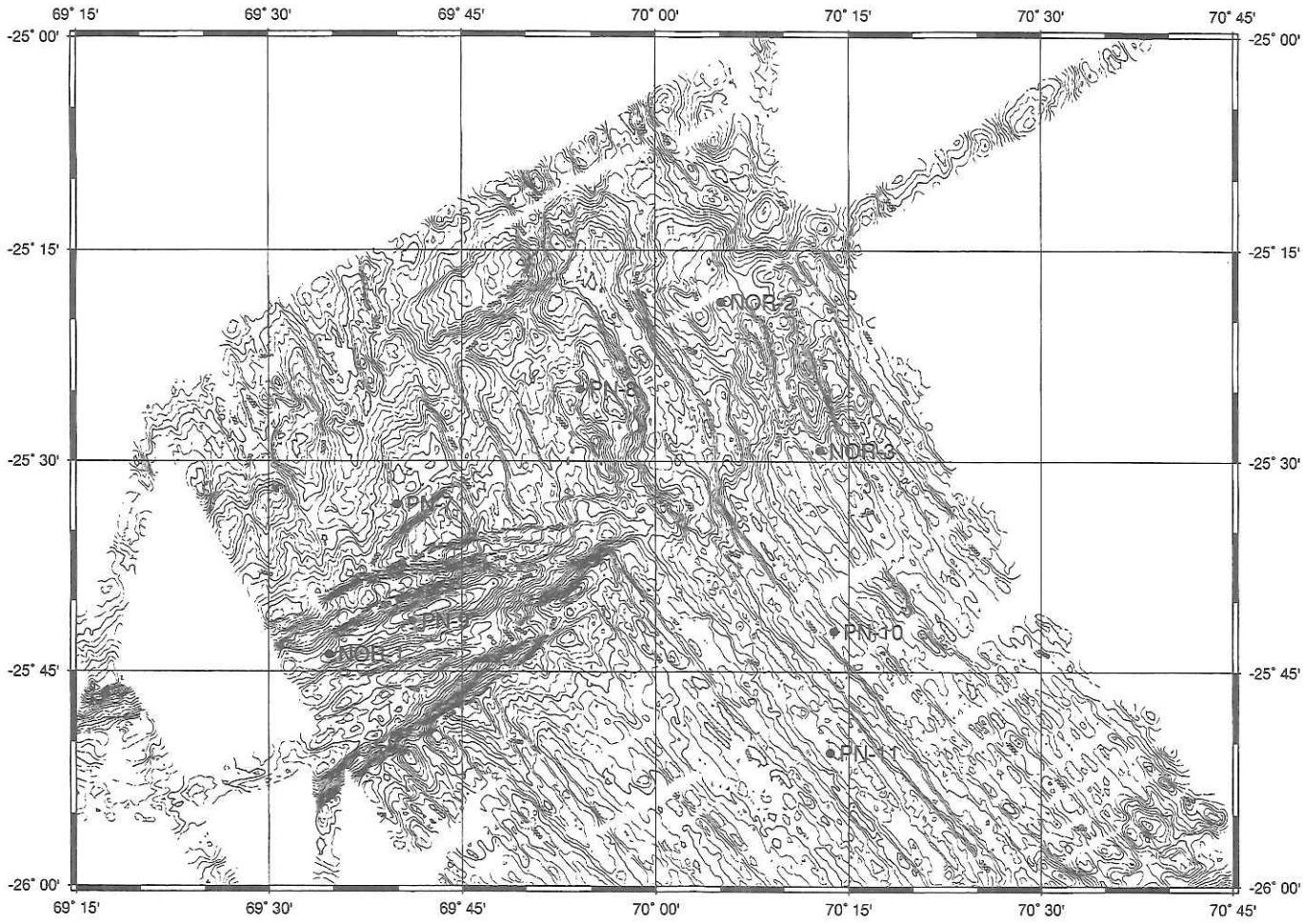

(PN:ORI net sampling, NOR:NORPAC net sampling)

12. Measurement of Aerosols (RaA, RaC', Mie-particles, Condensation nuclei) and Electrical Conductivity in the Atmosphere near the Sea Surface

Tatsuo TANJI[1] and Michio OKINO[1]

[1]*Muroran Institute of Technology*

1. Objective

To clarify the present condition of atmospheric environment we have made measurement of RaA, RaC', Mie-particles, condensation nuclei and electrical conductivity in the atmosphere near the sea surface over ocean while these ten years. As there were few example of the observation for aerosols over the Indian ocean, it was very useful to obtain the information on these area

2. Instrumentation and Measuring Method

To measure RaA and RaC's we adopted a filter pack method in which aerosols in sample air were collected on a membrane filter (1.0 mm pore size) and alpha events from radioactive aerosols on the filter were counted by a surface barrier type silicon semiconductor detector (HORIBA Ltd. 300SB-120L) fitted with multichannel pulse height analyzer (D. S. DAVIDSON CO., INC. MODEL 2056-C).We operated the system four or five times every cruising day. The system counted alpha events in the period of 8000 seconds of air sampling (about 6400 liters of sample air).

For Mie particle counting a light scattering type particle counter (RION CO., Ltd. KC-01) was used.It run automatically and counted aerosols in five ranges, i.e. 0.3-0.5 mm, 0.5-1.0 mm, 1.0-2.0 mm, 2.0-5.0 mm and over 5.0 mm in diameter. Usually we made it count those particles every 10 liters of sample air.

As a condensation nuclei counter we used a pollak type condensation nuclei counter (VIDEX Ltd. VDC-10). This instrument mainly consist of a pipe-shaped cloud chamber fitted with a lamp and photo cell at one and the other ends of the chamber respectively. It should operate every seventy eight seconds during all period of the cruise, however, it did not work well.

We used a Gerdien type conductivity meter to measure a atmospheric electrical conductivity, and set it at the starboard on the upper deck. Basically it consist of a cylindrical air condenser fitted with a vibrating reed electrometer(ADVANTEST CO., Ltd. TR-8401). It operated automatically and measured positive and negative conductivity for every five minutes alternately after Hakuho-Maru left the port of Singapore.

3. Example of Radioactive Aerosols Sampling

In this report we present a figure of one example of RaC' count which obtained by the method above mentioned. In this figure, the axis of ordinate is the RaC' count which is not rectified still and so not the concentration of Rn, and the axis of abscissa is the local time and days. Although the wind direction was almost south or south-east during these measuring term, the RaC' count showed the huge peak from 19th to 20th August.

All data on each items contained this figure are going to be analyzed in detail after the cruise.

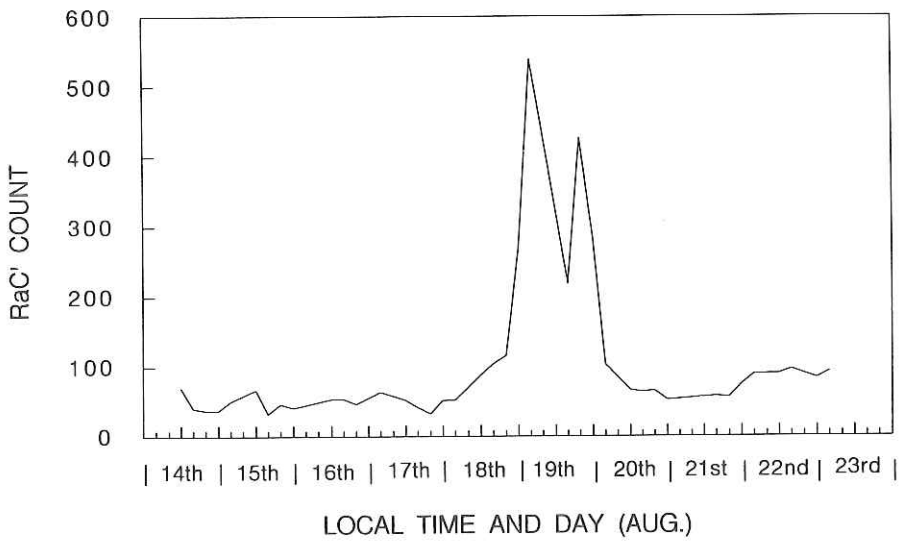

Fig. 12-1 Variation of RaC' Count from 14th to 23rd Aug.

13. The Horizontal Distribution of Background Aerosols in the Global Scale and Contribution of Continental Aerosols in the Maritime Atmosphere

Kazuhiko MIURA[1] and Kei SAITO[1]

[1] *Faculty of Science, Science University of Tokyo*

1. Objective

In previous papers [Miura et al. (1990,1991,1992)] measurements of back ground aerosols were presented which indicated that the following a), b) and c); a) in the northern hemisphere, farther off from the distance about 500km from the land, continental aerosols originated from human work were transported, b) in the western Pacific Ocean (165° E), when the dependence of Aitken particle concentrations on the latitude was observed, the results in the southen hemisphere were rather higher than that of in the northern hemisphere because there was the land near by, c) in a fixed point observation at the equator, it was found that the value of Aitken particle concentrations changed irregularity, i.e., we did not found a regular diurnal variation observed the land.

However, our data is not enough to discuss the influence of aerosols to a climate and to a background pollution at this stage. Further, in the Indian Ocean, there is hardly any data observed. Thus, it is necessary to observe background aerosols continuously in the global scale.

2. Instrumentation and Condition

We used the same apparatus as in our previous observation (1990,1991,1992).

2.1 Aerosol particles sampling

mesh (for an electron microscope)..... After the sampling on the mesh by using a low pressure type of cascade impactor the structure and morphology of the particles are observed by electron microscope. The sampling was carried out two times everyday. filter The composition of the sample is analyzed by an Ion-chromatography.
The sampling was carried out without interruption except when ship was stopped.

2.2 Size distribution measurement

We adopted a Pollak photoelectric nucleus counter to measure Aitken particles and used a light scattering type of particle counter to measure Mie particles. The measurements were made continuously by repeating each run of the time length 30min. and 20min. in succession, respectively.

2.3 Radon concentration measurement

Filter pack method was adopted to measure the concentration of radioactive substances in the air over the ocean. The system is operated four times everyday.

2.4 SO_2, NO_x measurement

To measure SO_2 and NO_x the sulfur dioxide meter by ultraviolet spectroscopy and the nitrogen oxide meter by chemi-luminous method were used, respectively. Through the full period of expedition voyage, the measurements were carrid out without interruption.

2.5 Atmospheric turbidity measurement

We adopted a Sunphotometor and measured the sunbeams at fine weather in the day time.

3. Observation Results and Summary

As an example variation curves of concentrations of Aitken particle and radon are shown Fig.1. We obtain radon concentrations by assuming radioactive equilibrium being established among Rn, RaA, RaB and RaC. From the figure shown in Fig.1, high Aitken particle concentrations measured like a pulse are thought to be the results from air contamination by pollutions due to ship herself. Thus, on the occasion of the observation by the aid of ship on the ocean, in particular, we have to pay attention to pollutions due to ship herself at all time. However, correlation was often found between concentrations of Aitken particle and radon.

The real cause for these events observed was unknown in present moment. We expect that these evidences obtained should be discussed in future together with the following; variation of meteorological conditions and air mass trajectories on each measuring spot.

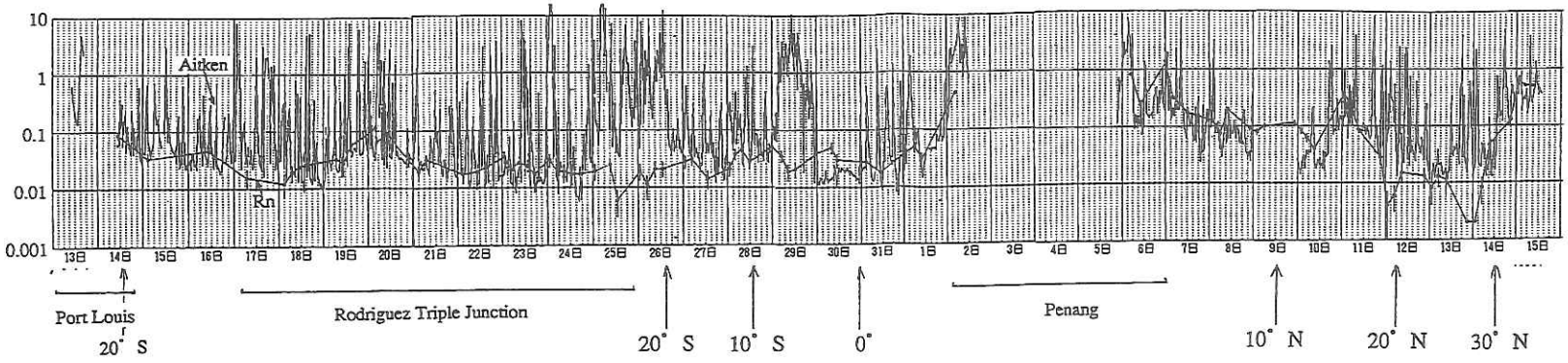

Fig. 13- 1. Aitken particle concentrations (1 / l) and Radon concentrations (Bq/m3).

14. Investigation of Latitude Effect on Cosmic-ray Intensity near the Sea-level

Masahide FURUKAWA[1]

[1]*Division of Environmental Health, National Institute of Radiological Sciences.*

1. Objective

In the Earths atmosphere, the distribution of cosmic-ray intensity changes as a function of both altitude and latitude. To estimate the human dose from cosmic rays, it is necessary to take into consideration these geographic factors. The purpose of this study was to investigate the actual distribution of cosmic-ray intensity near the sea-level by in situ measurements on a global scale. It will contribute to the study of environmental radiations in the atmosphere.

2. Measurement and Analysis

Cosmic-ray intensity and other environmental radiations were measured with a portable field system which was developed by Okano et al.(1980) and Kumagai and Okano (1982). The system consists of 3-in. diameter spherical NaI(Tl) and plastic scintillation detectors, an interface (multi-channel spectrometer), and a stereo magnetic tape recorder (Fig. 1).

The measurements were carried out on the upper deck of the vessel through the daylight hours every day during Legs. 1 and 2 (July 8, 1993 in Tokyo bay to August 10, 1993 in Mauritius, by way of Singapore and Sunda strait). At the same time, atmospheric pressure was measured during the cruise so that the pressure effect on the cosmic-ray intensity could be subtracted later. Locations of the measurement sites with NaI(Tl) scintillation detector are shown in Figure 2.

Analysis was made for absorbed energy spectra above 3 MeV by the peeling-off method, and the cosmic-ray intensity was calculated as the exposure rate (μR/h) from the ionizing component of the cosmic rays. The pressure effect was subtracted from the calculated intensity by a method of Minato et al.(1993).

3. Preliminary Result for Latitude Effect on Cosmic-ray Intensity

Figure 3 shows the variation of the cosmic-ray intensity with geographic latitude observed by the system with NaI(Tl) scintillation detector. In general, the intensity decreases with decreasing geographic latitude. The minimum value, about 2.6 μR/h, was observed at a geographic latitude of approximately 8.5° N.

From the view point that cosmic-ray intensity is dependent on the geomagnetic field, this geographic latitude can be considered the geomagnetic equator. Practically, this geographic latitude is equivalent to a geomagnetic latitude of about 2.3° S. This result approximately agree with theoretical estimation, and is interpreted in terms of the geomagnetic cut-off energy for the primary cosmic rays in space which increase with decreasing of the geomagnetic latitude (Kodama, 1968).

The latitude effect near the sea-level, the rate of change of cosmic-ray intensity with the geomagnetic latitude, was estimated to be about 0.016 μR/h/degree in this study area.

REFERENCES

Kodama,M.(1968) JARE Sci.Rept.Series A, 5, 1-61.

Kumagai,H. and Okano,M.(1982) A Portable Scintillation Spectrometer for Environmental Radiation Measurement. Sci.Rep.Inst.Phys.Chem.Res.,58, 1-10.

Minato,S., OBrien,K.O., Shimo,M., Sugino,M. and Moriuchi,Y. (1993) Simple and Convenient Carborne Survey Techniques for Detailed Evaluation of natural Background Radiation Dose Rates -Examples on Some Routes in Gifu Prefecture, Japan-. The 3rd Symposium on Environmental Radiation Monitoring Technology, proceedings, May 1993, Taiwan, E301-E310.

Okano,M., Izumo,K., Kumagai,H., Katou,T., Nishida,M., Hamada,T., and Kodama,M.(1980) Measurement of environmental radiations with a scintillation spectrometer equipped with a spherical NaI(Tl) scintillator. T.F.Gesell and W.M.Lowder eds., Natural Radiation Environment III, Technical Information Center, U.S.Department of Energy, 2, 896-911.

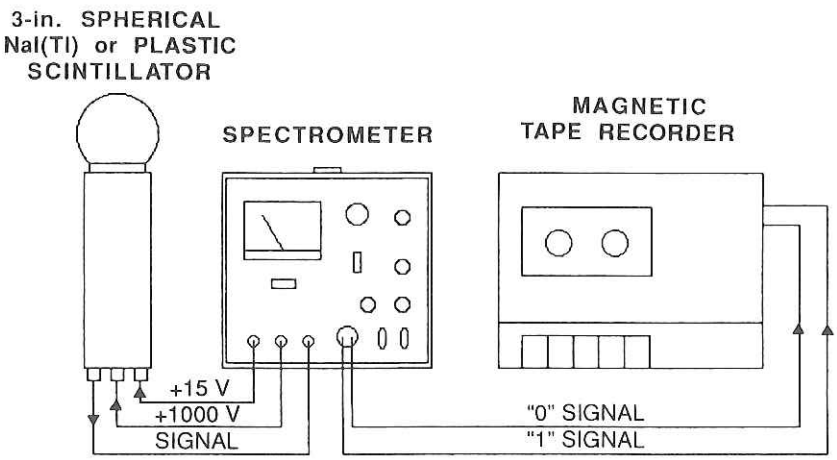

Fig. 14-1. Arrangement of the portable spectrometer used in this survey.

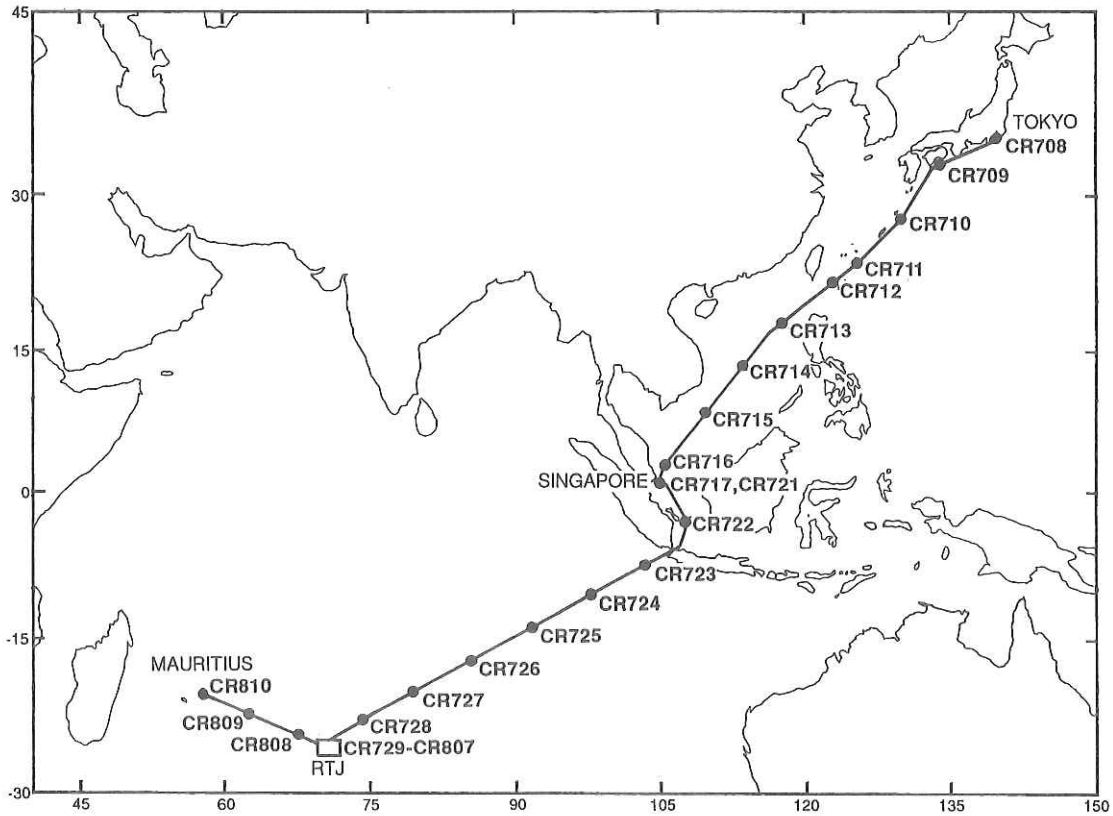

Fig. 14-2: Locations of the measurement sites with a NaI(Tl) scintillation detector.

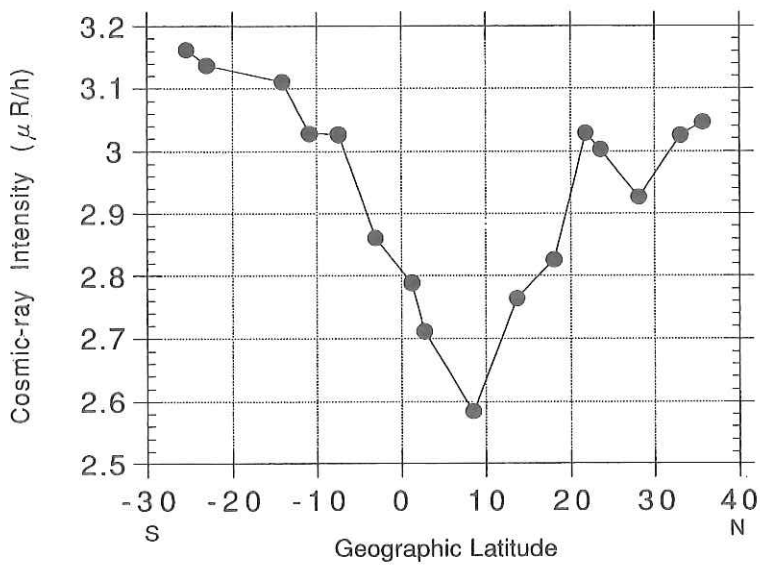

Fig. 14-3: Variation of the cosmic-ray intensity with geographic latitude observed in this study.

15. Thermal structure of atmospheric boundary layer over the Indian Ocean

Shigenori HAGINOYA[1] and Nobuyuki KINOSHITA[1]

[1] *Physical Meteorological Research Deopartment, Meteorological Research Institute, JMA*

1. Objective

In order to clarify the mechanism of the Asian Monsoon, which is caused through Air-Sea-Land interactions, the large-scale heat budgets over two different districts must be estimated by field observations. One of the districts is Tibetan-Himalaya Mountains Area and the other the Indian Ocean-South China Sea Area. Because of the vastness of the districts and their unsuitable conditions for observations, observatories or ships in these districts are so sparsely distributed that the basic meteorological data to clarify the mechanism of the Asian Monsoon are lacking. Since October 1991, the automatic observation of sea surface heat budget has been started in the Indian Ocean by VOS (Volunteer Observing Ship) to collect the above basic data and estimate heat budgets. The ship is Osaka-Maru (31,382 tons, Mitsui O.S.K.Lines Co. Ltd.). The observation is carried out 6 times a year on her round trip between Japan and Republic of South Africa through the South China Sea, the Strait of Malacca and the Indian Ocean. Sea surface heat budget affects atmospheric thermal structure and its motion, especially in the ABL (Atmospheric Boundary Layer). We cannot obtain enough data to clarify the mechanism of the Asian Monsoon from VOS observation only. The purpose of this cruise is to sound the vertical structure of atmosphere making use of aerological sonde observation, to collect the data of vertical thermal structure of ABL and to clarify the mechanism of atmospheric heat transfer.

2. Instrumentation and Condition

Omega sonde was used to obtain pressure, temperature, relative humidity, wind direction and wind speed up to 500hPa (about 5000m mean sea level). Omega sonde is the instruments which measure the wind using navaid networks. Observation was carried out from 16 August to 10 September (GMT). Table 1 shows the stations where the omega sonde were released. XBT (eXpendable Bathy Thermography) observation was carried out to check the SST (Sea Surface Temperature) obtained from Hakuho-Maru and to clarify the thermal structure of sea surface layer to the depth of 460m. Observation was carried out from 58E to 120E. Table 2 shows the stations where XBTs were released. One rain gauge and two rain detectors were installed the upper deck of the bridge to observe the existence of rainfall and the precipitation. To obtain the radiation data, a pyranometer and a long wave radiometer were also set up the same place. The recorders of above sensors recorded the data from Harumi to Harumi.

3. Principal Results

The vertical structure of virtual potential temperature, specific humidity, east-west wind component and north-south wind component were obtained from data analysis. Virtual

potential temperature is potential temperature in which influence of water vapor is under consideration. Figure 1 shows the results of omega sonde observations. Several parameters describe the ABL's characteristics. Figure 2 illustrates the parameters of ABL. Table 3 shows the results of parameters. Figure 3 shows the relation among the parameters of ABL. Table 4 summarizes the average quantitative feature of parameters. Mixed layer height in the low latitude (20S-20N) is nearly equal to the results that were obtained in the Pacific Ocean.

Figure 4 shows the results of XBT observation. It is found that the SST by Hakuho-Maru is about 0.2 degree Centigrade lower than the surface layer temperature measured by XBT.

In this cruise, the dew point meter did not work well. The dew point meter was checked by Asman ventilated dry and wet bulb thermometer. The results shows figure 5. Dew point measured by the dew point meter was calibrated by the empirical relation in the figure.

Heat budget analysis was carried out using the meteorological data of Hakuho-Maru instruments. Sensible (H) and latent (iE) heat flux of every minute are estimated by the bulk methodo (Kondo, 1975). Net radiation flux (Rn) was calculated by the following formula. Rn =(1-a)S+e(L-sTs4), where a:sea surface albedo(=0.06), S:global solar radiation, e:emissivity (=0.97), L:downward long wave radiation, s:Stefan-Boltzman's constant, Ts:SST. Figure 6 shows the results of heat budget analysis. Figure 7 shows the latitudinal variation of energy fluxes. Figure 8 shows the comparison of energy flux between Hakuho-Maru observation and that of Osaka-Maru. Present results of H+iE are two times smaller than that of Osaka-Maru.

4. Summary

It is the very valuable for marine meteorology that the data of ABL over the Indian Ocean and the South China Sea area were obtained. Parameters of ABL were useful for making the ABL model over the Ocean.

REFERENCES

Kondo, J., 1975: Air-sea bulk transfer coefficient in diabatic conditions. *Boundary-Layer Meteorol.*, **9**, 91-112.

Table 15-4 Average of parameters of ABL. ( ) indicates the standard deviation.

area	h Θv m	h q m	γ °C/km	Θvs-Θv °C	qs-q g/kg
Indian Ocean 25°S-20°S	997 (332)	1011 (357)	6.15 (1.85)	3.35 (1.04)	7.73 (1.25)
Indian Ocean 20°S- 5°N	788 (182)	632 (225)	4.87 (1.08)	2.26 (0.90)	8.43 (1.10)
South China Sea 4°N-20°N	494 (166)	488 (231)	4.27 (0.47)	2.83 (0.74)	9.08 (0.64)

Table 15-1. Omega sonde released station

St.No.	Date	Time GMT	Latitude 0.01°	Longitude 0.01°
001	1993-08-16	18:48	25.59 S	69.65 E
002	1993-08-17	00:34	25.34 S	69.99 E
003	1993-08-17	03:27	25.32 S	69.97 E
004	1993-08-17	06:07	25.30 S	69.96 E
006	1993-08-17	08:55	25.41 S	69.90 E
007	1193-08-17	12:02	25.33 S	69.97 E
008	1993-08-18	04:00	25.37 S	69.98 E
009	1993-08-18	08:09	25.40 S	70.03 E
010	1993-08-18	14:00	25.32 S	69.93 E
011	1993-08-19	02:59	25.57 S	69.98 E
012	1993-08-19	09:00	25.62 S	69.89 E
013	1993-08-19	13:04	25.71 S	69.68 E
014	1993-08-19	17:49	25.67 S	69.73 E
015	1993-08-20	03:23	25.81 S	70.02 E
016	1993-08-20	09:07	25.70 S	70.23 E
017	1993-08-20	13:30	25.80 S	70.20 E
018	1993-08-21	03:05	25.95 S	70.34 E
019	1993-08-21	08:55	26.13 S	70.41 E
020	1993-08-21	13:26	26.12 S	70.57 E
021	1993-08-22	03:04	26.18 S	70.94 E
022	1993-08-22	08:56	26.12 S	71.16 E
023	1993-08-22	13:15	26.04 S	71.32 E
024	1993-08-23	03:00	25.76 S	70.21 E
025	1993-08-23	08:57	25.58 S	70.00 E
026	1993-08-23	13:26	25.43 S	70.00 E
027	1993-08-24	03:00	25.31 S	70.01 E
028	1993-08-24	08:52	24.75 S	70.02 E
029	1993-08-24	13:14	24.00 S	69.66 E
030	1993-08-25	03:06	23.97 S	69.65 E
031	1993-08-25	08:51	24.00 S	69.65 E
032	1993-08-25	13:21	24.00 S	69.66 E
033	1993-08-26	00:03	22.24 S	71.11 E
034	1993-08-26	05:50	21.13 S	72.17 E
035	1993-08-26	11:49	19.93 S	73.22 E
036	1993-08-26	18:00	18.66 S	74.32 E
037	1993-08-26	23:58	17.46 S	75.34 E
038	1993-08-27	05:50	16.29 S	76.35 E
039	1993-08-27	11:58	15.02 S	77.42 E
040	1993-08-27	17:57	13.97 S	78.34 E
041	1993-08-28	00:01	12.71 S	79.37 E
042	1993-08-28	05:52	11.54 S	80.35 E
043	1993-08-28	11:54	10.40 S	81.30 E
044	1993-08-28	17:50	9.38 S	82.17 E
045	1993-08-28	23:59	8.06 S	83.22 E
046	1993-08-29	05:56	6.81 S	84.26 E
047	1993-08-29	11:49	5.59 S	85.27 E
048	1993-08-29	17:42	4.55 S	86.21 E
049	1993-08-29	23:55	3.23 S	87.37 E
050	1993-08-30	05:47	2.00 S	88.48 E
051	1993-08-30	11:49	0.88 S	89.49 E
052	1993-08-30	18:02	0.36 N	90.43 E
053	1993-08-30	23:59	1.53 N	91.33 E
054	1993-08-31	05:58	2.52 N	92.08 E
055	1993-08-31	11:58	3.52 N	92.85 E
056	1993-08-31	17:56	4.58 N	93.66 E
057	1993-09-07	23:51	4.68 N	106.53 E
058	1993-09-08	02:53	5.31 N	107.05 E
059	1993-09-08	06:00	6.00 N	107.59 E
060	1993-09-08	08:56	6.66 N	108.11 E
061	1993-09-08	11:58	7.31 N	108.64 E
062	1993-09-08	14:55	7.94 N	109.16 E
064	1993-09-08	20:49	9.17 N	110.19 E
065	1993-09-08	23:54	9.76 N	110.85 E
066	1993-09-09	03:03	10.35 N	111.57 E
067	1993-09-09	05:56	10.75 N	112.17 E
068	1993-09-09	08:53	11.22 N	112.89 E
069	1993-09-09	11:59	11.73 N	113.66 E
070	1993-09-09	14:54	12.21 N	114.39 E
071	1993-09-09	17:46	12.66 N	115.08 E
072	1993-09-09	20:47	13.15 N	115.83 E
073	1993-09-09	23:50	13.61 N	116.53 E
074	1993-09-10	03:16	14.15 N	117.36 E
075	1993-09-10	06:06	14.59 N	118.04 E
076	1993-09-10	08:55	15.05 N	118.69 E
077	1993-09-10	11:55	15.82 N	119.01 E
078	1993-09-10	14:53	16.57 N	119.34 E
079	1993-09-10	17:46	17.30 N	119.65 E
080	1993-09-10	20:47	18.08 N	120.08 E

Table 15-2. XBT released station

St.No.	Date	Time JST	Latitude ° - '	Longitude ° - '
X058	93/08/15	00:45:27	20-48 S	058-00 E
X059	93/08/15	04:31:58	21-13 S	059-00 E
X060	93/08/15	08:19:38	21-39 S	060-00 E
X061	93/08/15	12:14:54	22-03 S	061-00 E
X062	93/08/15	16:07:36	22-28 S	062-00 E
X063	93/08/15	19:59:47	22-53 S	063-00 E
X064	93/08/15	23:45:33	23-17 S	064-00 E
X065	93/08/16	03:26:36	23-41 S	065-00 E
X066	93/08/16	07:15:14	24-06 S	066-00 E
X067	93/08/16	11:16:49	24-33 S	067-04 E
X068	93/08/16	14:40:15	24-54 S	068-00 E
X069	93/08/16	18:22:03	25-19 S	069-00 E
X070	93/08/19	12:35:32	25-34 S	070-00 E
X0701	93/08/19	12:41:25	25-34 S	070-00 E
X071	93/08/22	16:22:41	26-11 S	071-00 E
X072	93/08/26	13:42:23	21-30 S	072-00 E
X073	93/08/26	19:28:45	20-13 S	073-00 E
X074	93/08/27	01:06:13	19-03 S	074-00 E
X075	93/08/27	06:52:51	17-54 S	075-00 E
X076	93/08/27	12:37:39	16-43 S	076-00 E
X077	93/08/27	18:23:59	15-35 S	077-00 E
X078	93/08/28	00:13:23	14-22 S	078-00 E
X079	93/08/28	06:48:19	13-11 S	079-00 E
X080	93/08/28	12:39:01	11-59 S	080-00 E
X081	93/08/28	19:05:47	10-52 S	081-00 E
X082	93/08/29	00:59:12	09-35 S	082-00 E
X083	93/08/29	07:37:00	08-21 S	083-00 E
X084	93/08/29	13:21:45	07-11 S	084-00 E
X085	93/08/29	19:10:28	05-58 S	085-00 E
X086	93/08/30	00:45:28	04-47 S	086-00 E
X087	93/08/30	06:51:22	03-40 S	087-00 E
X088	93/08/30	12:07:11	02-35 S	088-00 E
X089	93/08/30	17:47:25	01-28 S	089-00 E
X090	93/08/31	00:06:11	00-14 S	090-00 E
X091	93/08/31	06:42:58	01-05 N	091-00 E
X092	93/08/31	13:57:42	02-22 N	092-00 E
X093	93/08/31	22:52:49	03-40 N	093-00 E
X094	93/09/01	04:50:06	04-59 N	094-00 E
X095	93/09/01	10:21:35	06-08 N	095-00 E
X096	93/09/01	14:06:42	06-06 N	096-00 E
X097	93/09/01	19:06:50	06-00 N	097-00 E
X110	93/09/09	04:48:13	08-57 N	110-00 E
X1102	93/09/09	04:51:51	09-00 N	110-01 E
X111	93/09/09	09:32:14	09-52 N	111-00 E
X112	93/09/09	14:10:07	10-37 N	112-00 E
X113	93/09/09	18:14:08	11-17 N	113-00 E
X114	93/09/09	22:18:25	11-55 N	114-00 E
X115	93/09/10	02:16:28	12-35 N	115-00 E
X116	93/09/10	06:26:14	13-14 N	116-00 E
X117	93/09/10	10:36:44	13-53 N	117-00 E
X118	93/09/10	14:48:37	14-32 N	118-00 E
X119	93/09/10	20:43:08	15-45 N	119-00 E
X120	93/09/11	05:11:19	17-55 N	120-00 E

Table 15-3. Parameters of ABL

St.No.	hΘv m	hq m	γ ˚C/km	Θv ˚C	q g/kg	Θvs ˚C	qs g/kg
001	1043	1191	7.47	18.5	6.19	22.7	14.16
002	1100	1083	6.57	18.5	6.31	23.1	14.60
003	1043	1078	5.93	18.5	6.37	23.0	14.58
004	1026	983	6.44	18.7	6.44	23.0	14.42
006	1000	1048	6.93	19.0	6.44	22.9	14.52
007	1078	1087	8.09	19.5	6.96	23.1	14.60
008	1278	1304	5.93	19.5	6.19	22.8	14.65
009	913	1000	7.04	18.9	6.26	23.1	14.69
010	796	804	8.00	20.3	7.27	22.7	14.57
011	657	652	5.62	20.3	6.52	23.4	15.28
012	1313	570	5.52	20.8	6.44	22.8	14.66
013	1400	1400	5.00	20.8	7.37	23.0	14.19
014	1557	735	7.42	20.8	7.81	23.0	14.46
015	913	878	7.73	20.3	7.94	23.8	15.46
016	791	1043	9.28	20.0	7.00	23.8	15.13
017	835	800	7.86	20.2	8.00	24.4	15.86
018	1391	1730	3.48	19.3	6.11	24.6	16.15
019	1000	957	8.45	19.5	7.09	23.5	14.76
020	704	726	4.30	19.7	8.38	23.7	15.21
021	1696	1600	7.73	19.5	6.24	23.4	15.02
022	1470	1478	6.49	19.6	5.98	23.6	15.52
023	1478	1517	8.20	20.0	6.70	23.3	14.75
024	504	1800	8.51	20.8	5.85	23.5	15.03
025			5.23			23.4	14.98
026			3.22			23.3	14.97
027			1.57			22.7	14.43
028	787	800	4.54	23.0	10.44	23.9	15.41
029	478	522	3.00	23.4	11.08	24.0	15.39
030	348	348	5.80	20.6	10.05	23.3	14.89
031	869	861	7.45	21.4	8.22	23.9	15.46
032	1070	1000	6.57	20.6	7.60	23.8	15.44
033	700	696	3.61	21.3	7.94	25.2	16.35
034	657	639	4.12	22.2	9.07	25.8	16.99
035	770	800	4.54	23.2	10.00	25.8	17.23
036	522	422	3.79	23.0	10.75	26.6	17.81
037	917	904	4.77	24.2	10.05	25.2	16.35
038	800	800	7.19	25.0	9.79	27.8	18.95
039	778	709	5.49	25.0	10.36	28.8	19.90
040	609	565	4.38	26.7	12.63	29.0	20.04
041	370	348	4.77	26.3	12.40	29.0	20.17
042	930		6.31	27.1		29.0	20.20
043	652		4.95	27.7		29.7	20.94
044	700	630	4.12	30.0	14.18	30.1	21.32
045	991	943	4.25	27.3	12.35	31.0	22.22
046			4.36			31.2	22.56
047	1000	926	6.49	29.5	14.43	31.9	23.23
048	913	357	5.41	29.8	15.00	32.3	23.49
049	886	604	6.98	30.0	14.48	32.3	23.62
050	913	896	5.15	30.6	13.56	32.7	24.08
051	1000	543	5.00	31.4	15.21	32.7	23.91
052	913	661	5.08	31.2	15.34	32.9	24.21
053		891	3.32		16.57	33.1	24.45
054	526	370	3.61	30.9	15.46	32.9	24.34
055		200	3.61		14.00	32.9	23.75
056		435	3.48		16.00	32.4	23.75
057	561	600	4.28	30.0	15.36	33.5	24.89
058	652	600	3.66	31.0	15.46	33.4	24.75
059			3.81			33.5	24.96
060	400	304	3.81	29.0	15.98	33.3	24.65
061	696	491	4.56	30.7	14.15	33.0	24.34
062	643	491	4.64	30.6	15.98	32.8	24.19
064	783	774	4.33	30.6	15.46	32.9	24.25
065	652	565	5.00	30.9	15.31	33.0	24.34
066	561	478	3.87	31.1	15.75	33.1	24.64
067	674	643	3.61	31.4	15.72	32.9	24.25
068		1261	5.15		15.54	32.9	24.35
069	326	335	4.38	29.8	15.72	33.3	24.73
070	478	426	3.63	29.5	15.15	32.5	23.75
071	283	252	3.87	30.2	15.34	32.6	24.19
072	135	109	3.99	28.7	13.92	32.7	24.06
073	387	352	4.05	29.6	15.62	32.7	23.88
074	378	348	4.38	29.6	15.46	32.9	24.47
075	496	457	5.03	30.6	15.41	33.1	24.09
076		357	4.64		15.98	33.0	24.63
077			4.10			33.1	24.60
078	348	535	4.10	29.8	14.43	33.4	24.92
079	443	391	5.00	30.3	14.77	33.4	24.82
080						33.1	24.81

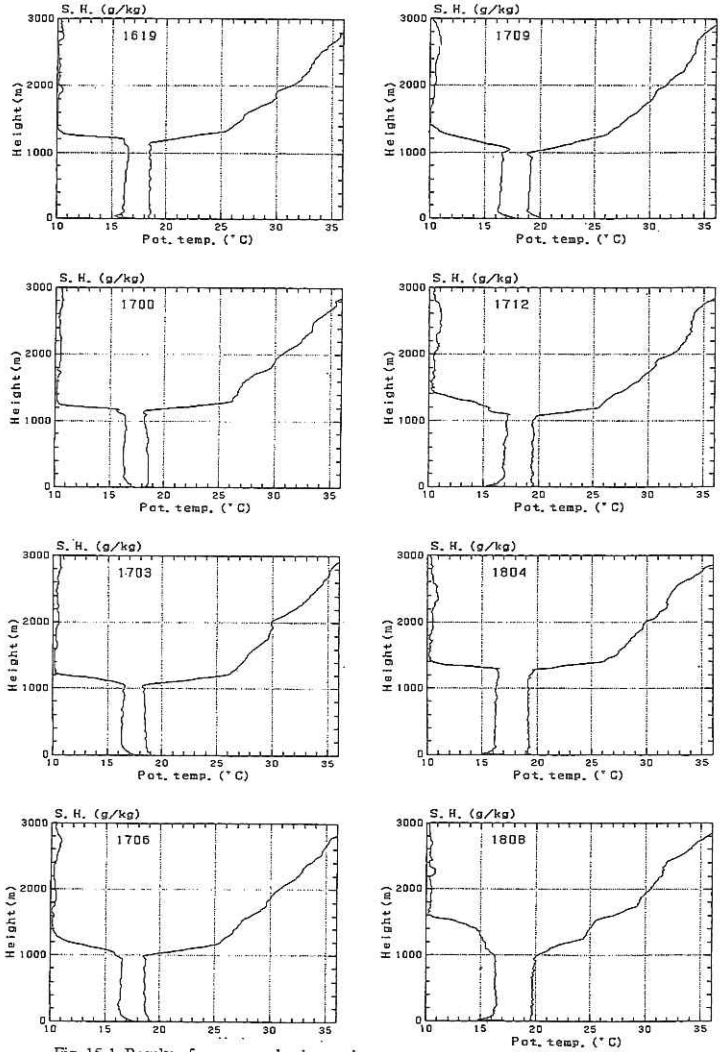

Fig. 15-1 Results of omega sonde observation.
(a)Vertical profile of virtual potential temperature and specific humidity(S.H.). Scale of S.H. is referred to Fig.15-2.

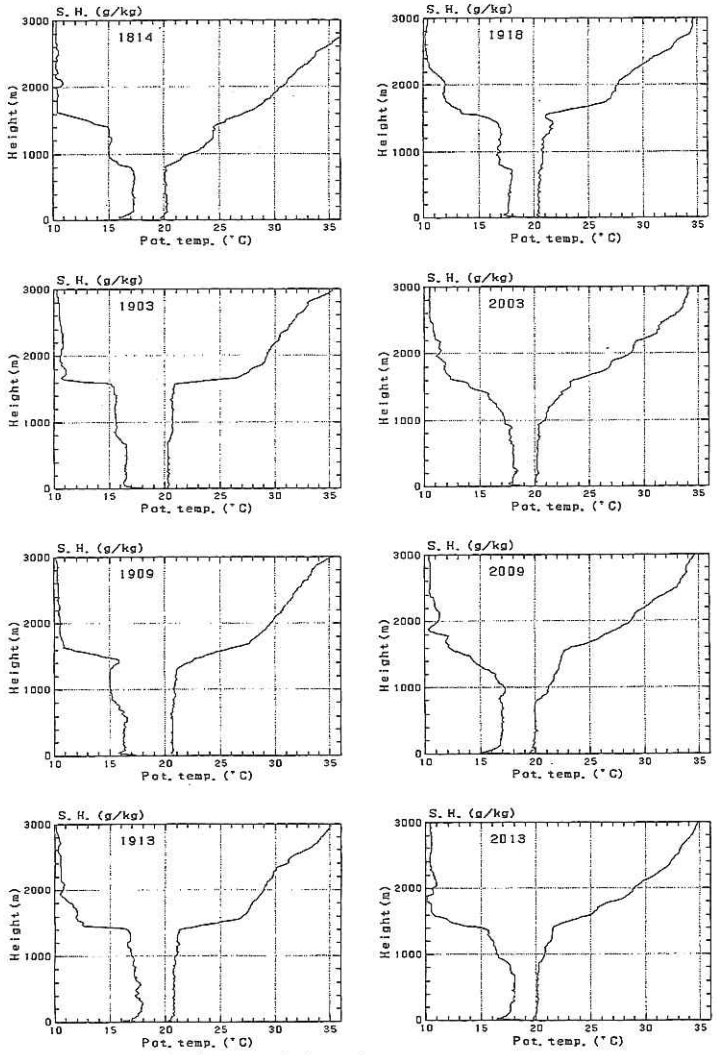

Fig. 15-1 Results of omega sonde observation.
(a)Vertical profile of virtual potential temperature and specific humidity(S.H.). Scale of S.H. is referred to Fig.15-2.

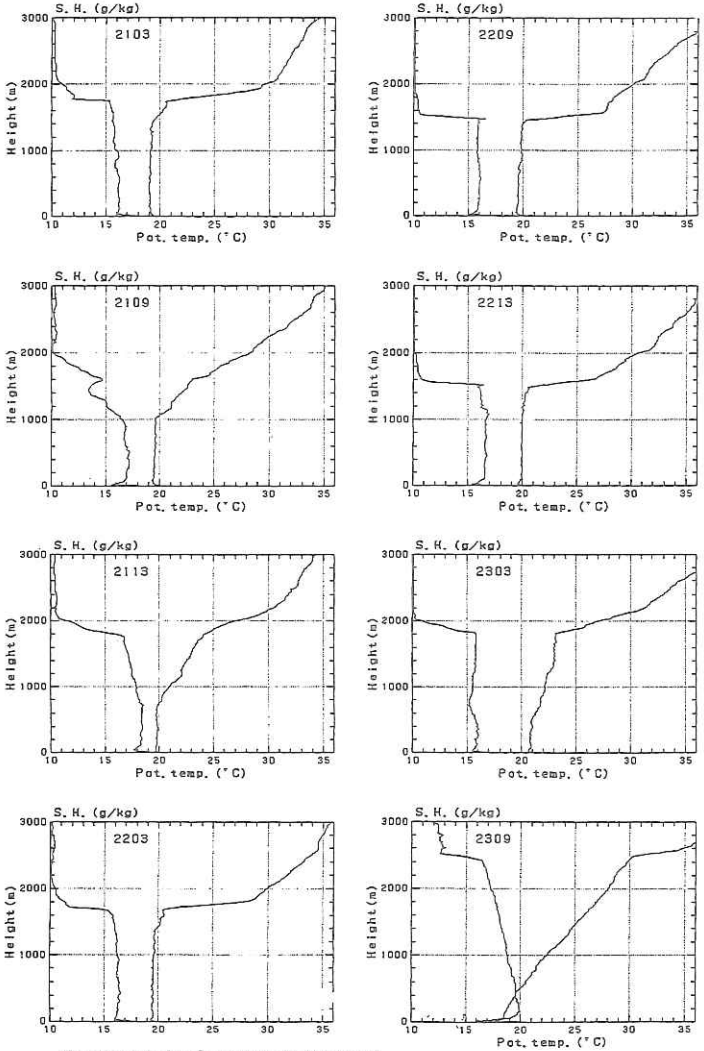

Fig. 15-1 Results of omega sonde observation.
(a)Vertical profile of virtual potential temperature and specific humidity(S.H.). Scale of S.H. is referred to Fig.15-2.

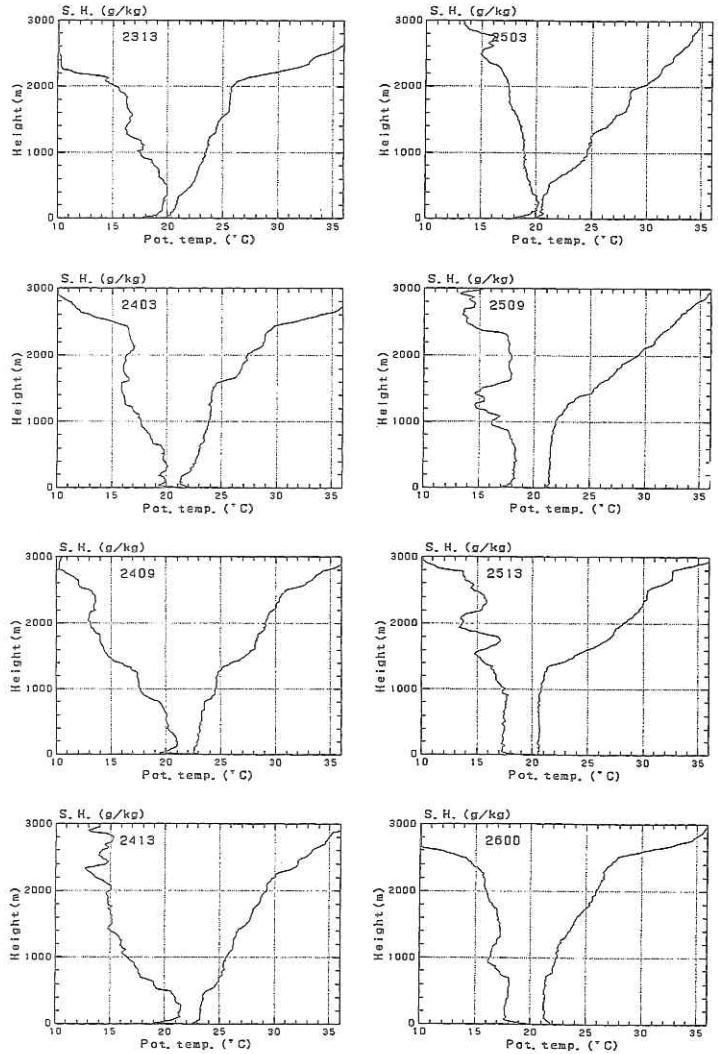

Fig. 15-1 Results of omega sonde observation.
(a)Vertical profile of virtual potential temperature and specific humidity(S.H.). Scale of S.H. is referred to Fig.15-2.

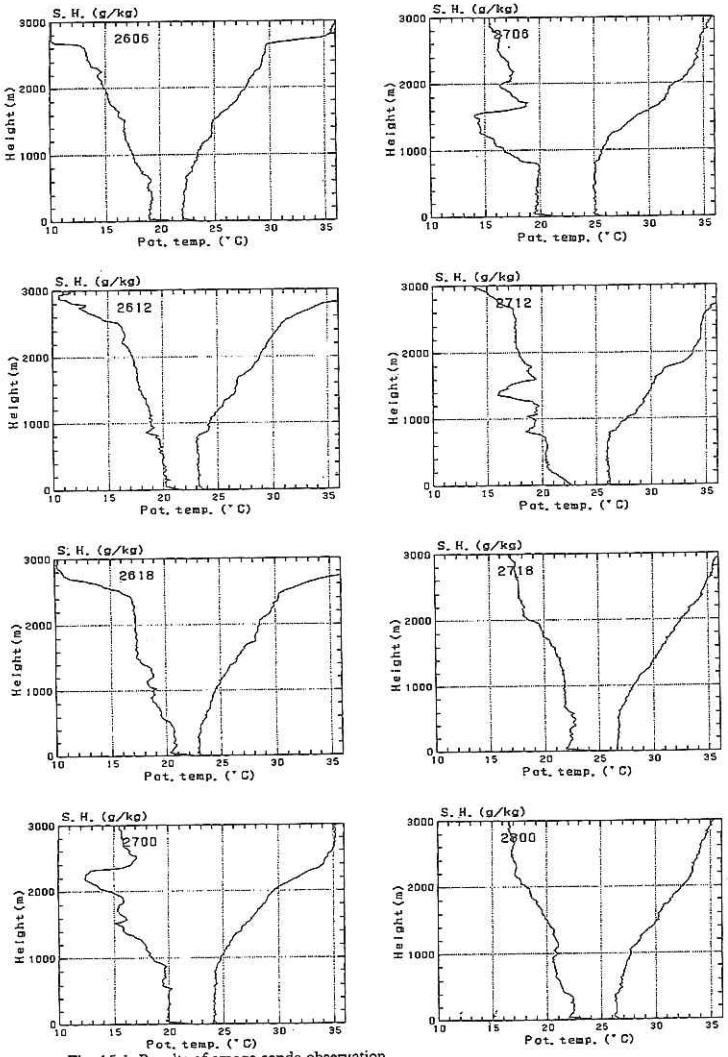

Fig. 15-1 Results of omega sonde observation.
(a)Vertical profile of virtual potential temperature and specific humidity(S.H.). Scale of S.H. is referred to Fig.15-2.

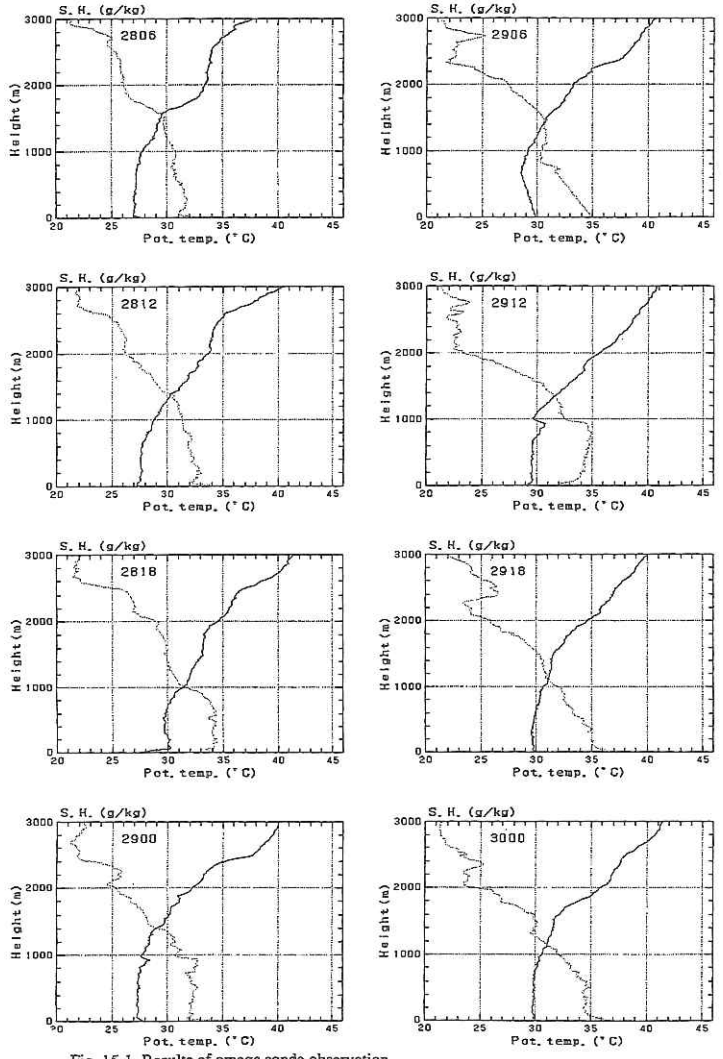

Fig. 15-1 Results of omega sonde observation.
(a)Vertical profile of virtual potential temperature and specific humidity(S.H.). Scale of S.H. is referred to Fig.15-2.

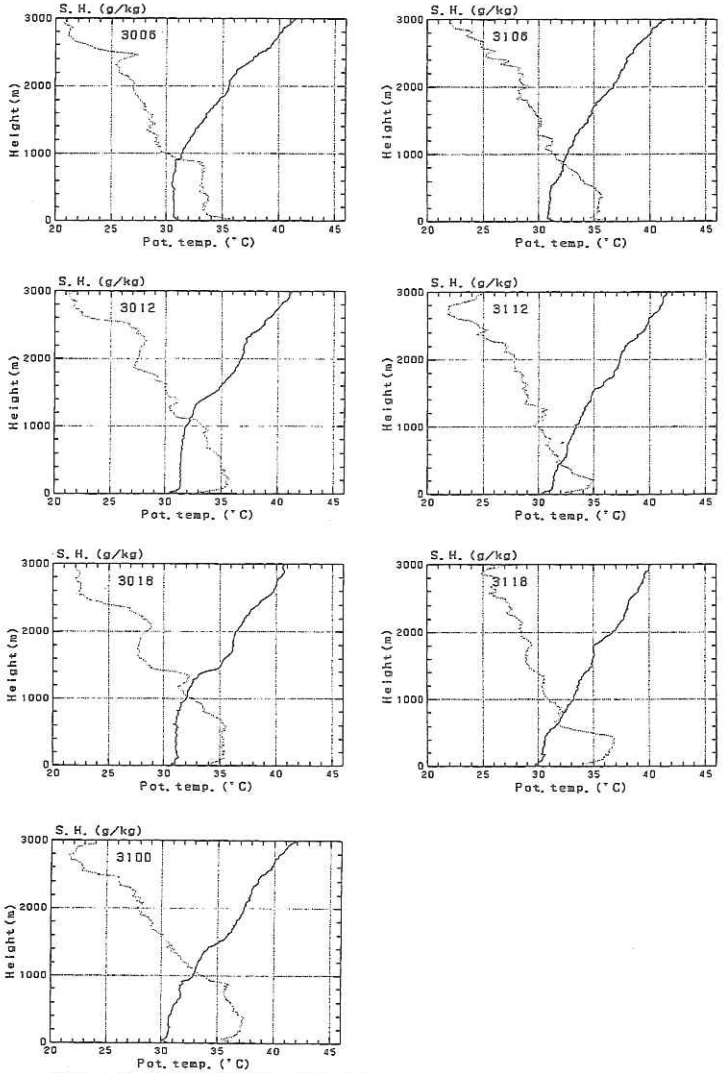

Fig. 15-1 Results of omega sonde observation.
(a)Vertical profile of virtual potential temperature and specific humidity(S.H.). Scale of S.H. is referred to Fig.15-2.

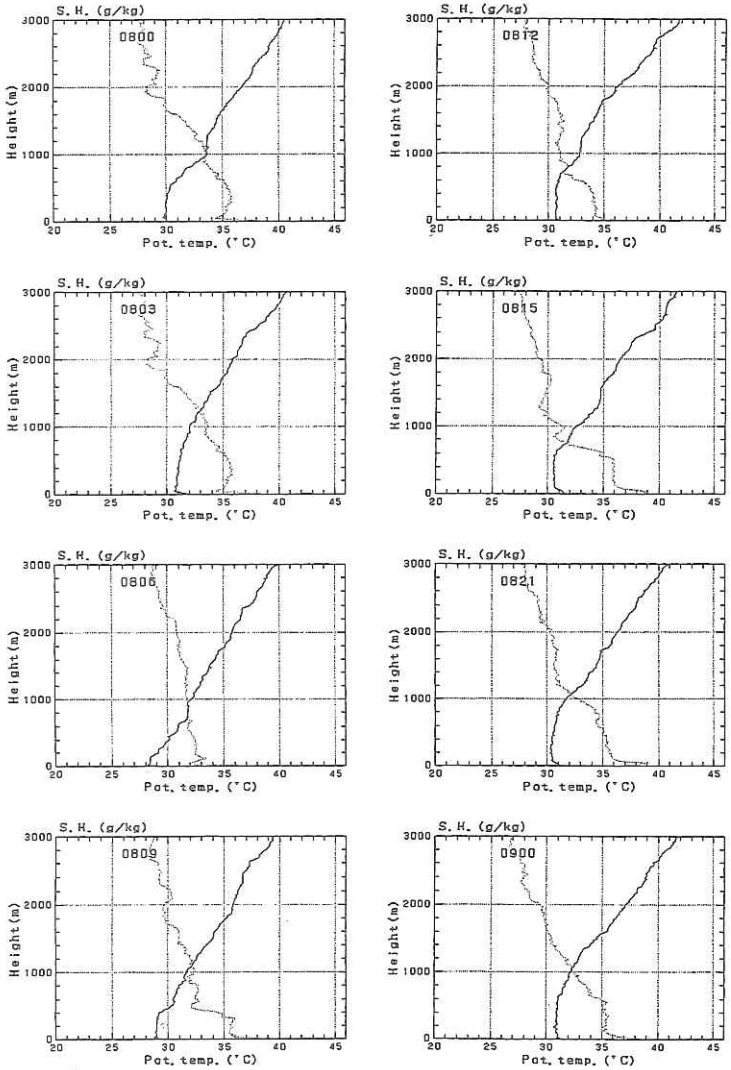

Fig. 15-1 Results of omega sonde observation.
(a)Vertical profile of virtual potential temperature and specific humidity(S.H.). Scale of S.H. is referred to Fig.15-2.

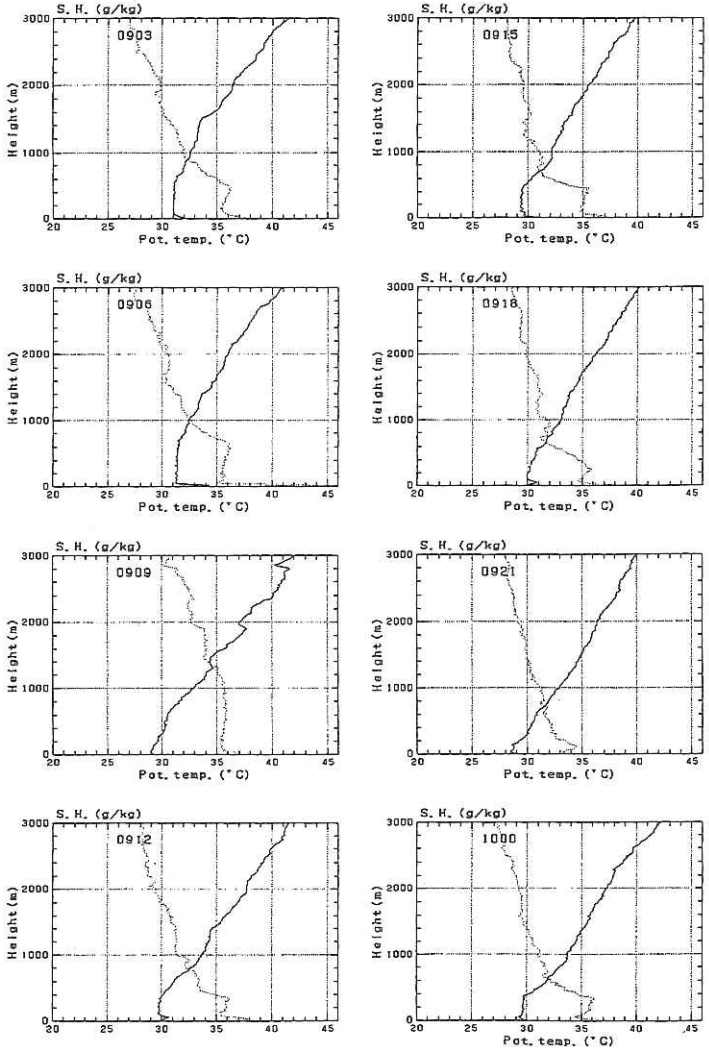

Fig. 15-1 Results of omega sonde observation.
(a)Vertical profile of virtual potential temperature and specific humidity(S.H.). Scale of S.H. is referred to Fig.15-2.

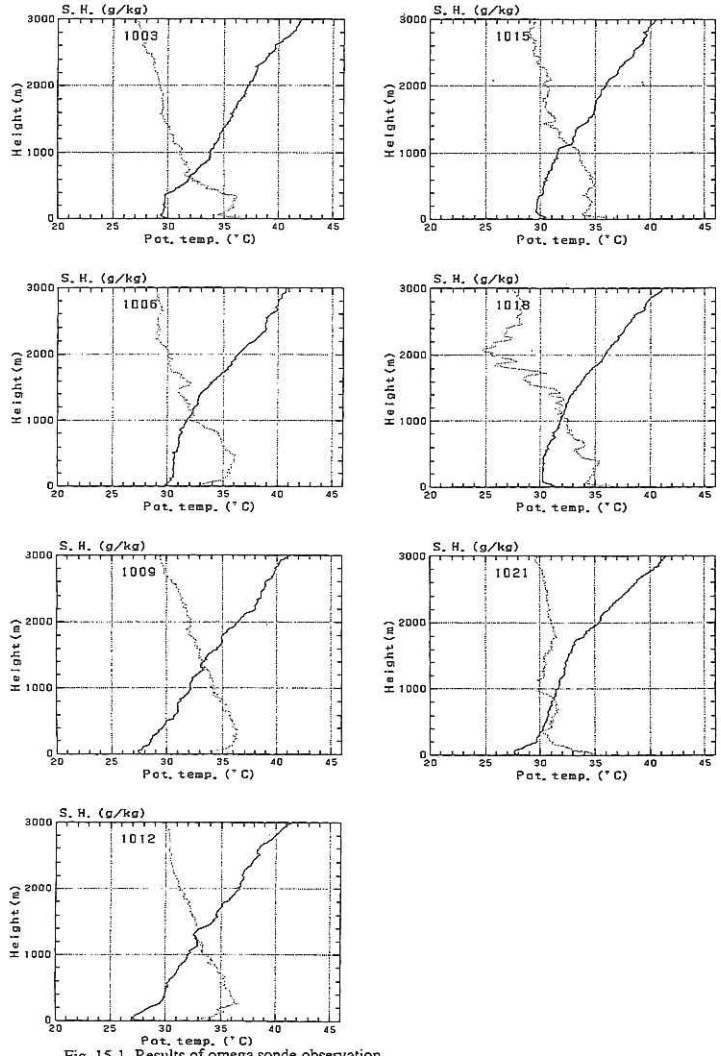

Fig. 15-1 Results of omega sonde observation.
(a)Vertical profile of virtual potential temperature and specific humidity(S.H.). Scale of S.H. is referred to Fig.15-2.

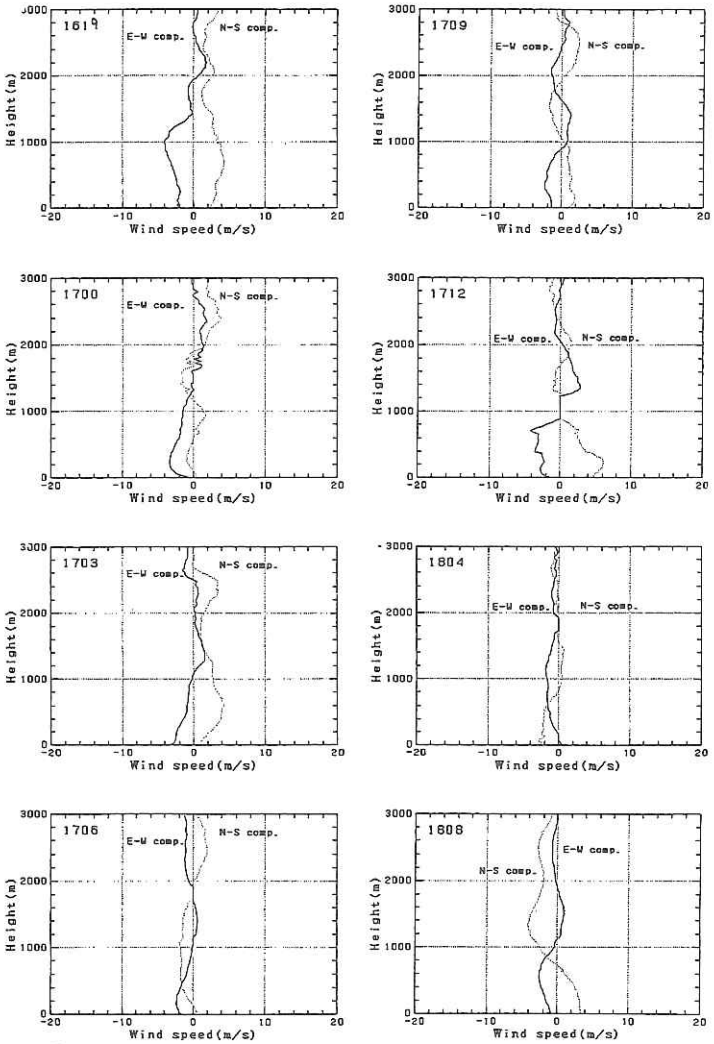

Fig. 15-1 Results of omega sonde observation.
(b)East-west and north-south component of wind speed. The number in the figure indicates released day and hour(GMT).

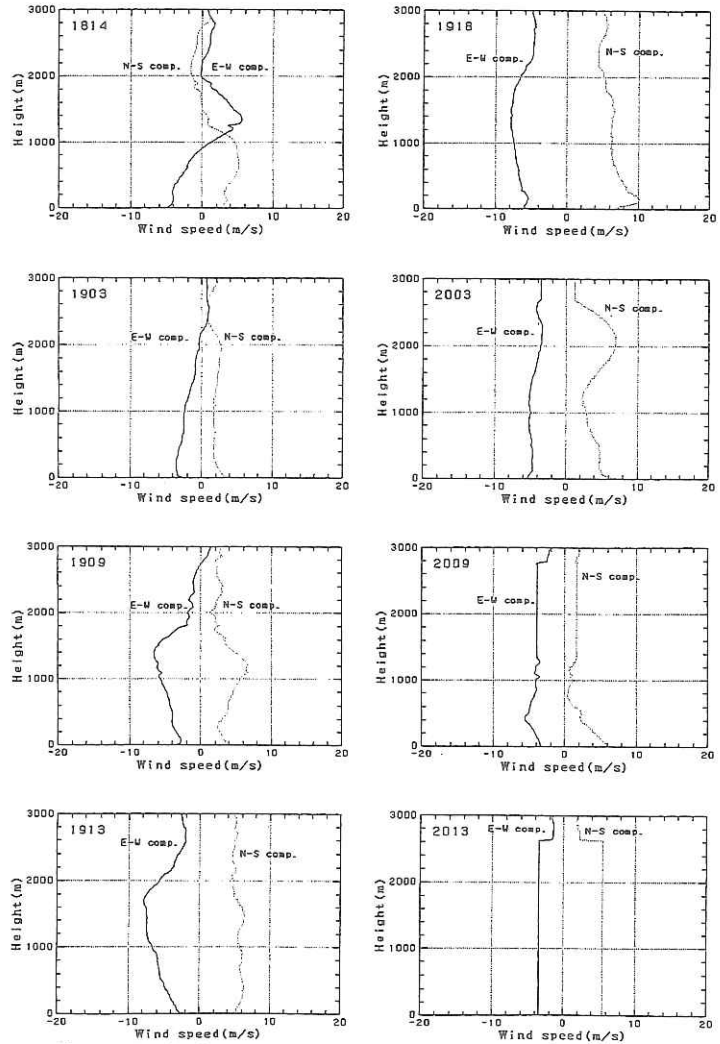

Fig. 15-1 Results of omega sonde observation.
(b)East-west and north-south component of wind speed. The number in the figure indicates released day and hour(GMT).

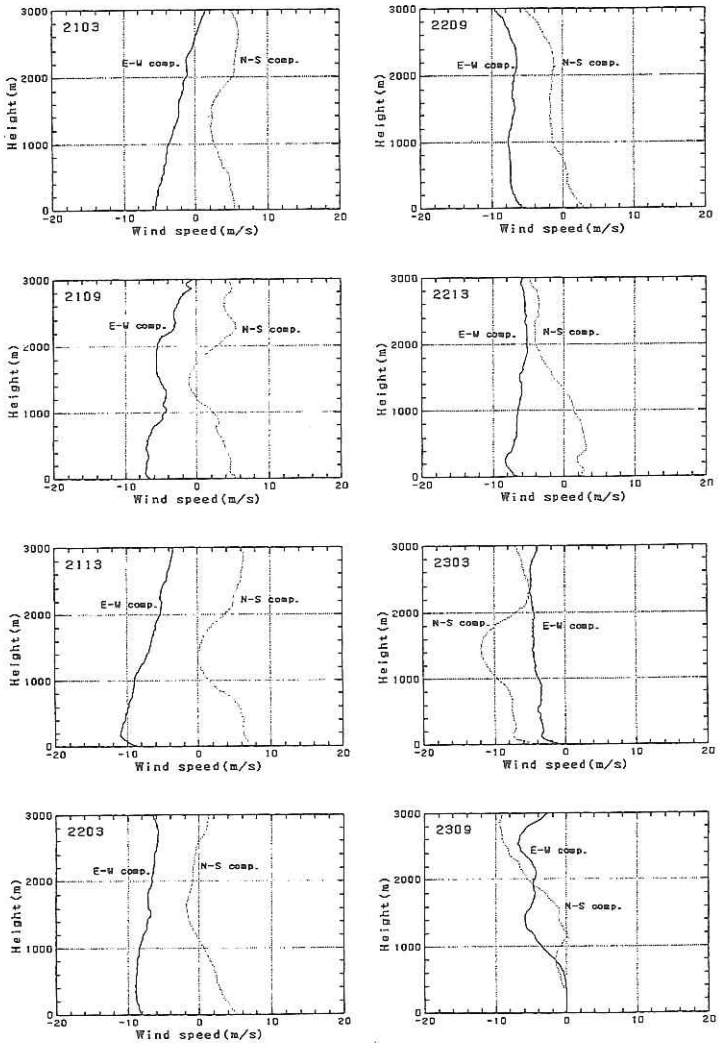

Fig. 15-1 Results of omega sonde observation.
(b)East-west and north-south component of wind speed. The number in the figure indicates released day and hour(GMT).

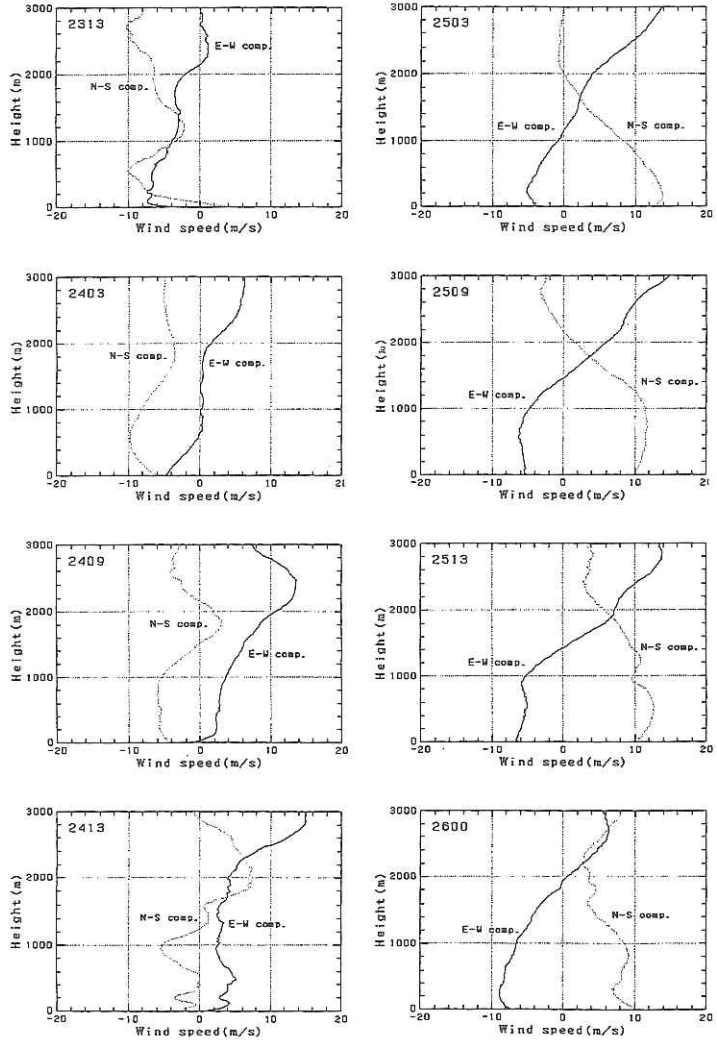

Fig. 15-1 Results of omega sonde observation.
(b)East-west and north-south component of wind speed. The number in the figure indicates released day and hour(GMT).

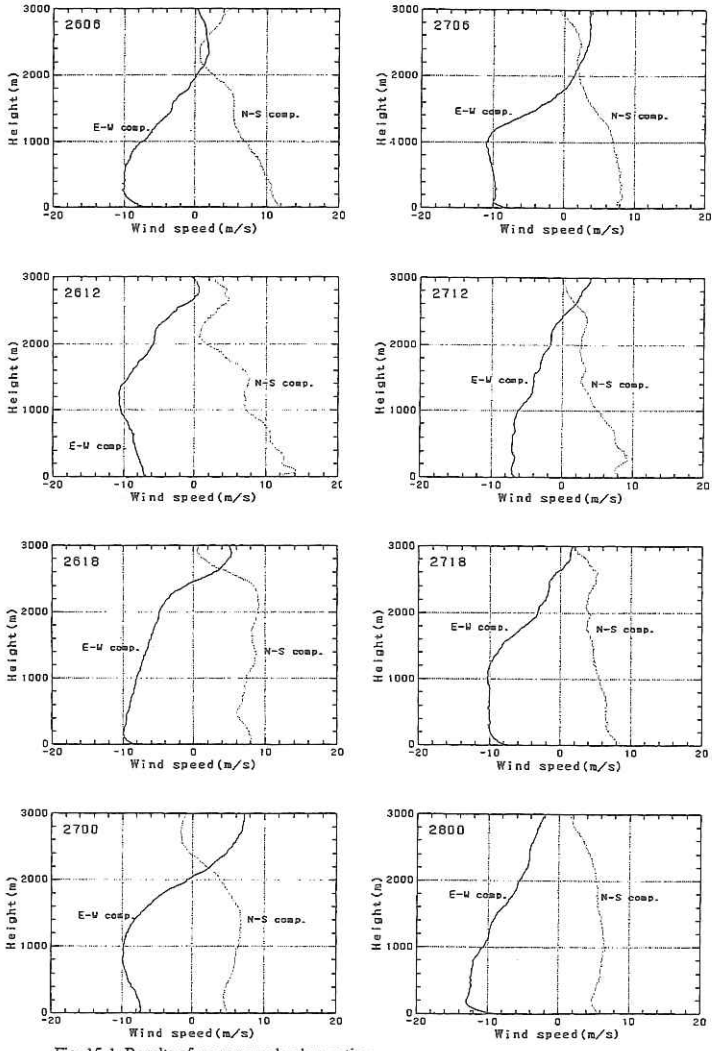

Fig. 15-1 Results of omega sonde observation.
(b)East-west and north-south component of wind speed. The number in the figure indicates released day and hour(GMT).

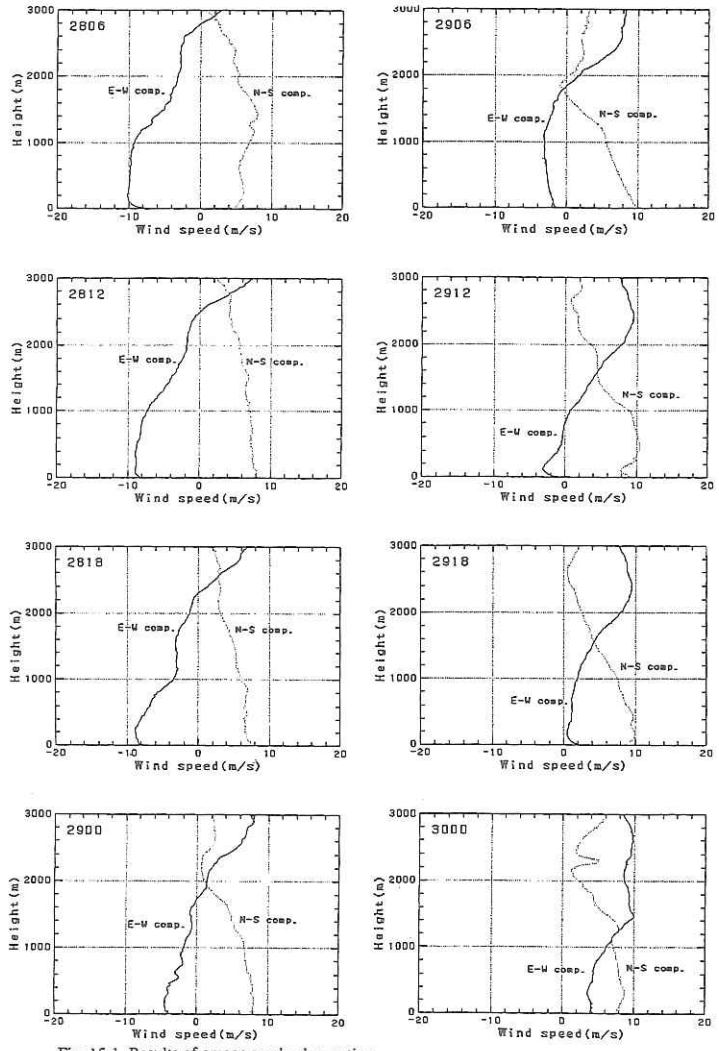

Fig. 15-1 Results of omega sonde observation.
(b)East-west and north-south component of wind speed. The number in the figure indicates released day and hour(GMT).

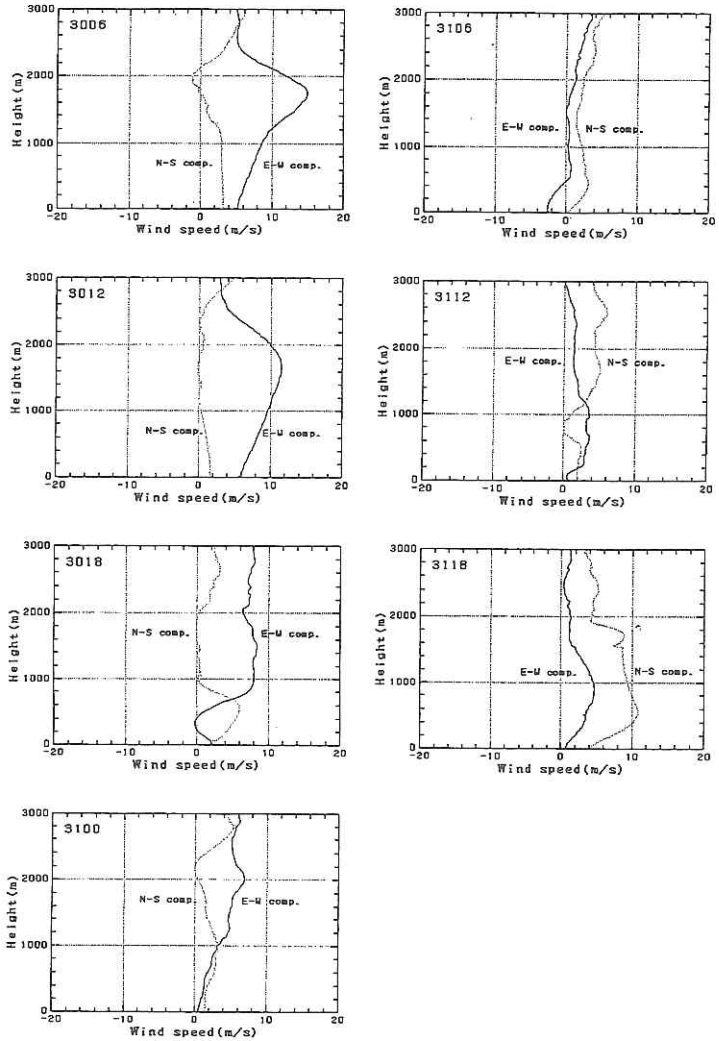

Fig. 15-1 Results of omega sonde observation.
(b)East-west and north-south component of wind speed. The number in the figure indicates released day and hour(GMT).

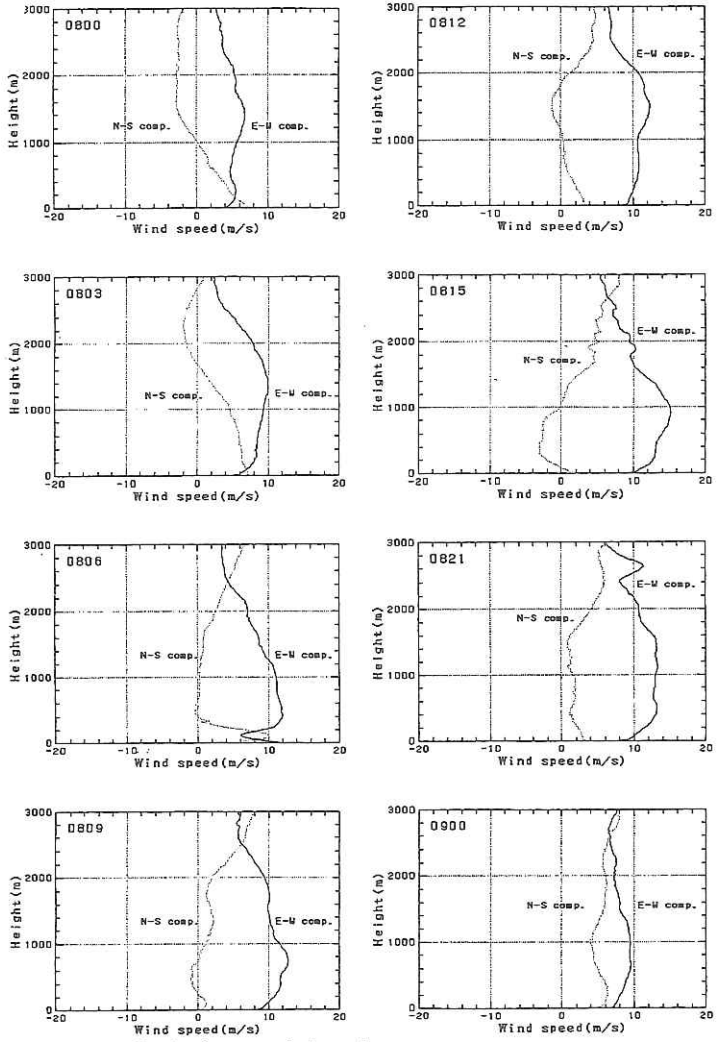

Fig. 15-1 Results of omega sonde observation.
(b)East-west and north-south component of wind speed. The number in the figure indicates released day and hour(GMT).

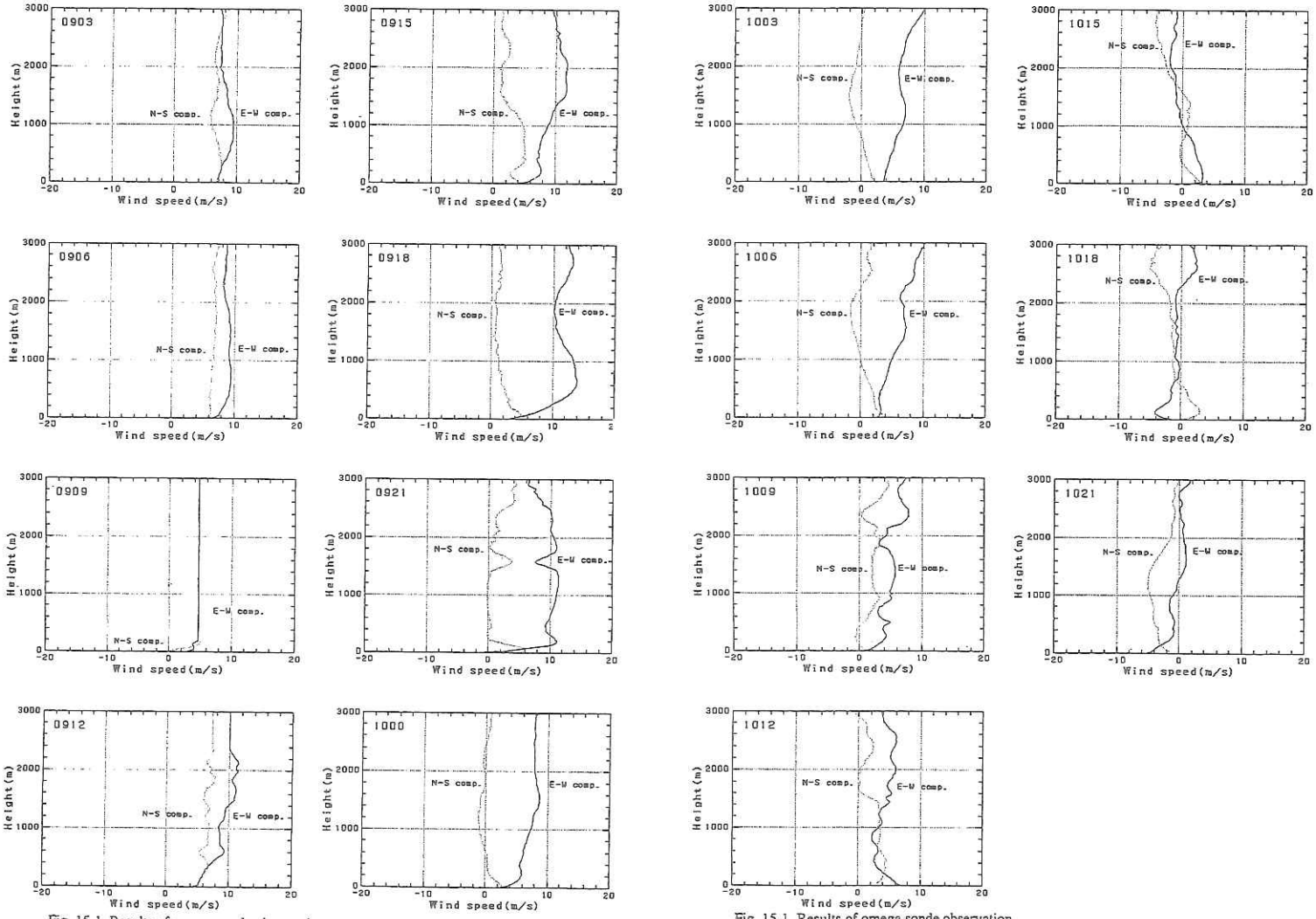

Fig. 15-1 Results of omega sonde observation.
(b)East-west and north-south component of wind speed. The number in the figure indicates released day and hour(GMT).

Fig. 15-1 Results of omega sonde observation.
(b)East-west and north-south component of wind speed. The number in the figure indicates released day and hour(GMT).

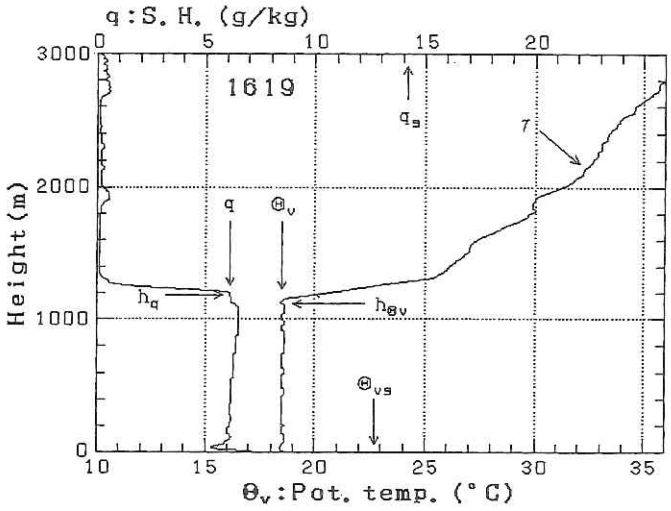

Fig. 15-2 Parameters of ABL. hqv:height of mixed layer defined by virtual potential temperature. hq:height of mixed layer defined by specific humidity. g:virtual potential temperature gradient of upper part of ABL. qv:virtual potential temperature of mixed layer. q:specific humidity of mixed layer. qvs:virtual potential temperature corresponded to SST. qs:saturated specific humidity corresponded to SST.

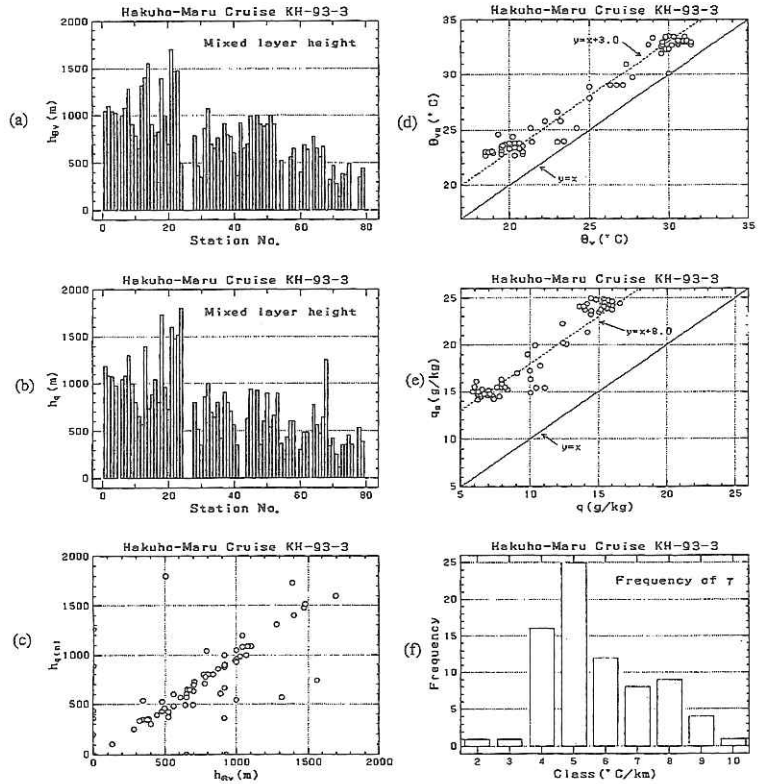

Fig. 15-3 The relation among the parameters of ABL. (a)station number vs. hqv, (b)station number vs. hq, (c)the relation between hqv and hq, (d)qv vs. qvs, (e)q vs. qs and (f)frequency distribution of g.

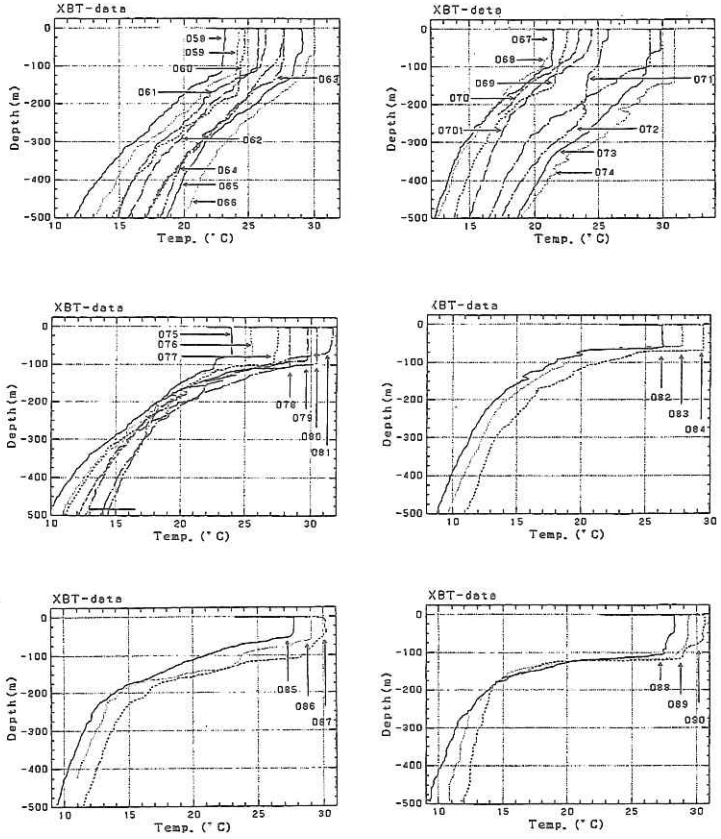

Fig. 15-4 Results of XBT observation.
(a)Vertical profile of temperature from surface to 500m in depth. Temperature scale corresponds to the left end profile. Other profiles are shifted one degree Centigrade respectively. The number indicates station number.

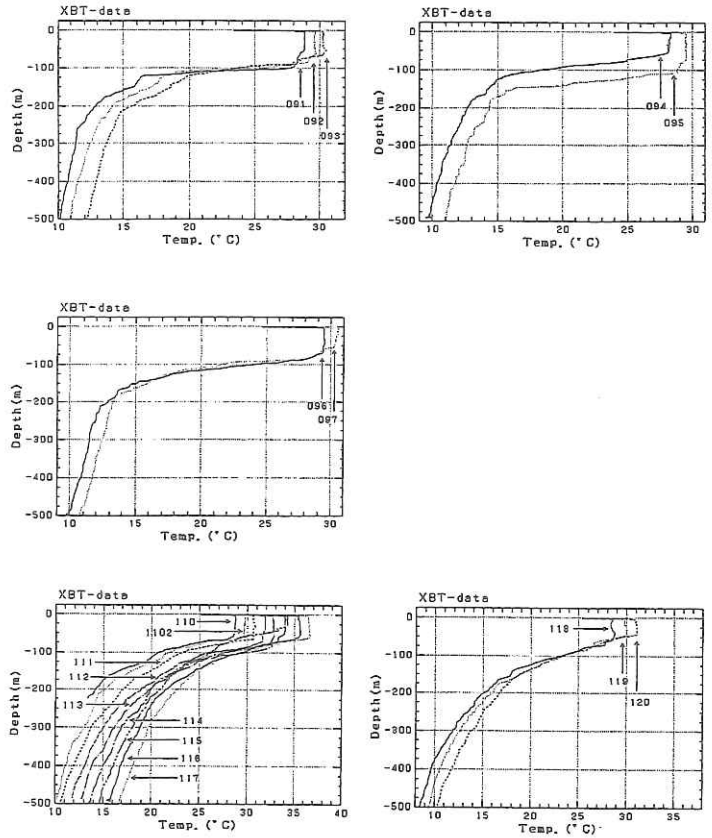

Fig. 15-4 Results of XBT observation.
(a)Vertical profile of temperature from surface to 500m in depth. Temperature scale corresponds to the left end profile. Other profiles are shifted one degree Centigrade respectively. The number indicates station number.

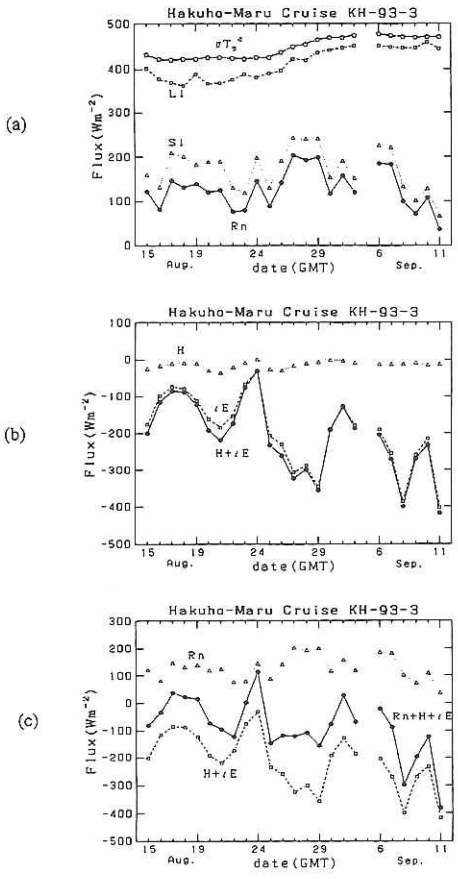

Fig. 15-6 The daily variation of energy fluxes. (a), (b) and (c) show net radiation flux, turbulent flux and net energy flux, respectively. Positive sign indicates the flux toward the sea surface.

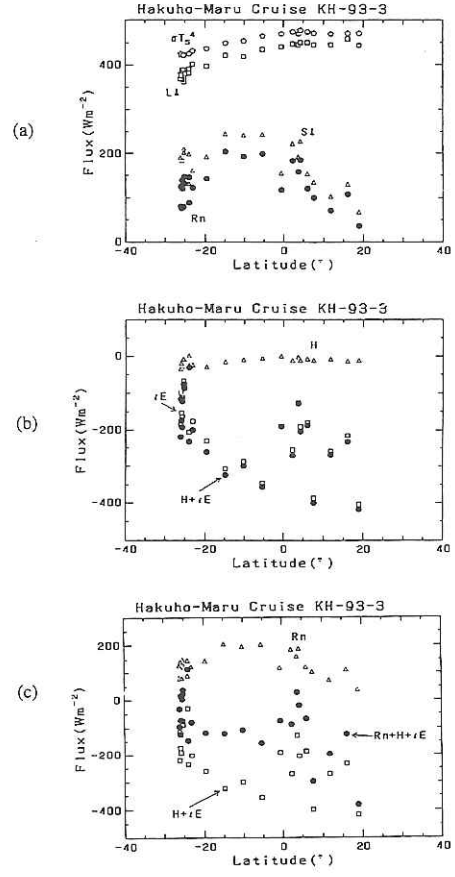

Fig. 15-7 The latitudinal variation of energy fluxes. (a), (b) and (c) are the same flux as in the figure 6(a), (b) and (c), respectively.

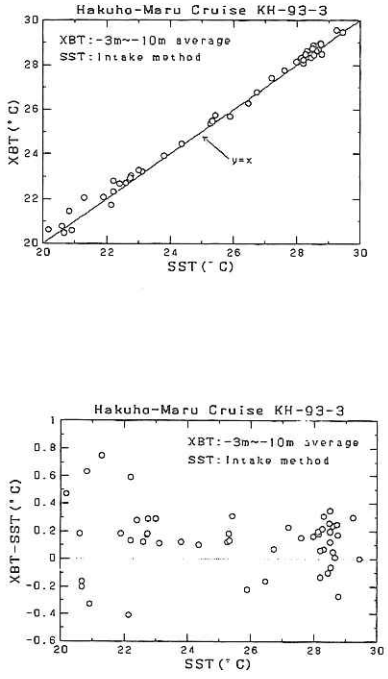

Fig. 15-4 Results of XBT observation.
(b)The relation between the SST from Hakuho-Maru and XBT. The latter data are average value from -3m to -10m. Upper figure is SST vs. XBT, lower SST vs. (XBT-SST).

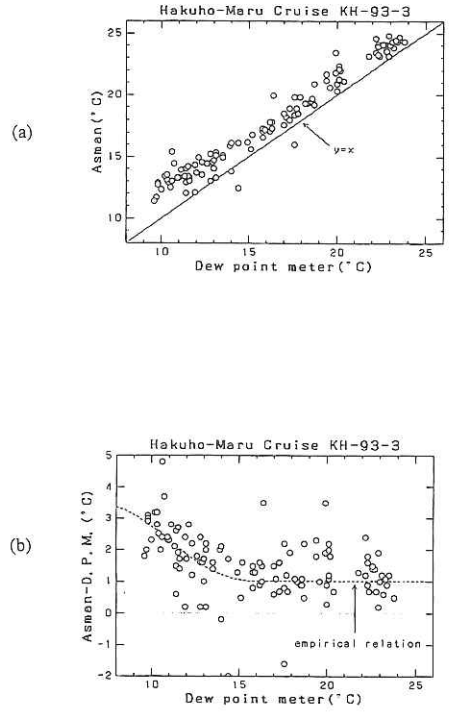

Fig. 15-5 (a)The relation of dew point measured by dew point meter (abscissa) and Asman ventilated dry and wet thermometer(ordinate). (b)Similar relation of (a), but the ordinate represents the difference of dew point measured by Asman and dew point meter. The dashed line indicates the empirical relation of calibration curve.

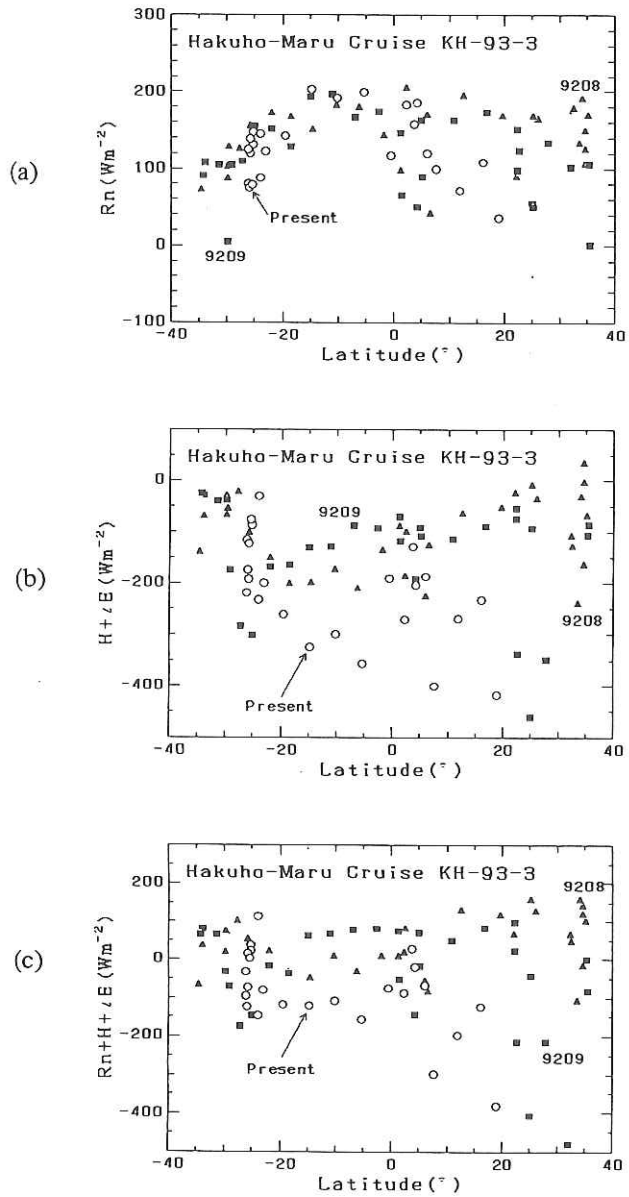

Fig. 15-8 Comparison of energy flux. Open circle shows Hakuho-Maru observation. "9208" and "9209" indicate the results of Osaka-Maru observation. "9208" means August 1992 and "9209" September 1992.